SYNTHESIS AND PROPERTIES OF SCANDIUM CARBOXYLATE METAL-ORGANIC FRAMEWORKS

Berenice González Santiago

A Thesis Submitted for the Degree of PhD
at the
University of St Andrews

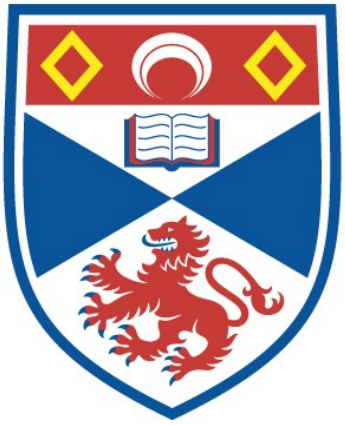

2015

Synthesis and properties of scandium carboxylate metal-organic frameworks

This thesis is submitted in partial fulfilment for the degree of

Doctor of Philosophy

in the Faculty of Science of the University of St Andrews by

Berenice González Santiago, MSc

September 2014

Supervisor: Prof. Paul A. Wright

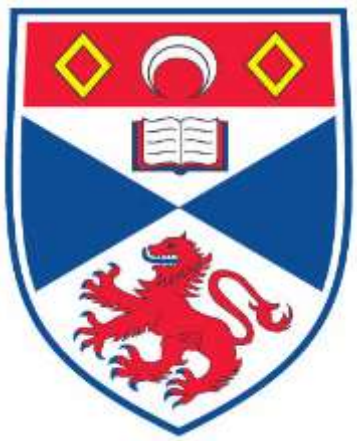

University of
St Andrews

Declarations

1. I, Berenice González Santiago, hereby certify that this thesis, which is approximately 40000 words in length, has been written by me, that it is the record of work carried out by me and that it has not been submitted in any previous application for a higher degree.

   I was admitted as a research student in September, 2010 and as a candidate for the degree of *Doctor of Philosophy* in October, 2011 the higher study for which this is a record was carried out in the University of St Andrews between 2010 and 2014.

   Date ……. Signature of Candidate ……..

2. I hereby certify that the candidate has fulfilled the conditions of the Resolution and Regulations appropriate for the degree of PhD in the University of St Andrews and that the candidate is qualified to submit this thesis in application for that degree.

   Date ……. Signature of Supervisor …….

3. In submitting this thesis to the University of St Andrews I understand that I am giving permission for it to be made available for use in accordance with the regulations of the University Library for the time being in force, subject to any copyright vested in the work not being affected thereby. I also understand that the title and the abstract will be published, and that a copy of the work may be made and supplied to any bona fide library or research worker, that my thesis will be electronically accessible for personal or research use unless exempt by award of an embargo as requested below, and that the library has the right to migrate my thesis into new electronic forms as required to ensure continued access to the thesis. I have obtained any third-party copyright permissions that may be required in order to allow such access and migration, or have requested the appropriate embargo below.

   Embargo on all of printed copy and electronic copy for the same fixed period of one year on the following ground: Publication would preclude future publication.

Date ……. Signature of Candidate ……

Signature of Supervisor ……

Acknowledgements

I am so grateful to CONACyT-Mexico for the scholarship awarded which made it possible to carry out my PhD. Also, many thanks to the School of chemistry at St. Andrews for co-funding. Thanks to SEP-complemento for the grant awarded for the term dates 2013-2014.

Firstly, I would like to express my sincerest gratitude to my supervisor Prof. Paul A. Wright, for the opportunity to be part of his group. Thanks for the feedback, suggestions, for your patience and taking time to answer my questions, and for the endless support you have given me in so many ways.

I thank Professor Alex Slawin and Dr. David Cordes at St. Andrews, Dr. Stephen Moggach and Jorge Sotelo at Edinburgh, for their help and support with the crystallography data. Thanks to Dr. Sharon Ashbrook, Dr. Valerie Seymour and Scott Sneddon for the collection and analysis of solid-state NMR data. I owe huge thanks to Mrs Silvia Williamson for the training on how to use the instruments, and for the collection of adsorption and thermal analysis data. Thanks to everyone in the Wright group including past members Dr. John Mowat, and Dr. Jurgen Kahr for all their background input on MOFs. I am lucky to have the ongoing support of great office mates; Dr. Magdalena Lozinska and David Prince. I would also like to give special thanks to Alessandro Turrina and Dr. Alex Greenway for helpful discussions about my research over the last year.

Thanks to all my friends here in St Andrews, with special thanks to Pernille Lau and J. Carlos H. Reta, for their company and kindness; to all my friends from Mexico, who have always brought a smile to my face. Also, I would like to thank Professors; Ana Maria Soto E., Miguel Angel Garcia S. and Hugo Sanchez S., for their enthusiasm and encouraging me to come here. I am hugely indebted to my mother and relatives for their endless support.

Dedicated to

The memory of my father

My family

And Salvador, who makes life fun.

Rise up like the sun
Labor till the work is done.

Abstract

This work investigated the synthesis, characterisation and properties of known and novel scandium carboxylate Metal-organic Frameworks (MOFs). The first part reports the performance of these Sc-MOFs as Lewis acid catalysts. The porous MOF scandium trimesate MIL-100(Sc) and the scandium terephthalates such as MIL-101(Sc), MIL-88B(Sc) and MIL-68(Sc) (prepared as the Sc-analogue for the first time), and scandium biphenyldicarboxylate MIL-88D(Sc) were prepared and tested as Lewis acid catalysts. Chromium MIL-101 and MIL-100 and scandium-exchanged zeolites were prepared for comparison. Moreover, successful encapsulation of the phosphotungstate polyoxometalates (POMs) in the cavities of MIL-101(Sc) enhanced the stability of this material. These scandium and chromium MOFs, POM-MOF composites and scandium-exchanged zeolite were tested as heterogeneous catalysts in the carbonyl ene reaction between α-methyl styrene and ethyl trifluoropyruvate. This showed that MIL-100(Sc) was the best catalyst for this reaction, achieving a conversion of 99% to the desired product. The stabilized MIL-101(Sc) was also very active, but less selective for this reaction. Acetalisation of acetaldehyde was also studied, and in this reaction the isoreticular MOFs MIL-88(B) and MIL-88D(Sc) were the most active and selective catalysts. For this reaction, the activity of MIL-100(Sc) was low, which was attributed to reduce pore size and blockage.

Functionalisation of the range of scandium terephthalates such as MIL-101(Sc), MIL-88B(Sc), MIL-68(Sc), Sc_2BDC_3,and MIL-53(Sc) particularly with $–NH_2$ groups, made up the second main part of this research. Solvothermal synthesis were performed at lower temperatures and using mixed solvents to synthesize these amino-terephthalate MOFs, often for the first time, and their adsorption properties were studied, particularly for the adsorption of CO_2.

The synthesis of pure $Sc_2(NH_2\text{-}BDC)_3$ and $Sc_2(Br\text{-}BDC)_3$ was achieved for first time by a solvothermal route, lower temperatures, and mixed solvents. This approach yielded large crystals suitable for single crystal diffraction and microcrystal IR spectroscopy. Post-synthetic modification (PSM) of $Sc_2(NH_2\text{-}BDC)_3$ was explored by incorporation of NO_2-groups into the framework by solvent-assisted ligand exchange. The adsorption properties of functionalised and post-modified materials were compared with those of Sc_2BDC_3 and $Sc_2(NO_2\text{-}BDC)_3$ for methanol and hydrocarbons This study demonstrated that Sc_2BDC_3 and $Sc_2(NH_2\text{-}BDC)_3$ give the higher uptakes while the –Br and $–NO_2$ forms display shape selectivity for n-alkanes over iso-alkanes.

Amino-functionalised MIL-53(Sc) was prepared for the first time using a mixed ligand approach, so that 10-20% of a second functionalised terephthalate ligand (NO_2, Br, $-(OH)_2$) was required for successful single phase synthesis in addition to amino-terephthalic acid. The materials were characterised using PXRD, TGA and gas adsorption, which confirms the samples show a range of behaviour for CO_2 adsorption. Notably, the `breathing´ behaviour is strongly dependent on the type of functionalisation.

Finally, the exploratory synthesis of novel scandium MOFs, using isophthalic acid (IA) and its amino and nitro- derivatives, 2,5-furandicarboxylate (FDA) and the porphyrin tetra(carboxyphenyl)porphyrin (TCPP) as linkers was carried out and six novel materials were synthesized, three of which gave crystals large enough for their structure to be determined by single crystal diffraction. Further characterisation was carried out by PXRD, TGA and solid-state NMR. Some of these materials have been shown to be porous to CO_2 and N_2.

Publications arising from this work

1. L. Mitchell, B. Gonzalez-Santiago, J. P. S. Mowat, M. E. Gunn, P. Williamson, N. Acerbi, M. L. Clarke and P. A. Wright.

Remarkable Lewis acid catalytic performance of the scandium trimesate metal organic framework MIL-100(Sc) for C–C and C=N bond-forming reactions.

Cat. Sci. Tech., 2013, 3, 606-617. DOI: 10.1039/c2cy20577g

2. Alex Greenaway, Berenice Gonzalez-Santiago, Paul M. Donaldson, Mark D. Frogley, Gianfelice Cinque, Jorge Sotelo, Stephen Moggach, Eleni Shiko, Stefano Brandani, Russell F. Howe and Paul A. Wright

In situ synchrotron IR microspectroscopy of CO_2 adsorption on single crystals of the functionalised MOF, $Sc_2(BDC\text{-}NH_2)_3$

Angew. Chem. Int. Ed., 2014, 53, 13483–13487. DOI: 10.1002/anie.201408369

Abbreviation	Explanation
$(OH)_2$-BDC	2, 5 -Dihydroxyterephthalic acid
3D	Three-dimensional
a	Unit cell parameter
b	Unit cell parameter
BDC	Terephthalic acid (Benzene dicarboxylic acid)
BET	Brunauer-Emmet-Teller
BPDC	Biphenyl-4,4-dicarboxylic acid
Br-BDC	2-Bromoterephthalic acid
BTC	Trimesic acid (Benzene tricarboxylic acid)
c	Unit cell parameter
CHN	carbon, hydrogen and nitrogen analysis
CP	Coordination Polymer
DMF	*N, N*- Dimethylformamide
DMSO	Dimethylsulfoxide
EDX	Energy dispersive X-ray spectroscopy
et al.	and others (Latin et alii)
FDA	2, 5-Furandicarboxylic acid
HKUST-1	Hong Kong University of Science and Technology Structure -1
IA	Isophthalic acid
IGA	Intelligent gravimetric analyser
IRMOF	Isoreticular MOF
IUPAC	International union of pure and applied chemistry
MAS	Magic angle spinning
MeOH	Methanol
MIL	Materials of Institut Lavoisier
MOF	Metal-Organic Framework
NH_2-BDC	2-Aminoterephthalic acid
NH_2-IA	5-Aminoisophthalic acid
NMR	Nuclear magnetic resonance
NO_2-BDC	2-Nitroterephthalic acid
NO_2-IA	5-Nitroisophthalic acid
PMA	Phosphomolybdic acid
POM	Polyoxometalate
PSM	Postsynthetic modification
PTA	Phosphotungstic acid
PXRD	Powder X-ray diffraction
SBU	Secondary Building Unit
SEM	Scanning electron microscopy
SIR	Semivariants representation
SXRD	Single-crystal X-ray diffraction
TCPP	*meso* Tetrakis(4-carboxyphenyl)porphyrin
TGA	Thermogravimetric analysis

Contents

Chapter 1: Introduction

1.1 Background: From Zeolites to MOFs

New developments in the synthesis of porous materials have attracted considerable interest because of their ability to interact with atoms, ions and molecules not only at their surfaces, but throughout their structure. In particular the development of zeolitic catalysts revolutionized the understanding and the rational design of surface and solid-state chemistry, and crystalline and porous aluminosilicates are found in numerous modern industrial applications.[1] Zeolites are crystalline aluminosilicates with an ordered framework structure built from corner-sharing SiO_4 and AlO_4 units (Figure 1.1). As-prepared zeolites typically contain inorganic cations such as Na^+, or organic alkylammonium cations that act as templates. However, some of these cations can be replaced by protons or by other cations of catalytic interest. The applications of these materials include ion exchange, adsorption/separation, and catalysis.[2-4]

Porous zeolites show outstanding performance as selective catalysts[5] and are among the most commercially important classes of industrial catalyst.[1, 6] For example in heterogeneous catalysis, zeolites have been successfully used in the chemical industry over a long period for large scale conversions, examples being the hydrocarbon conversions, where the conversion of methanol to hydrocarbon conversion is the most studied, isomerisation of xylenes, reforming gasoline to increase alkane branching, reaction of alcohols with ammonia, fine chemicals synthesis, and catalytic cracking[7]. However, zeolites do suffer drawbacks such as limited framework incorporation of different metals of interest in catalysis and also limited pore sizes, where there is a *ca.*1 nm limit. The pore size constraint is removed in the case of mesoporous silicates, but the lack of crystallinity of those materials reduces the ability to control and design the precise nature of their active sites and they have lower stability and Brønsted Lewis acidity.

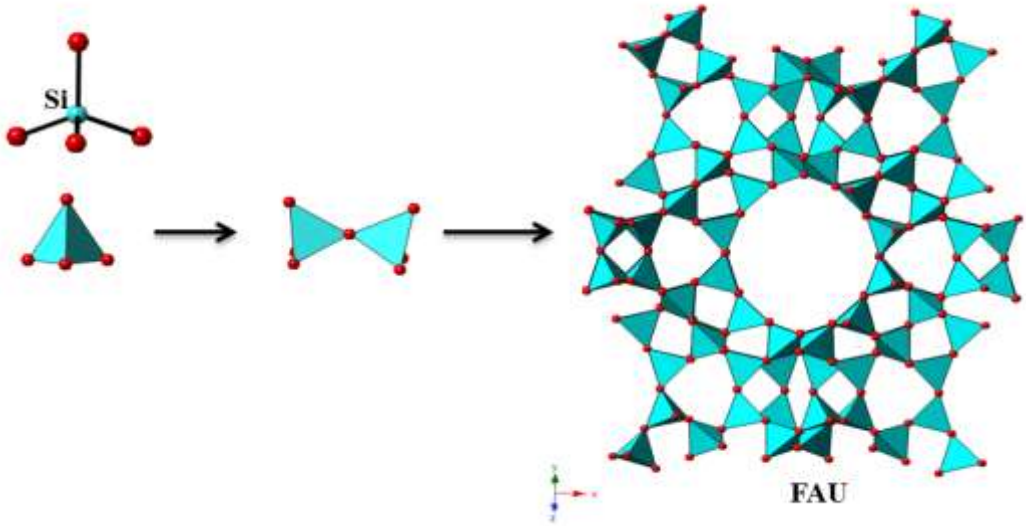

Figure 1.1: Zeolite structure FAU (faujasite Y). It has a 3-dimensional pore structure made of secondary building units 4, 6, and 6-6.

Extensive research on zeolites and the evolution of porous materials has led onto a new family of materials, known as coordination polymers (CP) and metal-organic frameworks (MOFs), which are built up of organic and inorganic components. These allow the pore size and chemical properties to be widely tuned. IUPAC[8] defined coordination networks as a subset of coordination polymers, and MOFs a further subset of coordination networks. The network of a MOF should contain potential voids as part of its assembly, while all other coordination compounds can be named as coordination polymers. Another characteristic that makes them different is that MOFs are by definition crystalline, whereas coordination polymers do not need to be.[9]

Metal-organic frameworks (MOFs)[10] have attracted enormous attention for potential applications in gas storage,[11-13] separation/purification,[14-18] drug delivery,[19] and catalysis.[12, 20-23] MOFs are crystalline materials generated by the association of metal ions and organic ligands. These materials can have a diverse range of framework architectures because of the wide variety of coordination geometries between the metal cations and the organic ligands, which assemble in 2D, and 3D structures.[10] The crystalline materials formed by a 3D

extended network involve metal ions connected through multidentate organic ligands, leading in many cases to a regular system of channels and cavities of molecular dimensions,[10] which have a cavity size that varies from microporous (smaller than 2 nm) to mesoporous (between 2 and 50 nm). MOFs are often described by their secondary buildings units (SBU),[24] which are essential to the design of directionality for the assembly of MOFs.

MOFs offer a breakthrough since they can combine many desired properties not observed in 'classical' porous solids and also have unprecedented pore sizes and surface areas suggesting their use as catalysts. MOFs possess significant potential catalytic advantages over zeolites, particularly in high-value added processes that do not require activation or regeneration at high temperatures. Among these potential advantages is the fact that the surface areas of MOFs are very high and they can be prepared with pore sizes much greater than can be achieved with zeolites. Furthermore, MOFs can possess almost endless chemical variety. Nevertheless these materials have the major disadvantage, of being much less thermally and hydrothermally stable compared with zeolites. The main properties of the MOFs and zeolites are summarized in Table 1.1.

Table 1.1: Comparison between zeolites and MOFs

Properties	**Zeolites**	**MOFs**
Surface area (BET)	Around 200–500 $m^2 g^{-1}$	Up to 5000 $m^2 g^{-1}$
Pore volume	Around 0.1–0.5 $cm^3 g^{-1}$	over 1 $cm^3 g^{-1}$
Thermal stability	Mostly stable above 523 ^oC	Not usually stable above 300 ^oC
Metal site density	Low percentage of other metal in framework. Typically transition metal cations are unstable in framework.	High percentage of metal frameworks that can act as Lewis acid or redox sites

Among the MOFs reported so far, some of the most interesting frameworks have been synthesized in metal carboxylate systems, where di- and trivalent metals have been combined with di- and tricarboxylic acids, often resulting in high symmetry structures. In 1999 two important MOFs were reported, a copper-based MOF known as HKUST-1[25] (now commercially available from BASF as Basolite™ C300) and the zinc based MOF, MOF-5.[26] The highly porous HKUST-1 has an open-framework that consists of dimers of Cu(II) in paddlewheels connected to four bridging benzene tricarboxylates (BTC), creating a square planar geometry around two adjacent copper sites(Figure 1.2).[27]

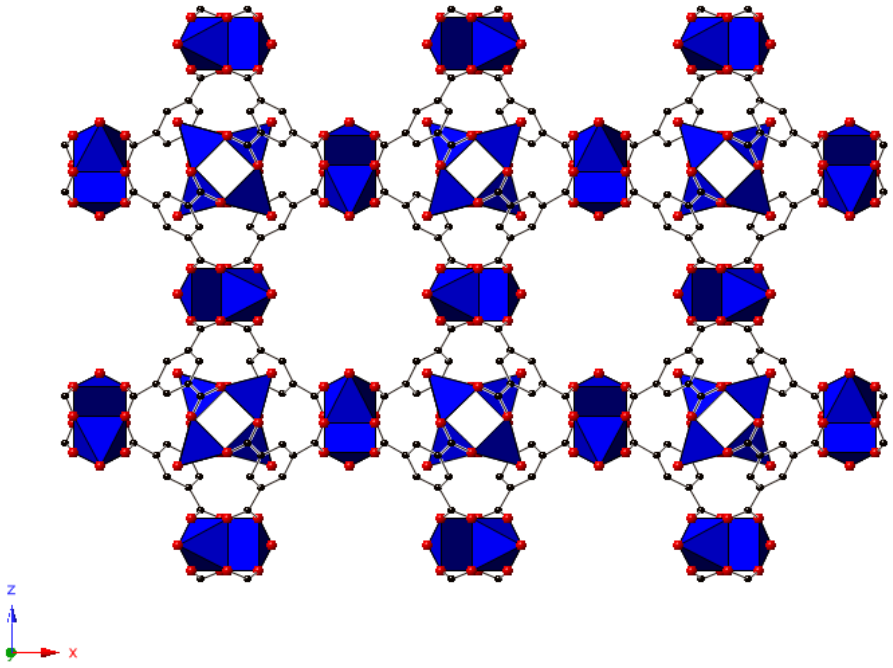

Figure 1.2: Images of the structure of HKUST-1[27]. Blue polyhedra represent the square pyramidal CuO_5 (C and O atoms are represented for red and black).

MOF-5 is a cubic 3-dimensional extended lattice composed of Zn_4O inorganic clusters connected by the terephthalate linker (1,4-benzenedicarboxylate or BDC). The prototypical MOF-5 structure, shown in Figure 1.3, the first 3-D metal organic framework structure reported to be stable to solvent removal, demonstrating permanent, reversible adsorption for nitrogen gas at standard conditions. A series of frameworks that have structures based on the

topology of MOF-5, with the building block $Zn_4O(CO_2)_6$ and dicarboxylate links projecting along the axes of a primitive cube, and with the linkers varying in length and ring substituents,[28] has been prepared giving porous materials with different pore sizes without changing the original cubic topology. They are known as isoreticular MOFs (IRMOFs).[11, 28-30] Figure 1.3 shows a series of IRMOF-n (n = 1 through 7, 8, 10, 12, 14, and 16) labelled respectively.

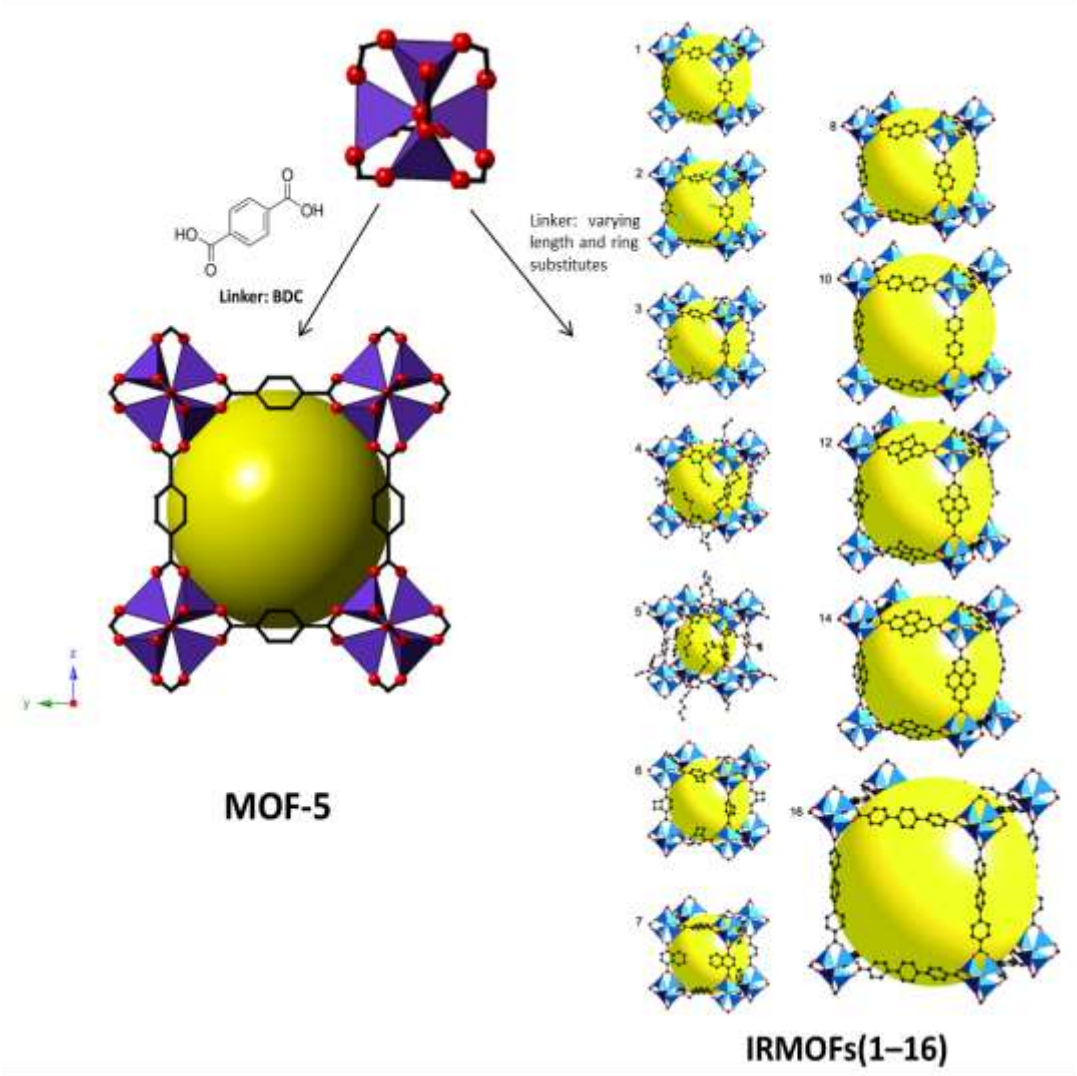

Figure 1.3: Coordination of structural units of MOF-5 framework and IRMOFs. ZnO4 tetrahedra (purple and blue polyhedral in MOF-5 and IRMOFs, respectively) (C and O atoms are represented for red and black spheres), yellow sphere represents the largest sphere that can occupy the pores (diameter of 12 Å in MOF-5) into the framework.[11, 30, 31]

A large number of MOFs with carboxylate frameworks have been synthesized over the last years. Férey *et al*[10] have synthesized an extensive series of carboxylate MOFs, members of the MIL-n family (Materials of Institute Lavoisier-n). A couple of the most extensively studied are MIL-101[32] and MIL-100,[33] both prepared initially with Cr^{3+}, with large pore structures containing mesoporous cavities. MIL-100 is prepared with the 1,3,5-benzenetricarboxylate (BTC) linker whereas MIL-101 is crystallised with the 1,4-benzenedicarboxylate (BDC) linker. Both structures contain supertetrahedra (ST) (Figure 1.4), [34] where each vertex of each supertetrahedron is occupied by a $Cr_3(\mu_3\text{-}O)$ trimer. MIL-100 and MIL-101 were the first examples of crystalline porous solids exhibiting mesoporous cages. In MIL-100, trimesate linkers are on the faces of the supertetrahedra, while in MIL-101 terephthalate linkers are on the edges of the supertetrahedra.

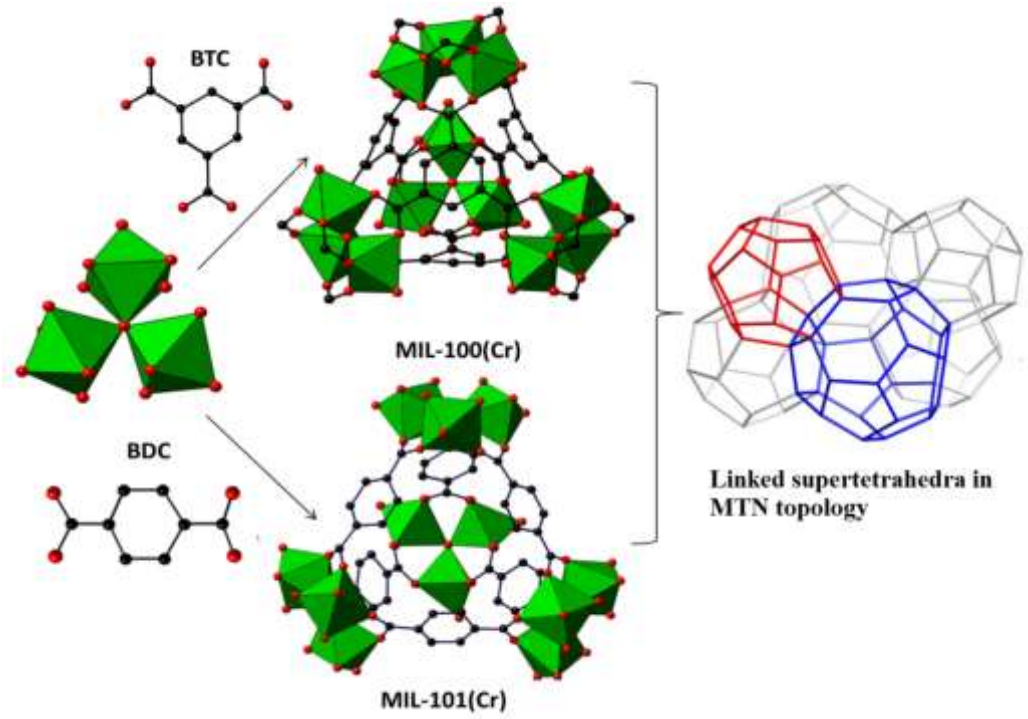

Figure 1.4: MIL-100 and MIL-101 super-tetrahedral units. Each unit is assembling in supertetrahedra in a 3D MTN zeolite topology. MTN network with a single smaller cage (blue) and larger cage (red) identified. Each vertex represents the centre of a tetrahedral unit, either an AlO_4 or SiO_4 tetrahedra in ZSM-39 or the super-tetrahedral building unit of MIL-101.

The supertetrahedra link through vertices forming a 3-D network of corner-sharing polyhedra with an augmented version of the 3D MTN zeolite topology.[35] Within the supertetrahedra in MIL-100 there are two cage forms, one is a pentagon dodecahedron with an internal diameter of *ca*. 25 Å, and pentagonal pore openings of 4.8 × 5.8 Å. The other cage forms as a polyhedron with 12 pentagonal and 4 hexagonal faces. The internal diameter is *ca*. 29 Å, and the large hexagonal pores are 8.6 Å.[33]. By contrast the supertetrahedra in MIL-101 have an internal diameter of 8.6 Å; with two larger different cages of internal diameters of 29 Å and 34 Å, linked via windows with dimensions of 12.5 Å and 16.3 Å. After synthesis the cages in MIL-101 are filled with a large number of guest molecules, including excess mainly terephthalic acid, which must be removed to activate the structure. In the structure of both MIL-100 (Cr) and MIL-101 (Cr), the chromium trimer is formed with three chromium atoms coordinated to the same μ_3 oxygen atom. Two out of the three Cr atoms in each trimer are coordinated to a water molecule, which can be removed, creating empty metal sites with Lewis acid properties, whereas the third is coordinated by a hydroxyl group to maintain the charge balance.

MIL-88 is another series of isoreticular MOFs, the first of which was reported in the iron form.[36] The ligands used in the synthesis of MIL-88 can be found in Table 1.2. This framework consists of both one dimensional channels and trigonal bipyramidal cages (Figure 1.5). Subsequent studies on the flexibility of materials MIL-88B (Cr and Fe) showed a large breathing behavior upon adsorption of polar gases.[37, 38] Similar behavior was observed with MIL-88B(Sc).[39, 40]

Table 1. 2: Summary of isoreticular MIL-88 materials prepared with Fe^{3+}. [36]

		Cell parameters		
MOF	**Ligand**	**a (Å)**	**c (Å)**	**V ($Å^3$)**
MIL-88A	Fumaric acid	11.18	14.68	1500
MIL-88B	Terephthalic acid	11.05	18.99	1980
MIL-88C	Naphthalene-2,6-dicarboxylic acid	10.22	23.60	2020
MIL-88D	4,4'-Biphenyldicarboxylic acid	12.05	27.50	3500

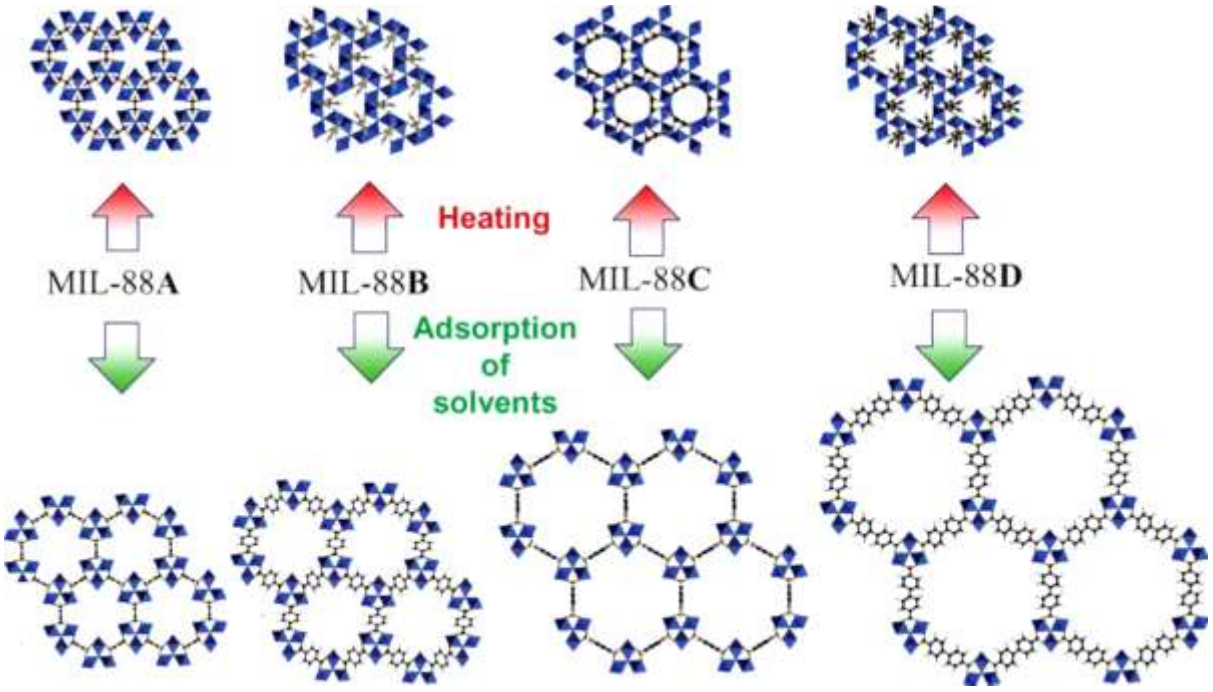

Figure 1.5: Representation of the isoreticular MIL-88. View of the simulated ''closed'' and ''open'' phases of the isoreticular MIL-88 reversibly obtained upon dehydration and adsorption of solvents, respectively.[34]

MIL-53[41] is another material widely studied because of its breathing behaviour and flexibility in response to changing temperature. The first report based on chromium (Cr^{3+}), was published by Serre et al,[42] and MIL-53 with other trivalent metals has been reported. [40, 43-46] This MOF has the formula MOH(BDC), M = Cr, Al, Fe, Ga, In, Sc; BDC = 1,4-

benzenedicarboxylate). Since MIL-53(Cr) was prepared, denoted as as-synthesized MIL-53 (MIL-53as), studies demonstrate that the channels of the as-prepared material are filled with residual ligands (BDC) or solvent molecules, resulting in a narrow-pore (*np*) form. Upon calcination at elevated temperatures (MIL-53h) to remove guest molecules, the material opens to exhibit a porous structure which is referred to as the large-pore (*lp*) form. At room temperature the MOF readsorbs atmospheric water to give narrow pore (*np*) hydrated MIL-53lt. This transition between the MIL-53ht dehydrated form and the hydrated MIL-53lt is fully reversible (Figure 1.6), and shows a very large breathing effect, the pores being closed in the presence of water molecules (MIL-53lt) and reopened when the water molecules are removed (MIL-53ht).

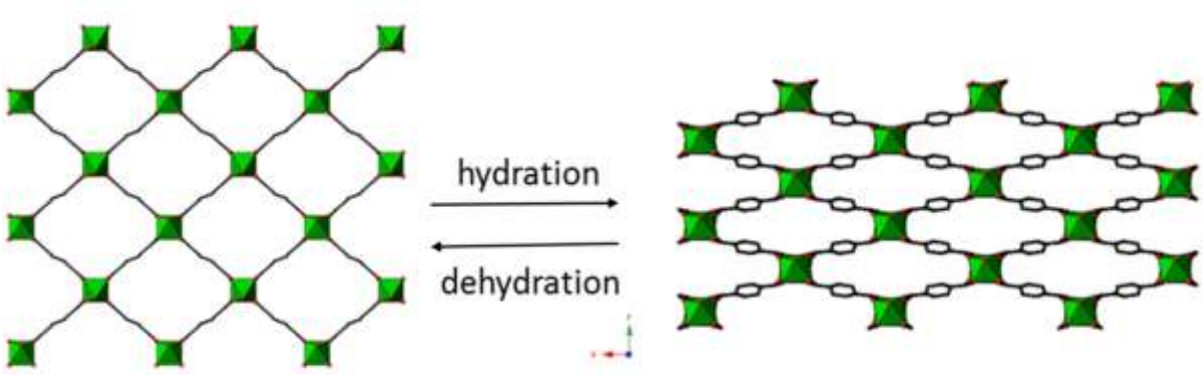

Figure 1.6: View of the pore systems of MIL-53(Cr); showing the breathing of the framework. (Left) MIL-53ht (large pore), and (right MIL-53lt (hydrated).[42]

MIL-53 is isostructural with MIL-47,[47] general chemical composition [M(X)(BDC)], where for MIL-53, X = OH, M = M^{+3} and for MIL-47, X = O, M = M^{4+}. The difference between these MOFs is that in MIL-53 there is a hydroxide bridge between trivalent cations, whereas in the activated MIL-47 bridges tetravalent cations μ_2-O. MIL-68[48] is another material synthesized with BDC; the framework is a polymorph of MIL-53. MIL-68 has been reported previously for V, Fe, Ga, In, Al[48-51] and as result of the work in this thesis, Sc[23] (chapter 3).

MIL-68 has a framework structure containing a hexagonal array of large pore channels and small triangular tunnels connected to the metal hydroxide chains creating a 'kagome lattice'. Unlike MIL-53, MIL-68 does not breathe.[41] Figure 1.7 shows the structure for the two polymorphs of $V^{III}(OH)[OOC–C_6H_4–COO]$, MIL-47(V) and MIL-68(V).

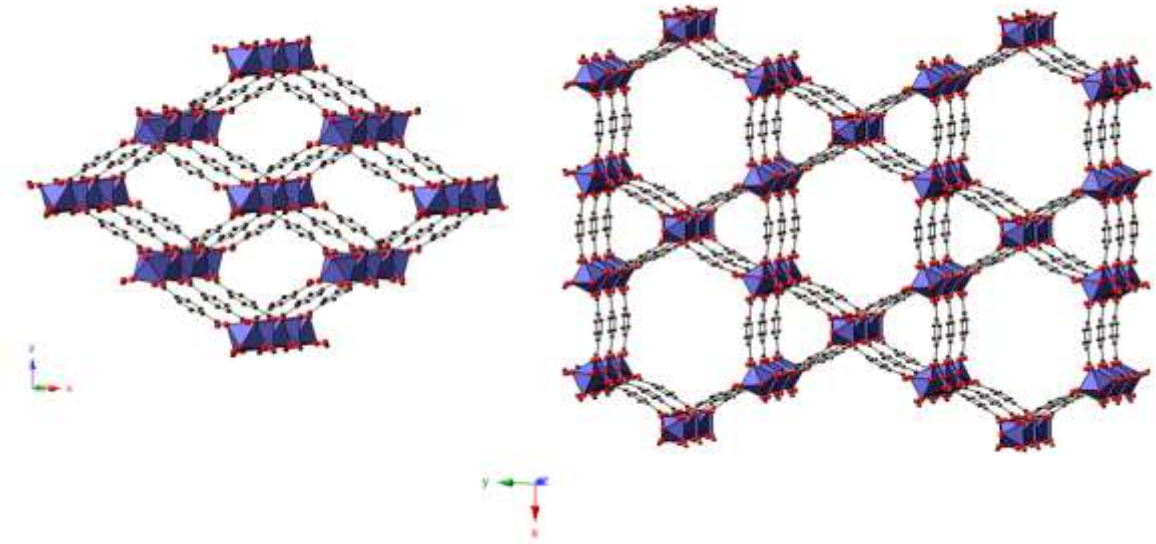

Figure 1.7: Image of the framework of MIL-47(V)(left) and MIL-68(V)(Right), two polymorphs of $V^{III}(OH)[OOC–C_6H_4–COO]$. VO_6 octahedra are shown in violet, red and black spheres represent carbon and oxygen atoms. [47-48]

1.2 Scandium Metal Organic-Frameworks

Among the metals used in the synthesis of MOFs, the trivalent cations are the most widely studied. In the Wright group there is a specific interest in preparing MOFs with scandium for their application in adsorption and catalysis.[23,40,52-54] The chemistry of scandium is dominated by that of its trivalent ion, Sc^{3+} (d^0). The ionic radius of Sc^{3+} is 74.5 pm so that the chemical properties and crystal chemistry of scandium are intermediate between those of aluminium (Al^{3+}, 53.5 pm) and the rare earth yttrium (Y^{3+}, 90 pm). Scandium has historically been classified as a rare earth element, together with yttrium and the lanthanides. Perles et al.[55] reported the first scandium based metal-organic framework, which is composed of layers of Sc_2O_{11} corner sharing dimers connected by the dicarboxylate linker succinic acid (Figure

1.6). However, this material did not show any uptake for gases. Gandara et al.[56] later reported the synthesis of scandium-squarate, but the internal pore space cannot be accessed by gas molecules due to the small size of the windows between cages. The scandium croconate[57] is another scandium carboxylate material, which is formed by discrete heptanuclear OH-μ-O–scandium cluster in a molecular complex $[Sc_7(croc)_6(H_2O)(OH)_7O]$.

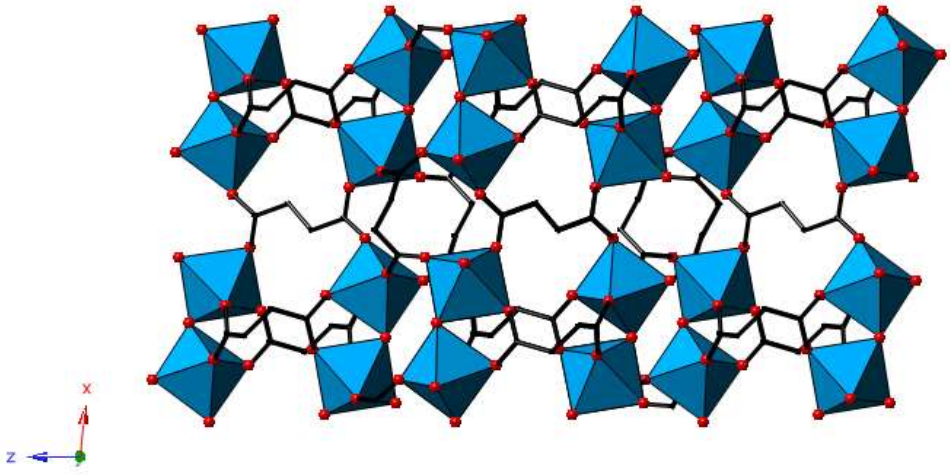

Figure 1.8: Structure of the first scandium succinate MOF. Scandium octahedra are shown in blue, red spheres represent oxygen. [55]

Syntheses using di and tri- carboxylate linkers have been widely studied; many of the resulting MOFs exhibited high thermal stability and both rigid and flexible frameworks capable of high adsorption uptake and novel adsorption behavior. Dietzel and coworkers [58] reported a material using as linker the 2,5-dihydroxyterephthalic acid, which crystalline material was the first report of the scandium trimer unit with the MIL-88 framework, however this did not show any uptake for nitrogen gas at -196 ℃, although careful studies may have shown some breathing behaviour with solvents. Figure 1.9 shows the framework of this MOF.

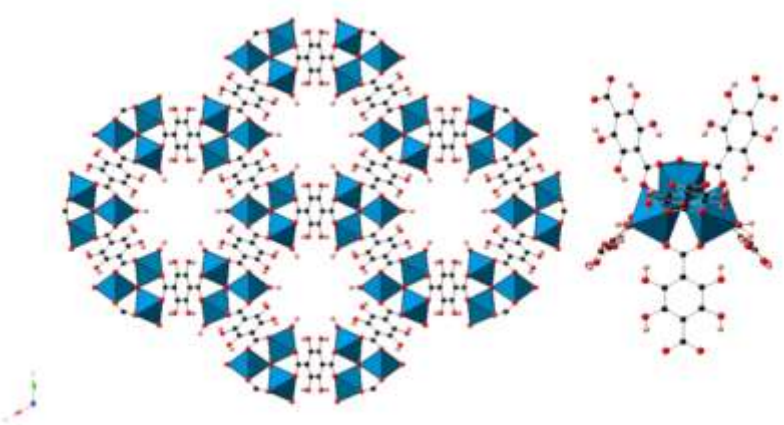

Figure 1.9: (Left) Crystal structure of scandium MIL-88 prepared with 2, 5-dihydroxyterephthalic and (right) trimeric building block. ScO_6 octahedra are shown in blue, black, red and pink spheres represent carbon, oxygen and hydrogen atoms of the linker. (Hydroxy groups are disordered).[58]

The MOF known as Sc_2BDC_3[59] was the first reported permanently porous material based on scandium. This framework is composed of chains of octahedral Sc^{3+} bridged by terephthalate groups (Figure 1.10), where each scandium is separated by three bridging carboxylates of the terephthalates from another, forming a chain of isolated ScO_6 octahedra, which is linked to six other adjacent chains generating an array of triangular channels. Sc_2BDC_3 displays a change in the symmetry observed on the adsorption of CO_2 from orthorhombic *Fddd* to monoclinic *C2/c*. Studies of its functionalisation with NO_2 and NH_2-groups have been published as well, [53] a topic that will be treated in more detail later.

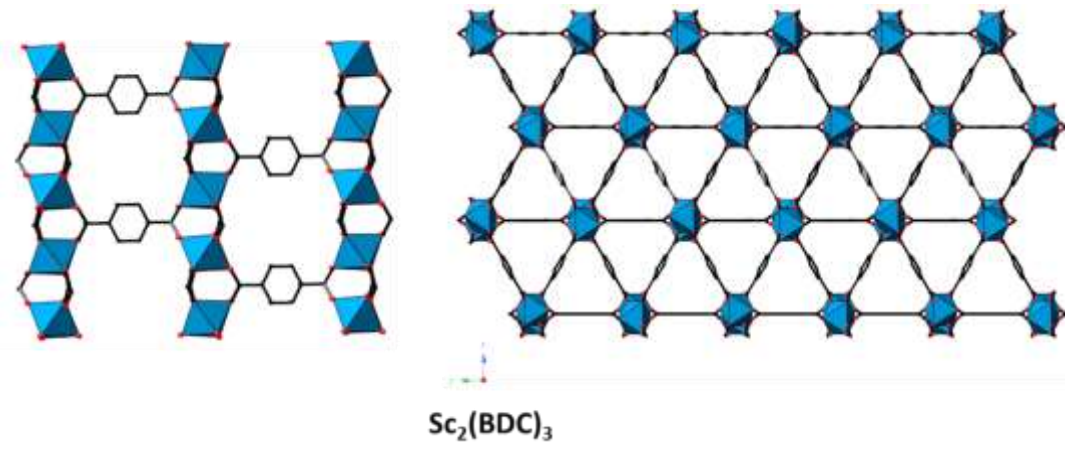

Figure 1.10: Structure of the layers of terephthalates connecting the chains (left) in framework of Sc_2BDC_3 (right). H atoms not shown.[59]

Mowat et al.[40] reported scandium versions of the MIL-88B(Sc), MIL-100(Sc) and MIL-101(Sc). The structure types for the solids MIL-100(Sc), and MIL-101(Sc), are illustrated in Figure 1.11. MIL-101 was obtained only within mixtures with MIL-88(Sc), with which it is polymorphic. For MIL-100(Sc), the powder patterns were not of high enough quality to permit structure refinement, but it was possible using the Le Bail method[60] to refine the cubic unit cell parameters as $Fd\bar{3}m$, a = 75.436(8) Å.

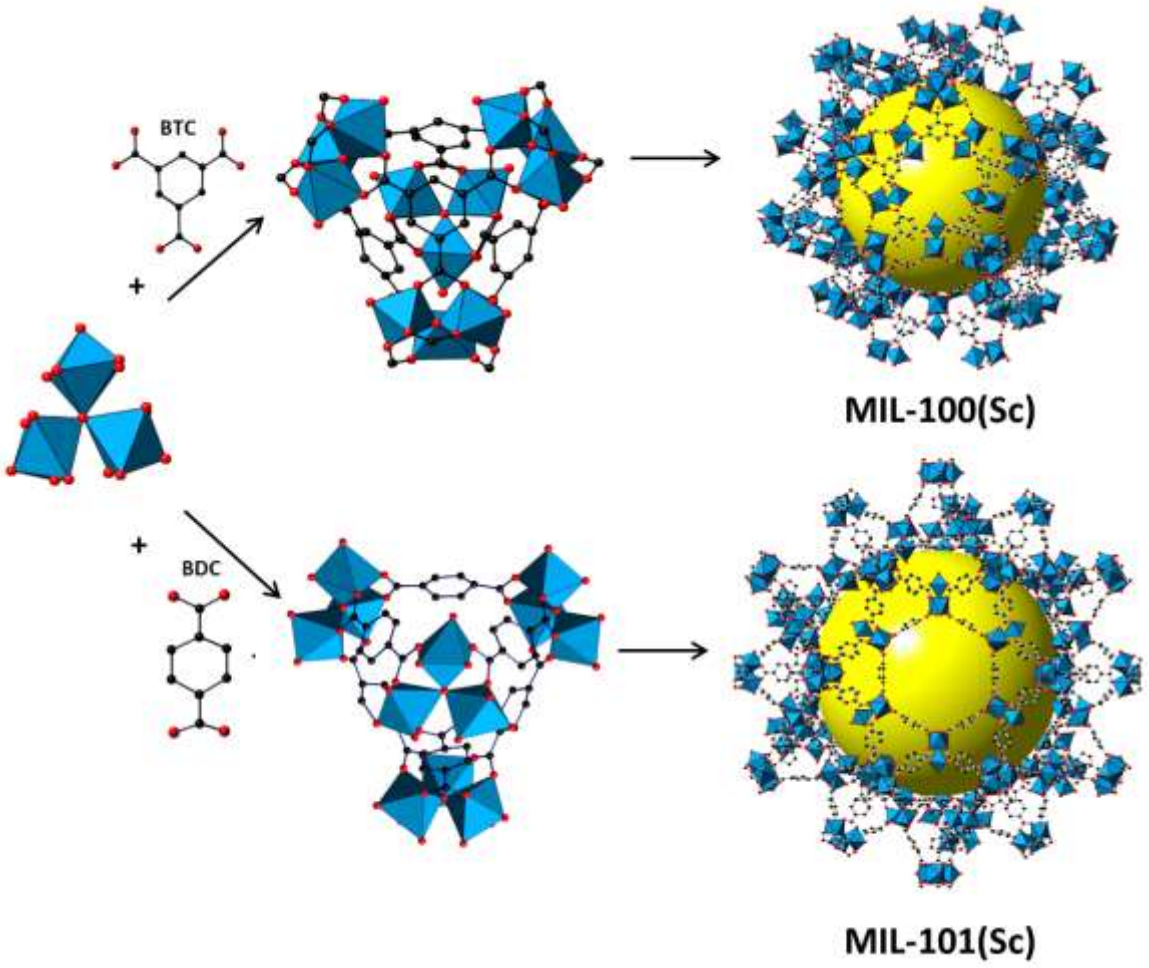

Figure 1.11: Structures of MIL-100(Sc) and MIL-101(Sc) assembled by trimers linked to the BTC (top) and BDC (bottom) respectively. [40]

Figure 1.12 shows the structure of the framework MIL-88(Sc). Studies of this material showed that the as-prepared material was indexed in the hexagonal cell typical of MIL-88, $P\bar{6}2c$, with a = 11.18 Å, c = 19.47 Å. Other published studies[39] show that the synthesis of MIL-88B(Sc), followed by solvent exchange with acetone and desolvation under vacuum

gives a solid with permanent porosity to N_2 of 0.25 cm^3 g^{-1}, indicating the importance of the activation procedure on opening the framework in the case of MIL-88(Sc). Recently, the synthesis of MIL-88D(Sc) was reported. [23] This MOF is based on the biphenyldicarboxylate linker, but the results of its flexibility behaviour suggesting the structure is much more rigid than the MIL-88B(Sc). These scandium carboxylates provide a promising starting point for studies of the Lewis acid catalytic performance of porous MOFs. The structure of MIL-88D(Sc) is shown in Figure 1.13.

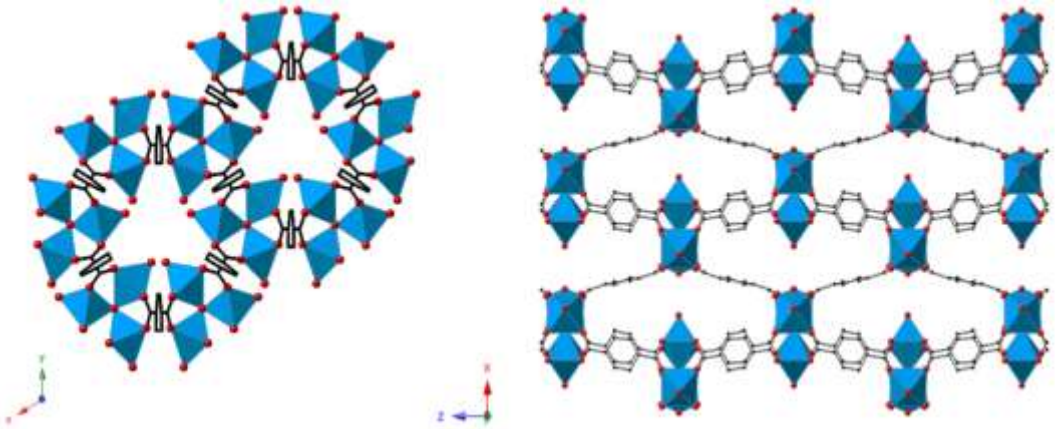

Figure 1.122: Views of the framework of as-prepared MIL-88B(Sc), down (left) the *z* axis and (right) the *y* axis.[40]

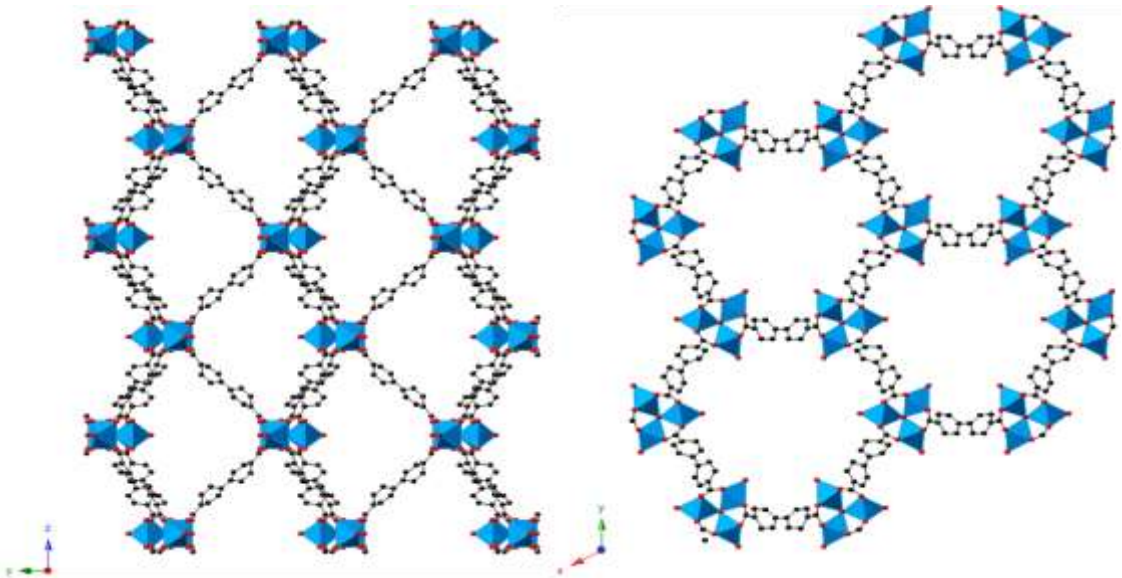

Figure 1.13: Views of the framework of as-prepared MIL-88D(Sc), down (left) the *x* axis and (right) the *z* axis.[23]

MIL-53, the most widely studied MOF in the carboxylate system due to its breathing properties, has been prepared with scandium by Mowat et al.[54] This framework is composed of infinite, corner-sharing, $ScO_4(OH)_2$ chains with the Sc^{3+} cations bridged by μ_2 hydroxyl groups. This material had solvent molecules (DMF) in the channels (Figure 1.14). Upon removal of solvent it gives a closed form which possesses the smallest cell volume yet observed for MIL-53, and which undergoes a transition at higher temperatures to a very narrow pore (*vnp)* structure.

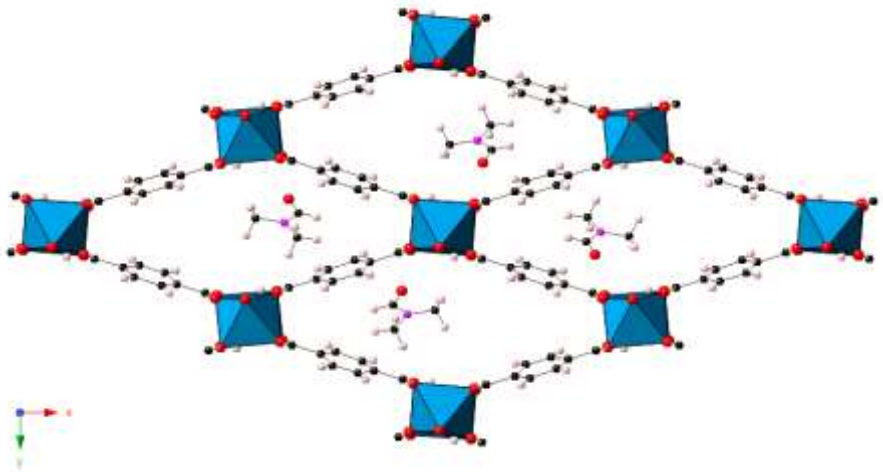

Figure 1.14: Structure of MIL-53(Sc)-DMF viewed down the channels parallel to the *z*-axis.[54]

This material has a highly flexible framework and the gas adsorption isotherm on this MOF is commonly characterized by a prominent step, in fact the isotherm is doubly S-shaped, and this is associated with structural changes upon change in pressure or temperature. The second, characteristic, inflection in the isotherm is typical for the adsorption/desorption behaviour for MIL-53, usually termed "breathing" or "gate opening". The gas adsorption analysis on MIL-53(Sc) shows no uptake at -196 ℃ for N_2 as in this case MIL-53(Sc) has smaller pores than the other analogues so at that temperature no pore opening occurs, however, at -77 ℃ it does adsorb CO_2. The process of adsorption occurs in two steps starting from the closed pore form, starting at low pressure (no adsorption), with a first step to get the

narrow pore form allowing moderate CO_2 adsorption uptake and then opening fully to the large pore form *(lp)* at higher partial pressures (Figure 1.15).

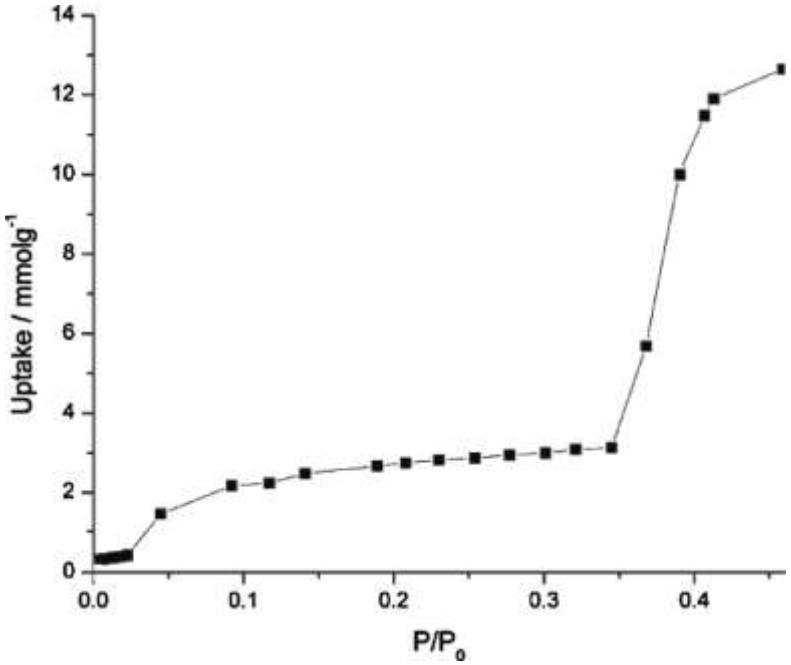

Figure 1.15: CO_2 isotherm measured at -77 ^{o}C on MIL-53(Sc). Reprinted with permission of the Royal Society of Chemistry.[54]

Beyond BDC and BTC as linkers to prepare scandium materials, the use of other ligands has been explored with a large tri-carboxylate linker 1,3,5-tris(4-carboxyphenyl)benzene (BTB), biphenyl-3,3',5,5'-tetracarboxylate and thiophene-2,5-dicarboxylate.[39, 61] Sc-BTB (Figure 1.16) is a large pore scandium carboxylate composed of the trimeric scandium cluster linked to 1,3,5-tris(4-carboxyphenyl)benzene with BET surface area of 1233 m^2g^{-1} and pore volume of 0.62 cm^3g^{-1}. For the biphenyl-3,3',5,5'-tetracarboxylate and the thiophene-2,5-dicarboxylate linkers, the frameworks are assembled from the $[Sc_2(\mu_2\text{-}OH)(O_2CR)_4]$ building block, these are named as NOTT-400 and NOTT-401 respectively (see Figure 1.17), both materials exhibit thermal stability and permanent porosity. [39, 61]

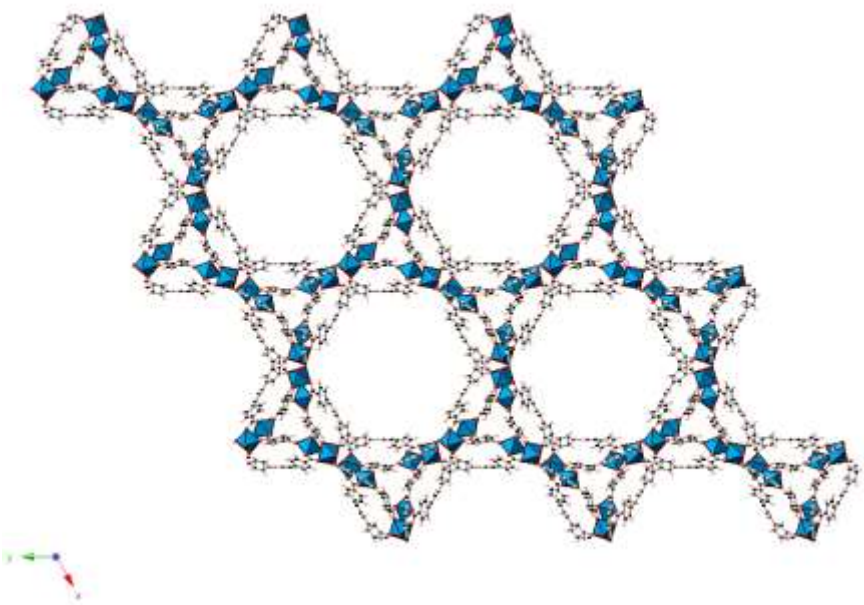

Figure 1.16: View of the three-dimensional framework Sc-BTB along the *z*-axis, which shows the channels of the structure. [39]

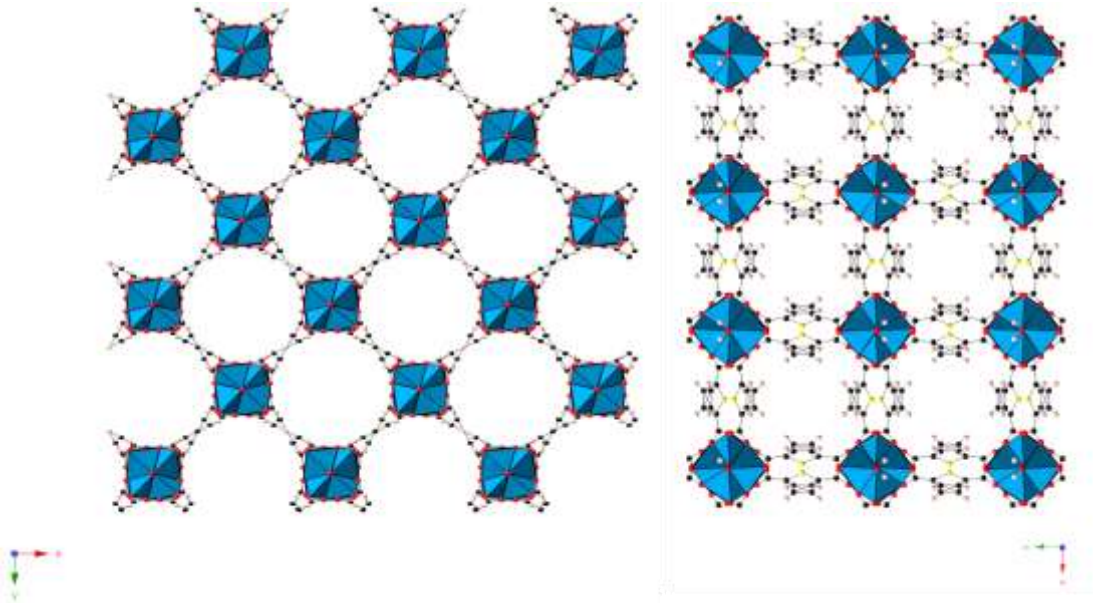

Figure 1.17: Structure of the frameworks NOTT-400 (left) and NOTT-401 (right). [61]

Scandium has been found to be of interest in MOF synthesis for application in gas adsorption and catalysis. One of the objectives in this thesis is exploring the synthesis of scandium MOFs with different linkers, extending the work started by Miller[62] and followed by Mowat.[62,63] Carboxylates linkers and large molecule such as Tetra(4-carboxyphenyl)porphyrin (TCPP) will be investigated. Fateeva et al,[64] published the use of

this porphyrin with iron (Fe^{3+}) assembling the MOF MIL-141(A). Additionally, synthesis of scandium MOFs containing linkers with functional groups, especially amines, is investigated.

1.2.1 Functionalised scandium MOFs

The structural versatility of MOFs has the potential to enable more selective adsorbents to be designed because their pore size and shape can be tuned by the addition of functional groups that enhance the physical and chemical properties of these materials. Functionalised MOFs can be prepared either by utilizing functional organic ligands that can be used directly in the synthesis (the isoreticular approach)[30] or by post-synthetic modification (PSM)[65] of the material after the formation of the crystalline structure. Functionalisation of MOFs is desirable because it is possible to make them more selective toward CO_2, CH_4, and H_2. For example, functionalised MIL-53(Fe)-$(CF_3)_2$ adsorbs N_2 at -196 ℃ (BET surface area of 100 mmol g^{-1}) and differently functionalised X-MIL-53(Fe) where X=Cl, Br, CH_3, adsorbs a higher amount of CO_2 at 30 ℃ and low pressure in comparison to the non-functionalised solid MIL-53(Fe), which has two steps in its isotherm.[66] The functional groups make the framework more rigid, allowing access of CO_2 under those conditions.

The scandium forms of MIL-53 and the Sc_2BDC_3 MOF have previously been prepared with nitro-terephthalate linkers, and microcrystalline $Sc_2(NH_2\text{-}BDC)_3$ has been prepared hydrothermally (although usually with an unreacted Sc_2O_3 impurity). [53, 54] For Sc_2BDC_3, the CO_2 adsorption is strongly affected by functionalisation, where the presence of amino groups increases the uptake at low pressures, due to stronger interactions with the CO_2, unlike NO_2 groups which reduce the adsorption because of their steric bulk (Figure 1.17). However, synthesis of amino- and especially bromo-functionalised Sc_2BDC_3 has proved problematical, due to the high temperature involved. The reported synthesis commonly leads to ligand

decomposition or even, in the case of the bromo-form, of reaction of the carboxylate linker with the solvent.

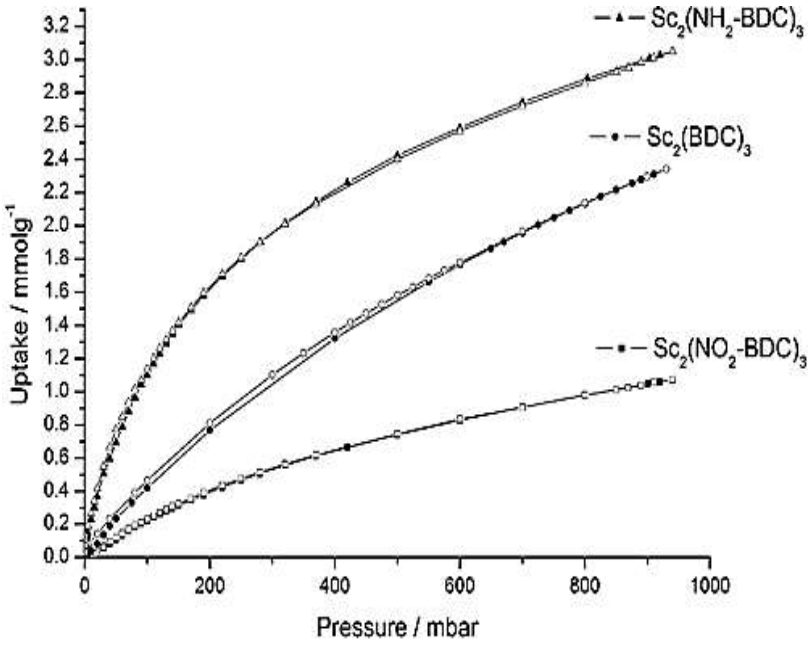

Figure 1.18: Carbon dioxide adsorption isotherms at 0 ^{0}C on Sc_2BDC_3, $Sc_2(NH_2\text{-}BDC)_3$, and $Sc_2(NO_2\text{-}BDC)_3$. Filled symbols, adsorption branch; open symbols, desorption branch. Reprinted with the permission of the American Chemical Society [53]

In the case of MIL-53(Sc) (Figure 1.18), functionalisation has been explored with NO_2 groups and studies of the CO_2 adsorption show that there is greatly increased uptake at low pressure, which confirms the crystallography result, where the structure is propped open by the bulky nitro groups that induce permanent porosity. CO_2 adsorption isotherms of MIL-53(Sc) and nitro form are shown in Figure 1.19. Considering that NH_2 does not have the bulky group, synthesis of MIL-53(Sc) with amine groups are worth exploring especially given the variation of CO_2 adsorption behaviour reported for the other trivalent metal forms of NH_2-MIL-53(M) (M= Al, Cr, In, Fe, Ga).[67]

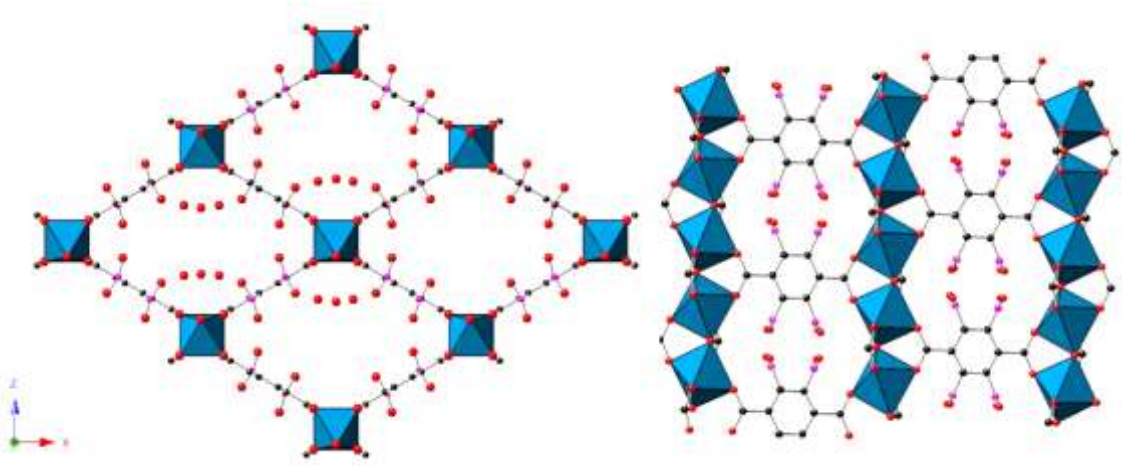

Figure 1.19: Structure of the MIL-53(Sc)-NO_2 from single crystal data on the as-prepared sample viewed down the channels. ScO_6 is the blue octahedral. C, N, and O atoms represented by black, magenta and red spheres). [54]

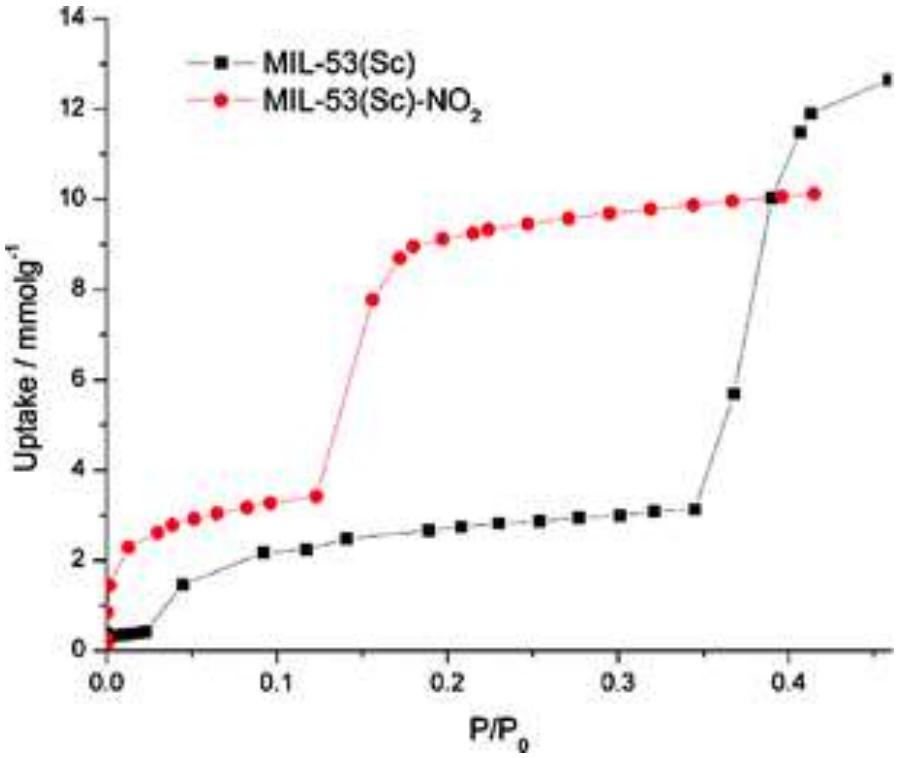

Figure 1.20: CO_2 adsorption isotherms measured at -77 ℃ on the MIL-53 (Sc) (black squares) and the –NO_2 functionalised material MIL-53(Sc)-NO_2 (red circles). Reprinted with permission of the Royal Society of Chemistry.[54]

Besides functionalisation by isoreticular and PSM approaches, another synthetic route has emerged with the use of mixed functionality of the ligands (or with and without functionality).[68-70] Previously, Stock and co-workers[70] demonstrated that the 'mixed linker

approach' of differently functionalised linker molecules can enhance the adsorption properties of MOFs. This was a method of interest in this work because it was found to be possible by this route to synthesize materials that are not readily accessible by direct synthesis, such as NH_2-MIL-53(Sc). Additionally, the post-synthetic solvent-assisted ligand exchange (SALE) method[71] was investigated in an attempt to prepare core-shell structures so this method was also investigated.

1.2.2 MOF-POM composites

Introducing species into MOFs pores either as guests or as part of the framework is of interest for applications in catalysis because their properties can be significantly enhanced. Among the different species, the use of polyoxometalates (POMs)[72] has attracted considerable interest. POMs can be strong Brønsted acids, and these classes of inorganic cluster anions comprising early transition metal cations (typically tungsten(VI), molybdenum(VI) or vanadium(V) centres) bridged by oxide anions extra space between have and abundant coordination sites on their oxygen-rich surface that could give rise to catalytic activity.

Keggin-type POMs (Figure 1.20) have been widely used, which have a general formula of $[XM_{12}O_{40}]^{n-}$; where X is the heteroatom, commonly phosphorus (P^{5+}), and M can be molybdenum or tungsten. Studies of POMs encapsulated in MOFs have been reported for MIL-101(Cr), MIL-100(Fe) and HKUST-1.[73-78] Phosphotungstic acid (PTA) encapsulated in MIL-101(Cr) has been applied as a catalyst for the Knoevenagel condensation of benzaldehyde with ethyl cyanoacetate.[75] With this in mind, it is desirable to evaluate the encapsulation of POMs in scandium MOFs as a route to improved catalysts.

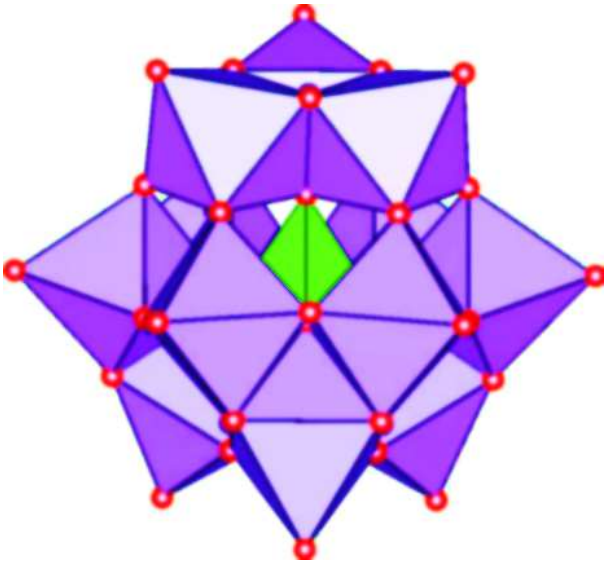

Figure 1.213: Polyhedral representation of the α-Keggin $[PX_{12}O_{40}]^{3-}$ anion, where X can be molybdenum or tungsten. PO_4 tetrahedra are in green, whereas MO_6 octahedra are in violet.

1.2.3 Applications of MOFs in catalysis

The nature of the self-assembly of MOFs leads to materials with open framework structures, where the porosity maybe accessible for gas adsorption, storage and potentially catalytic applications. On this basis, the potential of MOFs for catalysis can be foreseen since, in principle, the adequate design and selection of organic linkers allows the preparation of MOFs with a local structure similar to metal coordination complexes with catalytic activity.

Catalysis is a wide field in applied science and involves many areas of chemistry, notably organometallic chemistry, surface chemistry and materials science. Globally more than 90% of chemical manufacturing processes utilize catalysts.[7] By definition, a catalyst is defined as a substance that increases the rate of attainment of chemical equilibrium without itself undergoing chemical change. Catalysts are commonly divided into two main types: heterogeneous and homogeneous. Homogeneous catalysts are in the same phase as the reactants, whereas heterogeneous catalysis involves the use of a catalyst in a different phase from the reactants allowing facile catalyst recovery and recyclability.

Several MOFs with accessible metal sites have been reported, opening the possibility of their use in Lewis acid catalysis.[23, 79, 80] Lewis acid catalysis is of great interest in organic synthesis and many different Lewis acids have been applied in industry (including titanium alkoxides, for example) usually under strictly anhydrous conditions.[81] The presence of even a small amount of water stops the reaction, because most Lewis acids immediately react with water rather than the substrates and decompose, and this has restricted the use of Lewis acids in organic synthesis.

Heterogeneous catalysis was one of the earliest proposed applications for MOFs. The earliest reports of MOF-based catalysis was a description in 1994 by Fujita and co-workers[82] on the cyanosilylation of aldehydes (Scheme 1.1) by $Cd(4,4\text{-bpy})_2(NO_3)_2$, (bpy = bipyridine) (Figure 1.21) in which the cadmium center is the active Lewis-acid site. Filtration and recovery of the MOF demonstrated the reaction to be fully heterogeneous, with no observed further conversion in the reaction mixture after removal of the solid, suggesting that the active sites exist mainly in or more probably at the surface of the solid.[83] Tests separately using the ligand (4,4'-bpy) or $Cd(NO_3)_2$ as catalysts proved that they do not catalyse the reaction.

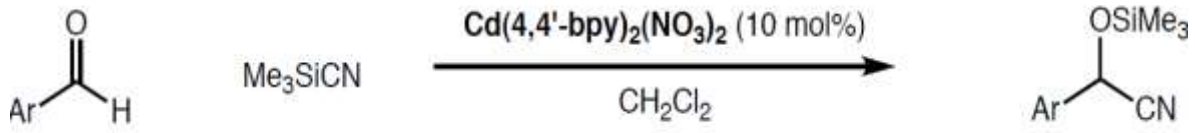

Scheme 1.1: Cyanosilylation of benzaldehyde catalysed by $Cd(4,4\text{-bpy})_2(NO_3)_2$ at 40 ^{0}C, 24 hours). Benzaldehyde (0.5 mmol) and cyanotrimethylsilane (1.0 mmol) with a CH_2Cl_2 (1.5 mL) gave 77% conversion.

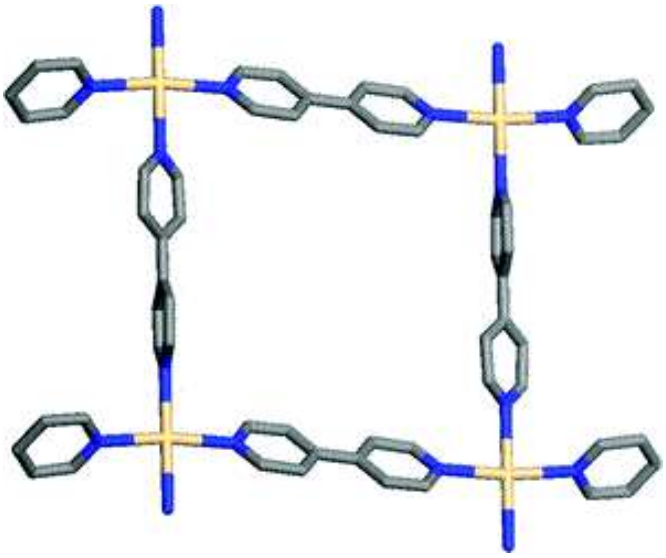

Figure 1.22 4: Structure of 2D network of $Cd(4,4'\text{-bpy})_2(NO_3)_2$. Cd = gold segment; N = blue segment; C = gray segment; Br = red segment.[82]

Several publications of MOFs reported their use as Lewis acid catalysts with active metal sites. These are bond to coordinating solvent molecules in the as-prepared materials, and the solvent can be easily removed by heating in vacuum. K. Schlichte et al.[84] described the use of HKUST-1($Cu_3(BTC)_2(H_2O)_3 \cdot xH_2O$) in Lewis acid catalysis, but dehydration of the material prior to use has to be performed to produce coordinatively unsaturated Cu(II) sites. These are able to act as a selective catalyst for the cyanosilylation of aldehydes and ketones. Other metal–organic frameworks have shown similar Lewis acid catalytic activity. For example $Mn_3[(Mn_4Cl)_3BTT_8(CH_3OH)_{10}]_2$ (Figure 1.22), was found to catalyse both the cyanosilylation of aromatic aldehydes and the Mukaiyama-aldol reactions.[20] This material contains a three-dimensional pore structure, with a pore diameter of 10 Å, and has two different types of Mn^{2+}, which are five-coordinate and two-coordinate with the separation between them being 3.420(8) Å.

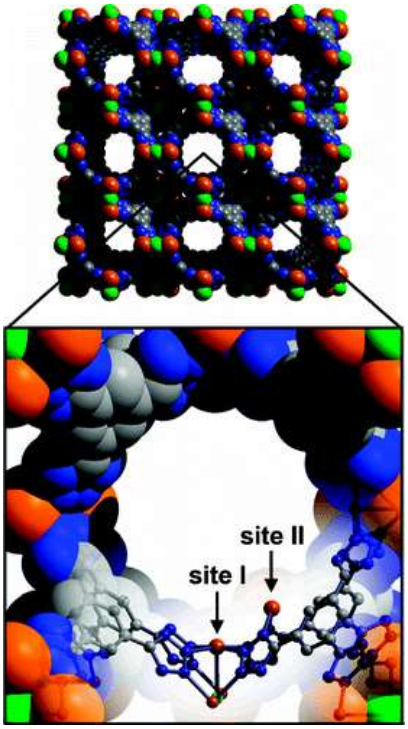

Figure 1.23: Structure of $Mn_3[(Mn_4Cl)_3BTT_8(CH_3OH)_{10}]_2$. Spheres represent to atoms: (Mn) orange, (Cl) green, (Carbon) gray, and (Nitrogen) blue; H atoms and bound MeOH molecules are omitted for clarity. Reprinted with the permission of the American Chemical Society [53]

Alaerts and co-workers[85] demonstrated the activity of activated $Cu_3(BTC)_2$ [(HKUST-1)], which has Cu^{2+} sites that can act as Lewis Acids. $Cu_3(BTC)_2$ showed stability, re-usability, a fully heterogeneous catalysts in the isomerisation of α-pinene oxide to campholenic aldehyde. Dhakshinamoorthy *et al*[86] have tested Fe(BTC) as a heterogeneous catalyst in the reaction of epoxides with alcohols and amines (Scheme 1.2). The structure of Fe(BTC) remains unknown due to its poor crystallinity but it showed good catalytic activity in the reaction of styrene epoxide with methanol (69 % conversion after 20 minutes). Scheme 1.3 shows the proposed mechanism with Fe(III) as Lewis acid.[86] MIL-100(Fe) has also been tested as Lewis acid catalyst and compared with Fe(BTC) in acetalization of benzaldehyde with methanol giving in both cases a conversion of 84%.

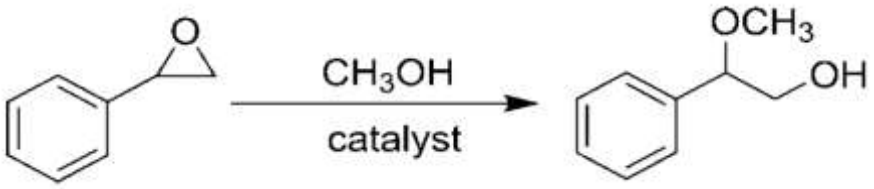

Scheme 1.2: Reaction of styrene oxide with methanol. Reaction conditions: Conditions: styrene oxide (2 mmol), catalyst (50 mg, 0.2 mmol of Fe) and methanol (5 mL) at 40 ^{o}C.[86]

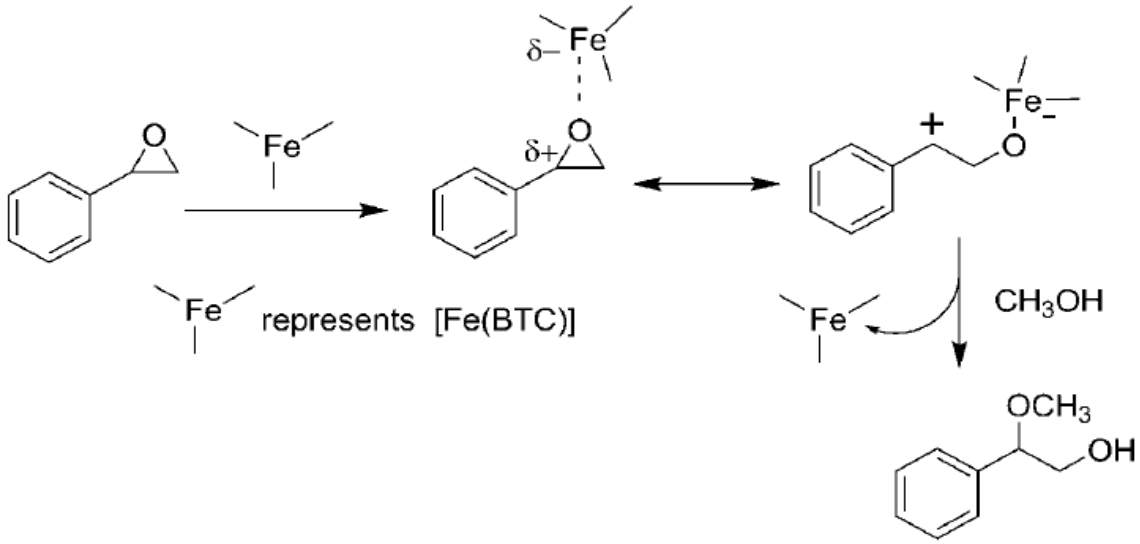

Scheme 1.3: Proposed mechanism for the ring opening of styrene oxide with methanol catalysed by [Fe(BTC)].[86]

The catalytic activity observed for MOF materials is directly related to their metal cation components and it well known that scandium is an excellent Lewis acidic cation. For example scandium triflate is commonly used in organic synthesis as a Lewis acid catalyst.[87] Studies using scandium triflate in organic synthesis demonstrate higher catalytic activity than that observed for other lanthanide triflates ($Ln(OTf)_3$), and it is recyclable and homogeneous. This led to exploration of the use of MOFs containing rare earth elements (scandium and yttrium) as catalysts,[88] for example a scandium metal-organic framework based on squaric acid proved to be an efficient heterogeneous catalyst both in cyanosilylation and acetalization of carbonyl compounds,[56] although this is likely to have resulted from catalysis sites on the

external surface, because it has a non-porous framework. It is therefore desirable to test porous scandium MOFs as catalysts as studied in this work, and these will be compared to Cr-MOFs, POMs encapsulated in MOFS and scandium-exchanged zeolites. Previously the inclusion of scandium ions in zeolite Y by vapor-phase exchange has been reported by Olmos et al.[89] The zeolite H-USY and $Sc(OTf)_3$ were mixed and transferred in a closed reactor, and heated at 350°C for 3 days under flowing nitrogen. This material was tested as a Lewis acid catalyst for a Diels-Alder reaction. In this thesis the scandium ion exchange in zeolite Y and Beta is described.

There are two types of reactions of interest in this investigation. The carbonyl ene reaction and acetalization.[90, 91] The carbonyl ene reaction is used in organic synthesis for commercial processes, one example of which is the production of menthol, a chemical used to give peppermint flavouring and smell to many products including toothpastes, pharmaceuticals and chewing gum. For this reaction it is desirable to improve the selectivity and to carry it out heterogeneously.

The carbonyl ene reaction occurs between an alkene bearing an allylic hydrogen and a carbonyl compound (Scheme 1.4). This reaction is accompanied by the migration of the double bond (enophile) to an olefin with an allylic hydrogen (ene). The ene component is an alkene (or enol), which can react with a quite broad range of enophiles. C–C bond-forming reactions between carbonyl compounds and nucleophilic reagents most frequently employ a metal-based nucleophile and typically result in metal ion-containing waste. Atom-efficient C–C bond-forming reactions are now rising in importance due to the demand for developing reactions that do not generate waste.

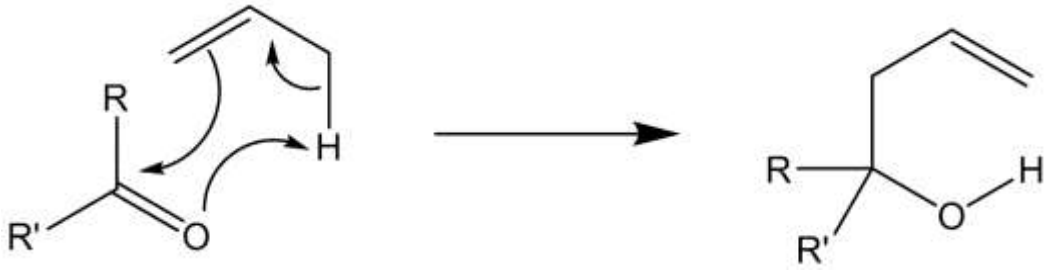

Scheme 1.4: General carbonyl ene reaction.

Acetalization is commonly used in the synthesis of fine chemicals. This type of reaction is a selective protection route of carbonyl groups in the presence of other functionalities during the reactions of multifunctional organic molecules. Besides the interest in acetals as protecting groups, many of them have applications as flavours or fragrances in cosmetics, food, beverage additives and detergents. Previously, the catalysts used in the acetalization reactions were generally homogeneous Brønsted acids, Lewis acids, and a number of transitional metal complexes including Rh, Pd, and Pt.[91] Although good results were obtained, the separation of the products from the catalyst system after the reaction was still difficult and the noble metal catalysts used were quite expensive and usually unstable. Therefore, to design and synthesize a catalytic system that may be stable, easily separable, and reusable has long been pursued.

MOFs have been used as catalyst in this type of reaction. Gándara *et al.*[56] have reported acetalization of benzaldehyde with trimethyl orthoformate (Scheme 1.5), using a layered indium-based MOF as a catalyst. The corresponding dimethylacetal is obtained in up to 97% yield, in relatively short reaction time (1 h) and under mild conditions 60 ^{o}C using 10 mol % of catalyst.

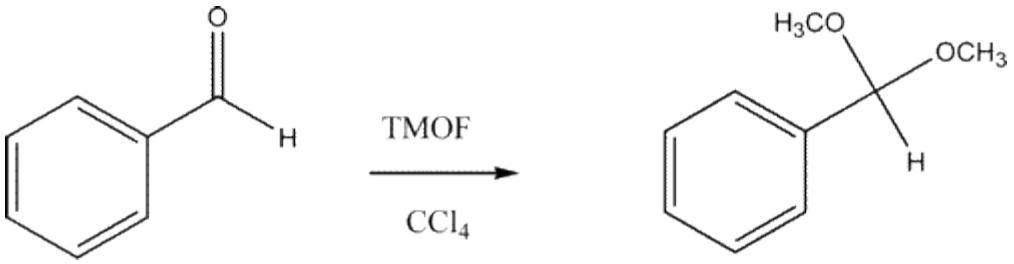

Scheme 1.5: Acetalization of benzaldehyde (2.54 mmol) and trimethyl orthoformate (TMOF, 1.30 mmol) in tetrachloromethane (3 mL) at reflux temperature.

1.3 Aims

The aim in this thesis is to investigate the synthesis, characterisation and applications in adsorption and catalysis of known and novel scandium MOFs.

1.3.1 Objectives

(i) Investigate catalytic performance of know and novel scandium MOFs as Lewis acid for prototypical Lewis acid catalyzed reactions of carbonyl and acetalization.

(ii) To modify and optimize the synthesis of targeted "functionalised" MOFs, particularly amino-functionalised MOFs, with the aim of preparing materials of interest in the selective adsorption of vapors. As part of this study, to examine the potential applicability of solvent-assisted linker exchange (SALE) for the modification of adsorption properties.

(iii) To explore the synthesis of novel scandium carboxylate MOFs, using carboxylate linkers, characterising them as adsorbents and where possible determine their crystal structures.

1.4 References

1. S. Kulprathipanja, *Zeolites in Industrial Separation and Catalysis*, Wiley-VCH UK, 2010.

2. P. A. Jacobs, E. M. Flanigen, J. C. Jansen and v. B. H., *Introduction to Zeolite Science and Practice*, Elsevier, Netherlands, 2001.

3. A. Corma, *Chem. Rev.*, 1997, 97, 2373-2420.

4. P. A. Wright, *Microporous Framework Solids*, RSC, UK, 2008.

5. A. Corma and H. Garcia, *Chem. Rev.*, 2003, 103, 4307-4365.

6. J. Hagen, *Industrial Catalysis*, Wiley-VCH 2006.

7. J. M. Thomas and W. J. Thomas, *Principles and practice of heterogeneous catalysis*, Wiley-VCH, Germany, 1997.

8. IUPAC, *http://www.iupac.org*.

9. S. R. Batten, S. M. Neville and D. R. Turner, in *Coordination Polymers: Design*, The Royal Society of Chemistry, 2009, 5-7.

10. G. Ferey, *Chem. Soc. Rev.*, 2008, 37, 191-214.

11. O. M. Yaghi, M. O'Keeffe, N. W. Ockwig, H. K. Chae, M. Eddaoudi and J. Kim, *Nature*, 2003, 423, 705.

12. A. U. Czaja, N. Trukhan and U. Muller, *Chem. Soc. Rev.*, 2009, 38, 1284-1293.

13. G. Férey, C. Serre, T. Devic, G. Maurin, H. Jobic, P. L. Llewellyn, G. De Weireld, A. Vimont, M. Daturi and J.-S. Chang, *Chem. Soc. Rev.*, 2011, 40, 550-562.

14. R. Krishna and J. M. van Baten, *Langmuir*, 2010, 26, 8450-8463.

15. L. Hamon, P. L. Llewellyn, T. Devic, A. Ghoufi, G. Clet, V. Guillerm, G. D. Pirngruber, G. Maurin, C. Serre, G. Driver, W. van Beek, E. Jolimaitre, A. Vimont, M. Daturi and G. Ferey, *J. Am. Chem. Soc.*, 2009, 131, 17490-17499.

16. S. Couck, J. F. M. Denayer, G. V. Baron, T. Rémy, J. Gascon and F. Kapteijn, *J. Am. Chem. Soc.*, 2009, 131, 6326-6327.

17. B. Liu and B. Smit, *Langmuir*, 2009, 25, 5918-5926.

18. H. B. Tanh Jeazet, C. Staudt and C. Janiak, *Dalton Trans.*, 2012, 41, 14003-14027.

19. P. Horcajada, C. Serre, M. Vallet-Regí, M. Sebban, F. Taulelle and G. Férey, *Angew. Chem. Int. Ed.*, 2006, 45, 5974-5978.

20. S. Horike, M. Dinca, K. Tamaki and J. R. Long, *J. Am. Chem. Soc.*, 2008, 130, 5854-5855.

21. K. Leus, S. Couck, M. Vandichel, G. Vanhaelewyn, Y. Y. Liu, G. B. Marin, I. Van Driessche, D. Depla, M. Waroquier, V. Van Speybroeck, J. F. Denayer and P. Van der Voort, *Phys. Chem. Chem. Phys.*, 14, 15562-15570.

22. D. Farrusseng, S. Aguado and C. Pinel, *Angew. Chem. Int. Ed.*, 2009, 48, 7502-7513.

23. L. Mitchell, B. Gonzalez-Santiago, J. P. S. Mowat, M. E. Gunn, P. Williamson, N. Acerbi, M. L. Clarke and P. A. Wright, *Cat. Sci. Tech.*, 2013, 3, 606-617.

24. D. J. Tranchemontagne, J. L. Mendoza-Cortes, M. O'Keeffe and O. M. Yaghi, *Chem. Soc. Rev.*, 2009, 38, 1257-1283.

25. S. S.-Y. Chui, S. M.-F. Lo, J. P. H. Charmant, A. G. Orpen and I. D. Williams, *Science*, 1999, 283, 1148-1150.

26. H. Li, M. Eddaoudi, M. O'Keeffe and O. M. Yaghi, *Nature*, 1999, 402, 276.

27. C. Petit, S. Wrabetz and T. J. Bandosz, *J Mater Chem*, 2012, 22, 21443-21447.

28. N. L. Rosi, M. Eddaoudi, J. Kim, M. O'Keeffe and O. M. Yaghi, *Angew. Chem. Int. Ed.*, 2002, 41, 284-287.

29. N. L. Rosi, J. Kim, M. Eddaoudi, B. Chen, M. O'Keeffe and O. M. Yaghi, *J. Am. Chem. Soc.*, 2005, 127, 1504-1518.

30. M. Eddaoudi, J. Kim, N. Rosi, D. Vodak, J. Wachter, M. O'Keeffe and O. M. Yaghi, *Science*, 2002, 295, 469-472.

31. O. M. Yaghi, G. Li and H. Li, *Nature*, 1995, 378, 703-706.

32. M. Latroche, S. Surble, C. Serre, C. Mellot-Draznieks, P. L. Llewellyn, J. H. Lee, J. S. Chang, S. H. Jhung and G. Ferey, *Angew. Chem. Int. Ed.*, 2006, 45, 8227-8231.

33. G. Férey, C. Serre, C. Mellot-Draznieks, F. Millange, S. Surblel, J. Dutour and I. Margiolaki, *Angew. Chem., Int. Ed.*, 2004, 43, 6296.

34. C. Mellot-Draznieks, *J Mater Chem*, 2007, 14, 4348-4358.

35. C. Baerlocher, W. M. Meier and D. H. Olson, *Atlas of Zeolite Framework Types*, Elsevier, 2007.

36. S. Surble, C. Serre, C. Mellot-Draznieks, F. Millange and G. Ferey, *Chem. Commun.* , 2006, 284-286.

37. C. Serre, C. Mellot-Draznieks, S. Surble, N. Audebrand, Y. Filinchuk and G. Férey, *Science*, 2007, 315, 1828-1831.

38. C. Mellot-Draznieks, C. Serre, S. Surblé, N. Audebrand and G. Férey, *J. Am. Chem. Soc.*, 2005, 127, 16273-16278.

39. I. A. Ibarra, X. Lin, S. Yang, A. J. Blake, G. S. Walker, S. A. Barnett, D. R. Allan, N. R. Champness, P. Hubberstey and M. Schroder, *Chem. Eur. J.*, 2010, 16, 13671-13679.

40. J. P. S. Mowat, S. R. Miller, A. M. Z. Slawin, V. R. Seymour, S. E. Ashbrook and P. A. Wright, *Micropor. Mesopor. Mat.*, 2011, 142, 322-333.

41. G. Ferey and C. Serre, *Chem. Soc. Rev.*, 2009, 38, 1380-1399.

42. C. Serre, F. Millange, C. Thouvenot, M. Nogues, G. Marsolier, D. Louer and G. Férey, *Journal of the American Chemical Society*, 2002, 124, 13519-13526.

43. T. Loiseau, C. Serre, C. Huguenard, G. Fink, F. Taulelle, M. Henry, T. Bataille and G. Ferey, *Chem. Eur. J.*, 2004, 10, 1373-1382.

44. T. R. Whitfield, *Solid State Sci.*, 2005, 7, 1096-1103.

45. C. Volkringer, T. Loiseau, N. Guillou, G. Ferey, E. Elkaim and A. Vimont, *Dalton Trans.*, 2009, 2241-2249.

46. E. V. Anokhina, M. Vougo-Zanda, X. Wang and A. J. Jacobson, *J. Am. Chem. Soc.*, 2005, 127, 15000-15001.

47. K. Barthelet, J. Marrot, D. Riou and G. Férey, *Angew. Chem. Int. Ed.*, 2002, 41, 281-284.

48. K. Barthelet, J. Marrot, G. Ferey and D. Riou, *Chem. Commun.*, 2004, 520-521.

49. A. Fateeva, P. Horcajada, T. Devic, C. Serre, J. Marrot, J.-M. Grenèche, M. Morcrette, J.-M. Tarascon, G. Maurin and G. Férey, *Eur. J. Inorg. Chem.*, 2010, 2010, 3789-3794.

50. C. Volkringer, M. Meddouri, T. Loiseau, N. Guillou, J. Marrot, G. Ferey, M. Haouas, F. Taulelle, N. Audebrand and M. Latroche, *Inorg. Chem.*, 2008, 47, 11892-11901.

51. Q. Y. Yang, S. Vaesen, M. Vishnuvarthan, F. Ragon, C. Serre, A. Vimont, M. Daturi, G. De Weireld and G. Maurin, *J Mater Chem*, 2012, 22, 10210-10220.

52. S. R. Miller, P. A. Wright, T. Devic, C. Serre, G. Ferey, P. L. Llewellyn, R. Denoyel, L. Gaberova and Y. Filinchuk, *Langmuir*, 2009, 25, 3618-3626.

53. J. P. S. Mowat, S. R. Miller, J. M. Griffin, V. R. Seymour, S. E. Ashbrook, S. P. Thompson, D. Fairen-Jimenez, A.-M. Banu, T. Düren and P. A. Wright, *Inorg. Chem.*, 2011, 50, 10844-10858.

54. J. P. S. Mowat, V. R. Seymour, J. M. Griffin, S. P. Thompson, A. M. Z. Slawin, D. Fairen-Jimenez, T. Duren, S. E. Ashbrook and P. A. Wright, *Dalton Trans.*, 2012, 41, 3937-3941.

55. J. Perles, M. Iglesias, C. Ruiz-Valero and N. Snejko, *Chem. Commun.*, 2003, 346-347.

56. F. Gandara, B. Gomez-Lor, M. Iglesias, N. Snejko, E. Gutierrez-Puebla and A. Monge, *Chem. Commun.*, 2009, 2393-2395.

57. M. C. Bernini, N. Snejko, E. Gutierrez-Puebla and A. Monge, *CrystEngComm*, 2011, 13, 1797-1800.

58. P. D. Dietzel, R. Blom and H. Fjellvag, *Dalton Trans.*, 2006, 2055-2057.

59. S. R. Miller, P. A. Wright, C. Serre, T. Loiseau, J. Marrot and G. Férey, *Chem. Commun.* , 2005, 3850-3852.

60. A. Le Bail, *Powder Diffraction*, 2005, 20, 316-326.

61. I. A. Ibarra, S. Yang, X. Lin, A. J. Blake, P. J. Rizkallah, H. Nowell, D. R. Allan, N. R. Champness, P. Hubberstey and M. Schroder, *Chem. Commun.* , 2011, 47, 8304-8306.

62. S. R. Miller, PhD Thesis, University of St. Andrews, 2007.

63. J. P. S. Mowat, PhD Thesis, University of St Andrews, 2012.

64. A. Fateeva, S. Devautour-Vinot, N. Heymans, T. Devic, J.-M. Grenèche, S. Wuttke, S. Miller, A. Lago, C. Serre, G. De Weireld, G. Maurin, A. Vimont and G. Férey, *Chem. Mat.*, 2011, 23, 4641-4651.

65. S. M. Cohen, *Chem. Rev.*, 2011, 112, 970-1000.

66. T. Devic, F. Salles, S. Bourrelly, B. Moulin, G. Maurin, P. Horcajada, C. Serre, A. Vimont, J.-C. Lavalley, H. Leclerc, G. Clet, M. Daturi, P. L. Llewellyn, Y. Filinchuk and G. Ferey, *J. Mater. Chem.*, 2012, 22, 10266-10273.

67. P. Serra-Crespo, E. Gobechiya, E. V. Ramos-Fernandez, J. Juan-Alcaniz, A. Martinez-Joaristi, E. Stavitski, C. E. Kirschhock, J. A. Martens, F. Kapteijn and J. Gascon, *Langmuir*, 2012, 28, 12916-12922.

68. W. Kleist, F. Jutz, M. Maciejewski and A. Baiker, *Eur. J. Inorg. Chem.*, 2009, 3552-3561.

69. W. Kleist, M. Maciejewski and A. Baiker, *Thermochim. Acta*, 2010, 499, 71-78.

70. H. Reinsch, S. Waitschat and N. Stock, *Dalton Trans.*, 2013, 42, 4840-4847.

71. S. Takaishi, E. J. DeMarco, M. J. Pellin, O. K. Farha and J. T. Hupp, *Chem. Sci.*, 2013, 4, 1509-1513.

72. M. Ammam, *J. Mate.r Chem.*, 2013, 1, 6291-6312.

73. N. V. Maksimchuk, M. N. Timofeeva, M. S. Melgunov, A. N. Shmakov, Y. A. Chesalov, D. N. Dybtsev, V. P. Fedin and O. A. Kholdeeva, *J. Catal.*, 2008, 257, 315-323.

74. C. Y. Sun, S. X. Liu, D. D. Liang, K. Z. Shao, Y. H. Ren and Z. M. Su, *J. Am. Chem. Soc.*, 2009, 131, 1883-1888.

75. J. Juan-Alcaniz, E. V. Ramos-Fernandez, U. Lafont, J. Gascon and F. Kapteijn, *J. Catal.*, 2010, 269, 229-241.

76. R. Canioni, C. Roch-Marchal, F. Secheresse, P. Horcajada, C. Serre, M. Hardi-Dan, G. Ferey, J.-M. Greneche, F. Lefebvre, J.-S. Chang, Y.-K. Hwang, O. Lebedev, S. Turner and G. Van Tendeloo, *J. Mater. Chem.*, 2011, 21, 1226-1233.

77. J. Song, Z. Luo, D. K. Britt, H. Furukawa, O. M. Yaghi, K. I. Hardcastle and C. L. Hill, *J. Am. Chem. Soc.*, 2011, 133, 16839-16846.

78. D. Y. Du, J. S. Qin, S. L. Li, Z. M. Su and Y. Q. Lan, *Chem. Soc. Rev.*, 2014, 43, 4615-4632.

79. D. Liu and C. Zhong, *J. Phys. Chem. Lett.*, 2010, 1, 97-101.

80. A. Dhakshinamoorthy, M. Alvaro and H. Garcia, *Chem. Commun.* , 2012, 48, 11275-11288.

81. S. Kobayashi and C. Ogawa, *Chem. Eur. J.*, 2006, 12, 5954-5960.

82. M. Fujita, Y. J. Kwon, S. Washizu and K. Ogura, *J. Am. Chem. Soc.*, 1994, 116, 1151-1152.

83. J. Lee, O. K. Farha, J. Roberts, K. A. Scheidt, S. T. Nguyen and J. T. Hupp, *Chem. Soc. Rev.*, 2009, 38, 1450-1459.

84. K. Schlichte, T. Kratzke and S. Kaskel, *Micropor. Mesopor. Mat.*, 2004, 73, 81-88.

85. L. Alaerts, E. Séguin, H. Poelman, F. Thibault-Starzyk, P. A. Jacobs and D. E. De Vos, *Chem. Eur. J.*, 2006, 12, 7353-7363.

86. A. Dhakshinamoorthy, M. Alvaro and H. Garcia, *Chem. Eur. J.*, 2010, 16, 8530-8536.

87. S. Kobayashi, *Eur. J. Org. Chem.*, 1999, 15-27.

88. J. Perles, N. Snejko, M. Iglesias and M. A. Monge, *J Mater Chem*, 2009, 19, 6504-6511.

89. A. Olmos, B. Louis and P. Pale, *Chem. Eur. J.*, 2012, 18, 4894-4901.

90. M. L. Clarke and M. B. France, *Tetrahedron*, 2008, 64, 9003-9031.

91. F. Gorla and L. M. Venanzi, *Helv. Chim. Acta.*, 1990, 73, 690-697.

Chapter 2: Experimental Methods and Characterisation Techniques

2.1 General synthesis

For this investigation most of the synthesis reactions were performed hydro- or solvothermally, which involves the use of Teflon-lined autoclaves (Figure 2.1). The Parr type, 23 mL autoclave and a 40 mL autoclave were used in this work. Chemicals were purchased from commercial suppliers; Aldrich, VWR, Acros, and BDH chemicals. The typical synthesis is as follows, a metal source (scandium nitrate or chloride) is mixed with the linker, generally in the form of a carboxylic acid, in a solvent (DMF = N,N´-dimethylformamide) or mixture of solvents , where the solvent controls the solubility, and therefore the availability of the organic linker during the crystallization. The homogenized reaction mixtures are transferred to a Teflon-lined autoclave and solvothermally treated with different synthesis parameters, including temperature and heating times. After heating, the autoclaves are cooled and the mixtures filtered, washed with solvent, then the materials are dried overnight at 60^{o}C. Characterisation of the product phases is initially performed by powder X-ray diffraction (PXRD). Characterisation methods included PXRD, EDX, CHN, and TGA.

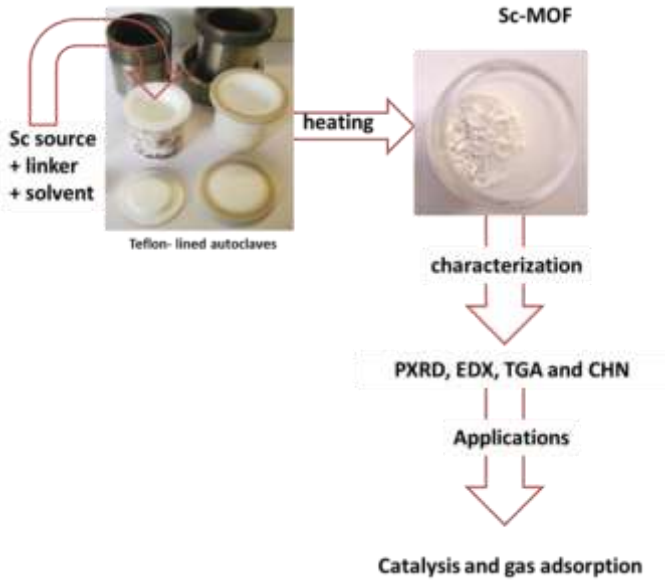

Figure 2.1: Characterisation carried out on MOFs prepared in this thesis.

Table 2.1 describes the target products prepared in this work. Details of the syntheses of each MOF reported are given in the relevant chapters 3 - 5. Where single crystals of sufficient quality were present, their structures were determined by single crystal X - Ray diffraction (SXRD). In particular cases solid-state NMR was used to determine structural details, and dissolution followed by solution NMR was used to confirm the composition of the organic linkers presents. The adsorption properties were measured either gravimetrically or volumetrically and the catalytic performance was evaluated in test reactions for Lewis acid catalysis. The experimental details of catalytic reactions are given below.

Table 2.1 List of MOFs of interest in this work, with chemical formula of their fameworks.

MOF	Ligand	Chemical Formula
MIL-100(Sc, Cr)	BTC	$M_3O(OH)(H_2O)_2(C_9H_3O_6)_2$
MIL-101(Sc, Cr)	BDC	$M_3O(OH)\ (H_2O)_2(C_8H_4O_4)_3$
MIL-88B(Sc)	BDC	$Sc_3O(OH)(H_2O)_2(C_8H_4O_4)_3$
MIL-88D(Sc)	BPDC	$Sc_3O(OH)(H_2O)_2(C_{14}H_8O_4)_3$
MIL-68(Sc)	BDC	$Sc(OH)(C_8H_4O_4)$
NH_2-MIL-101(Sc)	NH2-BDC	$Sc_3O(OH)(NH_2\text{-}C_8H_3O_4)_3$
NH_2-MIL-88B(Sc)	NH2-BDC	$Sc_3O(OH)(NH_2\text{-}C_8H_3O_4)_3$
NH_2-MIL-68(Sc)	NH2-BDC	$Sc_3(OH)(NH_2\text{-}C_8H_3O_4)$
NH_2-MIL-53(Sc)	NH2-BDC	$Sc_3(OH)(NH_2\text{-}C_8H_3O_4)$
$Sc_2(BDC)_3$	BDC	$Sc_2(C_8H_4O_4)_3$
$Sc_2(NH_2\text{-}BDC)_3$	NH2-BDC	$Sc_2(NH_2\text{-}C_8H_3O_4)_3$
$Sc_2(Br\text{-}BDC)_3$	Br-BDC	$Sc_2(Br\text{-}C_8H_3O_4)_3$
$Sc_2(NO_2\text{-}BDC)_3$	NO2-BDC	$Sc_2(NO_2\text{-}C_8H_4O_4)_3$
Sc(IA)-1	IA	$Sc_3O(OH)\ (H_2O)_2(C_8H_4O_4)_3$
Sc(IA)-2	IA	$Sc_2(C_8H_4O_4)_3$
$Sc(NH_2\text{-}IA)$	NH2-IA	$Sc_{2(}NH_2\text{-}\ C_8H_3O_4)_3$
Sc(FDA)-1	FDA	$Sc_2(C_6H_2O_5)_3$
Sc(FDA)-2	FDA	$Sc_2(C_6H_2O_5)_3{\cdot}x$DMF

2.2 X-ray Crystallography [1,2]

2.2.1 Background: Origin of X-rays

Light has a dual nature, which refers to the fact that it can behave both like a wave and a particle. The electromagnetic spectrum (Figure 2.2) is the range of all possible frequencies of electromagnetic radiation, including X-rays, which have wavelength of the order of bond and of interatomic distances in crystals.

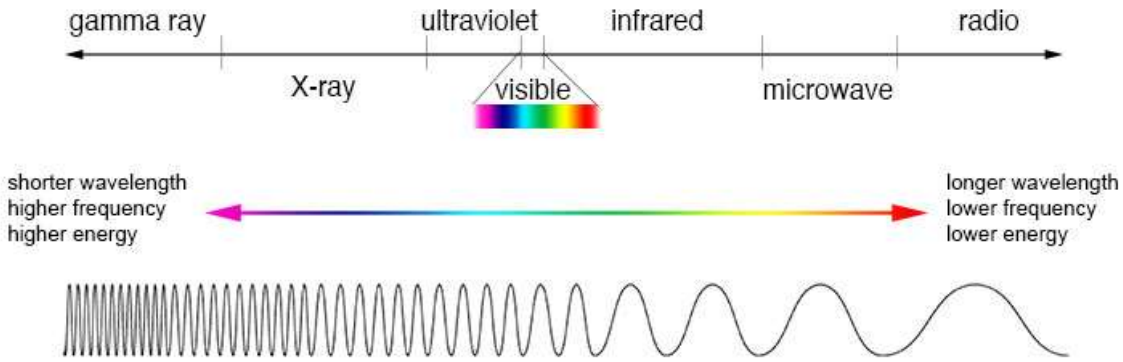

Figure 2.2: Electromagnetic spectrum

X-ray crystallography is the branch of science associated with the determination of the crystal structures by the analysis of X-ray diffraction. X-rays themselves are part of the electromagnetic spectrum as a form of electromagnetic radiation they have a frequency $\nu=c/\lambda$ (where λ is the wavelength and c the speed of light) and each photon has energy $E=h\nu=hc/\lambda$. X-rays have wavelength between 0.1 and 100 Å, and typically those with wavelength around 1 Å, are used for diffraction experiments to determine crystal structures where interatomic distances are also on the order of Å.

X-rays are produced in the laboratory as the result of bombarding a metal target anode by energetic electrons. This results in excitation of electrons from core levels and subsequent relaxation of higher energy electrons to fill these vacancies results in energy lost with well-

defined energies (characteristic of inter level transitions) in the X-ray region of the electromagnetic spectrum.

X-Ray diffraction results from a combination of two different phenomena: (a) scattering by each individual atom and (b) interference between the waves scattered by these atoms. Bragg's law explains how diffraction results in diffracted beam related to the incident X-ray beam. A collimated beam of X-rays incident on a specimen is diffracted by the crystalline phases in the specimen according to Bragg's law, Equation (2.1) (Figure. 2.3).

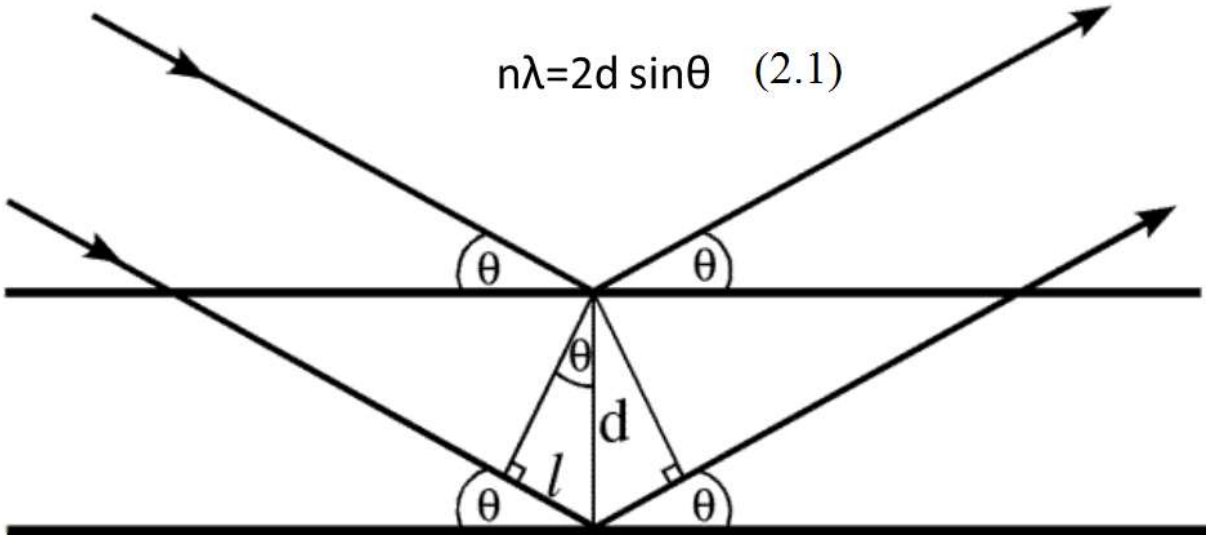

Figure 2.3: Representation of Bragg's Law

where *d* is the spacing between atomic planes in the crystalline phase and λ is the X-ray wavelength. The intensity of the diffracted X-rays is measured as a function of the diffraction angle 2θ and gives rise to peaks for each set of wave vectors which make up diffraction patterns. The position of a diffraction peak is independent of the atomic positions within the cell and entirely determined by the size and shape of the unit cell of the crystalline phase, whereas the diffracted intensities depend on the position of atoms within the unit cell. Each peak in a diffraction pattern arises from a unique set of repeating planes in the structure. Miller planes, which are oriented in all different directions in three-dimensional space, can be

identified by a set of three integers (h, k, l), known as Miller indices, that denote the orientation of the planes with respect to the axes (unit cell).

XRD[3] is a powerful method for structure determination or estimation of lattice constants if standard methods serve to identify the diffracting phase. This method is a non-destructive technique and determines the structural properties (phase composition, lattice parameters, thermal expansion, strain, grain size, etc), measuring thickness of thin films and multi layers, and giving the atomic arrangements to obtain a diffraction pattern, which contains information about the atomic arrangement within the crystal. A crystal is a regular, 3D-ordered arrangement of atoms over a large scale. The atoms may be of a single type or the repetition of a complex arrangement of many different types of atoms. Each repeating part of the 3-dimensional array is called a unit cell (Figure 2.4). The crystal can also be thought of as consisting of two separate parts: the lattice and the motif. The lattice is an ordered arrangement of points in space, while the motif consists of the simplest arrangement of atoms which is repeated at every lattice point to build up the crystal structure.

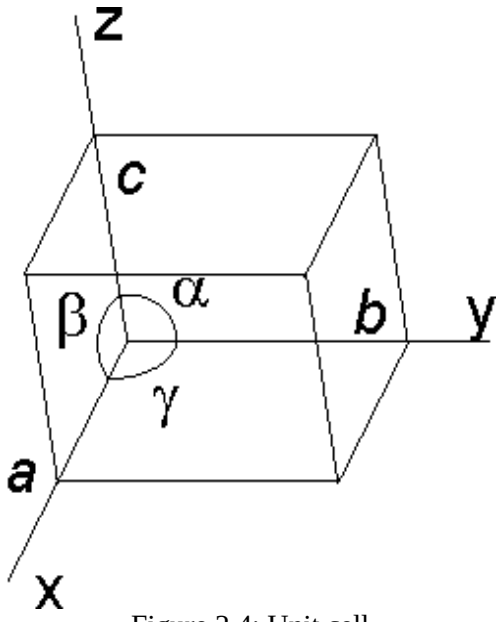

Figure 2.4: Unit cell

Crystal structures results from energy minimization in the atomic arrangement and give rise to unique properties. X-ray crystallography involves the ideas of point symmetry of molecules, where molecules are classified and grouped based on their symmetry, with additional translational symmetry to give periodic structures. Symmetry elements are used to define seven different crystal systems according to their unit cell symmetry and into 14 lattice systems according to their Bravais lattices (arrangement of lattice points in the unit cell) (Table 2.2). The lattice centring can be P (Primitive): simple unit cell; F (Face-centred): additional lattice point in the centre of each face; I (Body-centred): additional lattice point in the centre of the cell; C (Centred): one additional lattice point in a face centre; R (Rhombohedral) : trigonal class only.

Table 2.2: Seven crystal systems make up fourteen Bravais lattice types in three dimensions.

System	Number of Lattices	Lattice Symbol	Restriction on crystal cell angle
Cubic	3	P I F	a=b=c α =β =γ=90°
Tetragonal	2	P, I	a=b≠c α=β =γ=90°
Orthorhombic	4	P, C, I, F	a≠b≠c α=β =γ=90°
Monoclinic	2	F, C	a≠b≠c α=β=90 °≠β
Triclinic	1	P	a≠b≠c α≠β≠γ
Trigonal	1	R	a=b=c α=β =γ <120° ,≠90°
Hexagonal	1	P	a=b≠c α=β=90° γ=120°

The spacing between adjacent, Miller planes (h, k, l) depends on the unit cell shape and size.

- For an orthorhombic unit cell we can write

$$\frac{1}{d_{hkl}^2} = \frac{h^2}{a^2} + \frac{k^2}{b^2} + \frac{l^2}{c^2} \qquad (2.2)$$

Which, becomes for a cubic cell:

$$\frac{1}{d_{hkl}^2} = \frac{h^2 + k^2 + l^2}{a^2} \qquad (2.3)$$

Since the diffraction angle is given by Bragg's Law ($sin\theta = n\lambda/2d$) it is clear that the diffraction angle depends on d_{hkl} and therefore on the cell geometry. There are two types of X-ray diffraction experiment that are typically used in the laboratory, powder diffraction and single crystal diffraction.

If large (> 20 μm) crystals are available diffraction can be performed by scanning a single crystal in a collimated beam and rotating it so that its crystal planes become oriented to satisfy Bragg's law. In principle it is therefore possible to measure the intensity for each reflection individually. For a microcrystalline powder, a sample contains micron sized single crystals in all possible orientations, so that orientational information is lost (Figure 2.5). In practice this leads to peak overlap and massive loss of information, so that the methods are applicable to different types of structural problems. The two XRD technique : single crystal and polycrystalline or powder applications are used to analyse or solve crystal structures of the materials prepared in this work.

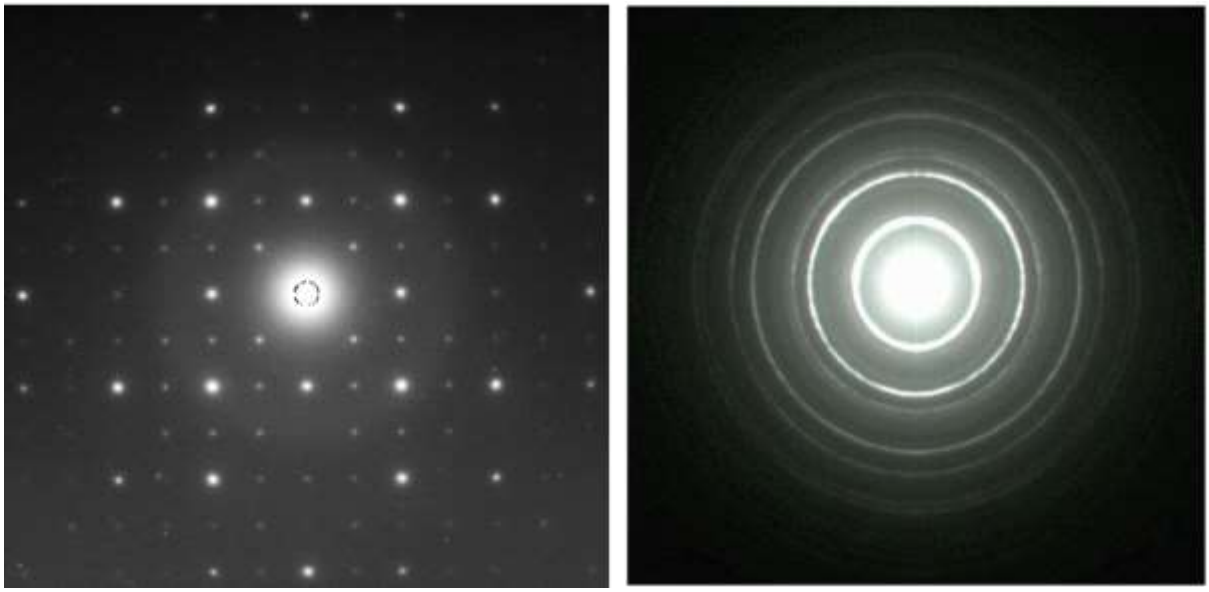

Figure 2.5: Representation of diffraction spots in a single crystal (left) and polycrystalline or powder (right).

2.2.2 Single crystal X-ray diffraction

Single crystal X-ray diffraction is one of the most common methods for the determination of the structures of new materials. However, this technique is limited by ability to grow crystals that are suitable for diffraction, typically larger than 0.02 mm in all dimensions but smaller can be studied. The technique enables determination of the unit cell and symmetry, and location of the atoms in the unit cell. This gives crystal-chemical information of bond distances and angles (and for MOFs, pore sizes and cavity dimension). For some unknown crystalline materials prepared in this thesis, single crystal XRD has been used to solve their structure. A schematic representation of single crystal is shown in Figure 2.6.

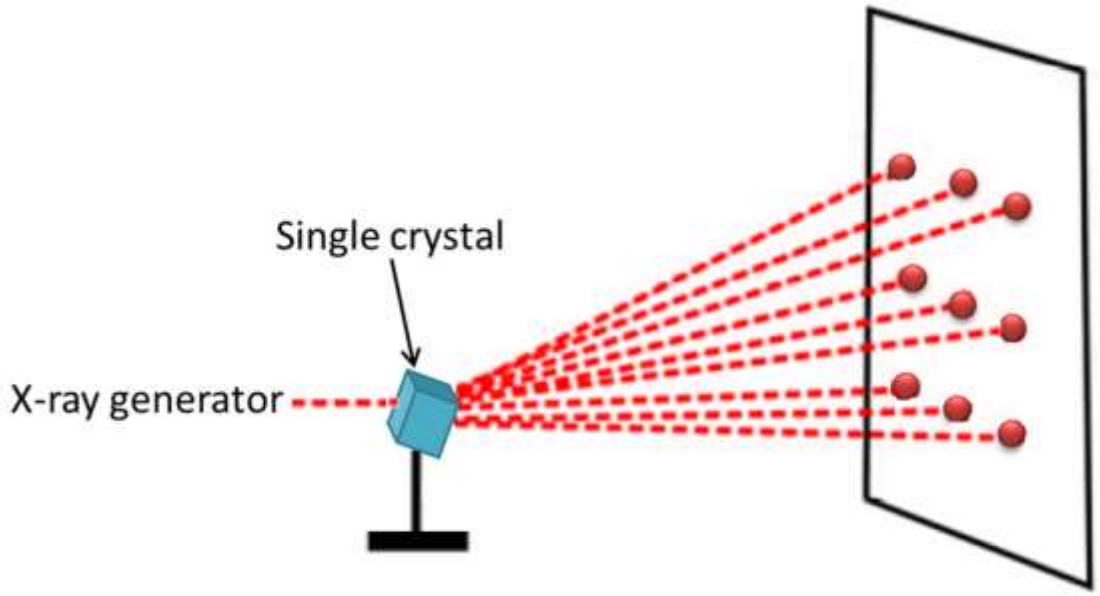

Figure 2.6 Schematic of single crystal diffraction

The single crystal method follows the steps: diffraction data collection, (*i*) taking the series of diffraction images and indexing the spots to determine the unit cell dimensions and the space group, (ii) data treatment, (iii) use of direct methods programs to determine phase of reflections and so derive the electron density in the unit cell, (iv) to attribute electron density to atoms to give a partial structure, (v) to refine the structure against the diffraction data. For any reflection, the intensity is related to the square of the structure factor (F).

. $$I_{hkl} \propto |F_{hkl}|^2 \qquad (2.4)$$

$$F_{hkl} = \sum f_n \exp\left[2\pi i\left(hx + ky + \ell z\right)\right] \bullet \exp \frac{-8\pi^2 u_n \sin^2 \theta}{\lambda^2} \qquad (2.5)$$

The structure factor (F_{hkl}) sums up the result of scattering from all of the atoms in the unit cell to make a diffraction peak from the [hkl] planes of atoms. The amplitude of scattered light is determined by fractional coordinates, (x,y z) and the efficiency of X-ray scattering at any angle by the group of electrons in each atom which is quantified by the scattering factor f_n further influenced by positional disorder (thermal vibration, u_n) of the atoms in the unit cell and can be isotropic (spherical) or anisotropic (elliptical). The electron density function ρ (see

Equation 2.6) completely determines the nature of the diffraction pattern, with a certain value at each point within the unit cell given by the coordinates (x, y, z), and the calculation of this function has to be done to obtain a structure of the crystal.

$$\rho_{xyz} = \frac{1}{V}\sum |F_{hkl}| \exp\left[-2\pi i\left(hx + ky + \ell z\right)\right] \qquad (2.6)$$

From Equation 2.4 the intensity is proportional to the square of the structure factor, therefore the phase of (F) cannot be determined directly, which is commonly referred to as the 'phase problem'. The common technique to solve the 'phase problem' is by using "Direct methods" developed by Karle and Hauptman,[4] which can retrieve the lost phases from the corresponding diffraction amplitudes, assuming that the structure is composed of discrete atoms and the electron density must be zero or an positive integer number, but never negative, so the combination with the amplitudes of the structure factor can give the probable phase to determine the structure.

Here for this investigation, programs SHELX and SIR software,[5] both implementing direct methods were used for crystal structure determination from single-crystal data collected on a Rigaku Mo MM-006 Saturn 92 diffractometer with Mo K_α radiation (λ = 0.71073 Å) or a Rigaku Cu MM007 HF with a Cu K_α radiation (λ = 1.54051 Å) and using the CRYSTALS suite of programs.[6]

2.2.3 Powder X-ray diffraction

Powder X-ray diffraction (PXRD) can be used to determine the crystallinity by comparing the integrated intensity of the sharp peaks to that of the background pattern, and allow observing phase changes or loss of crystallinity. The powder diffracts the X-Rays in accordance with Bragg's Law to produce cones of diffracted beams(Figure 2.7) so this results in considerable peak overlap compared to single crystal diffraction, due to the collapsing in

the ‘three dimensional’ diffraction pattern into a single, ‘2θ’ dimension. As a result, it is rarely possible to have enough unambiguous structure factor data to solve the phase problem by statistical ‘direct methods’ so that solution from powder X-ray data is more challenging than from single crystal data. Nevertheless, a considerable amount of information can be obtained.

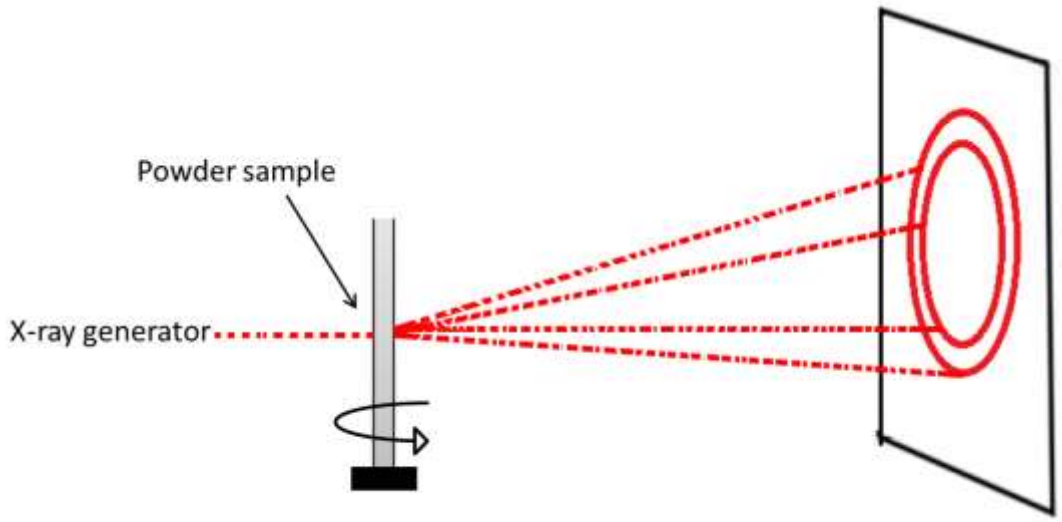

Figure 2.7: Schematic of powder X-ray diffraction.

Comparison of patterns obtained experimentally with databases (or with known or related structures) for phase identification can be achieved. For unknown structures, PXRD can determine unit cell from indexing the peaks observed in the diffraction pattern. The positions of the peaks together with the intensity are input using various algorithms the most useful of which are ITO,[7] DICVOL[3] and TREOR.[8] Thus, the unit cell is determined and via Le Bail refinement[9], the instrumental parameters and space group can be determined. The Le-Bail method is independent of the unit cell contents and is used to extract information on the intensities. If a starting model is available Rietvield refinement can be used to confirm and refine the structure.[10]

In order to refine the structure, the Rietveld[10] method was used. The refinement process[11] is a process of minimizing the difference between observed and calculated peak profiles upon refining atom positions, atom thermal motion, atom site occupancy parameters, peak shape, unit cell dimensions, zero dimensions, etc. The Rietveld method allows the refinement of a structural model including, lattice parameters, temperature vibrations, atomic positions and occupancies; using the Least-Square method.[12] The principle of the Rietveld method is to minimize the residual function to refine selected parameters, which equates to minimize the difference between an experimental pattern (observed data) and a model (calculated pattern). The calculated intensities are then compared to with the observed intensities, the value for the minimization function here called M (Equation 2.7), where: w, is a suitable weight calculated by errors for each reflection and the sum is over each data set; Y_o and Y_c are the observed and calculated intensities.

$$M = \sum w\left(Y_o - Y_c\right)^2 \qquad (2.7)$$

To know if the refinement is good enough there are reliability factors known as Residuals R; which are defined to compare the observed pattern vs the pattern calculated: the weighted R_{wp} is weighted to emphasize intense peaks over background, R_{exp} estimates the best value R for a data set and give an evaluation of how good the data are (see Equations below 2.8, where N and P represent the number of data point and number of refined parameters; and goodness of fit (GOF=χ^2). The GSAS software package with the EXPGUI[13] interface to perform Rietveld analysis is used (Figure 2.8). As part of the refinement process, additional scattering can be located using difference Fourier methods.

$$R_{wp} = \left[\frac{M}{\sum w\, y_o^2}\right]^{\frac{1}{2}} \qquad R_{\exp} = \left[\frac{N-P}{\sum w\, y_o^2}\right]^{\frac{1}{2}} \qquad GOF = \chi^2 = \left(\frac{R_{wp}}{R_{\exp}}\right)^2 \qquad (2.8)$$

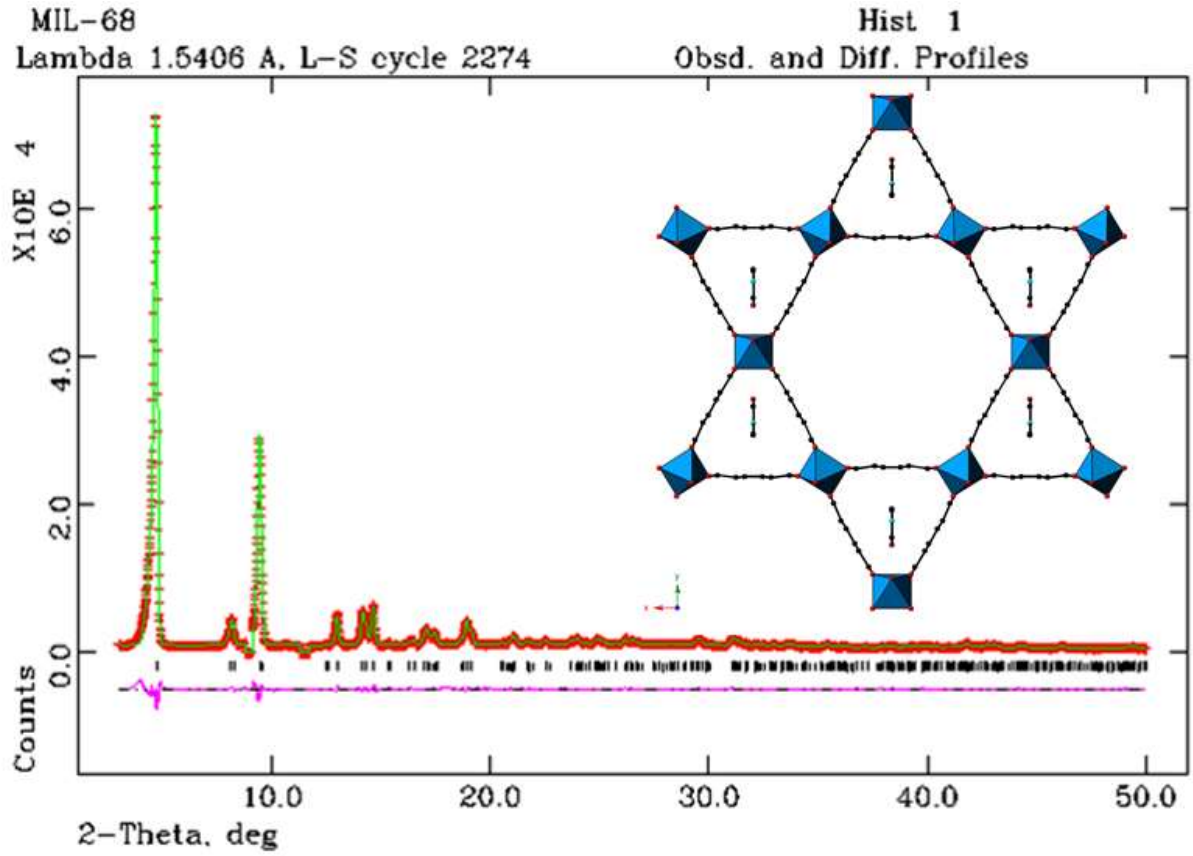

Figure 2.8: Rietveld plot of the refinement of the structure of MOF MIL-68(Sc), against X-ray powder diffraction data (λ =1.54056 Å, with values R_{wp} = 5.25%, R_p = 3.80%). Observed pattern, red crosses, fitted profile in green, difference curve between observed and calculated pattern in pink.

Phase identification in this work is performed by comparison of the diffraction pattern to those of known materials or to a database such as the International Centre for Diffraction Data's Powder Diffraction File or the Cambridge Structural Database (CSD).[14] PXRD patterns were collected on materials using PANalytical Empyrean and STOE STAD i/p diffractometers using Cu $K_{\alpha 1}$ X-radiation (λ = 1.54056 Å).

2.3 Nuclear Magnetic Resonance (NMR) Spectroscopy[15,16]

2.3.1 Introduction

NMR spectroscopy relies on the magnetic properties of the atomic nucleus; it measures the absorption of electromagnetic radiation in the radio frequency region (~10-800 MHz), radio waves have long wavelengths, and thus low energy and frequency. The principle of NMR comes from the spin of a nucleus generating a magnetic field. An atomic nucleus is a collection of protons and neutrons which, like electrons, possess a quantum mechanical property called spin which is characterised by an intrinsic spin angular momentum. Spin is a fundamental property of nature like electrical charge or mass. The nuclei are involved in the absorption process and generate a magnetic dipole when placed in a strong magnetic field (B_0) (Figure 2.9), spinning nuclei will align with or against the applied field creating energy difference (ΔE, Equation 2.9). The emitted radio frequency is directly proportional to the strength of the applied field (see Equation 2.10), γ is called the magnetogyric ratio, related to the ratio between the nuclear magnetic moment and angular moment.

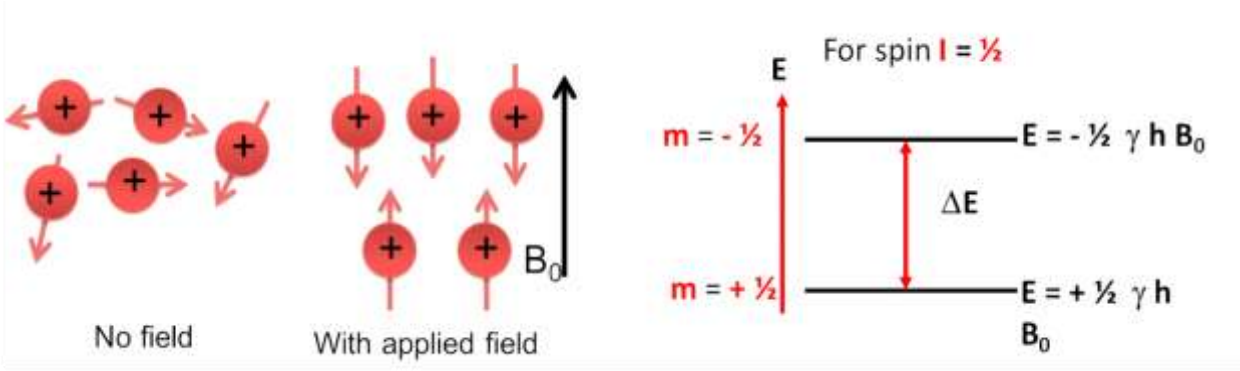

Figure 2.9: Alignment of nuclear spin in presence on the field B_o (left) and an example for spin I = ½ the energy gap between the 2 levels.

$$\Delta E = \gamma \hbar B_0 \quad (2.9)$$

Then, the applied magnetic field B_0 is measured in tesla (T), and the frequency ν of radiation used for resonance, measured in hertz (Hz), or megahertz (1 MHz = 10^6 Hz). The frequency with which the magnetization precesses about this field is defined as ω, the Larmor frequency. Figure 2.10 shows the precession around the axis (z) of the applied field when the aligned occurs at an angular frequency given by Equation 2.10. Consequently, increasing either the magnetic field strength or the magnetogyric ratio or both will result in an increase in the precession frequency.

$$\omega = \gamma B_0 \quad (2.10)$$

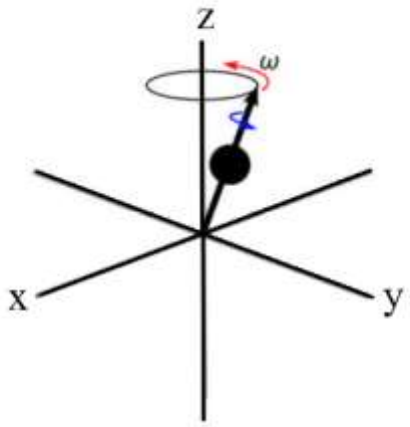

Figure 2.10: Precession of a magnetic moment around the axis of the applied field.

Then, the first part of the NMR experiment is the preparation of the nuclear spin system, which is placing in the external magnetic field B_0 so the magnetic moments of all the nuclei in the sample, so that is the result of net magnetisation (M) parallel to the B_0 axis. This is referred to as the bulk magnetisation vector which can be taken as a single magnetic moment (Figure 2.11).

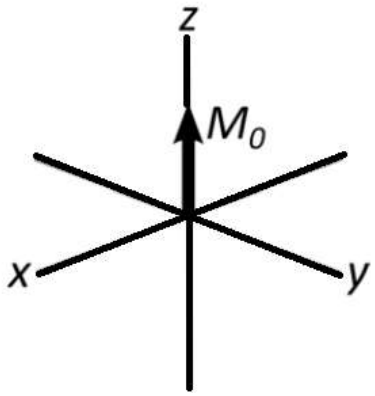

Figure 2.11: Illustration of the bulk magnetization vector.

In the second part of the NMR experiment is *perturbation:* the samples is irradiated with a pulse of plane-polarised radiofrequency (RF) radiation at the Larmor frequency and the detection, this last part take place when the RF field is turned off and its return to the initial state when the perturbation is removed. When the spin returns to its ground state level, the absorbed energy is emitted at the same radio frequency. The NMR signal is detected and recorded as function of time and is named a Free Induction Decay (FID) containing frequency information. This can be extracted by a Fourier Transformation to produce the frequency spectrum of the signal known as the NMR spectrum (Figure 2.12). NMR absorptions generally appear as sharp peaks and the height of each peak is proportional to the area under the peak.

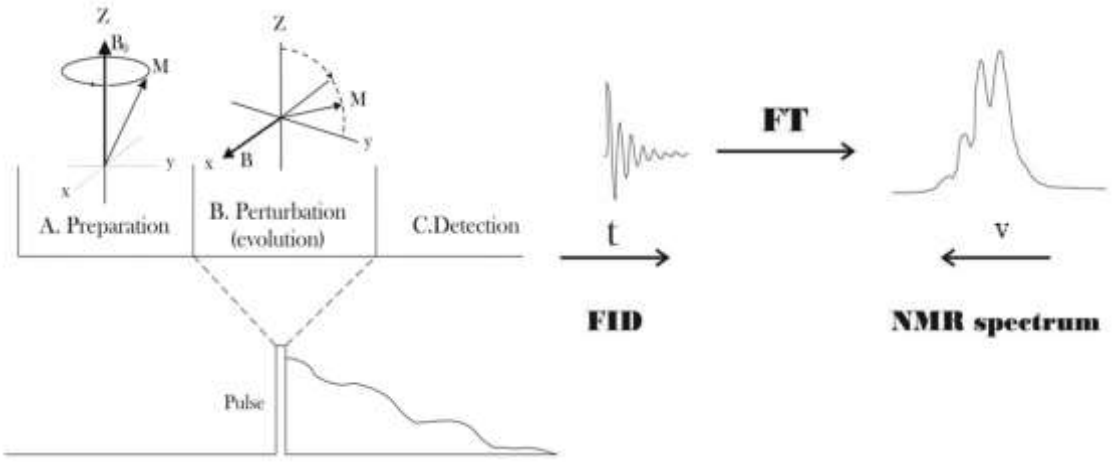

Figure 2.12: Schematic representation of NMR experiment.

2.3.2 The chemical shift

An NMR spectrum is a plot of the intensity of a peak against its chemical shift (δ), measured in parts per million (ppm). A chemical shift is defined as the difference between the resonance frequency of the observed proton and the reference compound, usually tetramethylsilane[16] (TMS), which gives a single peak upfield set at δ=0 ppm. The terms 'upfield' and 'downfield' describes the relative location of peaks on the NMR spectrum. The chemical shift depends on the local structural environment and it is sensitive to structural modifications and symmetry changes.

2.3.3 Magic Angle Spinning (MAS)[15]

The magnetic spin of an NMR-active nucleus interacts with surrounding magnetic and electric fields, leading to potential changes in the energies of resonance. In a solution, these effects are averaged out because the molecular motion is rapid and random due to Brownian motion and sharp NMR signals are obtained. In a crystalline solid, these interactions are anisotropic, so that in a stationary microcrystalline solid sample in a magnetic field there will be a range of interactions depending on the orientations of the crystallites to the applied magnetic field and this results in very broad signals. The interactions include chemical shift anisotropy (due to the generally non-spherical arrangement of electrons in bonding environments), internuclear dipolar interactions between NMR-active nuclei and internuclear quadrupolar interactions (for nuclei with non-1/2 spin, such as scandium-45, I = 7/2). These interactions all include a term $(3\cos 2\theta - 1)$, where θ is the angle that the internuclear vector makes with the magnetic field. Rotating the solid sample rapidly around an axis that is at an angle of 54.74° to the applied magnetic field Bo reduces this term to zero, if the rotation speed is high enough (which depends on the strength of the interactions to be averaged out). This is the technique of Magic Angle Spinning that has been employed to obtain the multinuclear high resolution solid state NMR spectra reported in this thesis.

2.3.4 NMR spectroscopy in this work

For catalytic evaluation using MOFs prepared in this thesis, solution-phase NMR has been used to monitor the reaction via the chemical shifts of reactants and products, ^{1}H NMR and ^{19}F NMR were carried out using a Bruker Avance 400 spectrometer at 400 Hz or a Bruker Avance 300 spectrometer at 300 Hz. Chemical shift information for each signal is given in part per million (ppm) relative to trimethylsilane (TMS). Chemical shifts for ^{19}F are relative to $CFCl_3$. (Figure 2.13)

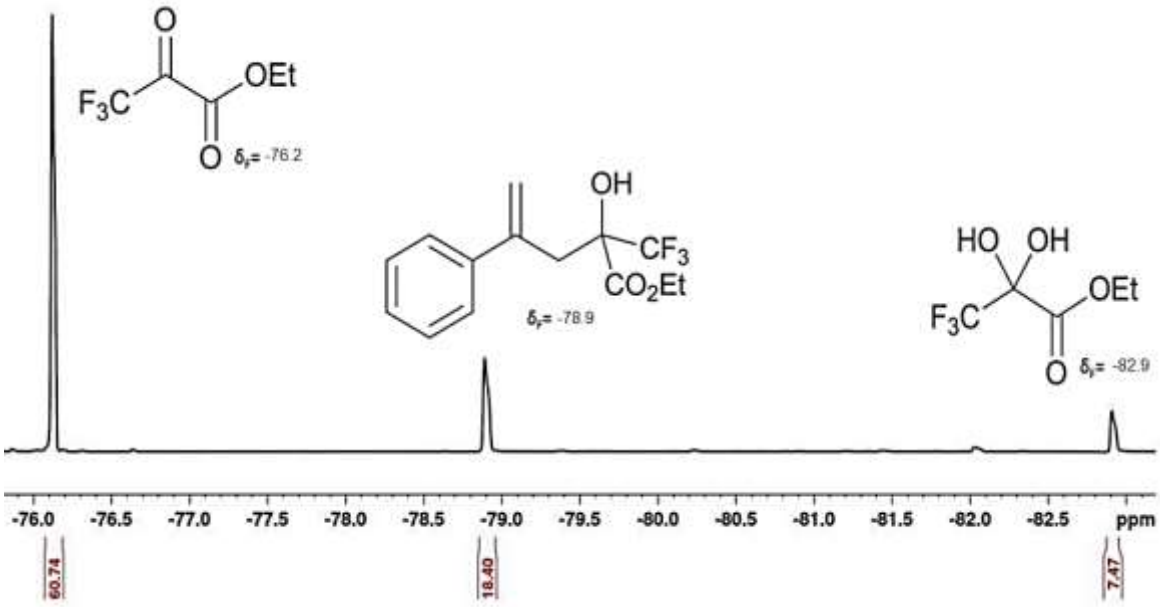

Figure 2.13: ^{19}F NMR spectrum (400 MHz, d_6-benzene of the mixture of control (catalyst-free) carbonyl ene reaction between ethyl trifluoropyruvate and α-methyl styrene): **δ;** -76.2 ppm (reactant), -78.9 ppm (product), -82.9 ppm (hydrated product).

Also, solution-phase NMR was used to characterise the amino functionalisation of MIL-53(Sc), which was prepared by a 'mixed-linker' approach; and in the post-synthethic modification of amino-functionalised Sc_2BDC_3 with nitro-terephthalate groups. Solution-phase ^{1}H NMR was used to confirm the ligands present in the material. The samples were digested in DMSO-d_6 and 0.3 mL of HNO_3 (0.2 M) followed by sonication for approximately 5 min leading to complete dissolution. Figure 2.14 shows a ^{1}H NMR spectra collected on

dissolved amino-functionalised MIL-53(Sc) (with 10% of NO_2-BDC), which has peaks attributed to the two ligands involved in its synthesis.

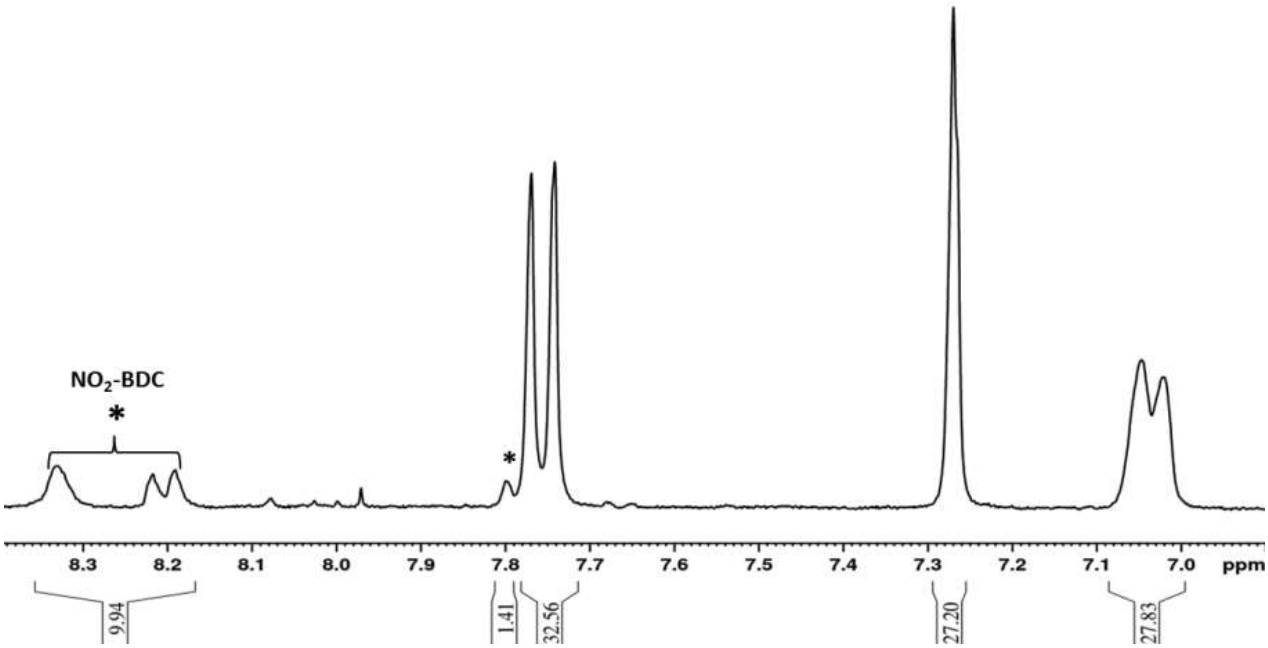

Figure 2.14: ^{1}H NMR of the digested NH_2-MIL-53(Sc). Chemical shift due to the resonances of NH_2-MIL-53(Sc) are presented in **δ;** 7.75 ppm, 7.3 ppm and between 7.0 and 7.1 ppm. *Signal attributed to the linker NO_2-BDC located in 7.8, 8.200, 8.248 and 8.358 ppm.

On the other hand, solid-state NMR is used as an approach to examine additional structural information of crystalline MOFs prepared in this thesis, in collaboration with the research group of Dr. Sharon Ashbrook at St Andrews. MAS NMR spectra were acquired using a Bruker Avance III spectrometer at B_0 field strength of 14.1 T, with Larmor frequencies of 145.782 MHz for ^{45}Sc, 600.130 MHz for ^{1}H and 150.903 MHz for ^{13}C. Powdered samples were packed into conventional 4 mm and 1.9 mm rotors, and rotated at MAS rates of 12.5 kHz and 40 kHz, respectively.

2.4 Chemical Elemental Analysis (CHN)

CHN is an analytical technique used to determine the organic content of a material. The elemental analysis is accomplished by combustion and determines weight percentage of

carbon, hydrogen and nitrogen. For the analysis the sample is burned in an excess of oxygen to form carbon dioxide, water and nitric oxide which can be extracted and weight percentage of each element determined. Elemental analysis was used to determine the relative amount of carbon, nitrogen and hydrogen present in the synthesized materials. Elemental analyses were performed by Elemental Analysis Service, London Metropolitan University, London, UK.

2.5 Scanning Electron Microscopy (SEM) and energy dispersive X-ray spectroscopy (EDX or EDS).

Scanning electron microscopy (SEM) is technique that can be used to determine particle morphology. An electron beam is produced by a heated tungsten filament and is accelerated and focussed to a narrow beam incident on the sample surface by two magnetic lenses, the condenser and objective lens (Figure 2.15). The condenser lens determines the beam current which impinges on the sample whereas the objective lens determines the final spot size. In the condenser lens are two pairs of scanning coils. The scan coils and objective lens direct and position the beam onto the sample so the electron beam is scanned over the surface of the sample. The focused beam produces secondary electrons at the sample and those electrons are collected by an electron detector, and amplified, and used to modulate the brightness of a cathode ray tube (CRT) so that every point that the beam strikes on the sample is mapped directly onto a corresponding point on the screen, resulting an image of the sample surface. In this thesis the morphology and size of crystal of materials of MOFs were analysed by SEM microscopy (Figure 2.16). SEM micrographs were taken on a JEOL JSM 5600 SEM electron microscope.

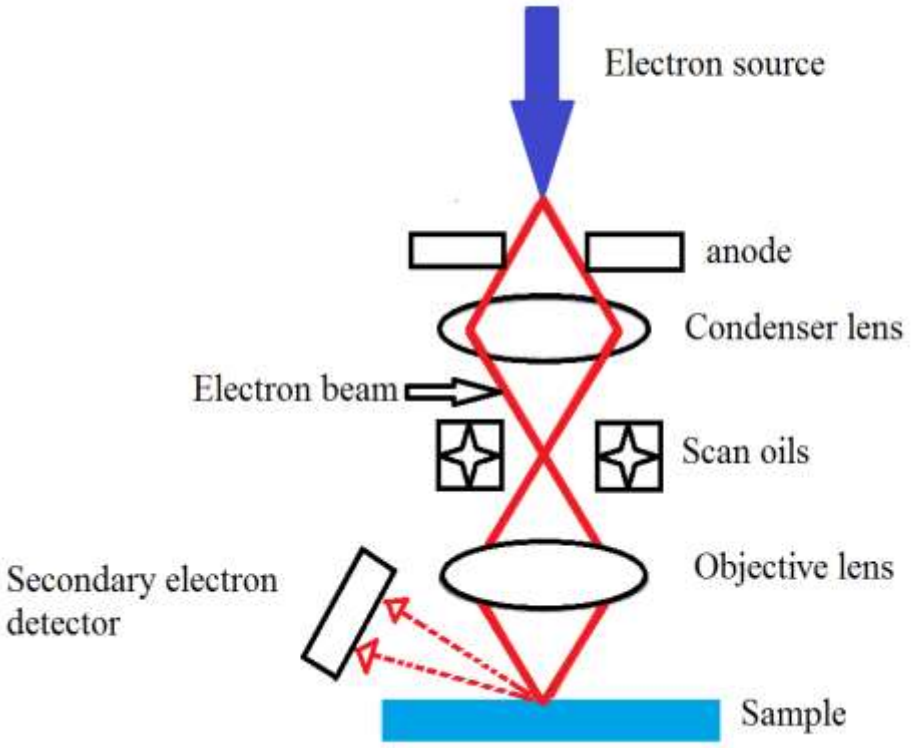

Figure 2.15: Schematic diagram illustrating the principle of SEM.

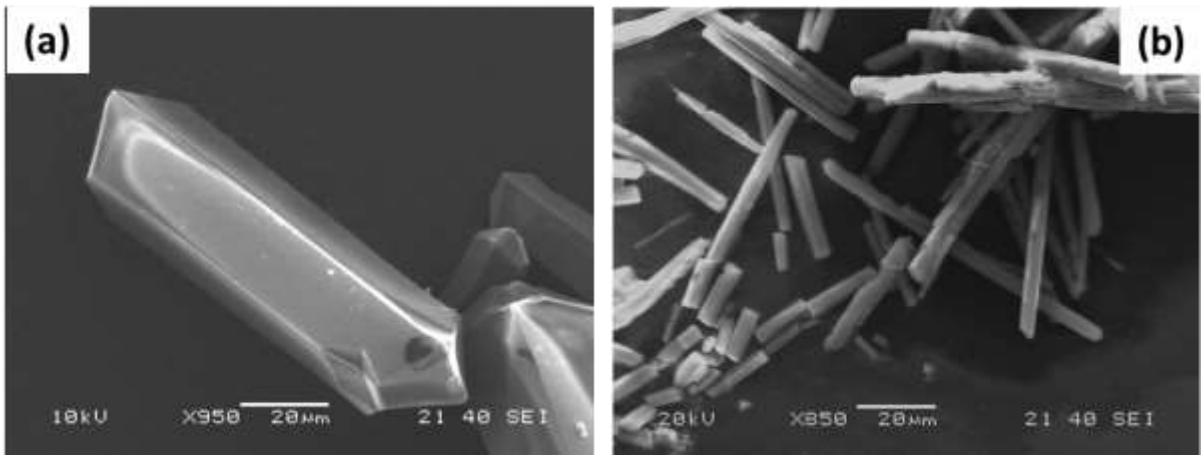

Figure 2.16: SEM images of MOF $Sc_2(NH_2\text{-}BDC)_3$ (a) and $Sc_2(Br\text{-}BDC)_3$ (b).

The presence of the metals and other heavy atoms was determined by energy dispersive X-ray spectroscopy (EDX or EDS) which analyses X-ray emission resulting from bombarding the sample with a high energy beam of electrons in the scanning electron. The bombarding electrons collide with the atoms in the material under examination, resulting in the ejection of

electrons. Subsequently, electrons transfer from a higher energy orbital to fill the vacancy and give up energy as an X-ray of characteristic energy. The energy of X-ray emitted is measured in an X-ray detector allowing identification of the elements and their abundance. Because the technique is performed in an electron microscope, and the beam size is small and focused, it is possible to perform selected area chemical analysis by this method. Figure 2.17 shows EDX spectrum from the MOFs $Sc_2(NH_2\text{-}BDC)_3$ and $Sc_2(Br\text{-}BDC)_3$ obtained with a JEOL 5600 SEM with an Oxford INCA energy 200 EDX system.

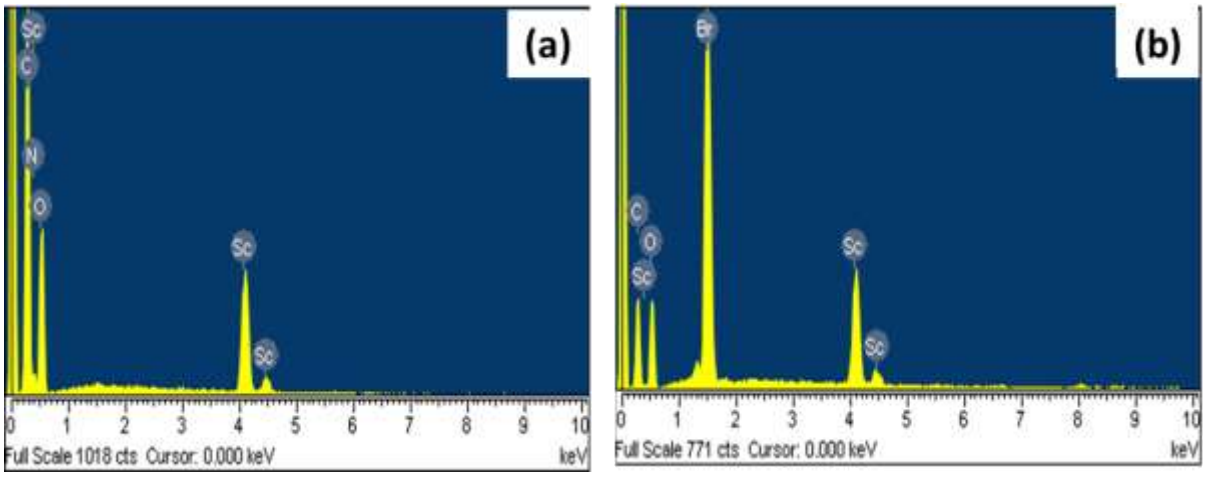

Figure 2.17: EDX spectrum of MOF MOF $Sc_2(NH_2\text{-}BDC)_3$. (a) and $Sc_2(Br\text{-}BDC)_3$ (b).

2.6 Gas adsorption[17-20]

Gas adsorption is one of many experimental methods available for the surface and pore characterisation of porous materials. Adsorption is defined as the concentration of gas molecules near the surface of a solid material. The adsorbed gas is called the adsorbate and the solid on which adsorption takes place is known as the adsorbent. Adsorption can be of two types: chemisorption, which involves the formation of bonds and physisorption where only dispersive, dipole-charge and quadrupole interactions are involved. For N_2, adsorption isotherms are measured at -196 ℃ usually, where interactions similar to those involved in liquefaction of N_2, are involved. When a material is exposed to a gas, an attractive force acts

between the exposed surface of the solid and the gas molecules. The result of these forces is characterised as physical (or van der Waals) adsorption, in contrast to the stronger chemical attractions associated with chemisorption.

The surface area of a solid includes both the external surface and the internal surface of the pores. Due to the weak bonds involved between gas molecules and the surface (<15 $kJmol^{-1}$) physical adsorption is a reversible phenomenon. Gas physisorption is considered non-selective, thus filling the surface step by step (or layer by layer) depending on the available solid surface and the relative pressure. The complete adsorption analysis at a single temperature is called an adsorption isotherm.

Figure 2.18 shows the IUPAC classification of the sorption isotherms. The six types of isotherms are described as follows:

- Type I isotherm is typical of monolayer chemisorption, or physisorption on microporous materials solids. The high adsorption at low relative pressure in this type is due to the narrow pore width and the high adsorption potential so that micropore filling with increasing pressure and the absorbed amount approaches a limiting value as $P/P_0 \rightarrow 1$.
- Type II isotherm represents the standard form of the isotherm on a non-porous or macroporous material with strong adsorbate-adsorbent interaction, where unrestricted monolayer-multilayer adsorption can happen. The point B in this type of isotherm indicates the stage at which the monolayer coverage is completed then the multilayer adsorption occurs.
- Type III isotherms are not common and describe adsorption on non-porous or macroporous adsorbent with weak adsorbate-adsorbent interactions.

- Types IV and V adsorption isotherms are typical of mesoporous materials with pore diameters between 2-50 nm. Type IV represent adsorption isotherm with hysteresis, which is associated with capillary condensation in mesoporous materials. The initial part of the type IV isotherm can be attributed to mono-layer adsorption similar to that observed in isotherm type II, whereas in the type V isotherm the initial part is related to weak interaction between the adsorbent and adsorbate as in the case of type III isotherm.
- Type VI shows the stepwise multilayer adsorption on a uniform, non-porous surface. This occurs for some materials with relatively strong fluid-wall forces, usually when the temperature is near the melting point for the adsorbed gas and can also be observed for MOFs that contain cages of different sizes (such as MIL-101). These isotherms were observed for krypton on graphitized carbons.

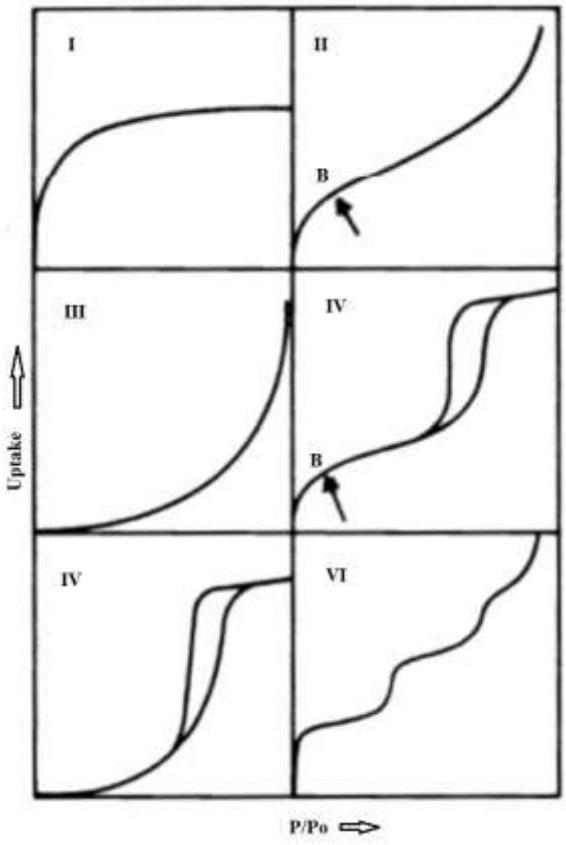

Figure 2.18: The six IUPAC standard adsorption isotherms.[18]

Brunauer, Emmett and Teller[18] developed a theory of multilayer adsorption to explain the form of the Type II isotherm. This 'BET' theory assumes that the uppermost molecules in adsorbed stacks are in dynamic equilibrium with the vapor. This means that, where the surface is covered with only one layer of adsorbate, equilibrium exists between that layer and the vapor, and so on. Since the equilibrium is dynamic, the actual location of the surface sites covered by one, two or more layer may vary but the number of molecules in each layer will remain constant. The theory gives Equation 2.11

$$\frac{P}{V(P_0 - P)} = \frac{c-1}{V_m c} * \frac{P}{P_0} + \frac{1}{V_m c} \qquad (2.11)$$

Where, c is the BET constant, P and P_0 are the equilibrium and the saturation pressure of adsorbates at the temperature of adsorption, V is the adsorbed gas quantity (for example, in volume units), and V_m is the monolayer adsorbed gas quantity.

BET isotherm analysis is applicable for mesoporous solids using a selected P range, and can be useful for comparing microporous solids. The adsorption isotherm of a MOF enables its surface area to be determined via this method, although the pores do not permit unlimited multilayer formation. Properties such as porosity, surface area, and pore size were measured and this information was used to compare the adsorption properties of the different MOFs prepared in this investigation. Sample preparation involved degassing the samples in a time period (4-12 h) at a temperature range of 60-250 ℃ under vacuum. The adsorption analysis for nitrogen was measured volumetrically at -196 ℃ using a Micromeritics Tristar II 3020, up to $P/P_0 = 1.0$, where P_0 is the saturation pressure. CO_2 adsorption isotherms were measured volumetrically at 0 ^{0}C and 25 ^{0}C using a Micrometrics 2020 porosimeter, and Hiden Isochema IGA gravimetric porosimeter was used for analysis at lower temperature -77 ℃ (196 K).

2.7 Gas Chromatography[19]

Chromatography is a method of separating different components of a sample, achieving separation over a stationary phase with the help of the mobile phase (carrier gas). Each component of the sample has properties which allow their different interaction with the stationary phase, so each component is delayed on an individual basis. If the flow rate, the characteristics of stationary and mobile phase and the column length are appropriate complete separation can be achieved.

The GC consists of an injection block, a column, and a detector. An inert gas flows through the system. The injection chamber is a heated cavity which serves to volatilize the compounds. A very small amount of liquid mixture is injected by syringe into the instrument and is volatilized in a hot injection chamber. Then, it is swept by a stream of inert carrier gas through a heated column. As the mixture travels through this column, its components equilibrate between the mobile and stationary phases, and thus separate into pure components. Each component passes through a detector at a different time and gives a chromatographic peak. The area under a chromatographic peak is proportional to the amount of analyte present in the chromatogram. By calculating the area of the peak the concentration of an analyte in the original sample can be determined.

Gas chromatography (GC) was used to follow the acetalisation reaction. 1 μl of sample was injected onto an HP-5 crosslinked 5% phenyl dimethylpolysiloxane capillary column fitted to a CE Instruments GC 8000 TOP machine equipped with a Flame Ionisation Detector (FID). The column temperature was kept constant at 130 ^{0}C, with helium used as the carrier gas (flow rate, 25 mL min). Table 2.3 lists the retention time for each component in the sample. Data was plotted and analysed using a Fisons Instruments DP700 integrator (Figure 2.19).

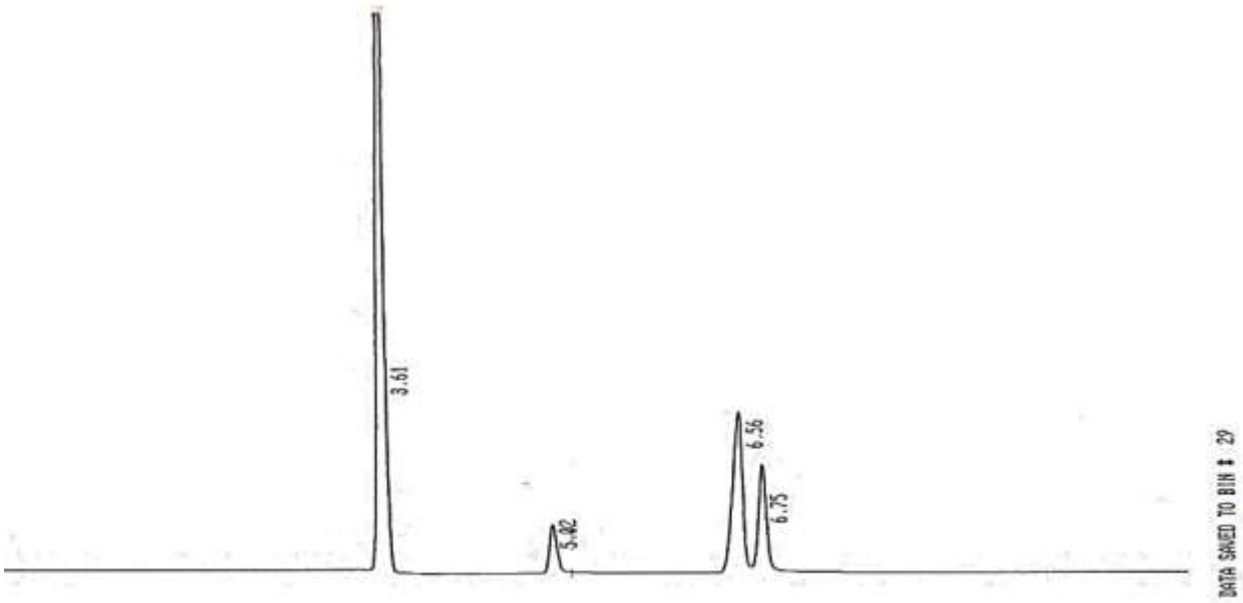

Figure 2.19: Gas chromatogram showing the product mixture of acetalisation of benzaldehyde with methanol, using nitrobenzene as an internal standard.

Table 2.3 Peaks in the GC traces.

Peak	Ret.time min	Component
1	3.61	Methanol
2	5.02	Benzaldehyde
3	6.56	Nitrobenzene
4	6.75	1,1 Dimethoxytoluene

2.8 Thermogravimetric Analysis (TGA)[20]

To check the thermal stability of the materials thermogravimetric analysis (TGA) was used. The technique measures how the weight changes when the temperature is increased. This technique can be used to determine the thermal stability and composition, and the measurement is normally carried out in air or in an inert atmosphere. A TGA analysis is performed by gradually raising the temperature range from 25°C to 800°C (Figure 2.20) under flowing air at a heating rate of 5 K min^{-1} routinely using a Netzsch TGA 760 or TGA 1000.

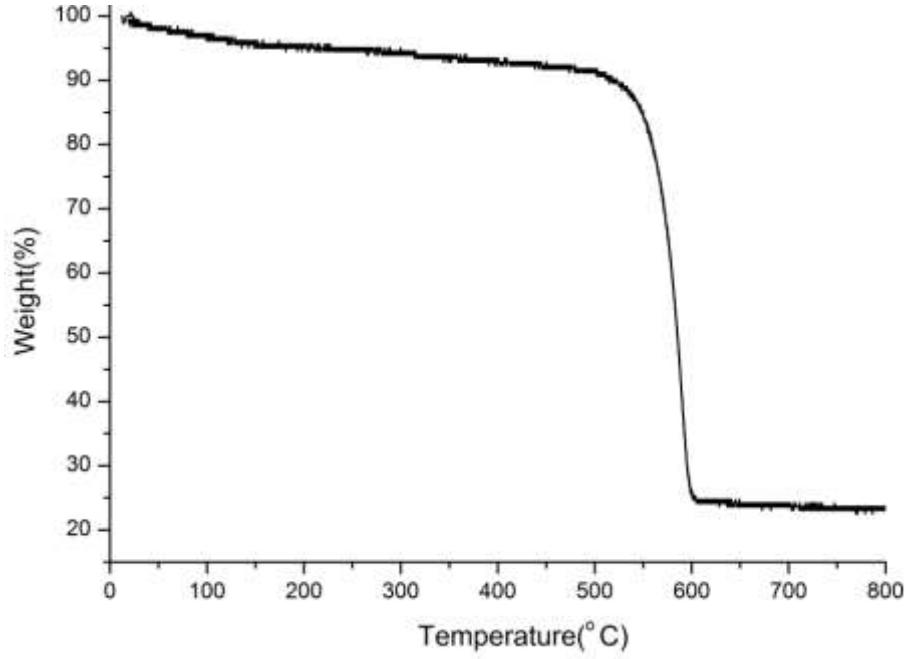

Figure 2.20: TGA curve of MIL-68(Sc)

2.9 References

1. M. Ladd and R. Palmer, *Structure Determination by X-ray Crystallography*, Springer, New York, USA, 2003.

2. C. Giacovazzo, H. L. Monaco, G. Artioli, D. Viterbo, M. Milanesio, P. G. Gastone Gilli, G. Zanotti, G. Ferraris and M. Catti, *Fundamentals of Crystallography*, OUP, New York, USA, 2011.

3. A. Boultif and D. Louer, *J. Appl. Crystallogr.*, 1991, 24, 987-993.

4. H. Hauptman, *Computers & Mathematics with Applications*, 1988, 16, 385-396.

5. G. M. Sheldrick, *Acta Cryst.*, 2008, A64, 112-122.

6. P. W. Betteridge, J. R. Carruthers, R. I. Cooper, K. Prout and D. J. Watkin, *J. Appl. Crystallogr.*, 2003, 36, 1487.

7. J. G. Huddleston, A. E. Visser, W. M. Reichert, H. D. Willauer, G. A. Broker and R. D. Rogers, *Green Chemistry*, 2001, 3, 156-164.

8. P.-E. Werner, L. Eriksson and M. Westdahl, *J. Appl. Crystallogr.*, 1985, 18, 367-370.

9. A. Le Bail, H. Duroy and J. L. Fourquet, *Mater. Res. Bull.*, 1988, 23, 447.

10. H. Rietveld, *Acta Cryst.*, 1967, 22, 151-152.

11. R. A. Scott and C. M. Lukehart, *Applications of Physical Methods to Inorganic and Bioinorganic Chemistry*, Wiley-Blackwell, UK, 2007.

12. D. Sayre, *Acta Crystallographica*, 1952, 5, 60-65.

13. B. H. Toby, *J. Appl. Crystallogr.*, 2001, 210-213.

14. Cambridge Crystallographic Data Centre (CCDC), http://www.ccdc.cam.ac.uk.

15. M. J. Duer, in *Solid-State NMR Spectroscopy Principles and Applications*, Blackwell Science Ltd, 2007,.

16. M. Bruch, *NMR Spectroscopy Technique*, CRC Press, USA, 1996.

17. S. Lowell and J. E. Shields, *Powder Surface area and porosity*, Springer, USA, 3 edition edn., 1991.

18. S. Braunauer, P. H. Emmett and E. Teller, *J. Am. Chem. Soc.*, 1938, 60, 309.

19. R. L. Grob and E. F. Barry, *Modern Practice of Gas Chromatography*, Wiley-Blackwell, USA, 2004.

20. J. Kenkel, *Analytical Chemistry for Technicians*, CRC Press, USA, Third Edition edn., 2003.

Chapter 3: Assessing the potential of scandium carboxylate MOFs in catalysis

3.1 Introduction

Research in the application of Metal-Organic Frameworks (MOFs) in catalysis has been increasing in the last years, in particular as Lewis acidic catalysts.[1-7] There are several Lewis acid catalyzed reactions such as cyanosilylation, acetalization, epoxidation, acylation and the ene reaction and many of them have been applied in industry.[8-11] Like zeolites, porous crystalline MOFs offer high surface areas that can host active sites accessible via well-defined pore openings, and therefore have potential in heterogeneous catalysis.[11-15]

It is has been demonstrated that scandium (Sc^{3+}) has Lewis acidic properties.[16-19] Studies in the reaction of 1-trimethylsiloxycyclohexene with benzaldehyde in dichloromethane (Scheme 3.1) was tested using scandium and lanthanide triflates, $M(OTf)_3$ (where M^{3+} = scandium, ytterbium and yttrium) as catalysts.[17] Results of this evaluation demonstrated that scandium triflate, $Sc(OTf)_3$ is a powerful homogeneous Lewis acid catalysts giving a yield of 81%, whereas the other triflates $Yb(OTf)_3$ and $Y(OTf)_3$ did not result in selective conversion. After use $Sc(OTf)_3$ is not deactivated while the common Lewis acidic compounds are, a characteristic that makes it reusable.

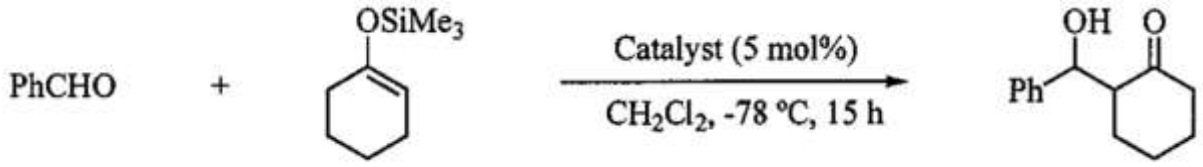

Scheme 3.1: Reaction of 1-trimethylsiloxycyclohexene with benzaldehyde in dichloromethane.

Several Lewis acids have been tested for C-C bond formation; however, this evaluation has been done in many cases in the homogeneous solution phase. Therefore, there is the aim to perform it in the heterogeneous form, allowing the catalyst to be recycled and avoiding waste and minimizing costs to industry. Considering that MOFs containing scandium can be used as

heterogeneous Lewis acid catalysts in organic synthesis, their applications in carbonyl ene reaction and acetalization are reported in this investigation. One example of carbonyl ene reaction is the production of menthol. Scheme 3.2 shows menthol production, which initially comes from β-pinene (obtained from pine trees usually applied in paper and furniture making. The current process involves the synthesis of (R)-citronellal from β-pinene, followed by an intramolecular ene reaction catalyzed by $ZnBr_2$ with 94% selectivity for the desired anti isomer of isopulegol, then hydrogenation to give menthol. [20]

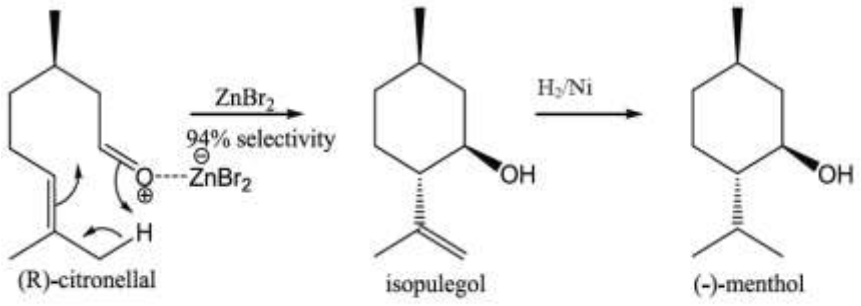

Scheme 3.2: Commercial process for menthol manufacture.[20]

This is just one example of the wide field of ene reactions. Here, in order to evaluate the possibility to use scandium MOFs as Lewis acid catalysts, the carbonyl ene reaction chosen is that between the alkene, α-methyl styrene and the (activated) carbonyl compound, ethyl trifluoropyruvate, resulting in C-C bond formation (Scheme 3.3). Here scandium MOFs, in particular those with trimeric units in their structure are powerful candidates because as mentioned earlier in the introduction of this thesis once that those structures have lost the water molecules from the trimer it is possible to create unsaturated metal sites that impart Lewis acidic properties to the material. Thus, the scandium MOF could activate the carbonyl group of the substrates.

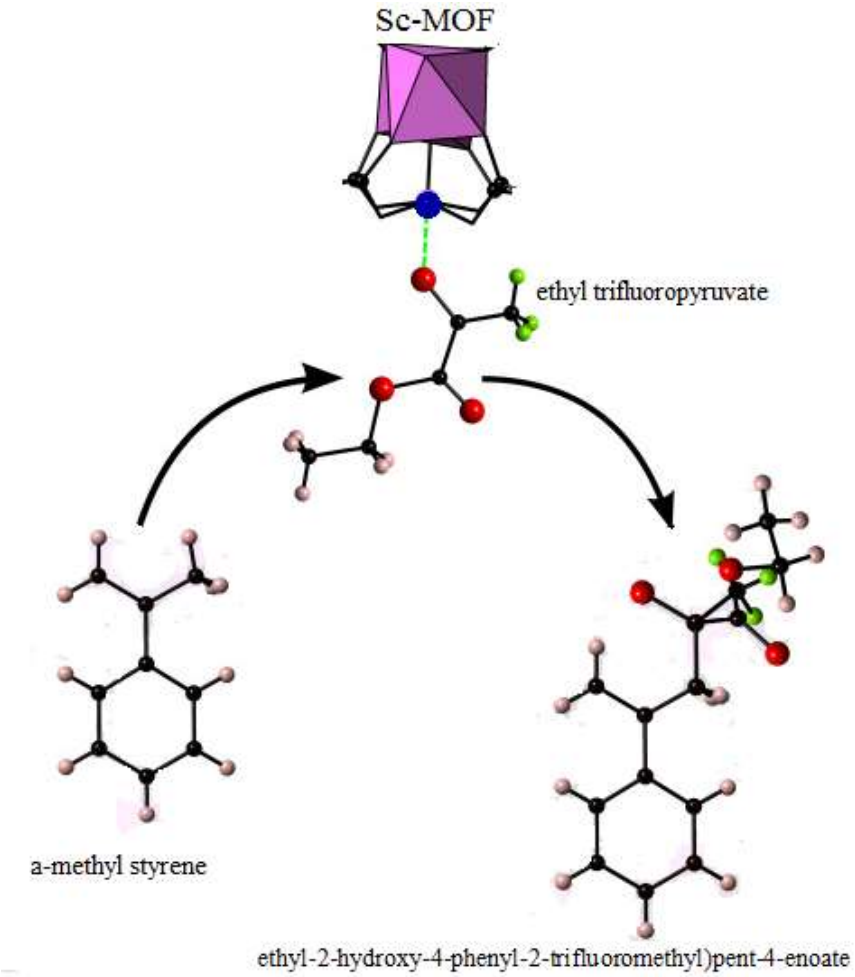

Scheme 3.3: Anticipated mechanism of reaction between α-methyl styrene and ethyl trifluoropyruvate catalysed by scandium MOFs. In (Sc-MOF) the blue sphere represents a coordinatively unsaturated active Lewis acid site. Red, pale and green spheres represent oxygen, hydrogen and fluorine atoms, respectively.

Acetalization of aldehydes is another organic reaction to evaluate. Although the formation of dimethyl acetals can be achieved with trimethyl orthoformate as the reagent the use of methanol is preferable due to its greater availability. In this way acetalization of various aliphatic and aromatic aldehydes with methanol has been reported with Al-MCM-41.[21] Recently, MOFs have also been reported as solid catalysts for the acetalization of benzaldehyde with methanol at room temperature.[22] A copper-containing MOF $Cu_3(BTC)_2$ was tested giving high selectivity and yields compared to zeolites and clays.

In this chapter the applications of scandium MOFs as catalysts are described. Therefore, the synthesis and characterisation of the MOFs selected as potential catalysts are described in the first part of this chapter and the second part describes the catalytic applications.

Scandium MOFs such as MIL-100(Sc) which is prepared with benzene-1,3,5-tricarboxylic acid and the isoreticular MIL-88B(Sc) and MIL-88D(Sc) based on terephthalate and 4,4-biphenyl-dicarboxylate respectively have been reported. MIL-101 is another selected MOF tested as a catalyst, however the reported synthesis only gave it within mixtures with MIL-88B(Sc). Thus, the objectives include synthesis of the pure form of MIL-101(Sc). In attempts to obtain the pure MIL-101(Sc) several variables were explored and it was found that use of a mixture of solvents, dimethylformamide and ethanol, yields pure MIL-101(Sc). Slight modification of the synthesis led to the first preparation of MIL-68 in the scandium form. The first report of this framework was published by Barthelet et al,[23] using vanadium. Syntheses of MIL-68 with other trivalent metals, such as gallium, indium, aluminium and iron have been reported. [24-26] This MOF is built up of a hexagonal array of large pore channels and small triangular tunnels, which are linked to the metal hydroxide chains creating a 'kagome lattice'. It is a polymorph of MIL-53 but it does not show the breathing behaviour of MIL-53.

In order to put into the context the catalytic activity of MOFs, scandium-exchanged zeolites were prepared. Scandium cations were introduced into extra-framework, charge-balancing cation positions of zeolites. Zeolites Y and Beta were chosen. Zeolite Y exhibits the large pore faujasite (FAU) structure (Figure 3.1) and crystallizes in the cubic space group $Fd\bar{3}m$ with a = 24.7 Å. It is available in the Na-form. Zeolite Beta[27] has a three dimensional large (8 Å) pore structure in which all extra-framework cations are accessible to adsorbed species. Zeolite Beta was available in the H-form.

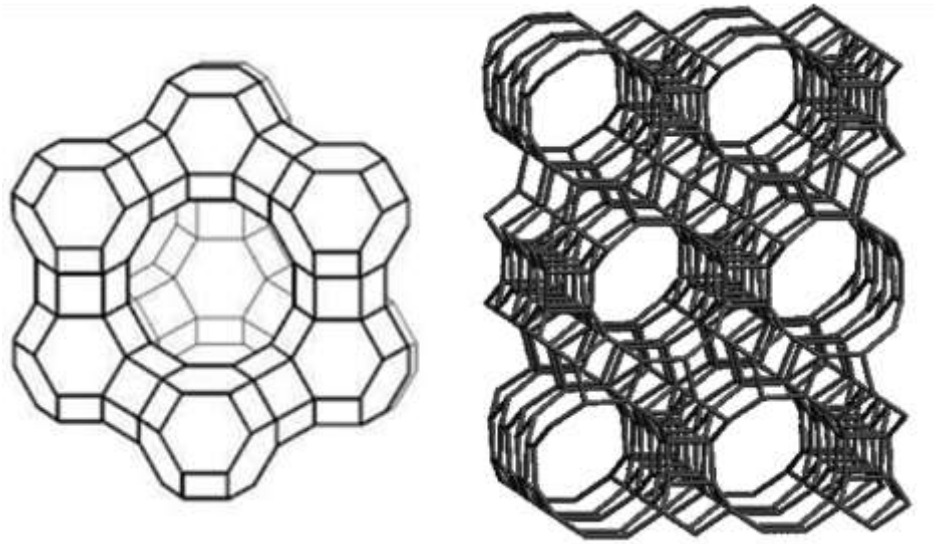

Figure 3.1: Framework structures of zeolites: (left) Zeolite Y and (right) zeolite Beta. T-O-T linkages are represented by linear 'bonds' between tetrahedral cation positions.

Finally the direct synthetic encapsulation of polyoxometalates (POM) in scandium MOFs is explored. From a practical point of view there are two techniques to encapsulate POMs into MOFs, by direct synthesis or post-synthetically method. Here, the direct synthetic method is used to encapsulate Keggin POMs (13–14 Å in diameter). Phosphotungstic acid monohydrate (PTA) or phosphomolybdic acid monohydrate (PMA), are used in the preparations, and properties of these POMs can be found in Table 3.1.

Table 3.1: POMs used for encapsulation in MOF

POM	**Formula**	**Name**	**Molar mass**
PTA	$H_3PW_{12}O_{40}{\cdot}xH_2O$	Phosphotungstic acid hydrate	2880.05
PMA	$H_3PMo_{12}O_{40}{\cdot}xH_2O$	Phosphomolybdic acid hydrate	1825.25

3.2 Experimental

3.2.1 Synthesis and characterisation

3.2.1.1 Synthesis of MOFs

A series of scandium and chromium MOFs were prepared using the ligands shown in Figure 3.2 by following the published syntheses or via their slight modification.[28-30] The synthesis of scandium MOFs were carried out via a solvothermal route using scandium nitrate ($Sc(NO_3)_3$ 99.9%, Metal Rare Earth Limited) or scandium chloride solution ($ScCl_3$). The $ScCl_3$ solution was prepared by dissolving scandium oxide (Sc_2O_3, 75 mmol; Stanford Materials Corporation, 99.99%) in a stoichiometric amount of HCl (18.6 mL, Fischer Scientific; 38%) to produce $ScCl_3$ 1.45 M upon heating. Upon cooling the solution is made up to 100 mL with distilled water.

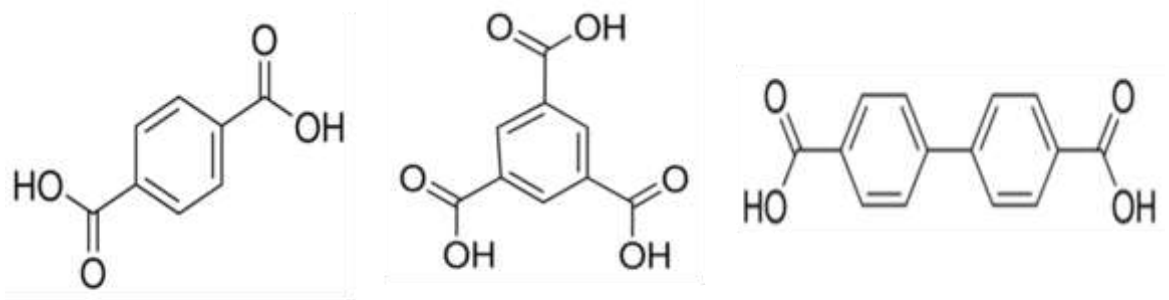

Figure 3.2: Carboxylic acid used as sources of carboxylate linkers in the synthesis of MOFs.

The synthesis of chromium MOFs for comparison involved chromium oxide (Cr_2O_3 ; Aldrich 98%) and chromium chloride ($CrCl_3$; Aldrich, 98 %). Also, solvents were purchased and used with further purification, such as N,N-dimethylformamide (DMF, Acros, 98%), ethanol (EtOH, VWR, 99.8%), toluene (Aldrich, 99.8 %), dichloromethane (DCM; Aldrich 99.8) and deionised water. The linkers used in this chapter were; trimesic acid (BTC= benzene-1,3,5-

tricarboxylic acid; Aldrich, 95%), terephthalic acid (BDC= benzene-1,4-dicarboxylic acid; Aldrich, 98%) and biphenyl-4,4′-dicarboxylic acid (BPDC; Aldrich 98%). The general procedure for synthesis of MOFs is carried out as follows: the metal source and the ligand were dissolved in the solvent and heated in a Teflon-lined steel autoclave at the temperature and time, as outlined in Table 3.2. The resulting solid was washed with the solvent used in the synthesis and dried at 60 °C. Product identification was carried out using powder x-ray diffraction and the samples were characterised further by chemical analysis, gas adsorption and NMR as required. Synthetic conditions of each MOF prepared in this chapter are detailed below and summarized in Table 3.2.

Table 3.2: Reaction conditions for the preparation of scandium and chromium MOFs (incusing the solvent:linker ratio S/*l*).

Metal source (M^{3+})	**Ligand** (*l*)	**Millimoles**		**Molar ratio (S/*l*)**			**Temp.** (^oC)	**Time** (h)	**MOF**
		M^{3+}	*l*	DMF	EtOH	H_2O			
$Sc(NO_3)_3$	BTC	0.9	0.4	600			150	48	MIL-100(Sc)
$Sc(NO_3)_3$	BDC	0.4	0.9	300			110	48	MIL-88B(Sc)
$ScCl_3$	BDC	0.58	0.64	80	120		80	24	MIL-101(Sc)
$ScCl_3$	BDC	0.46	0.46	80	200	600	90	12	MIL-68(Sc)
$Sc(NO_3)_3$, $ScCl_3$	BPDC	0.5	0.5	300			110	72	MIL-88D(Sc)
$CrCl_3$	BDC	0.4	0.7			800	220	8	MIL-101(Cr)
Cr_2O_3	BTC	0.5	0.4			300	220	96	MIL-100(Cr)

a) ***MIL-100(Sc)***: The synthesis of MIL-100(Sc) $[Sc_3O(OH)(H_2O)_2(C_9H_3O_6)_2]$ was performed using $Sc(NO_3)_3 \cdot 3H_2O$ (0.9 mmol) and trimesic acid (BTC= benzene-1,3,5-tricarboxylic acid**,** 0.4 mmol; Aldrich, >95%) in DMF (10 mL). The homogenized reaction mixture was transferred to a Teflon-lined autoclave and heated at 150 ℃ for 48 h. After heating, the autoclave was cooled and the mixture filtered, washed with ethanol and dried at 60 ℃.

b) ***MIL-88B(Sc)***: The MOF with formula $[Sc_3O(OH)(H_2O)_2(C_8H_4O_4)_3]$ was prepared using $Sc(NO_3)_33{\cdot}H_2O$ (0.4 mmol), and terephthalic acid (BDC= benzene-1,4-dicarboxylic acid , 0.9 mmol; Aldrich 98 %) in DMF for 72 h at 110 ^oC. The resulting solid was filtered, washed firstly with DMF and followed with ethanol, the MOF was dried at 60 ℃ for 12 h.

c) ***MIL-101(Sc):*** Initially the synthesis of MIL-101(Sc) $[Sc_3O(OH)(H_2O)_2(C_8H_4O_4)_3]$ was attempted with Sc $(NO_3)_33{\cdot}H_2O$ (0.6 mmol) as the metal source and terephthalic acid (BDC, 0.6 mmol; Aldrich > 98 %,) in DMF (10 mL) for 24 h at 100 ^oC. Results of this synthesis yielded crystalline products and were identified within mixtures that also contained MIL-88B(Sc). Thus, attempts to improve the purity and porosity of MIL-101(Sc) involved exploration of solvents and other source of metal. It was possible to prepare the pure material by a new route, using $ScCl_3$ solution (0.58 mmol, 1.45 M) and BDC (0.64 mmol) in a solvent mixture DMF (4 mL) and EtOH (5 mL). The homogenized reactions mixture was transferred to a Teflon-lined autoclave and heated at 80℃ for 24 h. After heating, the autoclave was cooled and the mixture filtered and washed with ethanol, methanol or DMF before drying in oven at 60 ^oC overnight.

d) ***MIL-68(Sc)*** : The MOF with formula $Sc(OH)(C_8H_4O_4){\cdot}0.3DMF$ was prepared for first time by solvothermal reaction of scandium chloride (0.46 mmol) and terephthalic acid (0.46 mmol) in DMF (3.0 mL), H_2O (water, 5.0 mL), and EtOH (ethanol, 5 mL) heated at 90 ℃ for 12 h in a Teflon-lined Parr autoclave. After the heating time, the autoclave was cooled and the mixture is filtered, washed with ethanol and dried overnight at 60 ℃.

e) ***MIL-88D(Sc)***: $Sc_3O(OH)(H_2O)_2(C_{14}H_8O_4)_3$ Two samples were synthesised, *"sample a"* using $Sc(NO_3)_33{\bullet}H_2O$ (0.60 mmol) and *"sample b"* prepared with $ScCl_{3aq}$ (0.50

mmol, 1.45 M). In each synthesis 0.50 mmol of BPDC (Aldrich 97%) was added into DMF (10 mL) and heated at 110 ℃ for 72 h. The resulting solid was washed with DMF followed by ethanol and dried at 60 ℃ for 12 h.

f) ***MIL-101(Cr):*** The synthesis of MIL-101(Cr) with formula $Cr_3O(OH)(H_2O)_2(C_8H_4O_4)_3$ (as a comparison for catalysis) was carried out using $CrCl_3$ (0.4 mmol; Aldrich, 98 %), water and terephthalic acid (BDC, 0.7 mmol; BDH chemicals 97 %) using the synthetic conditions in Table 3.2. The solution was mixed and stirred then transferred to a Teflon-lined autoclave and heated at 220 ℃ for 8 h. After the heating time, the autoclave was cooled and the mixture is filtered, washed and dried overnight at 60 ℃. To remove unreacted terephthalic acid MIL-101(Cr) was sonicated in suspension with DMF for 1 hour at 65 ℃.

g) ***MIL-100(Cr)***: The synthesis of MIL-100 (Cr) $Cr_3O(OH)(H_2O)_2(C_9H_3O_6)_2$ was prepared via a mixture of chromium oxide (Cr_2O_3 , 0.5 mmol; Aldrich 98%), trimesic acid (0.4 mmol; Aldrich 95%) and hydrofluoric acid (5 M, 1 mL) in water (22.5 mL), which was heated to 220℃ for 4 days in Teflon-lined autoclave and then cooled to room temperature. The green precipitate was collected and washed with water then dried overnight at 60℃.

3.2.1.2 Preparation of scandium-exchanged zeolites Y and Beta

Zeolite Na-Y (Si/Al=2.49) was repeatedly ion-exchanged with an aqueous 3.0 M NH_4Cl solution under reflux conditions and subsequently thoroughly washed with distilled water. Then zeolite NH_4Y (1 g, 3.9 mmol of Al) was exchanged with Sc^{3+} using $Sc(NO_3)_33{\bullet}H_2O$ (1.32 mmol) in 100 mL of water, at room temperature for 24 h. Then it was filtered, and the recovered zeolite material was washed. The ion-exchange procedure was repeated 3 times in this case. Zeolite H-Beta (0.23 g; Zeolyst CP811E-22 H-Beta, Si/Al=17) was exchanged four

times with Sc^{3+} using $Sc(NO_3)_3$ (0.009 M) at room temperature for 24 h. The concentration of scandium in the ion-exchange zeolites was measured by EDX.

3.2.1.3 Encapsulation of POM into scandium MOFs via direct synthesis.

The synthesis of scandium MOFs with the addition of different quantities of phosphotungstic acid monohydrate (PTA) or phosphomolybdic acid monohydrate (PMA) was explored in this experiment. The scandium MOFs, MIL-100(Sc), MIL-101(Sc) and MIL-88D(Sc) were chosen because their cages are accessible through microporous windows and channel (MIL-88D) of about 12 and 16 Å. The synthesis involves dissolution of the ligand (BTC, BDC or BPDC) and the scandium chloride together with the addition of POM (PTA or PMA), and the reaction mixture was transferred in a Teflon-lined autoclave and heated at the synthetic conditions previously stablished for the relevant MOF preparation (Table 3.2).

Table 3.3 lists the POMs used in each MOF. As an example synthesis of POM (PTA) in MIL-101(Sc), a successful encapsulation in this work involves the use of terephthalic acid (BDC, 0.64 mmol), $ScCl_3$ solution (0.58 mmol, 1.45 M) and 0.048 mmol of PTA, all together in in a solvent mixture DMF (4 mL) and EtOH (5 mL). The resulted mixture was heated in a Teflon lined steel autoclave at 80 ℃ for 24 h. From the chemical formula of POM, it has 12 atoms of W (tungsten) in PTA or Mo (molybdenum) in PMA, so for the synthesis describe above PTA/MIL-101(Sc), Sc^{3+} (0.58 mmol, 1.45 M) and PTA (0.048 mmol) the theoretical molar ratio PTA to scandium (PTA/Sc) was 0.083 and so on for the other experiments. Several theoretical molar ratios (POM/Sc) were explored in a range between 0.02 – 0.083 for POM encapsulation in MIL-101(Sc).

In the case of MIL-100(Sc), synthesis involves trimesic acid (0.4 mmol), $ScCl_3$ (0.9 mmol, 1.45 M) and addition of POM (PTA or PMA) in a theoretical molar ratio (POM/Sc) range 0.025-0.083, in DMF (10 mL) and heated at 150 ℃ for 48 h, solids were washed with

methanol and dried overnight at 60 ℃. Encapsulation of POMs into MIL-88D(Sc), which was prepared using 0.50 mmol of biphenyl-4,4′-dicarboxylic acid (BPDC, 0.5 mmol; Aldrich 97%), $ScCl_3$ (0.50 mmol, 1.45 M) and POM (PTA or PMA) in a M.R. (POM/Sc) range 0.02-0.083, all together added into DMF (10 mL) and heated at 110 ℃ for 72 h. After heating, the autoclaves were cooled and the mixture filtered, washed with methanol and dried at 60℃

Table 3.3: MOFs used in encapsulation experiments. POM= PTA (phosphotungstic acid monohydrate) and PMA (phosphomolybdic acid monohydrate), (diameter of POM 13–14 Å). $ScCl_3$ solution (1.45 M) was used with the respective linker according table 3.2. M.R (Molar Ratio).

MOF	POM	Amount of POM (mmol)	Theoretical M.R. (POM/Sc)
MIL-100(Sc)	PTA	0.016-0.05	0.033-0.083
	PMA	0.016-0.05	0.025-0.04
MIL-101(Sc)	PTA	0.016-0.05	0.025-0.083
	PMA	0.016-0.05	0.025-0.083
MIL-88D(Sc)	PTA	0.01-0.05	0.020-0.04
	PMA	0.02-0.05	0.038-0.083

3.2.2 Catalytic tests

MOFs were activated in different ways. For MIL-88B and MIL-100(Sc), methanol was used to remove DMF from the pores. Samples were soaked in MeOH for 24 h, filtered and dried at 60 °C for 12 h. Activation of the other scandium MOFs and POM/MOFs involve the same condition used prior to N_2 adsorption measurements, i.e. heating the sample in a furnace under an inert atmosphere in a temperature range of 60-120 ^{o}C. In the case of the zeolites, these were activated by heating under inert atmosphere (nitrogen) at 550^{o}C. For chromium MOFs the activation was performed according to the literature, (heated under solvothermal conditions for 12 h at 90 °C in EtOH (20 mL) and further washed using a solution of NH_4Cl),[30, 31]

3.2.2.1 The carbonyl ene reaction

Scandium and chromium MOFs, scandium-exchanged zeolites and POM-loaded MOFs were tested as catalysts in the intermolecular carbonyl ene reaction between ethyl trifluoropyruvate and α-methyl styrene, stirred under N_2 for 8 h. The amount of the MOF used to catalyse the reaction was based on mol% metal cation within the MOF in order to eliminate any differences in the ligand weight. The product and substrate contain fluorine so this allowed the reaction to be monitored by ^{19}F NMR. Scheme 3.4 shows the chemical shift **δ** -76.2 ppm, whilst another at **δ** -78.9 ppm corresponds to that of the product. A hydration by-product has a chemical shift at **δ** -82.9 ppm and an unidentified resonance at 83.5 ppm was also observed in some cases, particular in zeolites with high percent.

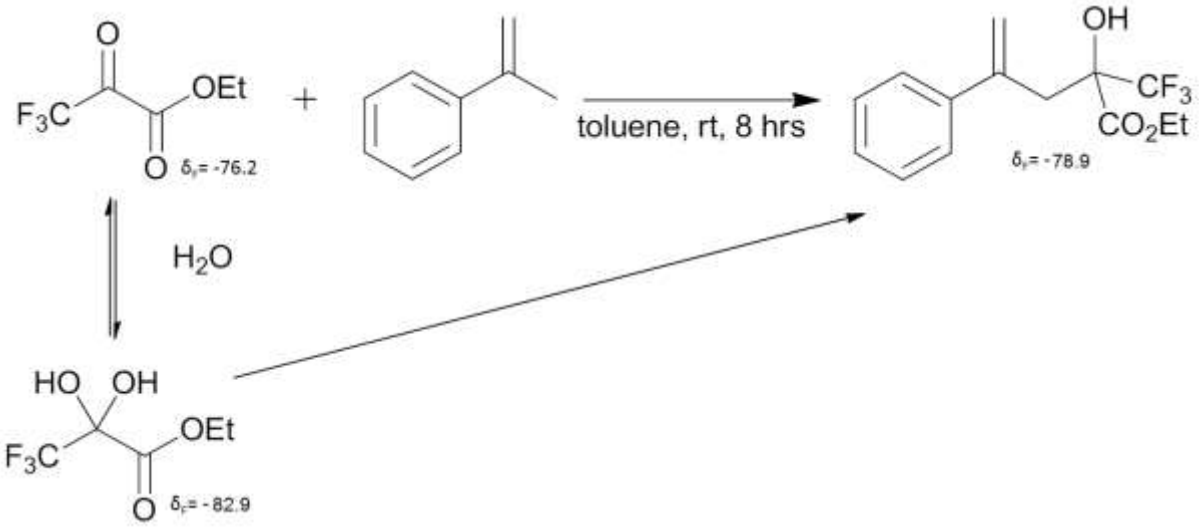

Scheme 3.4: Intermolecular carbonyl ene reaction between ethyl trifluoropyruvate and α-methyl styrene stirred under N_2 for 8 h, and ^{19}F NMR shifts of ethyl trifluoropyruvate, its hydration product and the ene product.

The reaction was performed under an inert atmosphere (dry N_2) to avoid the formation of a hydrate of ethyl trifluoropyruvate as far as possible. Liquid samples were taken from the settled reaction mixture, and filtered into an NMR tube with a d_6-benzene reference.

3.2.2.2 Acetalization of benzaldehyde and acetophenone

The acetalization of benzaldehyde and acetophenone was carried out with scandium-bearing MOFs as catalysts, using methanol as the reactant. MOFs were activated before the catalyst test. Catalytic reactions were carried out using the following the procedure: the required amount of activated catalyst (2.5% MOF) was placed in a 25 mL round-bottomed flask, aldehyde (1 mmol) or ketone (1 mmol) was added under N_2 flow and the substrate methanol (10 mmol), and addition of nitrobenzene as internal standard. The resulting suspensions were magnetically stirred at room temperature. Scheme 3.5 shows the general acetalization reaction. The reaction was monitored by GC, as samples of the solution were taken at intervals and the conversion and selectivity measured by following the yield of the desired product. (See chapter 2 for a typical GC trace).

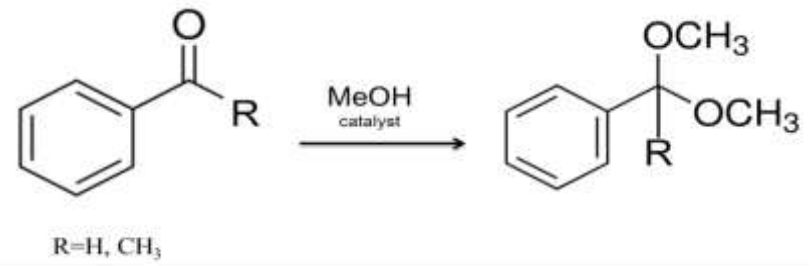

Scheme 3.5: Acetalization of benzaldehyde (R=H) and for acetophenone ($R=CH_3$).

3.3 Results and discussions of synthesis and characterisation of materials

The results discussed in this part focus in the synthesis of all materials for testing as catalysts. There are three sections, which are the synthesis of metal-organic frameworks (MOFs) using scandium and chromium, followed by results for scandium exchange in zeolites and finally the discussion of encapsulation of polyoxometalates in selected MOFs such as MIL-101(Sc), MIL-88D(Sc) and MIL-68(Sc).

3.3.1 Synthesis of known and novel Scandium MOFs

3.3.1.1 MIL-100(Sc), $Sc_3O(OH)(H_2O)_2(C_9H_3O_6)_2$

The solid obtained were identified as MIL-100(Sc) by powder X-ray diffraction (PXRD) (Figure 3.3). The reported structure of MIL-100(Cr)[29], was used and modified to simulate an expected pattern for MIL-100(Sc) by substitution of Sc for Cr and using the refined unit cell parameter, and confirmed assignment of the product as MIL-100(Sc).

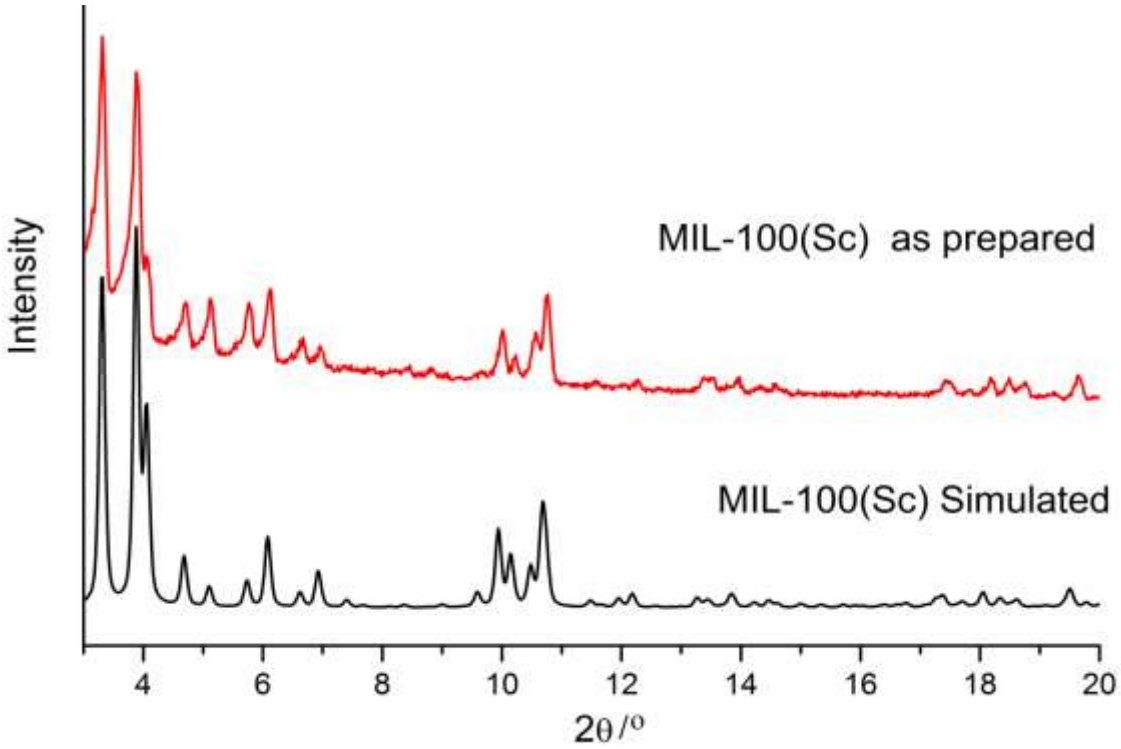

Figure 3.3: Comparison of experimental PXRD of as-prepared MIL-100(Sc) with that simulated for MIL-100(Sc).

Thermogravimetric analysis (TGA) of the sample showed a 15% weight loss up to 350 ℃ attributed to loss of residual solvent (Figure 3.4). N_2 adsorption isotherms shows a type 1/VI (Figure 3.5) with the presence of cages in the mesoporous regime. The material demonstrated BET surface area of 1385 m^2g^{-1} and pore volume 0.693 cm^3g^{-1}, close to that observed for MIL-100(Sc) synthesized by Mowat et al. (0.72 cm^3g^1). EDX analysis confirmed the presence of scandium in the MOF, Sc expected 21.80 wt %; 22.07 wt% measured. CHN

analysis on sample gives: C expected 34.97 wt% ; 34.51 wt% measured. N expected 0; 0.0 wt% measured.

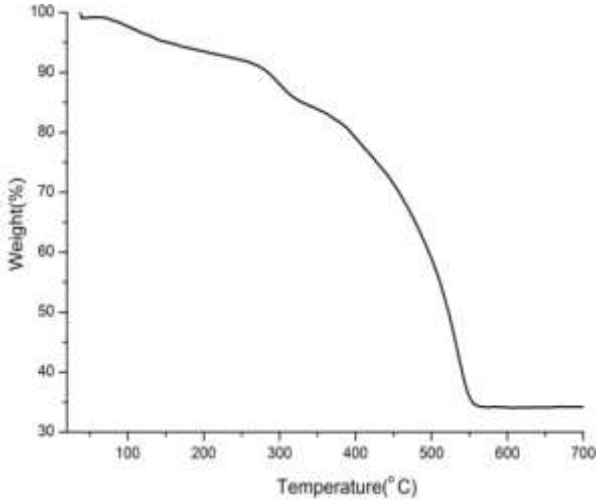

Figure 3.4: Thermogravimetric analysis of MIL-100(Sc) in flowing air.

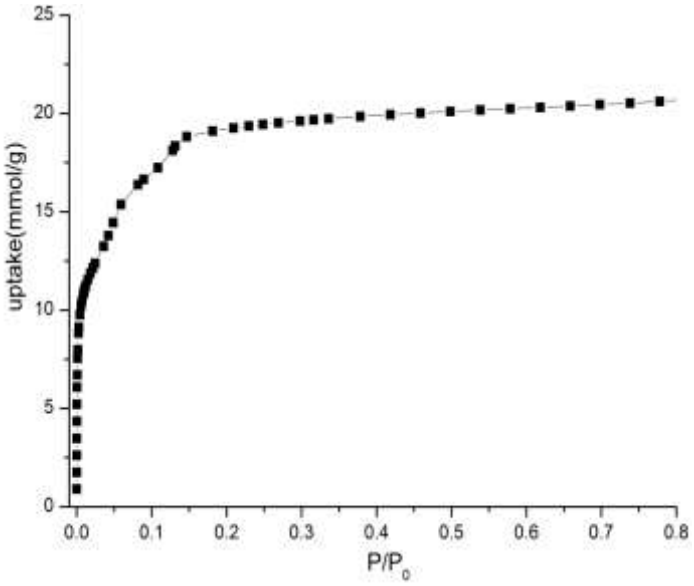

Figure 3.5: Nitrogen adsorption isotherm of MIL-100(Sc) measured at -196 ℃.

3.3.1.2 MIL-88B(Sc), $Sc_3O(OH)(H_2O)_2(C_8H_4O_4)_3$

Identification of the product phase was achieved by powder X-ray diffraction. In Figure 3.6 the PXRD patterns for MIL-88(Sc) samples are compared to the theoretical pattern from the published structure for MIL-88B(Sc).[28] The patterns obtained after washing with DMF and overnight drying at 60 ℃ (b) and of the dried sample washed thoroughly with methanol (c)

are compared with that of the simulated pattern (a). MIL-88(Sc) is an example of solid that shows marked breathing upon adsorption and desorption so that its diffraction pattern is strongly influenced by its state of solvation. The diffraction pattern of the sample washed with methanol and dried was indexed and shows that this MOF material exhibits the hexagonal symmetry and space group ($P\bar{6}2c$: a = 11.116 Å, c = 19.263Å), similar to that reported for MIL-88B(Cr), as-synthetized which is the solvated form, with guest species (pyridine) into the cages and the symmetry $P\bar{6}2c$: a = 11.028 Å, c = 18.972Å.[32]

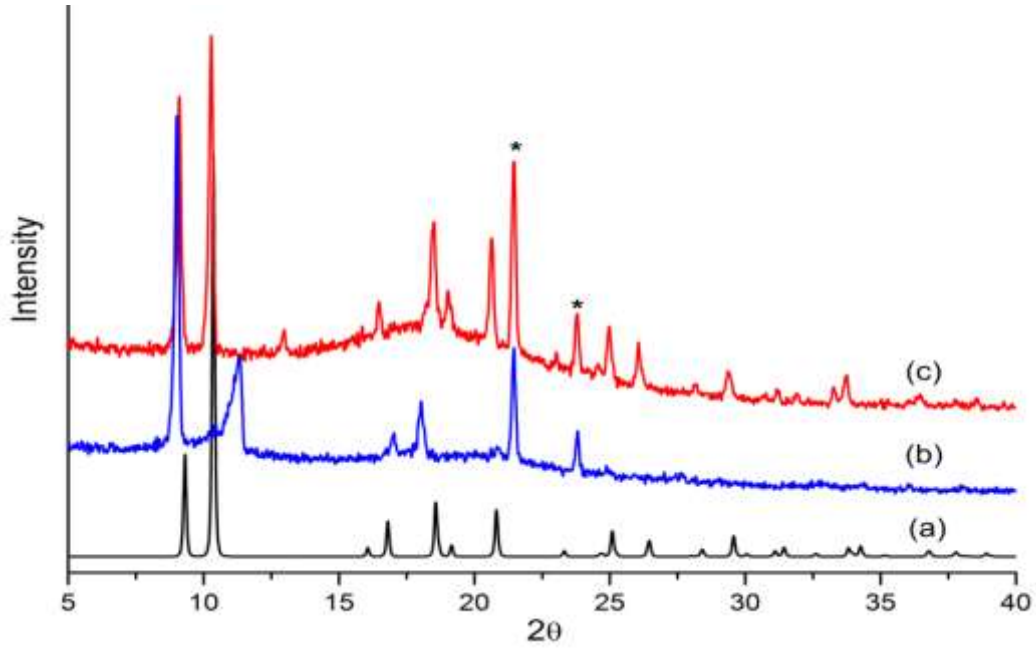

Figure 3.6: PXRD of MIL-88B(Cr); simulated (a), as- prepared (b) and washed with MeOH(c).* Diffractometer peaks.

This suggests that the topology of the framework is maintained while undergoing a large swelling effect. Figure 3.7 shows the structural swelling behaviour of MIL-88B.

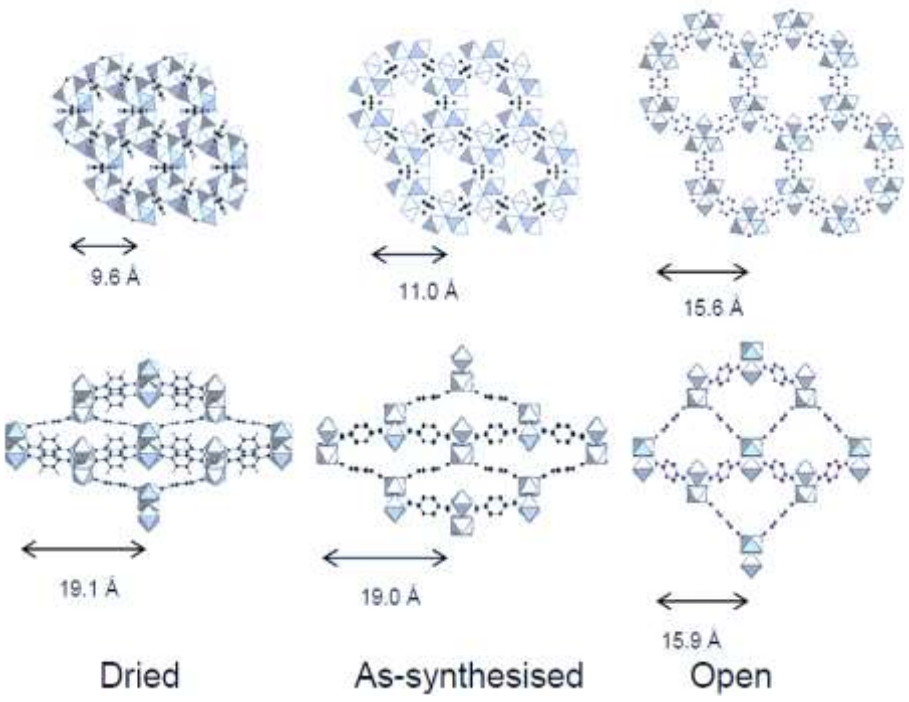

Figure 3.7: Structures of MIL-88B in its dry, as-synthesized and open forms; top: along the *c* axis; bottom: along the *a* axis. Reprinted with the permission of the American Association for the Advancement of Science.[33]

TGA analysis of the sample showed a weight loss of around 12% up to 300 ℃ attributed to the slow release of water or solvent molecules trapped in the cages within the structure (Figure 3.8, left). Nitrogen adsorption analysis demonstrated that MIL-88B(Sc) has isotherm type 2 characteristic of non-porous materials so it was not accessible to gas. The BET surface area of only 27 m^2g^{-1} (Figure 3.8, right), indicating that MIL-88(Sc) is in the closed form when heated under vacuum, and does not adsorb N_2. EDX analysis on MIL-88(Sc) confirmed the presence of metal in the MOF, Sc expected 19.37 wt%; 15.38 wt% measured. Elemental analysis on sample gives: C expected 41.40 wt%; 38.64 wt% measured, N measured 0.0 wt %.

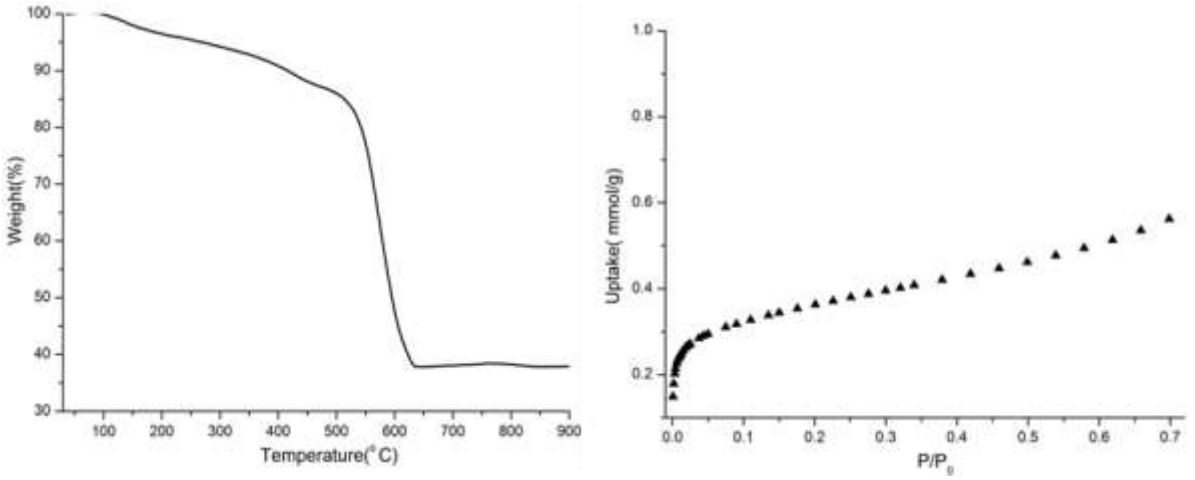

Figure 3.8: (Left) Thermogravimetric analysis of MIL-88(Sc) in flowing air and (right) isotherm for N_2 adsorption measured at -196 ℃ on MIL-88B(Sc).

3.3.1.3 MIL-101(Sc), $Sc_3O(OH)(H_2O)_2(C_8H_4O_4)_3$

Identification of the product phases was achieved by powder X-ray and comparison of the profile with a simulated pattern. The simulated pattern for MIL-101(Sc) was obtained using the reported structure of MIL-101(Cr) as model. Substitution of Sc for Cr gave the expected pattern for MIL-101(Sc) (Figure 3.9). TGA analysis of the sample showed an 18 % weight loss up to 300 ℃ (Figure 3.10). Elemental analysis on sample gives: C expected 41.40 wt%; 38.08 % wt measured, N measured 0.0 wt%.

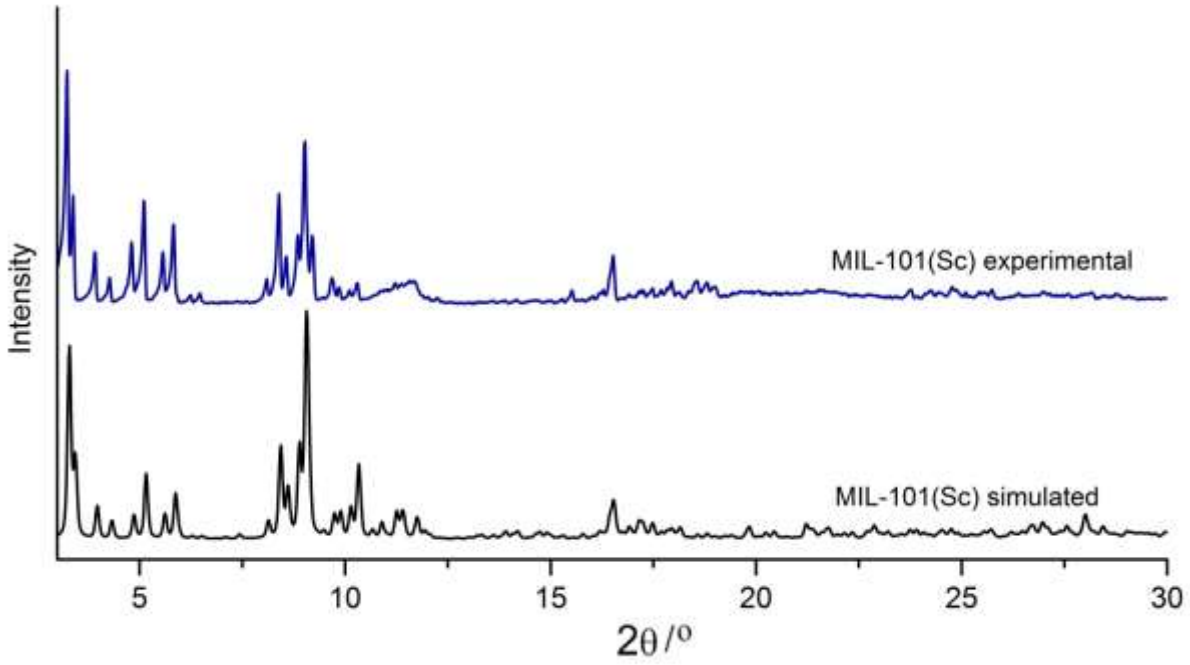

Figure 3.9: PXRD simulated pattern of MIL-101(Sc) below and as-prepared MIL-101(Sc).

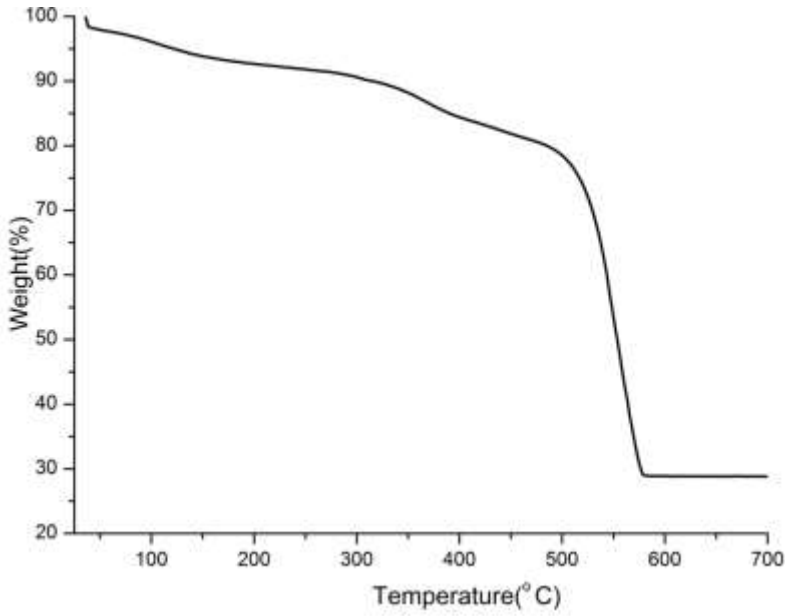

Figure 3.10: TGA of MIL-101(Sc) in flowing air.

For gas adsorption analysis, the samples were outgassed at 60 ℃ for 4 h under vacuum. Type I isotherms for N_2 adsorption demonstrated that the solids are microporous of which the steep increase of adsorbed quantity at low relative pressure indicates the available microporous volume.

When the sample was washed with DMF and degassed at 60 ℃ it exhibits 640 m^2g^{-1} surface area but when the sample was outgassed at120 ℃ the surface area was reduced to 160 m^2g^{-1}. The surface area of the sample washed with methanol and treated at 120 ^oC is 452 m^2g^{-1} in contrast to that washed with ethanol and degassed at 120 ℃, which gave a BET surface area of 155 m^2g^{-1}. The summarised data of this analysis is given in Table 3.4 and isotherms are shown in Figure 3.11.

Table 3.4: N_2 adsorption for MIL-101(Sc) washed with different solvents and degassed at different temperatures.

Solvent	**BET surface (area m^2g^{-1}) outgassing (at 60 ℃)**	**Solvent**	**BET surface area (m^2g^{-1}) outgassing(at 120 ℃)**
Ethanol	190	**Ethanol**	155
Methanol	540	**Methanol**	452
DMF	640	**DMF**	160

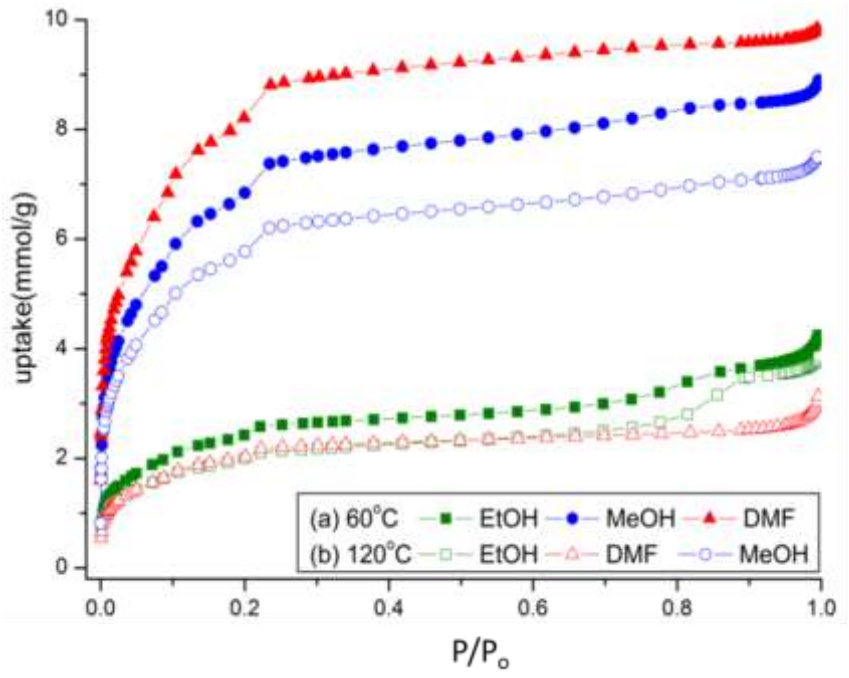

Figure 3.111: Isotherms for N_2 adsorption measured at -196 ℃ on MIL-101(Sc), degassed at 60 ℃ (a) and 120 ℃ (b).

PXRD measured after adsorption analysis and prolonged exposure to air demonstrated loss of crystallinity and recrystallization into MIL-88B(Sc) (Figure 3.12). The much lower stability of MIL-101(Sc) than MIL-101(Cr) is likely to be a result of the faster ligand exchange expected for Sc^{3+} than for the kinetically inert Cr^{3+}.

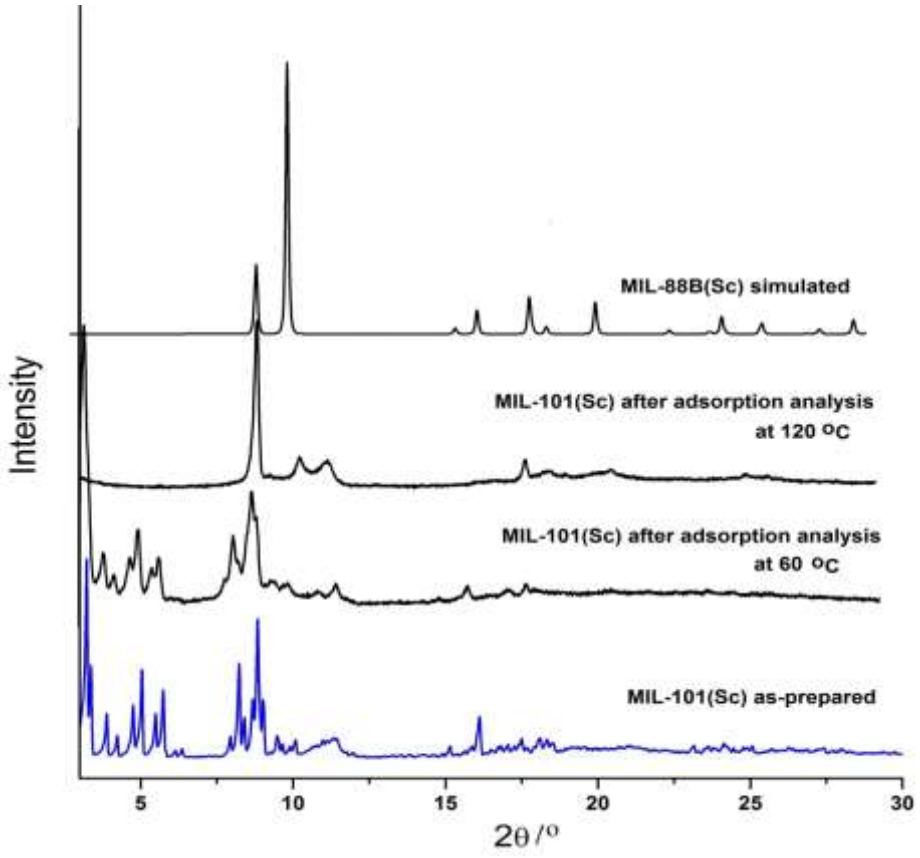

Figure 3.12: PXRD patterns: as-prepared MIL-101(Sc), MIL-101(Sc) sample after treatment at 60℃ and 120℃. Upon heating MIL-101(Sc) recrystallises into MIL-88B(Sc).

3.3.1.4 MIL-68(Sc), $Sc(OH)(C_8H_4O_4)$

In attempts to obtain pure MIL-101(Sc), the scandium analogue of the MOF known as MIL-68 was prepared for the first time. MIL-68 has previously been obtained with vanadium, gallium, indium, iron and aluminium.[23-26] The solid crystallised as acicular crystals > 100 μm long that were suitable for single crystal analysis (Figure 3.13). TGA (Figure 3.14) indicates

the structure loses around 8 wt% solvent before the major weight loss starts at 400℃, corresponding to the carboxylate decomposition.

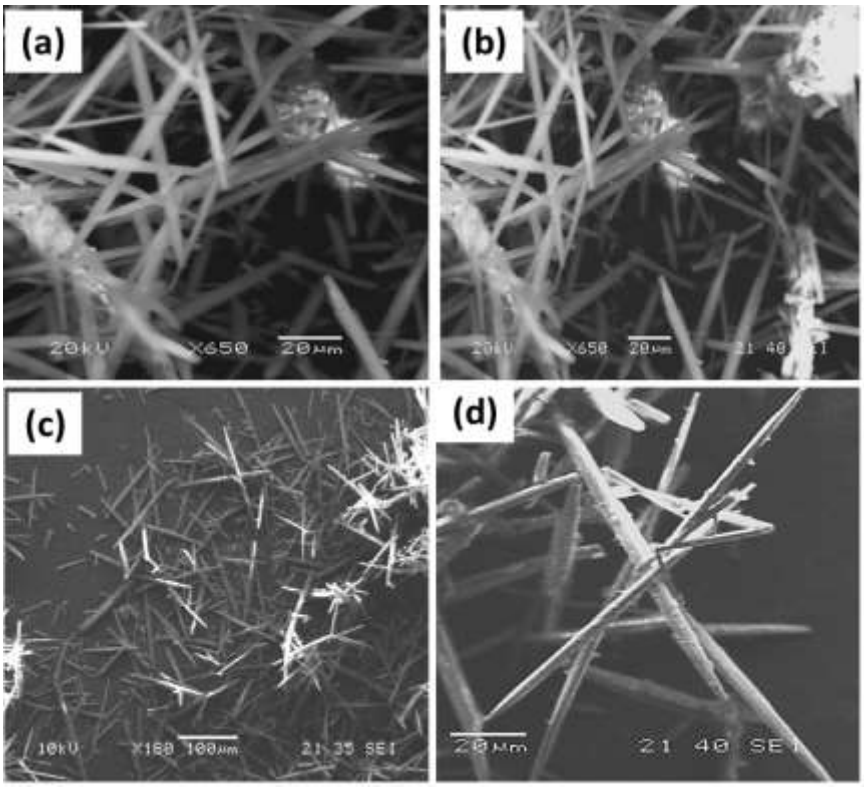

Figure 3.132: SEM images of MIL-68(Sc) needle-shaped crystals.

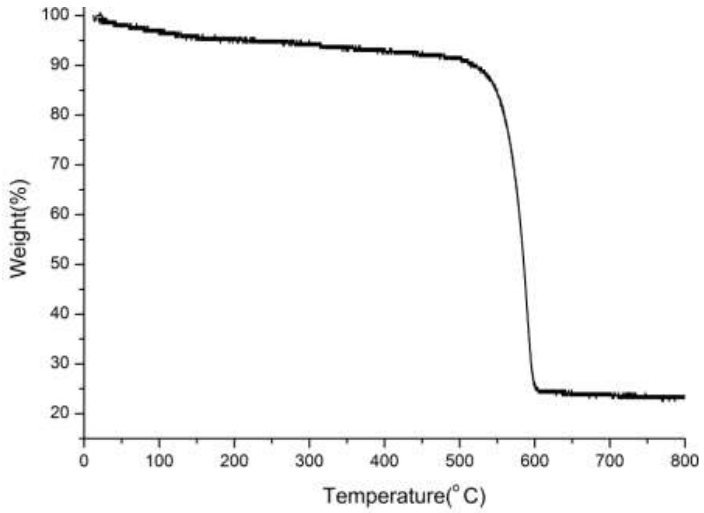

Figure 3.143: TGA of as-prepared MIL-68(Sc).

Figure 3.15 shows the experimental powder diffraction pattern of MIL-68(Sc) compared to the pattern simulated from the partial solution of the structure from single crystal data. The material crystallizes in the orthorhombic space group *Cmcm* with unit cell parameters of *a* =

21.577(7) Å, *b* = 37.523(11) Å, *c* = 7.320(2) Å, but the data was not of sufficent quality to complete the refinement (wR = 24.5%). Instead, the single crystal structure was used as a starting model that was Rietveld refined against laboratory powder diffraction using the GSAS suite of programs, and using constraints to maintain the framework with chemically reasonable distances.

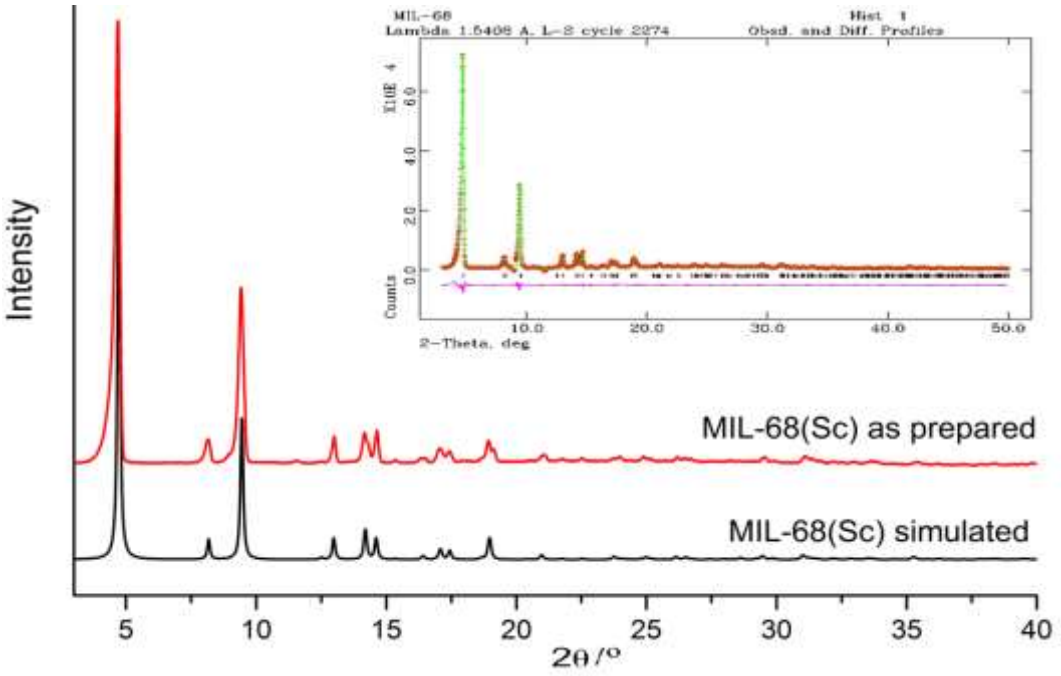

Figure 3.15: PXRD simulated pattern of MIL-68(Sc) and as prepared MIL-68(Sc), (inset) Rietveld refinement of MIL-68(Sc).

MIL-68 has a framework structure containing a three-dimensional network with infinite chains of octahedral units. Some extra-framework scattering was located in the narrow channel of MIL-68(Sc) in positions reported by Volkringer *et al.* for DMF molecules in MIL-68(In). A satisfactory fit to the data was achieved confirming the structural assignment (R_{wp} = 5.2%, R_p = 3.8%, Table 3.5). Figure 3.16 shows the framework structure of MIL-68(Sc) obtained by single crystal analysis. The Sc^{3+} cations are present in chains of $ScO_4(OH)_2$ corner-sharing octahedra linked through the terephthalate ligand, delimiting triangular and hexagonal channels (window diameters 16 Å) (CIF file available in Appendix A).

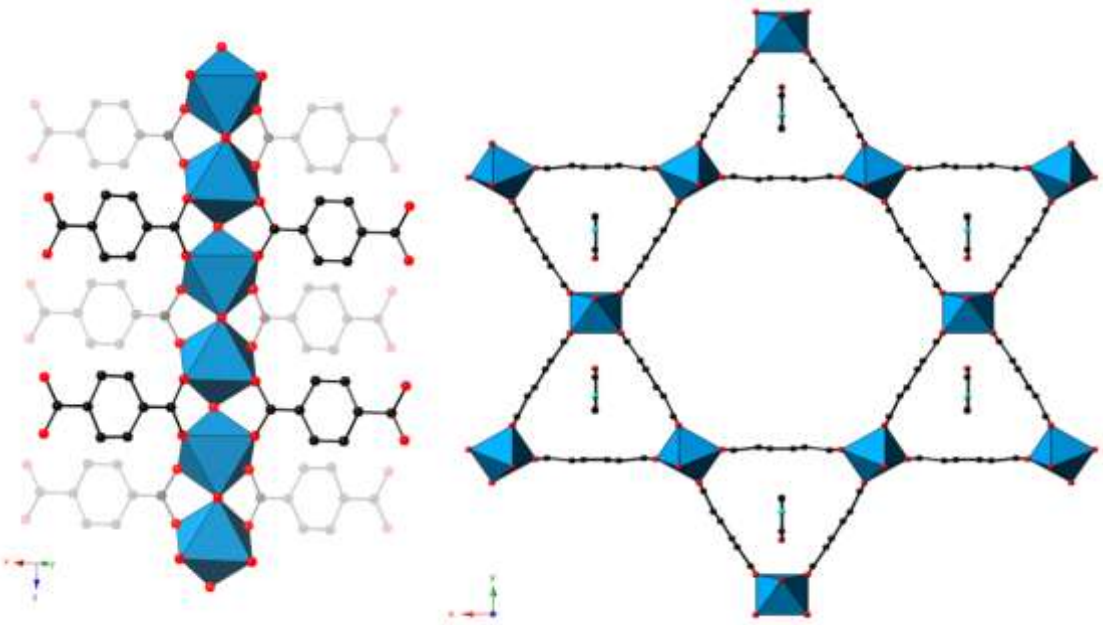

Figure 3.16: The framework structure of as-prepared MIL-68(Sc), $Sc(OH)(O_2CC_6H_4CO_2)$, (left) showing the chains of corner-sharing $ScO_4(OH)_2$ octahedra and (right) viewed down its channel axis, with the position of an extraframework DMF molecule shown.

Table 3.5: Structural data from Rietveld refinement on MIL-68(Sc)

Structure	**MIL-68(Sc)**
Formula unit	$Sc(OH)(O_4H_4C_8)$•0.3DMF
Crystal system	Orthorhombic
Space group	*Cmcm*
X-ray source	Cu $K\alpha_1$
Diffractometer	
Wavelength (Å)	1.54056
Unit cell (Å)	
a/Å	21.6834(12)
b/Å	37.0259(23)
c/Å	7.2956(3)
α/°	90
Volume/$Å^3$	5857.2(7)
R	0.0380
R_w	0.0525

Chemical analysis of as-prepared MIL-68(Sc), assuming inclusion of DMF as reported in the indium analogue was responsible for all the N in the solid, suggests a composition

Sc(OH)(BDC)•0.3DMF (calculated C, 43.0 wt%; H, 2.9%; N 1.9%: measured C, 45.2%; H 2.5%, N 1.9%). Only a small fraction of the estimated DMF was located by diffraction, presumably due to disorder. The adsorption properties of the material were studied using nitrogen and carbon dioxide adsorption. N_2 adsorption at -196℃ was performed on a heated (200 ℃) sample re-activated at 120℃ under vacuum for 4 h. MIL-68 has a large micropore opening (16 Å), however MIL-68(Sc) gave a BET surface area of only 202 m^2g^{-1} (3 $mmolg^{-1}$, pore volume of 0.1 cm^3g^{-1}) much lower than expected from the crystal structure uptake, and much lower than that reported from N_2 adsorption for MIL-68(Ga) 1117 m^2g^{-1}, pore volume of 0.46 $cm^3\ g^{-1}$).[24] Nevertheless, when CO_2 is used as the adsorbate, a type V isotherm is noticed in Figure 3.17 (A-2 sample re-activated at 200 ℃ under vacuum for 8 h), in which a step or an inflection point can be observed. The presence of the inflection point in isotherms could be attributed to filling of the large pore by CO_2 molecules.

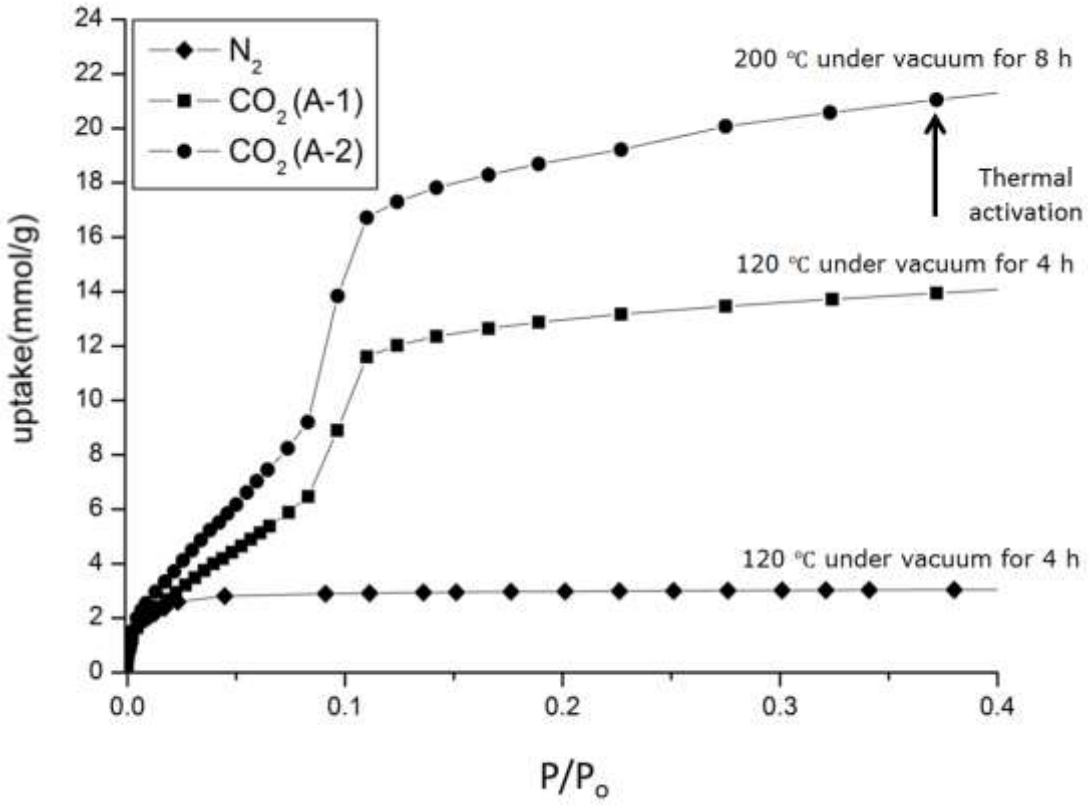

Figure 3.174: N_2 and CO_2 adsorption isotherms collected on MIL-68(Sc), measured at -196 ^{0}C and -77 ^{0}C respectively.

For a range of other permanently porous solids, our measurements show that the uptake in mmol g^{-1} at pore filling for N_2 (p/p_o = 0.9; T = -196 °C) is *ca*. 1.27× that of CO_2 at pore filling (p/p_o = 0.5, -77 °C), suggesting that the density of CO_2 under those conditions is 1.24× that of liquid N_2, i.e. 1.0 g cm^{-3}. This gives a pore volume of 0.6 and 0.8 cm^3 g^{-1} for A-1 and A-2 respectively as measured by CO_2 adsorption, much higher than measured via N_2 adsorption. It is therefore likely that surface restructuring resulting in pore blocking to N_2 but not CO_2 occurs during activation at 200℃ in vacuum. To confirm that the pores of the as-prepared material were accessible to molecules larger than CO_2, 80 mg of the as-prepared MIL-68(Sc) was immersed in a solution of 0.15 mL of N-(2-hydroxyethyl)ethylenediamine ($C_4H_{12}N_2O$) in 5 mL of toluene. The solid was filtered and dried, and the N content found to increase from 1.9% to 7.7%, indicating uptake of 28 wt% of the amine and confirming the porosity of the unheated sample for relatively large molecules.

3.3.1.5 MIL-88D(Sc), $Sc_3O(OH)(H_2O)_2(C_{14}H_8O_4)_3$

Previously, MIL-88D(Sc) was prepared by Mowat[34] using $Sc(NO_3)_3 \cdot 3H_2O$ as the metal source and the linker biphenyl-4,4′-dicarboxylic acid (BPDC) and N,N-diethylformamide as solvent, however the nitrogen adsorption showed a uptake of 8 mmol g^{-1}, less than predicted for MIL-88D(Sc), so that attempts to improve its porosity were made changing the solvent and metal source. Two samples were prepared ‘sample a’ using $Sc(NO_3)_3$ and ‘sample b’ prepared with $ScCl_{3aq}$. Comparison of powder diffraction pattern for the as-synthesised samples with that simulated pattern from the interpenetrated indium analogue[35] (Figure 3.18), suggests the structure is strongly interpenetrated.

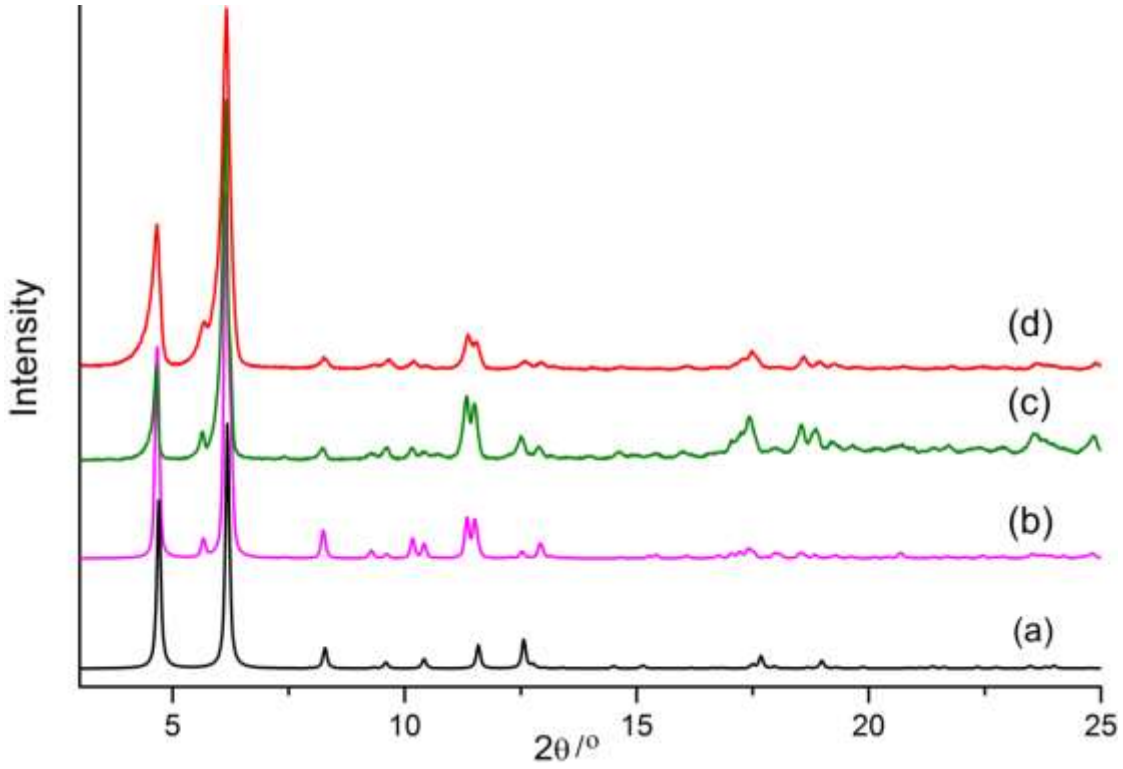

Figure 3.18: PXRD patterns, (a) simulated from non-interpenetrated MIL-88D(Sc), (b) simulated for the interpenetrated MIL-88D(In), (c) as-synthesised MIL-88D(Sc) 'sample a', (d) as-synthesised MIL-88D(Sc) 'sample b'.

TGA (Figure 3.19) of the as-prepared materials indicated 12 wt% loss of water or organic solvent until around 300 ℃ and further removal to 350 ℃ solvent removal before complete decomposition of the material to Sc_2O_3 at 450°C and completed by 600 ℃. Adsorption was carried out with nitrogen and prior to measurements the sample was heated at 120 ^{o}C under vacuum for 4 h. The Type 1 isotherm indicates the material is microporous. Figure 3.20 shows the N_2 adsorption for sample 'a', which gave a BET surface area of 886 m^2g^{-1} and sample 'b' 1243 m^2g^{-1}, the latter being close to that reported for interpenetrated MIL-88D(In).

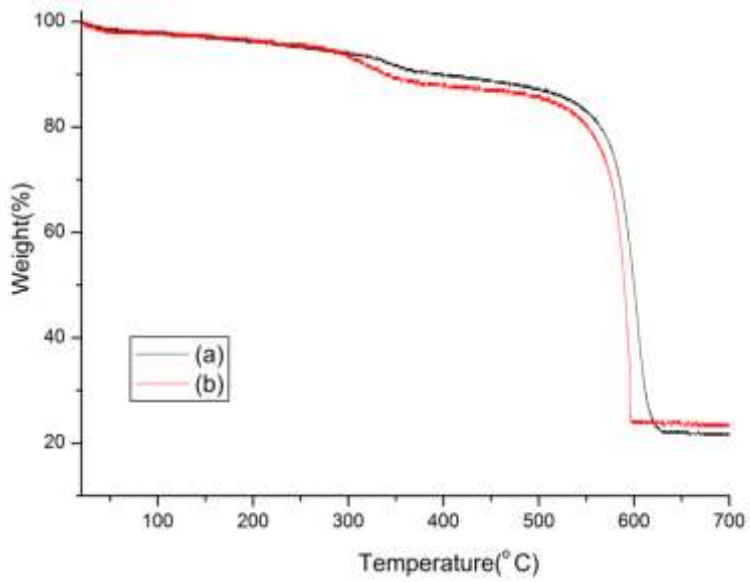

Figure 3.19: TGA of as-prepared MIL-88D(Sc), sample *a* and sample *b*.

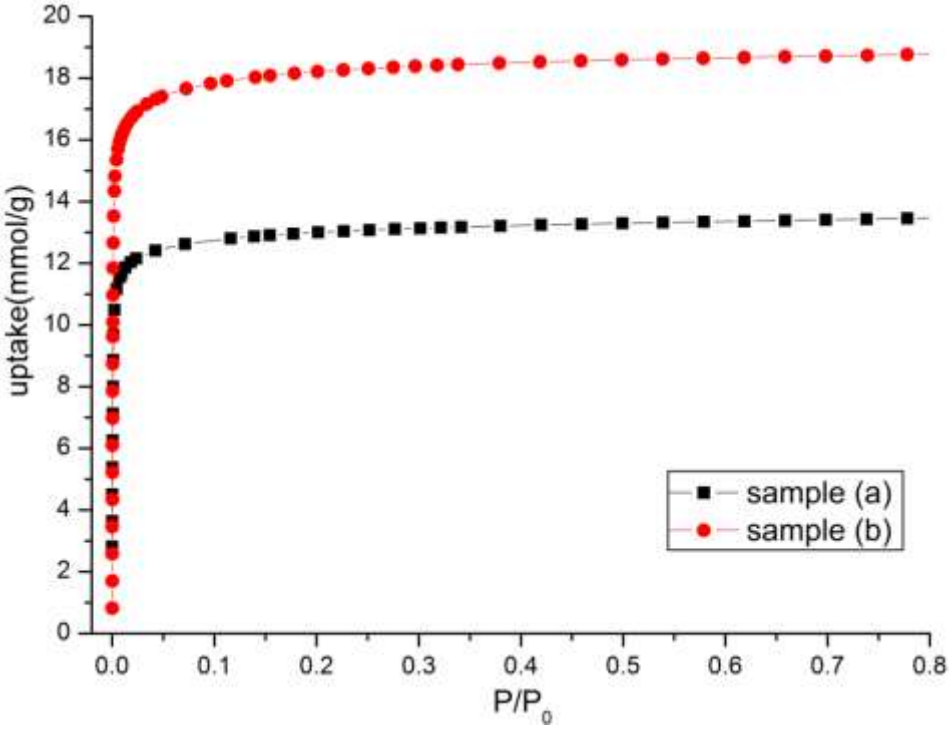

Figure 3.205: N_2 adsorption isotherms collected on two samples of MIL-88D(Sc).

3.3.1.6 MIL-101(Cr), $Cr_3O(OH)(H_2O)_2(C_8H_4O_4)_3$

The green solid obtained was confirmed as MIL-101(Cr) plus residual terephthalic acid (Figure 3.21). After ultrasound treatment the sample showed that the terephthalic acid was removed (Figure 3.21b).

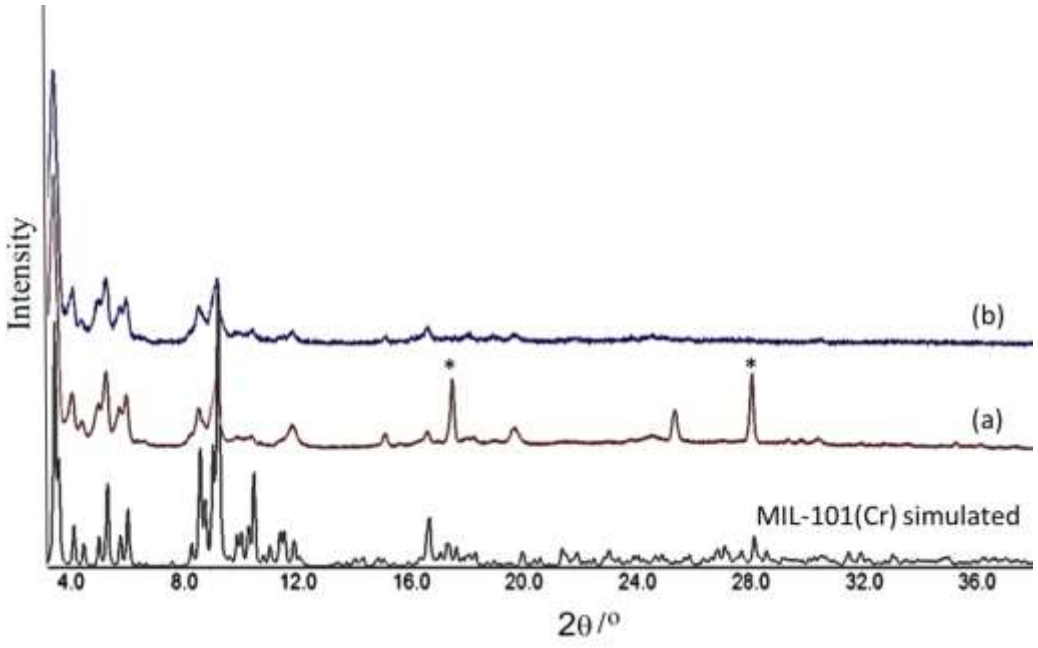

Figure 3.216: PXRD of MIL-101 Cr: simulated pattern, pattern of (a) material as-prepared and (b) sample treated with DMF. *terephthalic acid

TGA (Figure 3.22 left) revealed that MIL-101(Cr) was stable up to 300 ^{o}C with 15 % weight loss. N_2 adsorption (Figure 3.22, right) at -196 ℃ on MIL-101(Cr) indicates a BET surface area of 2162 m^2g^{-1} and pore volume of 1.53 cm^3g^{-1}. The solid has the same porosity as MIL-101(Cr) reported previously by Khan et al [36] for MIL-101(Cr).

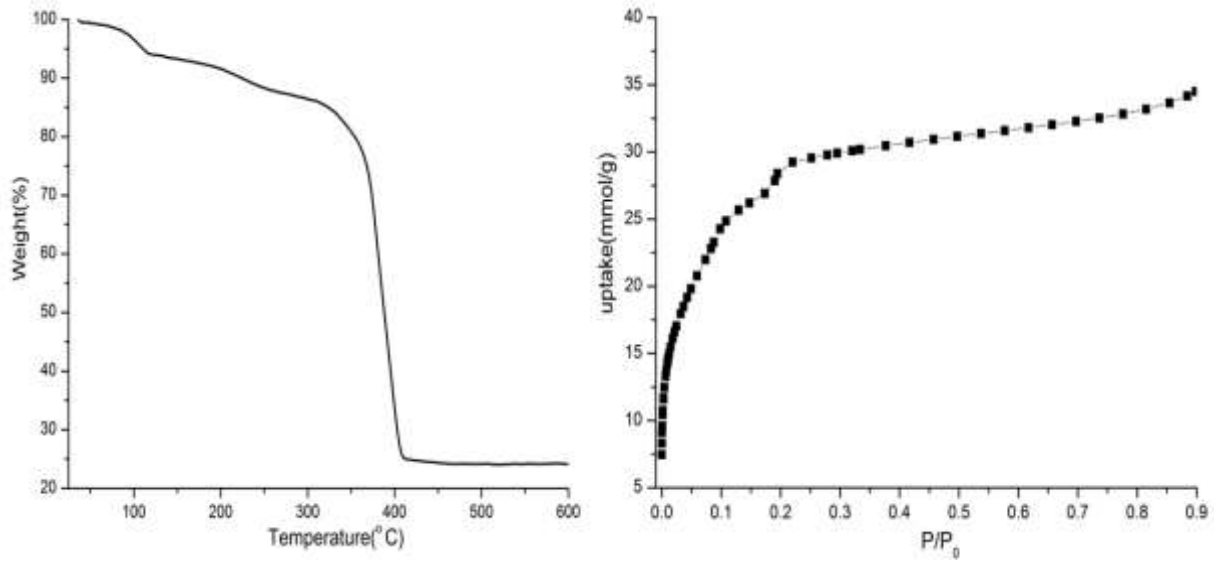

Figure 3.227: (Left) Thermogravimetric analysis of MIL-101(Cr). (Right) N_2 adsorption isotherm measured at -196 ℃.

3.3.1.7 MIL-100(Cr), $Cr_3O(OH)(H_2O)_2(C_8H_3O_4)_3$

The material was characterised by powder X-ray diffraction (PXRD) and this was compared to the theoretical patterns from the published structure (Figure 3.23).

TGA (Figure 3.24, left) revealed that MIL-100 (Cr) showed a 13 % weight loss up to 280 ^oC. Figure 3.24 (right) shows the isotherms for N_2 adsorption at -196 ℃ to MIL-100(Cr) with a BET surface area of 1431 m^2g^{-1} and a pore volume 0.79 cm^3g^{-1}. This pore volume is lower than reported for MIL-100(Cr) of Férey *et al.*, but is similar to that obtained for MIL-100 (Sc) in this work.

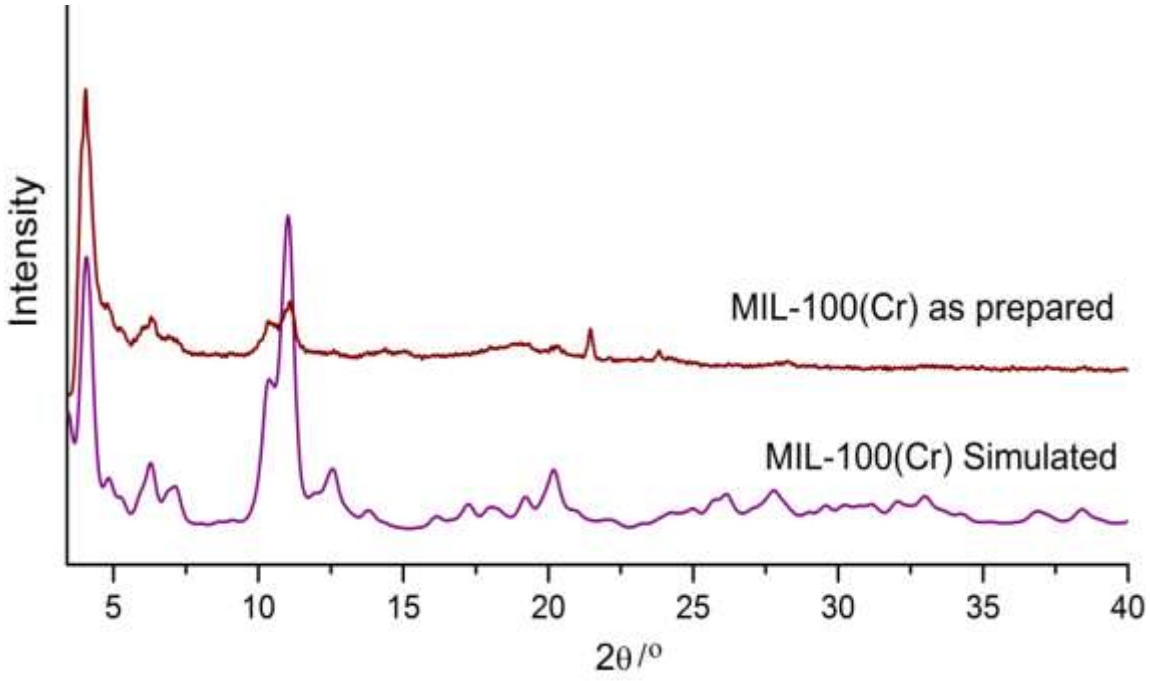

Figure 3.238: PXRD of MIL-100 (Cr): simulated and observed .

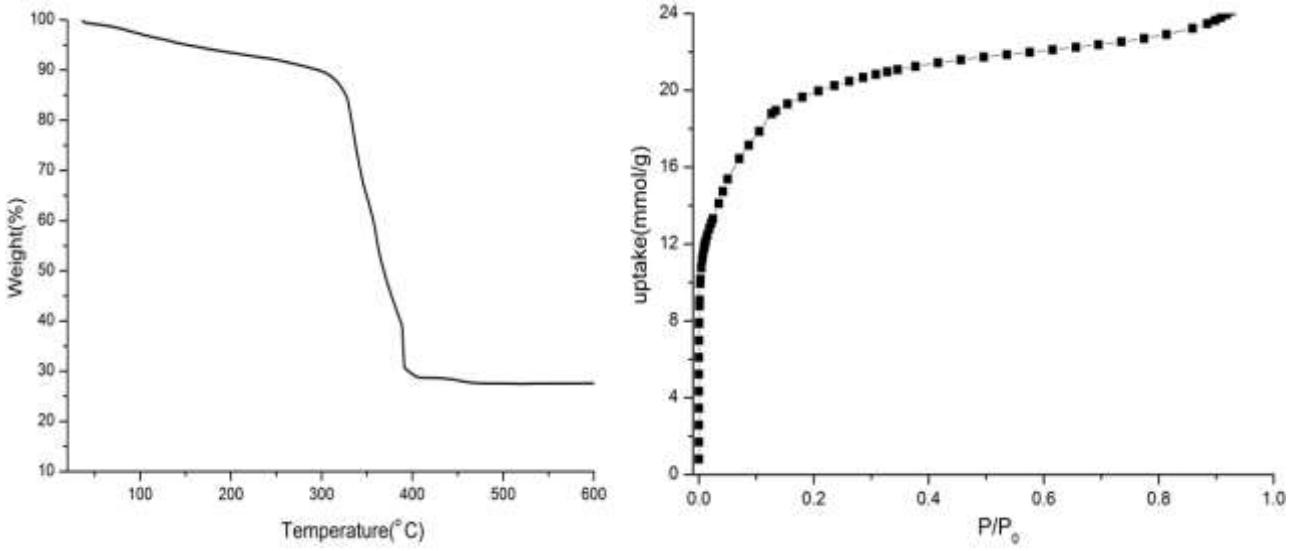

Figure 3.24: (Left) Thermogravimetric analysis of MIL-100 (Cr), (right) Nitrogen adsorption isotherm on MIL-100 (Cr) measured at -196 ℃.

3.3.2 Scandium-exchanged zeolites

Semi-quantitative analysis by EDX (Table 3.6) of the Sc^{3+} zeolite Y indicates almost complete removal of sodium and high scandium content (Figure 3.25). Similarly, Sc^{3+} has successfully been exchanged into zeolite Beta. If the negative charge on the zeolite frameworks due to incorporated Al^{3+} were balanced by cation-exchanged Sc^{3+}, a Sc^{3+}:Al^{3+} ratio of 1:3 would be expected. In both cases (Sc-Y, Sc-Beta) the measured amount of Sc^{3+} is greater than this. This could suggest some over exchange of scandium, with Sc^{3+} cations being associated with hydroxyl groups (e.g. , $[Sc(OH)_2]^+$ or $[Sc(OH)]^{2+}$).

Table 3.6: Elemental composition of scandium-exchanged zeolites.

	Atomic %			
	O	Al	Si	Sc
Sc-Y	54.95	7.95	30.4	6.6
Sc- Beta	61.18	2.025	35.54	1.25

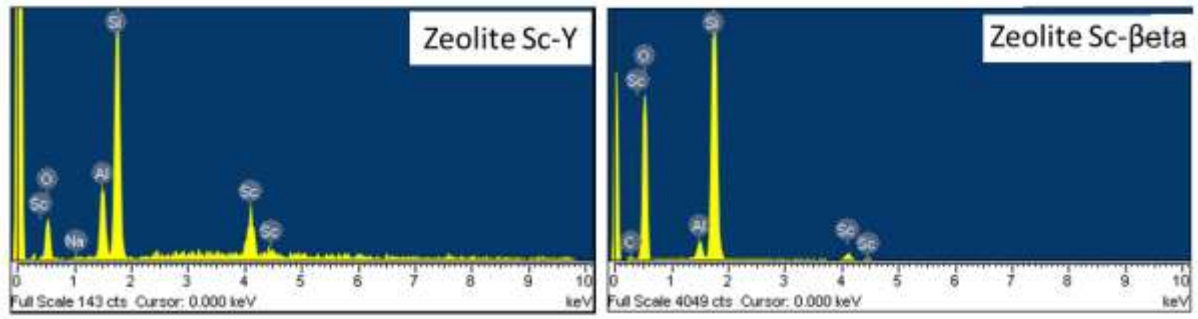

Figure 3.25: EDX spectra of zeolites: (Left) Zeolite Y and (Right) zeolite Beta.

The Sc-Y sample was calcined under air at 550℃ and zeolite Sc- Beta at 350℃ for 12 h respectively. The PXRD of scandium-exchanged zeolites were very similar to the original material (Figure 3.26) and proves the high crystallinity of the material. Adsorption of samples was measured at -196 ℃ and outgassing at 350 ℃ for 8 hours prior to analysis. The N_2

isotherms were reversible and mainly of Type I (with some Type II contribution due to uptake on external surfaces) and showed that the porosity was retained after scandium exchange (Figure 3.27).

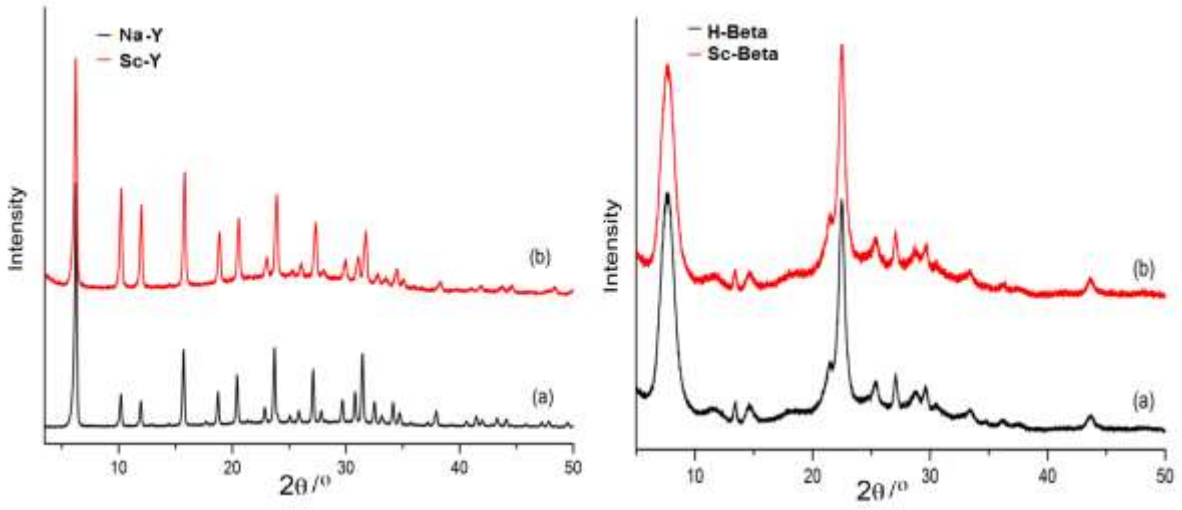

Figure 3.26: PXRD of zeolites: (Left) (a) zeolite Na-Y and (b) Sc- Y; and (right) zeolite H-Beta and (b) Sc-Beta.

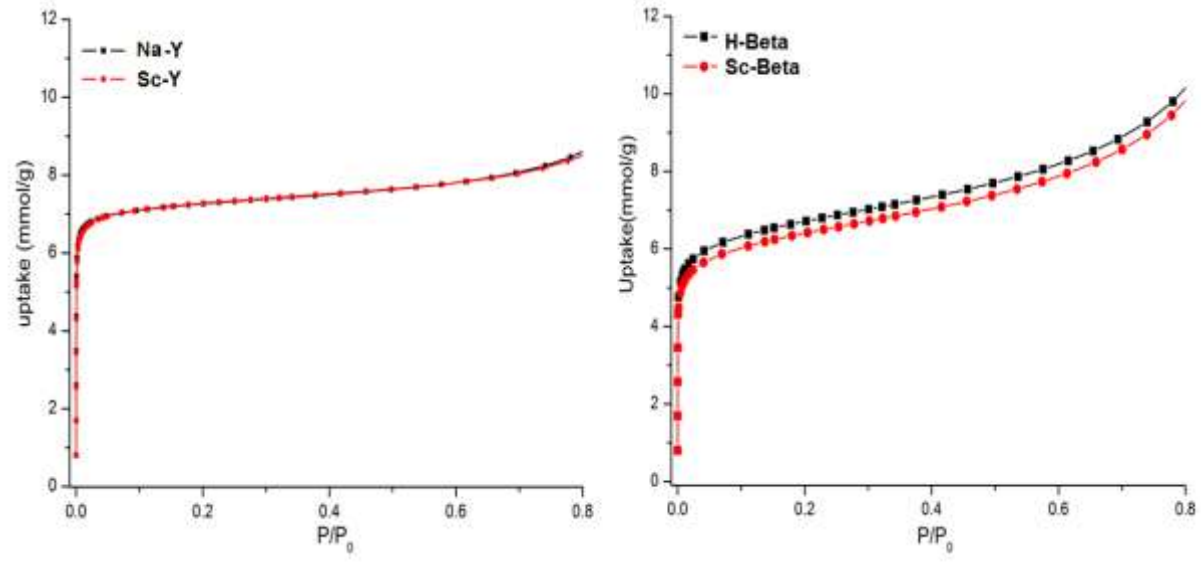

Figure 3.27: Isotherms for N_2 adsorption measured at -196 ℃ on Sc-exchanged zeolites;(Left) zeolite Na-Y (black) and Sc-Y(red); and (right) zeolite H-Beta (black) and Sc-Beta (red).

3.3.3 Encapsulation of polyoxometalates in scandium MOFs

3.3.3.1 MIL-100(Sc)

Results of the addition of different amounts of phosphotungstic acid (PTA) or phosphomolybdic acid (PMA) to the reaction mixture for the synthesis of MIL-100(Sc) are presented in Table 3.7.

Table 3.7: Encapsulation of polyoxometalates in MIL-100(Sc).

Entry	POM	Molar ratio (POM/Sc)		BET surface area m^2g^{-1}
		Theoretical	Calculated by EDX	
As-prepared	-	-	-	1385
1	PMA	0.028	0.018	1056
2	PMA	0.038	0.036	874
3	PTA	0.04	0.029	971
4	PTA	0.08	0.053	800

Figure 3.28 shows the PXRD of products of POM/MIL–100(Sc) syntheses. All preparations yield in crystalline solids but in the case of PMA, reactions gave mixtures with a second crystalline phase in addition to MIL-100. This is similar to results observed previously for POM/HKUST–1.[37] The diffraction patterns of samples containing PMA shows how the intensity of the second phase increases along with the increased amount of POM in the preparation. On the other hand, for samples containing PTA no peaks of extra phases are observed. However, a change in relative intensities at low angles is observed, suggesting a significant change in the electronic density within the pores in the framework. A similar situation was observed previously for MIL-101(Cr) and MIL-100(Fe).[38, 39] Nitrogen adsorption analyses of these samples were carried out to determine the BET surface area. Figure 3.29 shows the adsorption isotherms. In all cases uptakes decreased with loading of POMs..

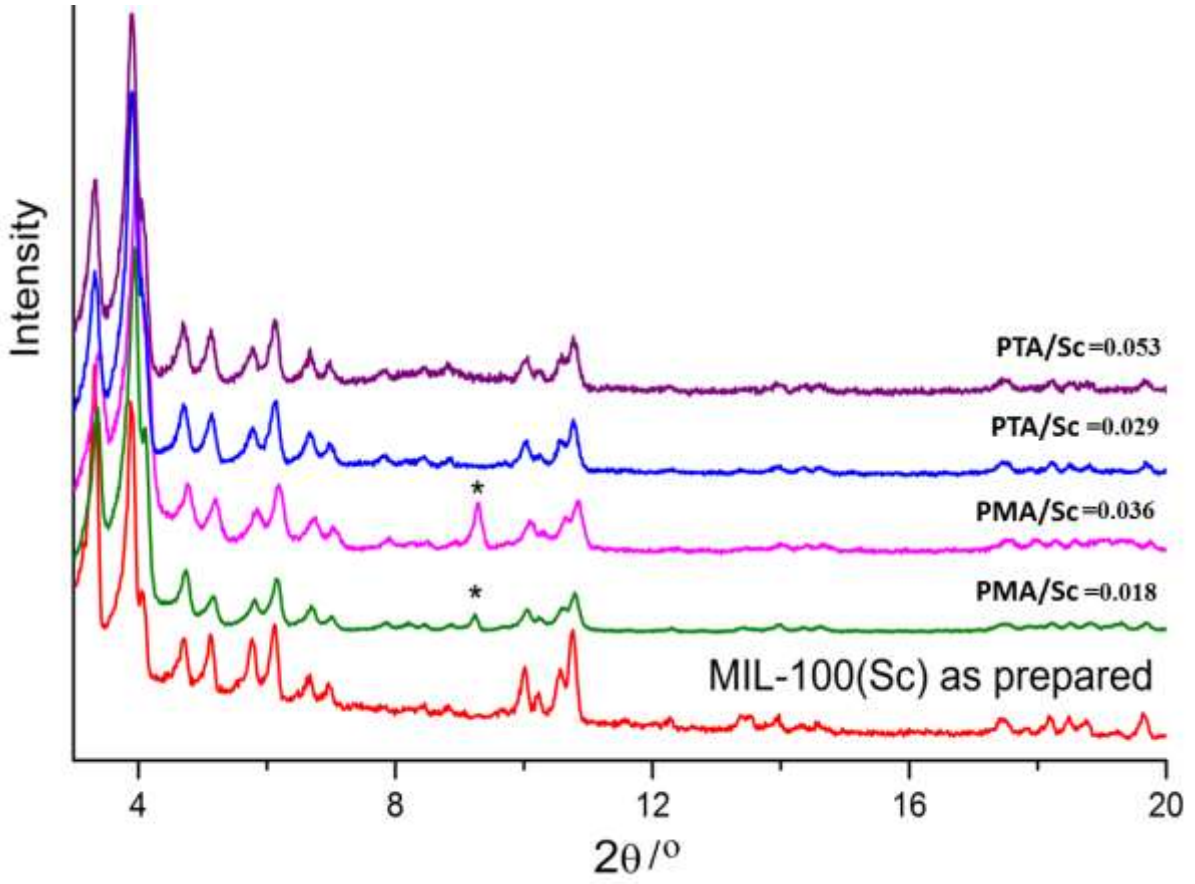

Figure 3.28: Simulated PXRD pattern of the as-prepared MIL-100(Sc) and samples prepared in the presence of different amount of added POMs. Reflection from additional phase asterisked.

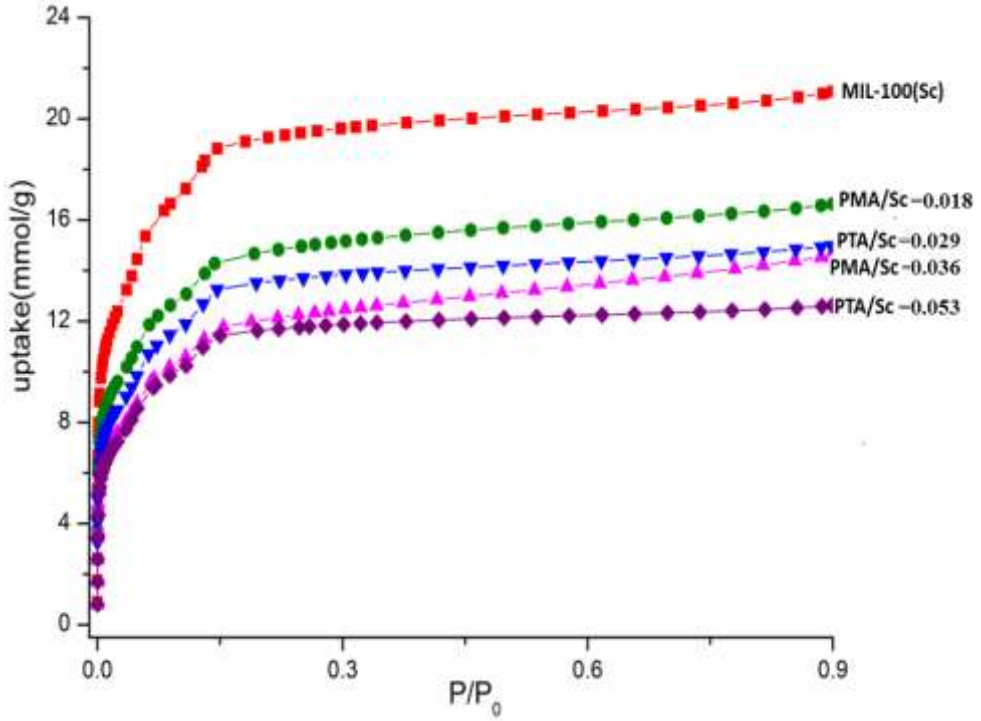

Figure 3.29: N_2 adsorption isotherms collected on MIL-100(Sc) and POM/MIL-100(Sc) at -196 ℃.

Characterisation by EDX confirms the presence of POM (Figure 3.30). In the samples containing PMA as a second phase, needle-like crystals are present (not shown).

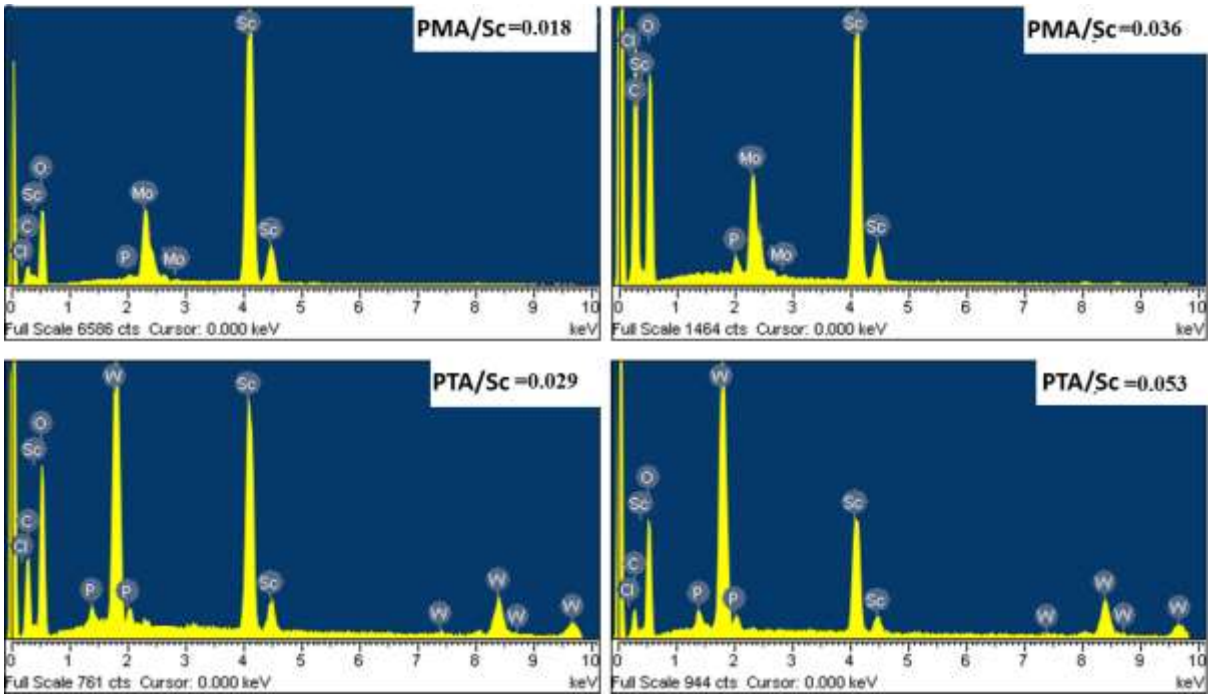

Figure 3.30: EDX analysis of MIL-100(Sc) samples preapred in the presence of POMs (PTA and PMA).

Thermogravimetric analyses of MIL-100(Sc) and sample (PTA(0.053)/MIL-100(Sc) are shown in Figure 3.31. TGA was carried out in flowing air. The sample with loaded PTA exhibits a lower weight loss than MIL-100(Sc) (as expected) and it is highly thermal stable, despite the presence of POM. There are two steps in the TGA, the first one caused by a loss of POM at 300 ^{o}C and the second by decomposition of the framework starting at 450 ^{o}C. The calculated values of additional POM are consisted with the residual mass observed experimentally for this sample (60 wt%).

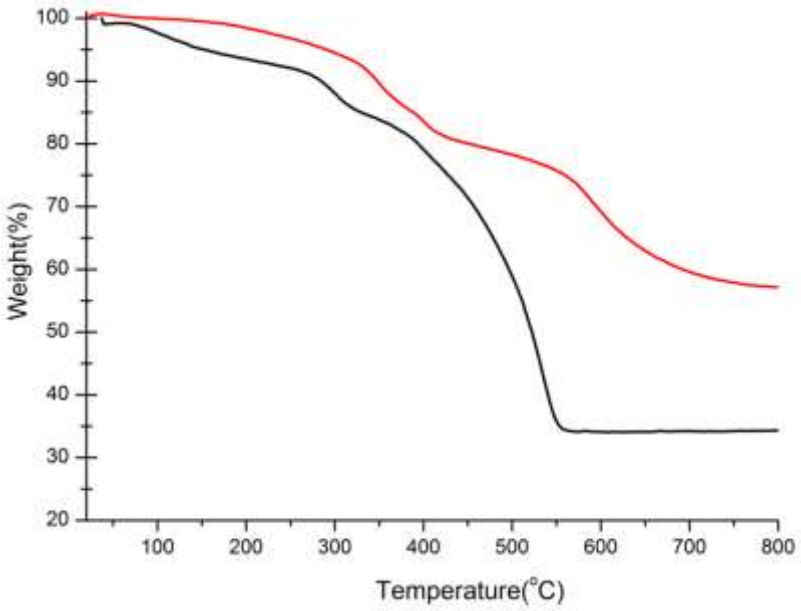

Figure 3.31: TGA of as-synthesised MIL-100(Sc) (black line) compared to as-synthesised (0.053) PTA/MIL-100(Sc) (red line).

3.3.3.2 MIL-101(Sc)

Results of encapsulation of POMs into the framework of MIL-101(Sc) are indicated in Table 3.7.

Table 3.8: Results of samples POM/MIL–101(Sc) prepared from different molar ratios.

Entry	POM	Molar ratio POM/Sc		BET surface area m^2g^{-1}
		Theoretical	Calculated by EDX	
as prepared	-	-	-	640
1	PTA	0.028	0.026	974
2	PTA	0.083	0.044	1200
3	PMA	0.028	0.023	91
4	PMA	0.083	0.041	273

Figure 3.32 shows the PXRD patterns of synthesized POM/MIL–101(Sc), all samples remaining crystalline. The PXRD of those samples prepared with PTA showed strong changes in the relatives intensities of the diffraction pattern, which suggests that PTA is encapsulated within the pores. Syntheses in the presence of PMA do not give MIL-101(Sc)

with strong differences in PXRD suggesting that a much lower degree of encapsulation was achieved.

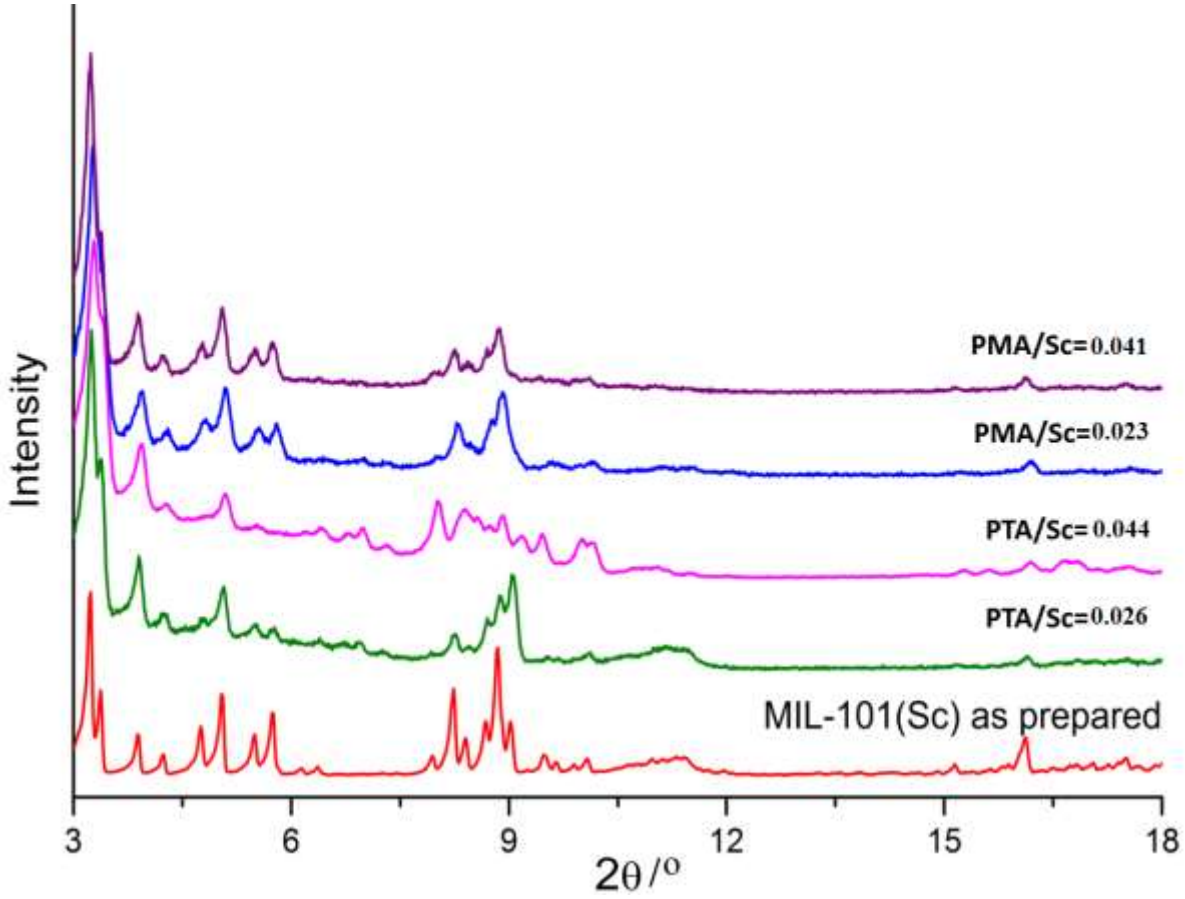

Figure 3.32: PXRD of MIL-101(Sc) as prepared and samples with different amount of POM.

Adsorption of N_2 was performed on the samples to provide information as to how the presence of POM affects the porosity. Nitrogen isotherms (Figure 3.33) show that for samples with encapsulated PTA the porosity is almost double than of as-prepared MIL-101(Sc). This indicates that the encapsulated POM increases the thermal stability of MIL-101(Sc). By contrast, adsorption analysis of nitrogen for PMA/MIL-101(Sc) showed a lower uptake that indicates that the POM is not encapsulated, and the stability of the MOF remains low.

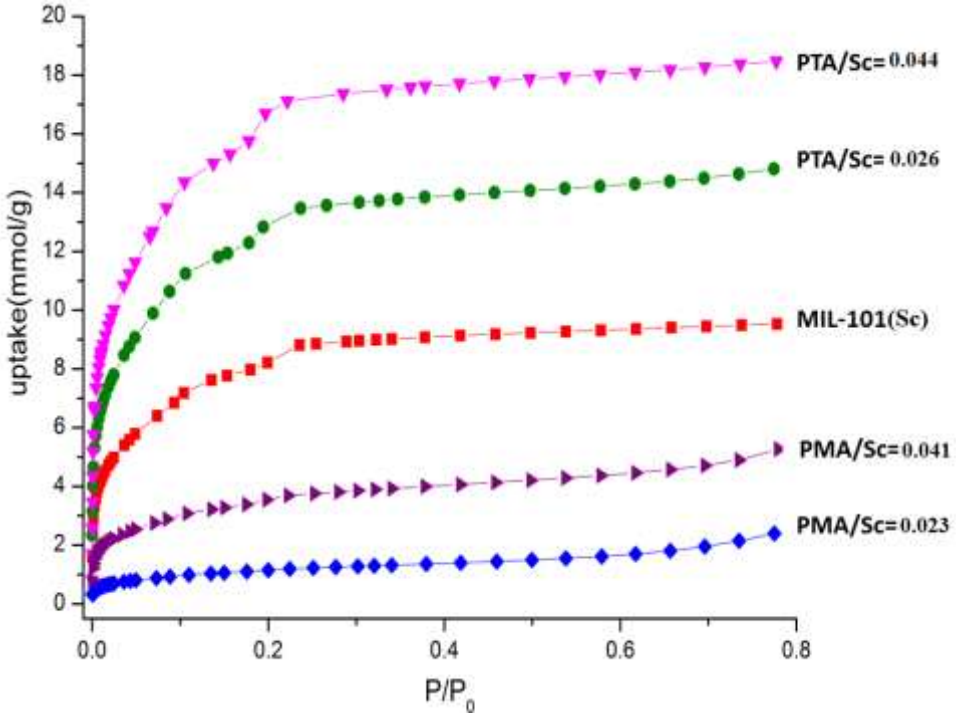

Figure 3.33: N_2 adsorption isotherms collected on MIL-101(Sc) and samples prepared with different amount of POM.

Figure 3.34 shows EDX spectra of POM-loaded MIL-101(Sc) samples and images of the samples are shown in Figure 3.35, confirming that PTA/MIL-101(Sc) crystallises as one phase as octahedral crystals, typical of MIL-101 material.

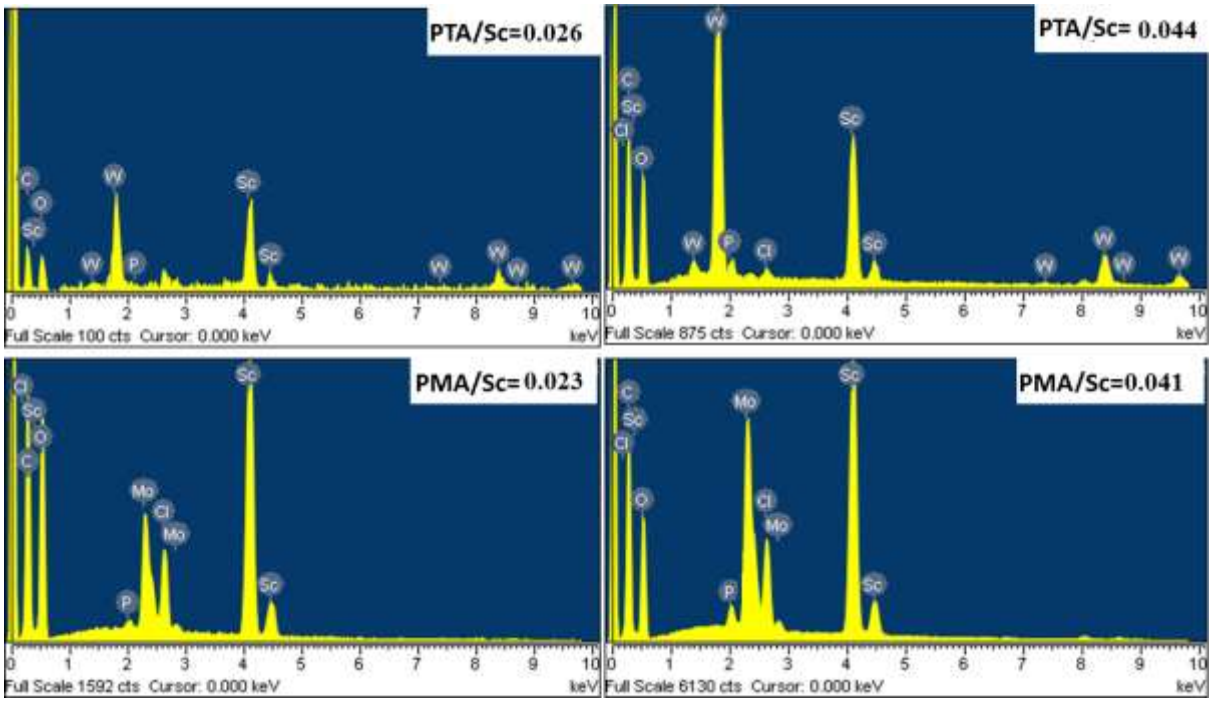

Figure 3.34: EDX analysis of samples loaded amounts of POM (PTA and PMA) into MIL-101(Sc).

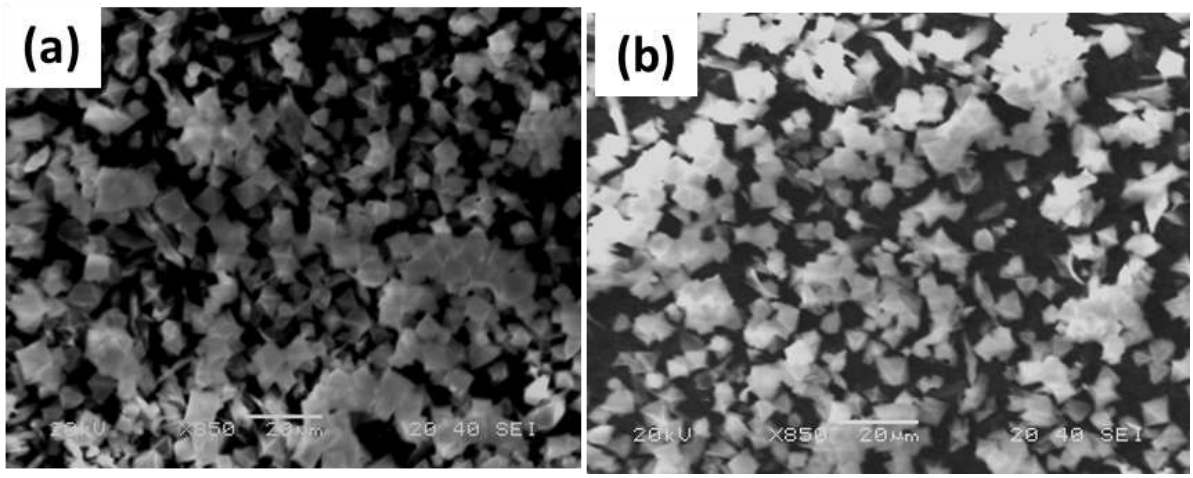

Figure 3.35: SEM images of crystals of PTA/MIL-101(Sc) in a molar ratio PTA/Sc 0.026 (a) and 0.044(b).

TGA of MIL-101(Sc) and a sample encapsulating PTA (PTA/Sc=0.044) are shown in Figure 3.36. The sample with encapsulated PTA exhibits a lower loss weight at high temperature than MIL-101(Sc) due to the presence of PTA decomposition products. The residual mass is 48 wt%, which is very close to the expected from the by EDX analysis.

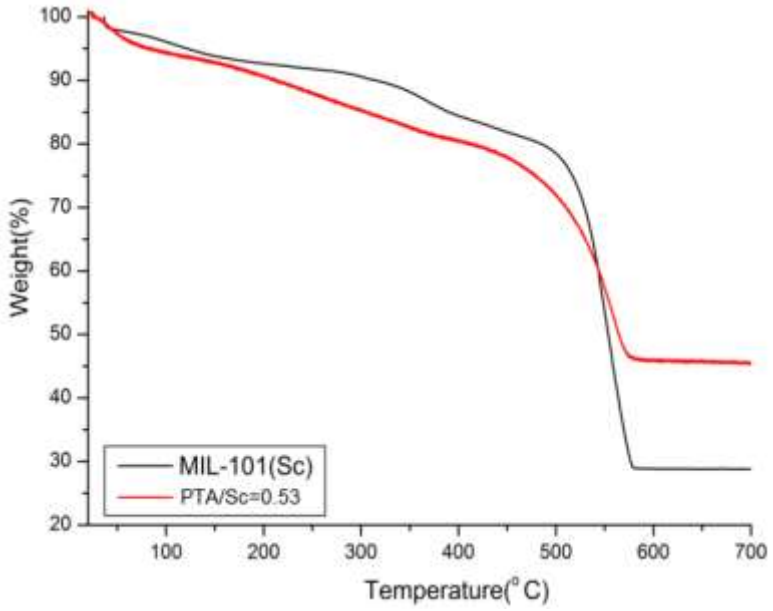

Figure 3.36: Thermogravimetric analysis of as-synthesized MIL-101(Sc)(black) compared to as-synthesized PTA/MIL-101(Sc) (red).

To check the crystallinity of the PTA/MIL-101(Sc) (PTA/Sc=0.53) after adsorption (which involves pre-heating at 120 ^{o}C), the diffraction pattern was collected. Previously, it had been found that MIL-101(Sc) re-crystallized into MIL-88B(Sc) after adsorption analysis, because the sample is activated by heating. Figure 3.37 shows the diffraction pattern after adsorption, which demonstrated that MIL-101(Sc)/PTA remains crystalline after heating and prolonged exposure to air.

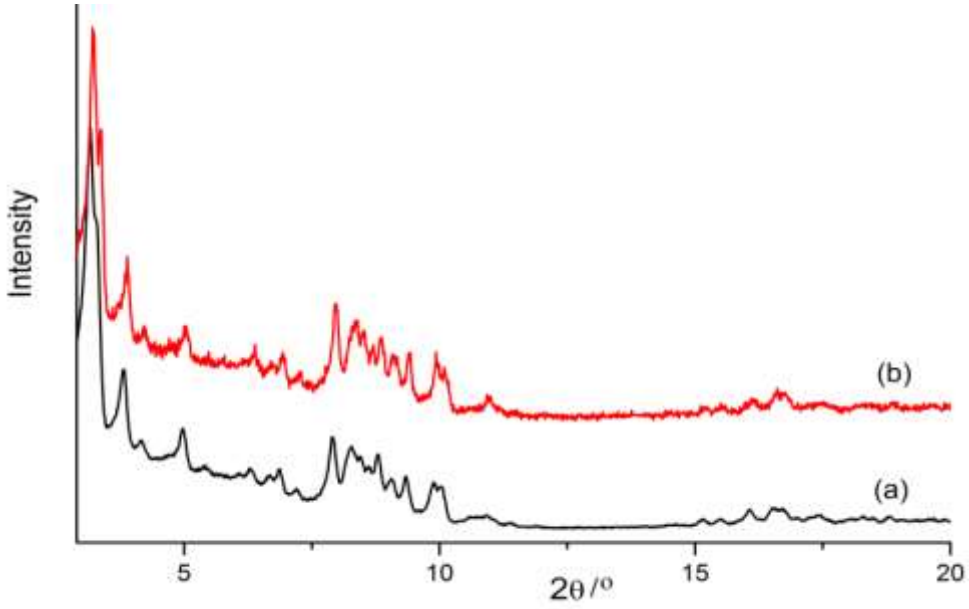

Figure 3.37: Powder x-ray diffraction pattern of PTA/MIL-101(Sc). (a) As-prepared sample and (b) sample after adsorption treatment at 120 ℃ and prolonged exposure to air.

3.3.3.3 MIL-88D(Sc)

Attempts were also made to encapsulate POM in MIL-88D(Sc) through direct synthesis. Table 3.9, gives the chemical composition of the final products.

Table 3.9: Results of samples POM/MIL–88D(Sc) prepared from different molar ratios and N_2 surfaces areas (BET) of the obtained samples.

Entry	POM	Molar ratio (POM/Sc)		BET surface area m^2g^{-1}
		Theoretical	Calculated by EDX	
As prepared				1243
1	PTA	0.022	0.021	546
2	PTA	0.041	0.031	502
3	PMA	0.038	0.036	755
4	PMA	0.067	0.050	605
5	PMA	0.083	0.062	283

All samples remain crystalline (Figure 3.38). For preparations with PTA the co-crystallisation of the POM occurs, but this is not observed for PMA-loaded samples. It was possible to explore in a range of values of molar ratio (POM/Sc) between 0.036 and 0.062.

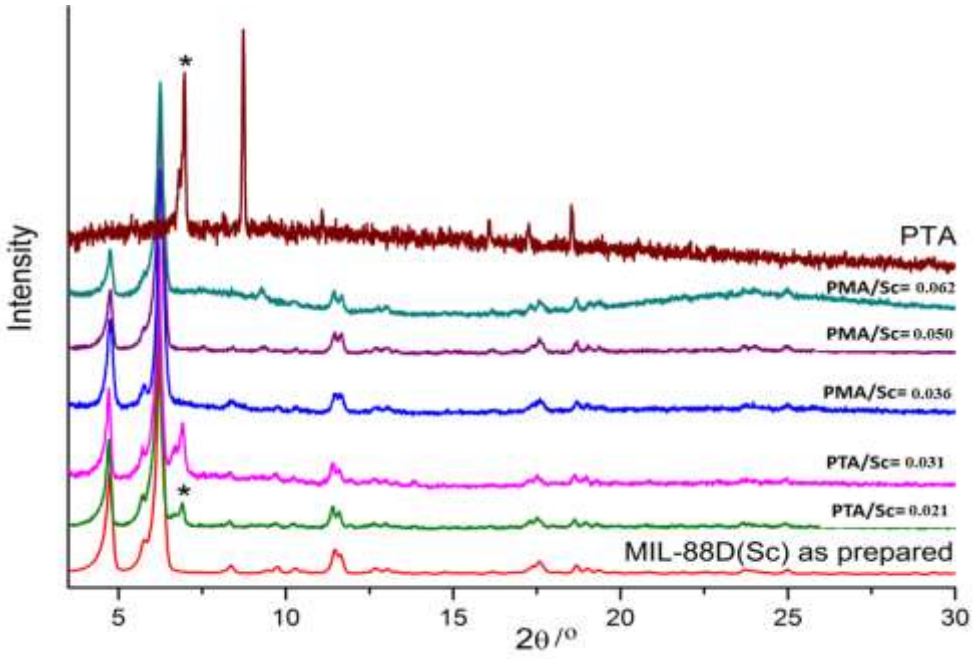

Figure 3.38: PXRD patterns of POM/MIL-88D(Sc). MIL-88D(Sc) as prepared red one, samples obtained with different amount of POM.

Figure 3.39 shows nitrogen adsorption isotherms, the BET surface area decrease from 1243 m^2g^{-1} to 502 m^2g^{-1} for sample which has a PTA/Sc ratio of 0.031 by EDX and for sample with the highest loading of PMA (0.062), the surface area decreases to 283 m^2g^{-1}, but with no changes in the PXRD pattern it is not possible to confirm that the POM is encapsulated.

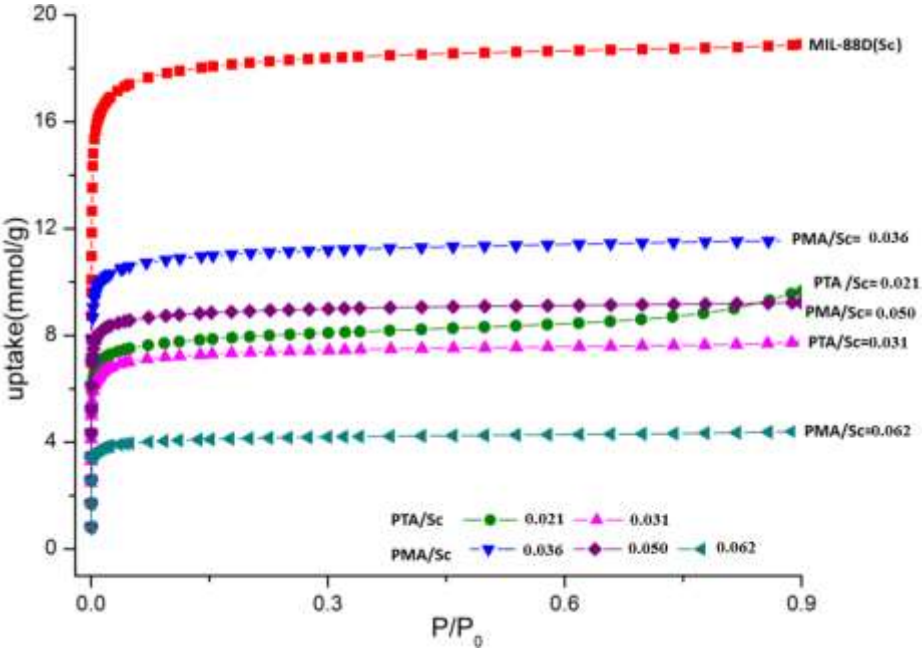

Figure 3.39: N_2 adsorption isotherms collected on POM/MIL-88D(Sc).

EDX showed POM present in the sample but it could be on the surface rather than in the framework (Figure 3.40). TGA analysis of the material (Mo/Sc= 0.062) shows that the materials are less thermally stable than MIL-88D(Sc) (Figure 3.41). The residual mass of the that sample is 58 %, this could confirm that this is the maximum amount of POM present into the structure despite de EDX analysis which found 0.062, indicated some of this POM was on the surface.

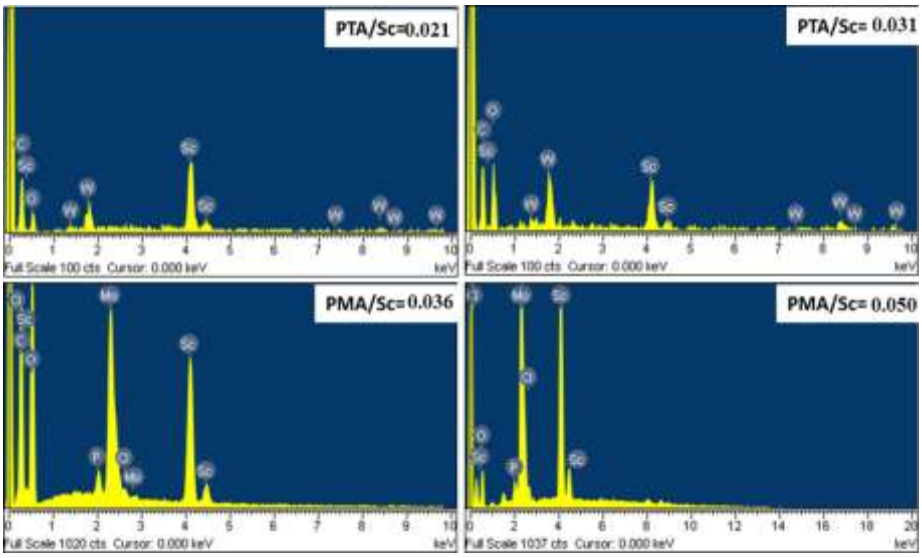

Figure 3.40: EDX analysis of samples of MIL-88D(Sc) prepared in the presence of added POMs (PTA and PMA).

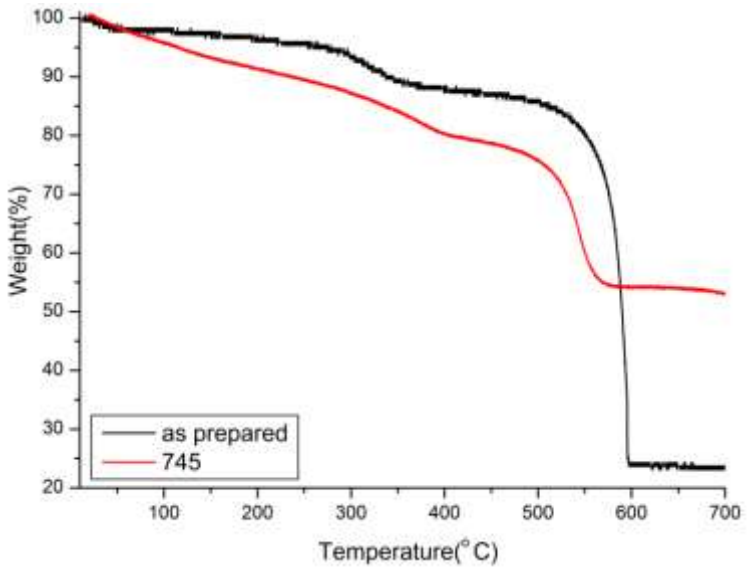

Figure 3.41: Thermogravimetric analysis of as-synthesised MIL-88D(Sc) (black one) compared to as-synthesised PTA/MIL-88D(Sc) (W/Sc= 0.062).

3.3.3.4 Discussion of POM encapsulation into MOFs

The results described for the synthesis of MOFs encapsulating POM suggest that it was successful for PTA in MIL-101(Sc). The SEM images show only particles with characteristic octahedral morphology and strong changes in intensities of the PXRD pattern. Furthermore, inclusion of POM increases stability of MIL-101(Sc), presumably by protecting Sc-O bonds

from hydrolysis in its structure, which otherwise leads to transformation to MIL-88B(Sc) in MIL-101(Sc). For the other syntheses, there was no conclusive evidence for POM encapsulation. The use of phosphomolybdic acid monohydrate (PMA) gave a second crystalline phase in the case of MIL-100(Sc) and for MIL-88D(Sc), co-crystallisation of PTA occurs.

For MIL-101(Sc), therefore, conclusive evidence for POM inclusion was observed (SEM and PXRD) and its encapsulation in the large cavities of the MOF stabilizes the structure against conversion to MIL-88B(Sc) upon heating, enabling MIL-101(Sc) with high surface area to be obtained. The sample contained PTA within MIL-101(Sc) was therefore used in catalytic experiments for comparison with other Lewis acidic MOFs.

3.4 Results and discussion of catalytic application

3.4.1 Catalytic application in carbonyl ene reaction

Scandium MOFs, POM/MOFs (PTA/MIL-100(Sc) and PTA/MIL-101(Sc)) were compared to Cr-MOFs and Sc^{3+}-exchanged zeolites in the carbonyl ene reaction.

3.4.1.1. Comparison of MOFs and zeolites in carbonyl ene reaction

The results for the carbonyl ene reaction between α-methyl styrene and ethyl trifluoropyruvate are found in Table 3.10. These show that there is some conversion (12 %, even in the absence of a catalyst). Among the scandium MOFs, MIL-100(Sc) is the most active, giving highly selective conversion (100% conversion, 99% selective). This performance is attributed to the presence of scandium sites that can undergo ligand exchange (for example of H_2O or MeOH on two thirds of the trimer sites). These sites can activate the carbonyl groups to the ene reaction. These sites are present within a stable, three-dimensionally connected large pore framework that retains crystallinity during catalysis reaction.

By comparison MIL-100(Cr) is less active, despite spectroscopic evidence that the Cr^{3+} site is stronger Lewis acid site.[40] Addition of POM (PTA) to MIL-100(Sc) reduces the conversion. No additional active Lewis sites are added and less Sc^{3+} is present. The activity of MIL-101(Sc) is surprisingly low, given that the active sites are the same as in MIL-100(Sc) and the structure also is a mesoporous framework. The reason for this low activity is that some of it converts to the less porous MIL-88B(Sc) during activation, as observed by XRD (Figure 3.44). It is therefore noteworthy that the MIL-101(Sc)/PTA (PTAM/Sc=0.53) composite gives an improved performance (99% conversion) although with lower selectivity (76%). The encapsulated POMs increase the stability of the solid but appear to introduce unselective acid

sites. Again, the stabilized MIL-101(Sc)/PTA (PTA/Sc=0.53) is more active than MIL-101(Cr), underlining the faster turnover rates over Sc^{3+} than Cr^{3+} in the same framework.

Table 3.10: Catalytic activities and selectivities for selected MOFs and zeolites for the carbonyl ene reaction of Scheme 3.3

Catalyst	**Reactant (%)**	**Product (%)**	**Hydrate (%)**	**Other (%)**
no catalyst	85	12	2	1
MIL-100(Sc)	0	99	0	1
PTA/MIL-100(Sc)	10	87	2	1
MIL-100(Cr)	29	65	4	2
MIL-101(Sc)	53	24	13	10
PTA/MIL-101(Sc)	1	76	10	13
MIL-101(Cr)	36	58	5	1
MIL-88B(Sc)	55	26	17	2
MIL-88D(Sc)	46	45	8	1
MIL-68(Sc)	11	33	24	32
Zeolite Beta (Sc)	16	20	45	19
Zeolite H-Beta	22	32	21	25
Zeolite Y(Sc)	7	30	12	51
Zeolite Y	17	20	43	20

Reaction monitored by NMR. Reaction conditions: α-methyl styrene (1.0 mmol, 0.13 mL), ethyl trifluoropyruvate (0.9 mmol, 0.1 mL), 2.5 % mol of MOF (Sc^{3+} or Cr^{3+}) catalyst, toluene (5 mL) stirred under N_2 for 8 h, at room temperature.

Neither MIL-88B(Sc) nor MIL-88D(Sc) give high conversions, despite containing the same $Sc_3(\mu_3O)$ trimers as MIL-100(Sc). In both cases this can be attributed to inaccessibility of the active sites. For MIL-88B(Sc), the flexible framework remains is a closed state (low porosity) in the apolar solvent, whereas for MIL-88D(Sc) the interpenetrated nature of the structure denies access to the internal pores for larger molecules. By corollary, this suggests that the

catalytic conversion over MIL-100(Sc) and MIL-101(Sc) is largely due to the active sites within the pores, rather than at the surface (Figure 3.42). This has been confirmed by Mitchell[41] using larger substrates in the carbonyl ene reaction.

MIL-68(Sc) is less active than MIL-100(Sc). It has no trimers and, in the perfect structure, no coordinatively unsaturated sites. It does have bridging hydroxyl groups, which may be active sites for the unselective conversion. Finally, the scandium-exchanged zeolites show relatively high conversions but low selectivity, possible because of the range of Sc^{3+} and $[Sc^{3+}(OH)_n]^{(3-n)+}$ site present in the pores. MIL-100(Sc) was therefore the most suitable catalyst for the carbonyl ene reaction. Figure 3.43 shows the PXRD of MOFs, MIL-68(Sc), MIL-88B(Sc), MIL-101(Sc) and PTA/MIL-101(Sc) after use in catalysis, and demonstrate that the solid remain crystalline.

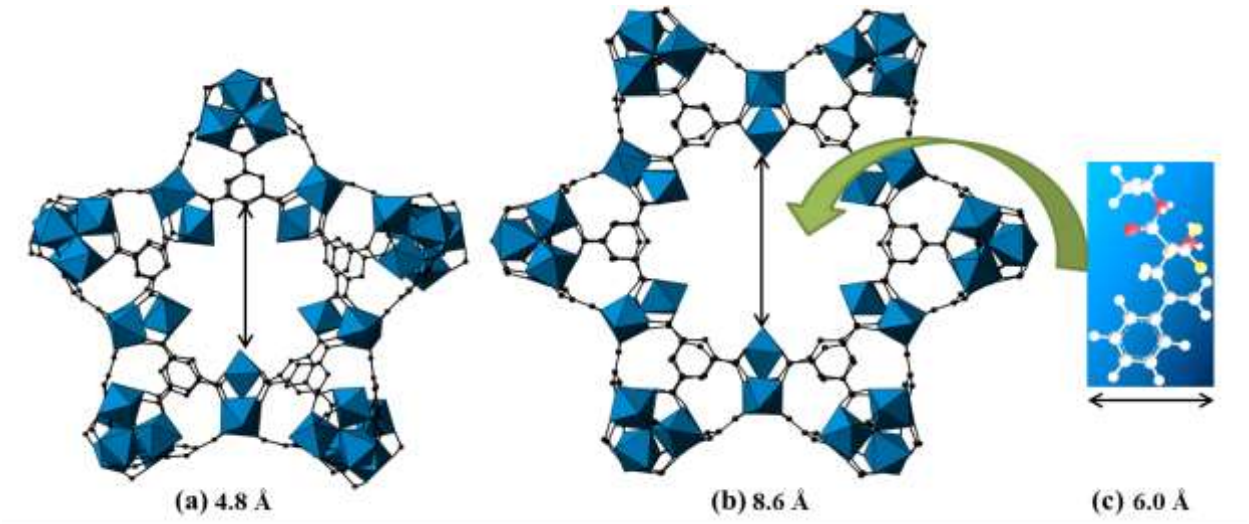

Figure 3.42: The two types of windows present in MIL-100 that control passage between cages: Pentagonal windows have a free diameter of 4.8 Å and large hexagonal windows have a free diameter of 8.6 Å.

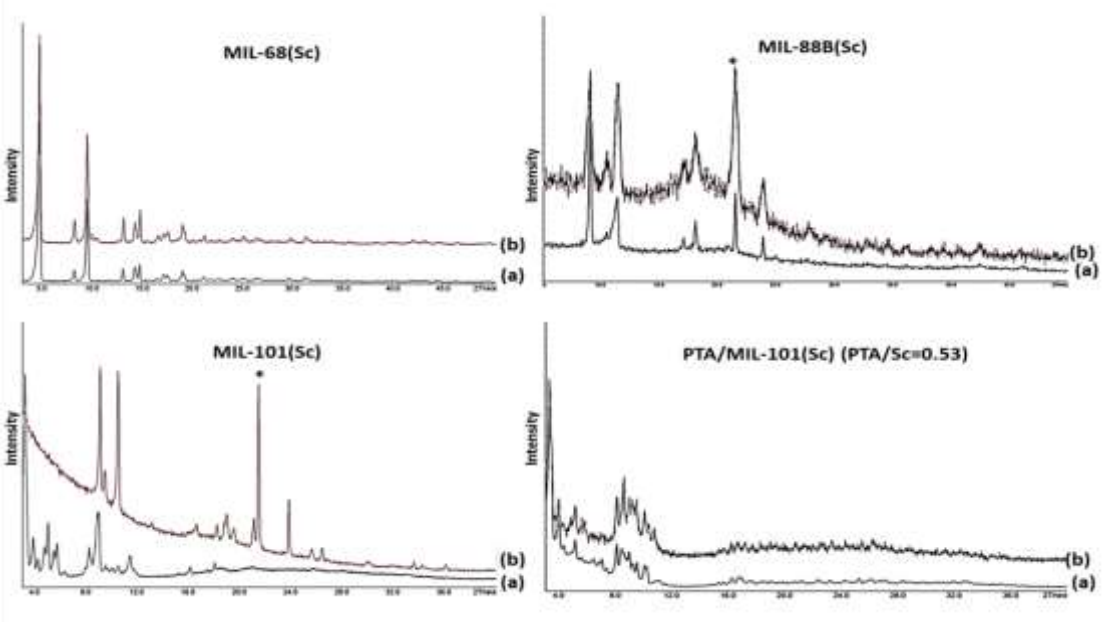

Figure 3.43: PXRD of the Sc MOF after use in catalysis

The heterogeneous nature of the catalyst over MIL-100(Sc) was studied. The carbonyl ene reaction was performed under the same conditions used previously, and after 2 h the catalyst was filtered off and the reaction was followed (Figure 3.44). Removal of catalyst stopped the reaction indicating the catalytic activity was entirely heterogeneous, and no Sc^{3+} leaching occurs.

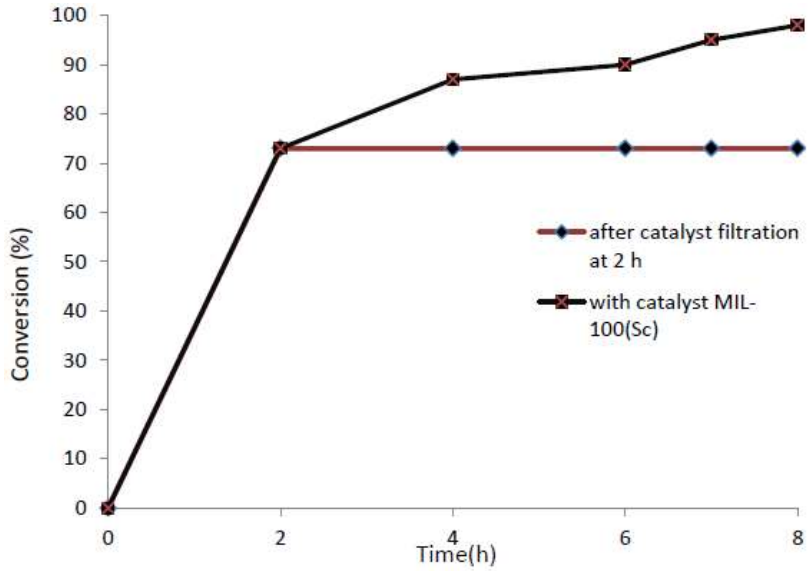

Figure 3.44: Plot of catalytic leaching test performed for MIL-100(Sc) in the carbonyl ene reaction

3.4.1.2 Effect of solvent in ene reaction

Previously, MOFs (Cr) have been tested as catalysts for the carbonyl ene reaction in dichloromethane.[20] In order to put the catalytic activity of MIL-100(Sc) into context, MIL-100(Sc), MIL-100 (Cr) and MIL-101 (Cr) were tested as catalysts in DCM as solvent. Results are summarized in Table 3.11. Using DCM as solvent MIL-100(Sc) demonstrated similar catalytic activity to that observed in toluene. MIL-100(Sc) gave 94.7 % conversion after 8 h, higher than the 43% obtained for MIL-100(Cr) over the same period. MIL-100(Cr) was tested for a longer time (16 h) and conversion obtained was 69%, similar to that result obtained when the reaction was performed in toluene (65 %). MIL-101(Cr) as catalyst gives a conversion of 55 %, although a 99 % conversion can be reached after 16 h of reaction. In summary, MIL-100(Sc) gives an excellent performance in DCM.

Table 3.11: Carbonyl ene reaction in Sc and Cr MOF in DCM.

Catalyst	% Reactant	%Product	%Hydrate
Control	84.4	11.6	4
MIL-100(Sc)	**0.2**	**94.7**	**5.1**
MIL-100(Cr)	53	43	4
MIL-100(Cr)*	26.5	69	4.5
MIL-101(Cr)	40.0	55.0	5.0
MIL-101(Cr)*	0.2	99.0	0.8

Reaction conditions: α-methyl styrene (1.0 mmol, 0.13 mL), ethyl trifluoropyruvate (0.9 mmol, 0.11 mL), 2.5%MOF (Sc^{3+} or Cr^{3+}) catalyst, DCM (5 mL) stirred under N_2 for 8 h, at room temperature.* Reaction for 16 h.

Finally, the use of methanol as solvent was investigated. MIL-88B(Sc) is known to breathe upon exposure to polar molecules such as methanol, so the ene reaction was performed in a polar solvent to investigate whether opening the structure could accelerate the reaction. However, with methanol as solvent the product obtained was the hydrated reactant (yield of

86%). When MIL-100 (Sc) was used, a high amount of the hydrated form was also obtained. This may be because methanol adsorbs at the active sites, blocking them to reactant molecules and allowing additional reaction. Therefore, the ene reaction should preferably be performed in the apolar solvents dichloromethane and toluene, but not in methanol.

3.4.1.3 Recyclability of MIL-100 (Sc)

One of the challenges in "green chemistry" is the design of highly selective catalytic materials that can be recycled without loss of activity and so reduce waste. Hence, recyclability over MIL-100(Sc) was explored. Results of this investigation showed a minimal loss of activity of the catalyst. After each reaction, the catalyst was filtered, then washed with toluene to remove any physisorbed reagents, and oven-dried at 60 ℃. The results obtained for re-usability can be seen in Table 3.12 under the same conditions as in Table 3.4. PXRD (Figure 3.45) indicated that MIL-100(Sc) retained crystallinity after catalysis.

Table 3.12 Recycling of MIL-100(Sc) as catalyst.

Catalyst	Cycle	Product (%)
MIL-100(Sc)	1	99
MIL-100(Sc)	2	96
MIL-100(Sc)	3	95

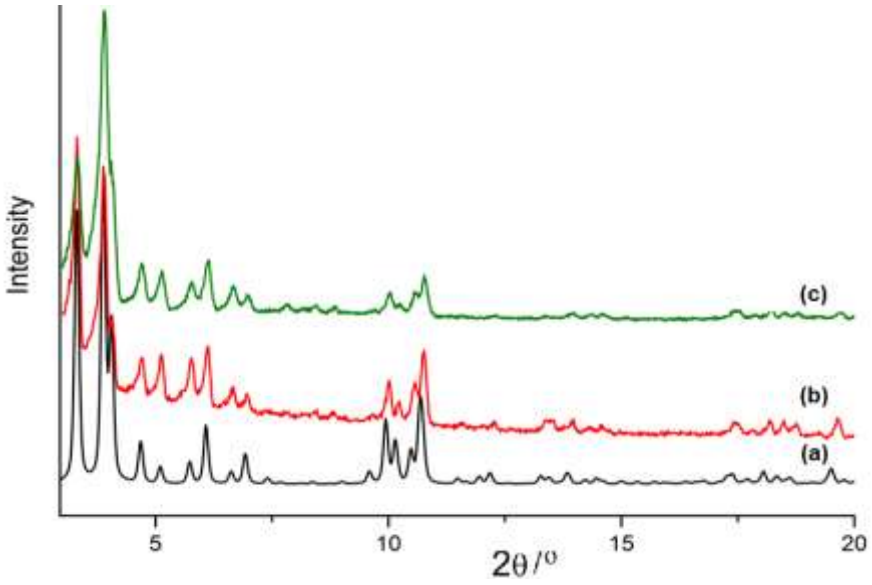

Figure 3.45: Comparison of MIL-100(Sc) PXRDs: (a) simulated, (b) as-prepared and (c) after third re-use.

For this series of scandium MOFs, MIL-100(Sc) was found to be a highly promising active Lewis acid catalyst. Its performance in a wide range of C-C and C=N bond forming reactions has subsequently been studied by Mitchell et al.[42]

3.4.2 Catalytic application in acetalization

3.4.2.1. Comparison of MOFs and zeolite(Y)

For the acetalisation of benzaldehyde, the blank experiment (without catalyst) resulted in 24% conversion but no conversion was observed when acetophenone was used as substrate. Table 3.13 lists the results and conditions for both reactions. The MOF MIL-100(Sc), showed low activity compared to MIL-88(Sc) and MIL-88D(Sc), even though all these solids have $Sc_3\mu_3O$ trimers and despite the high porosity of MIL-100(Sc). In the case of MIL-101(Sc) also gives low conversion. MIL-88D(Sc) gave the highest conversion, even though this framework is rigid in comparison with the MIL-88B(Sc) which opens up in polar solvents. The use of MIL-68(Sc) as a catalyst showed some activity but this is still low compared to MIL-88D(Sc) but higher compared to activity of MIL-100(Sc) or Sc-Y zeolite.

Table 3.13: Results of acetalisation reaction of benzaldehyde and acetophenone.

	Catalyst	Benzaldehyde dimethyl acetal % Conversion	Acetophenone % conversion
1	no catalyst	24	0
2	MIL-100(Sc)	6	9
3	MIL-88B(Sc)	67	3
4	MIL-88D(Sc)	87	2
5	MIL-101(Sc)	61	8
6	MIL-68(Sc)	45	2
8	Sc-Zeolite Y	10	0

Reaction conditions: Substrate: Methanol 1:10, catalyst amount (0.022 mmol MOF). Reactions were carried out at room temperature. Determined by GC.

The low activity of MIL-100(Sc), which was expected to be the most active catalyst, was investigated further; Figure 3.46 shows isotherms of MIL-100(Sc) before and after catalytic reaction. There is a decrease in BET surface area from 1385.3 to 630 m^2g^{-1}. The appreciable decrease in surfaces area suggests that the substrate is becoming strongly adsorbed in the pore of MIL-100(Sc) thus stopping the reaction and blocking active sites in the MOF. The XRD pattern of MIL-100(Sc) remains practically unchanged after reaction (Figure 3.47).

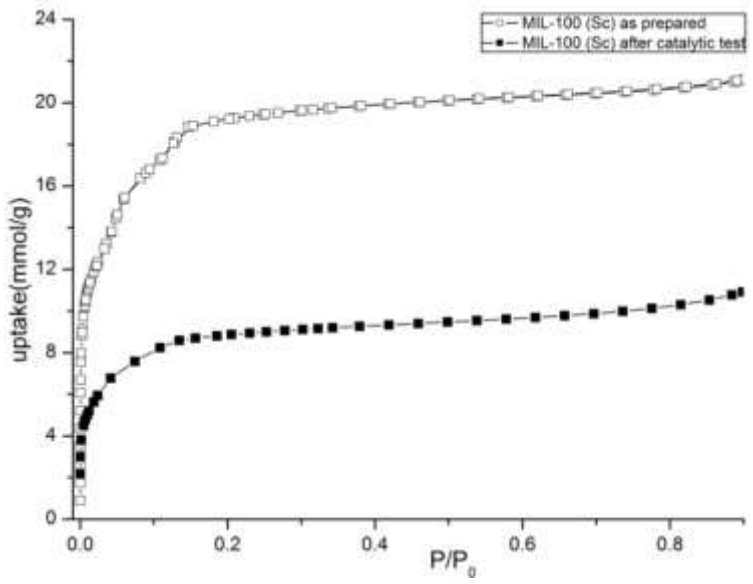

Figure 3.46: Nitrogen adsorption isotherm measured at -196 ℃ of as prepared (open squares) MIL-100(Sc) and after test in acetalization reaction (dark squares).

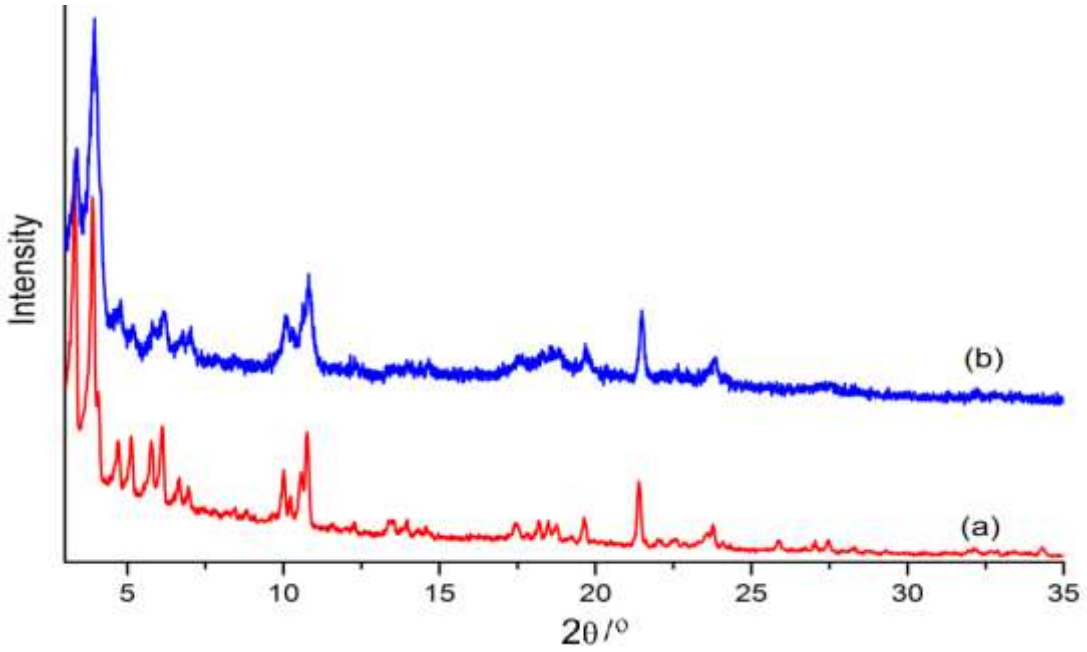

Figure 3.47: Comparison of PXRD MIL-100(Sc): (a) as-synthesized and (b) after use as catalyst in acetalization of benzaldehyde.

Acetophenone was much less active than benzaldehyde, in this case MIL-100(Sc) showed the highest activity, the yields obtained here are similar to those reported for the same reaction conditions by Dhakshinamoorthy et al [22] for the MOF $Cu_3(BTC)_2$ [HKUST-1].

3.4.2.2 Recyclability of MIL-88(Sc)

The re-use of MIL-88B(Sc) and MIL-88D(Sc) was investigated in the acetalization of benzaldehyde with the conditions given in Table 3.13. The materials were re-used three times with little loss of activity (Figure 3.48), when the catalyst was recovered from the reaction mixture it was washed with methanol, dried and analysed by powder XRD.

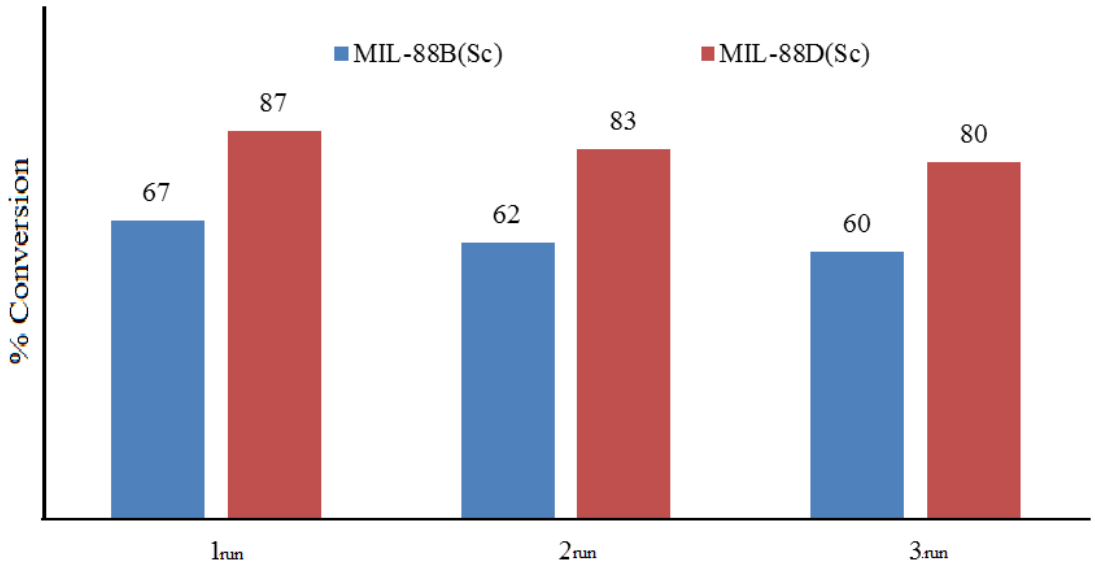

Figure 3.48: Recycling of MIL-88B(Sc) and MIL-88D(Sc). Conversions of each MOF re-used up to three times.

Figures 3.49 and 3.50 shows the XRD patterns of MIL-88B(Sc) and MIL-88D(Sc) after reaction. In both cases the structures remained crystalline after three uses but the XRD pattern of MIL-88B(Sc) after reaction indicated the unit cell had changed and then only partially closed upon losing methanol upon drying. PXRD before and after reaction show that MIL-88B(Sc) becomes much more ordered. The indexed post-catalysis pattern has a unit cell of a = 11.17 Å, c= 19.493Å in the hexagonal space group $P\bar{6}2c$.

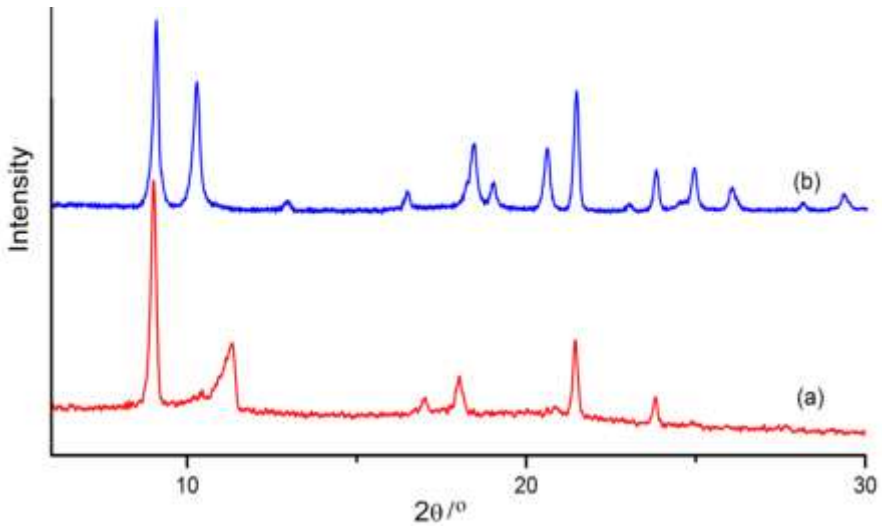

Figure 3.49: Comparison of PXRD MIL-88B(Sc): (a) as-synthesized and (b) after three uses as catalyst in acetalization of benzaldehyde.

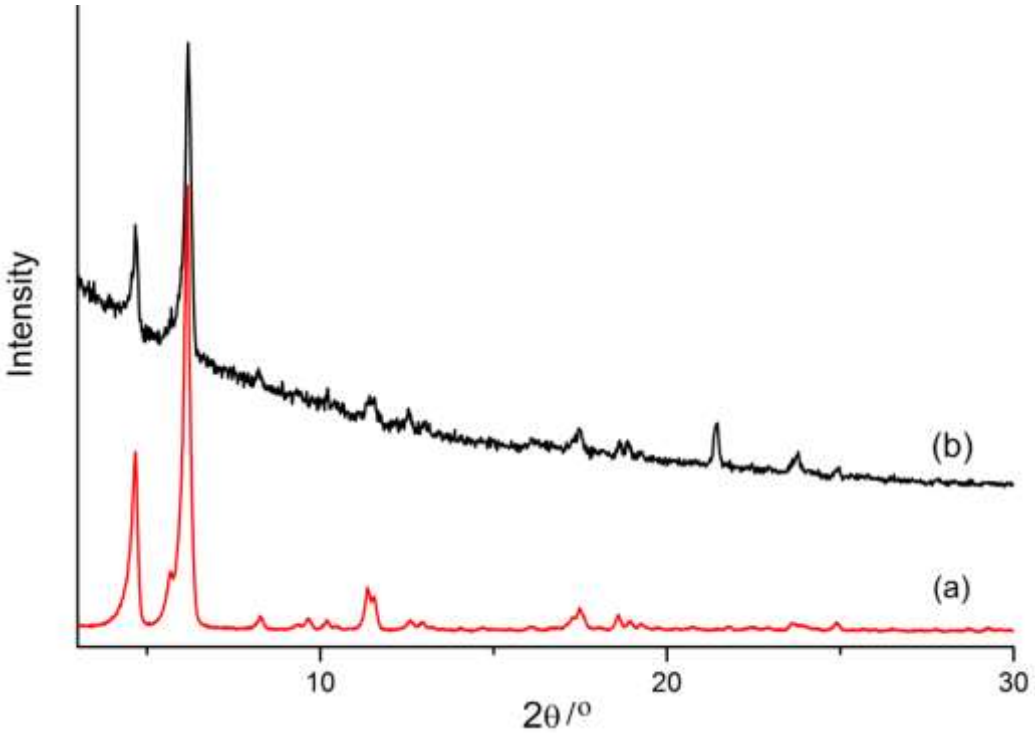

Figure 3.50: PXRD of MIL-88D (a) as-synthesized and (b) after use as catalyst.

As the catalysis reaction was performed in methanol it could suggest that in solution the MOF can take up methanol and partially opened the framework during catalysis and allow the reaction and then then partially closed upon losing methanol upon drying. Remarkably MIL-88B(Sc) after reaction has permanent porosity for N_2 even though the original material was not porous (Figure 3.51).

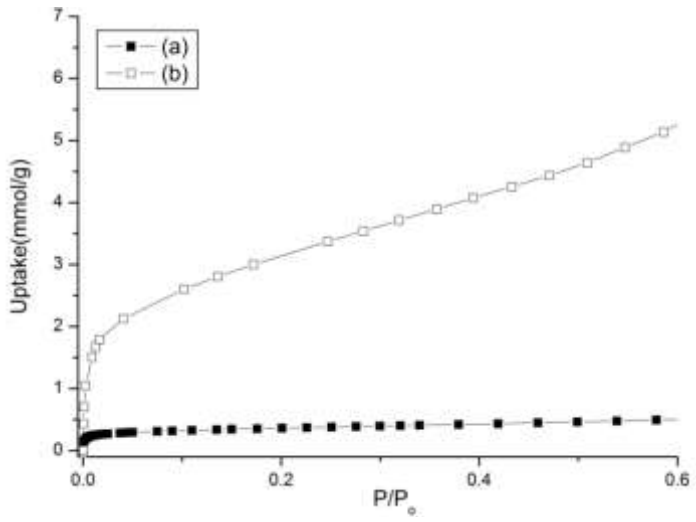

Figure 3.51: Nitrogen adsorption isotherms of MIL-88B(Sc) measured at -196 ℃: (a) as-prepared (dark squares) and (b) after test in acetalisation reaction (open squares).

3.5 Conclusion

The first part of this chapter described the synthesis and characterisation of known and novel scandium MOFs. The synthesis of MIL-100(Sc) and MIL-88B(Sc) was prepared by following reported methods and characterisation was performed using PXRD, thermal analysis, CHN analysis and gas adsorption. The synthesis of pure MIL-101(Sc) was achieved for the first time using a modified method of synthesis, which involves a mixture of solvents N,N'-dimethylformamide (DMF) and ethanol (EtOH) in the preparation. Studies of the adsorption properties of MIL-101(Sc) indicated that it recrystallised into MIL-88B(Sc) after heating at 120 ℃ and prolonged exposure to air. Also, using the mixed solvents method the synthesis of MIL-68(Sc) was prepared for the first time, crystallising as large crystals, and the structure was solved from single crystal diffraction and refined against X-ray powder diffraction data. The crystal structure of MIL-68(Sc) was measured by Rietveld refinement against X-ray powder diffraction data in the orthorhombic *Cmcm* symmetry. A satisfactory fit to the data was achieved, R_{wp} = 5.2%, R_p = 3.8%. DMF solvent molecules were collocated in the smaller triangular channels of as-synthesised MIL-68(Sc). The adsorption behaviour of the Sc-MOF was measured for N_2 and CO_2 at -196 ℃ and -77 ℃, respectively. Chromium MOFs, MIL-101 and MIL-100; and scandium-exchange zeolites Y and beta were prepared for comparison with scandium MOFs in catalytic tests.

The encapsulation of Keggin polyoxometalate phosphotungstate PTA by direct synthesis was explored in MIL-100(Sc), MIL-101(Sc) and MIL-88D(Sc). However, it was only certainly achieved in MIL-101(Sc). PMA added to MIL-100(Sc) preparations resulted in a second crystalline phase, while MIL-88D(Sc) loaded with PTA showed co-crystallisation of the POM. PTA encapsulated within MIL-101(Sc) enhances the MOF's hydrolytic stability, preventing the re-crystallisation to MIL-88B(Sc) and allowed a BET surface area of 1200 m^2g^{-1} to be achieved.

This series of scandium and chromium MOFs, POM/MOFs and scandium-exchanged zeolites were tested as heterogeneous catalysts in the carbonyl ene reaction between α-methyl styrene and ethyl trifluoropyruvate. From these results, MIL-100(Sc) was the best Lewis acid catalyst in this reaction. The POM-stabilised PTA/MIL-101(Sc) was also an active Lewis acid catalysts for this reaction, but the presence of the POM also catalyses side reaction, leading to reduce selectivities. By contrast, in the acetalisation of benzaldehyde with methanol the isoreticular MIL-88B(Sc) and MIL-88D(Sc) showed the highest conversions, but MIL-100(Sc) is not active. It is likely that the Sc^{3+} sites in MIL-100(Sc) have a high affinity for methanol and the presence of substrate and product blocks the pores.

In summary, MIL-100(Sc) is an excellent and reusable Lewis acid catalyst for C-C bond forming reactions, better than the well-known MIL-100(Cr) and MIL-101(Cr), but the reactions have to be performed in non-coordinating solvents.

3.6 References

1. L. Alaerts, E. Séguin, H. Poelman, F. Thibault-Starzyk, P. A. Jacobs and D. E. De Vos, *Chem. Eur. J.*, 2006, 12, 7353-7363.

2. J. Lee, O. K. Farha, J. Roberts, K. A. Scheidt, S. T. Nguyen and J. T. Hupp, *Chem. Soc. Rev.*, 2009, 38, 1450-1459.

3. K. K. Tanabe and S. M. Cohen, 2010, 49, 6766-6774.

4. A. Dhakshinamoorthy, M. Alvaro and H. Garcia, *Chem. Commun.* , 2012, 48, 11275-11288.

5. A. Dhakshinamoorthy, M. Alvaro, P. Horcajada, E. Gibson, M. Vishnuvarthan, A. Vimont, J.-M. Greneche, C. Serre, M. Daturi and H. Garcia, *ACS Catalysis*, 2012, 2, 2060-2065.

6. L. Mitchell, B. Gonzalez-Santiago, J. P. S. Mowat, M. E. Gunn, P. Williamson, N. Acerbi, M. L. Clarke and P. A. Wright, *Cat. Sci. Tech.*, 2013, 3, 606-617.

7. Y. Liu, K. Mo and Y. Cui, *Inorg. Chem.*, 2013, 52, 10286-10291.

8. J. M. Thomas and W. J. Thomas, *Principles and practice of heterogeneous catalysis*, Wiley-VCH, Germany, 1997.

9. A. Corma and H. Garcia, *Chem. Rev.*, 2003, 103, 4307-4365.

10. J. Hagen, *Industrial Catalysis*, Wiley-VCH 2006.

11. A. U. Czaja, N. Trukhan and U. Muller, *Chem. Soc. Rev.*, 2009, 38, 1284-1293.

12. J. Perles, M. Iglesias, C. Ruiz-Valero and N. Snejko, *Chem. Commun.* , 2003, 346-347.

13. D. Farrusseng, S. Aguado and C. Pinel, *Angew. Chem. Int. Ed.*, 2009, 48, 7502-7513.

14. F. Gandara, B. Gomez-Lor, M. Iglesias, N. Snejko, E. Gutierrez-Puebla and A. Monge, *Chem. Commun.*, 2009, 2393-2395.

15. A. Corma, H. García and F. X. Llabrés i Xamena, *Chem. Rev.*, 2010, 110, 4606-4655.

16. S. Kobayashi, *Synlett*, 1994, 689-701.

17. S. Kobayashi, *Eur. J. Org. Chem.*, 1999, 15-27.

18. S. Kobayashi and C. Ogawa, *Chem. Eur. J.*, 2006, 12, 5954-5960.

19. D. A. Evans and J. Wu, *J. Am. Chem. Soc.*, 2005, 127, 8006–8007.

20. M. E. Gunn, University of St Andrews Undergraduate Research Project report, 2009.

21. S. Ajaikumar and A. Pandurangan, *J. Mol. Catal. A: Chem.*, 2008, 290, 35-43.

22. A. Dhakshinamoorthy, M. Alvaro and H. Garcia, *Adv. Synth. Catal.*, 2010, 352, 3022-3030.

23. K. Barthelet, J. Marrot, G. Ferey and D. Riou, *Chem. Commun.* , 2004, 520-521.

24. C. Volkringer, M. Meddouri, T. Loiseau, N. Guillou, J. Marrot, G. Ferey, M. Haouas, F. Taulelle, N. Audebrand and M. Latroche, *Inorg. Chem.*, 2008, 47, 11892-11901.

25. A. Fateeva, P. Horcajada, T. Devic, C. Serre, J. Marrot, J.-M. Grenèche, M. Morcrette, J.-M. Tarascon, G. Maurin and G. Férey, *Eur. J. Inorg. Chem.*, 2010, 24, 3789-3794.

26. Q. Y. Yang, S. Vaesen, M. Vishnuvarthan, F. Ragon, C. Serre, A. Vimont, M. Daturi, G. De Weireld and G. Maurin, *J. Mater. Chem.*, 2012, 22, 10210-10220.

27. J. M. Newsam, M. M. J. Treacy, W. T. Koetsier and C. B. D. Gruyter, *Proc. Roy. Soc. Lond. A*, 1988, 420, 375-405.

28. J. P. S. Mowat, S. R. Miller, A. M. Z. Slawin, V. R. Seymour, S. E. Ashbrook and P. A. Wright, *Micropor. Mesopor. Mat.*, 2011, 142, 322-333.

29. G. Férey, C. Serre, C. Mellot-Draznieks, F. Millange, S. Surblé, J. Dutour and I. Margiolaki, *Angew. Chem. Int. Ed.*, 2004, 43, 6296-6301.

30. G. Férey, C. Mellot-Draznieks, C. Serre, F. Millange, J. Dutour, S. Surblé and I. Margiolaki, *Science*, 2005, 309, 2040-2042.

31. P. L. Llewellyn, S. Bourrelly, C. Serre, A. Vimont, M. Daturi, L. Hamon, G. De Weireld, J. S. Chang, D. Y. Hong, Y. Kyu Hwang, S. Hwa Jhung and G. Ferey, *Langmuir*, 2008, 24, 7245-7250.

32. S. Surble, C. Serre, C. Mellot-Draznieks, F. Millange and G. Ferey, *Chem. Commun.*, 2006, 284-286.

33. C. Serre, C. Mellot-Draznieks, S. Surble, N. Audebrand, Y. Filinchuk and G. Férey, *Science*, 2007, 315, 1828-1831.

34. J. P. S. Mowat, PhD thesis, University of St Andrews, 2012.

35. Y. Liu, J. F. Eubank, A. J. Cairns, J. Eckert, V. C. Kravtsov, R. Luebke and M. Eddaoudi, *Angew. Chem. Int. Ed.*, 2007, 46, 3278-3283.

36. N. A. Khan, I. J. Kang, H. Y. Seok and S. H. Jhung, *Chem. Eng. J.*, 2011, 166, 1152-1157.

37. Y. Q. Lan, S. L. Li, X. L. Wang, K. Z. Shao, D. Y. Du, H. Y. Zang and Z. M. Su, *Inorg. Chem.*, 2008, 47, 8179-8187.

38. N. V. Maksimchuk, M. N. Timofeeva, M. S. Melgunov, A. N. Shmakov, Y. A. Chesalov, D. N. Dybtsev, V. P. Fedin and O. A. Kholdeeva, *J. Catal.*, 2008, 257, 315-323.

39. R. Canioni, C. Roch-Marchal, F. Secheresse, P. Horcajada, C. Serre, M. Hardi-Dan, G. Ferey, J.-M. Greneche, F. Lefebvre, J.-S. Chang, Y.-K. Hwang, O. Lebedev, S. Turner and G. Van Tendeloo, *J Mater Chem*, 2011, 21, 1226-1233.

40. G. T. Palomino, C. P. Cabello and C. O. Areán, *Eur. J. Inorg. Chem.*, 2011, 1703-1708.

41. L. Mitchell, PhD Thesis, University of St Andrews, 2014.

42. L. Mitchell, P. Williamson, B. Ehrlichova, A. E. Anderson, V. R. Seymour, S. E. Ashbrook, N. Acerbi, L. M. Daniels, R. I. Walton, M. L. Clarke and P. A. Wright, *Chem. Eur. J.*, 2014, 20, 17185-17197.

Chapter 4: Functionalisation of scandium terephthalate MOFs

4.1 Introduction

Over the last years many studies on MOFs have addressed their functionalisation,[1-7] because in this way the adsorption properties of the framework can be modified. For example the functionalisation by amino groups has been demonstrated to increase the affinity of these materials toward CO_2.[3, 8-14] The functionalisation of MOFs can be achieved in two ways. One is through direct synthesis, which involves the use of the functionalised linker of interest and the other one is by post-synthetic modification (PSM)[6] of the material. One of the first reports with direct synthesis was published by Yaghi's group.[15] Assembling zinc oxide clusters and different linear carboxylates MOFs gave rise to 16 structures defined as isoreticular (IR) MOFs with the MOF-5 topology. These results demonstrated it was possible to modify the properties of the structures by varying the organic linker. This led to the functionalisation of many MOF by other research groups.

For the MIL family of MOFs (MIL = Materials Institute Lavoisier),[16] functionalisation via direct synthesis has been explored extensively in the terephthalate system with the trivalent metal cations Fe^{3+}, Cr^{3+} and Al^{3+}, for MOFs such as MIL-88B, MIL-101, MIL-68 and MIL-53.[5, 14, 17-22] Syntheses with Fe^{3+} and amino-terephthalic acid were the first reports for the amino-functionalisation of the terephthalate frameworks MIL-88B, MIL-101 and MIL-53.[17] Later studies on these materials demonstrated that the adsorption properties are enhanced by the presence of the amino-groups, for example for the uptake of ethanol, which was higher for the amino-functionalised compared to the non-functionalised MOFs. [23]

Functionalisation with the amino-functionalised linker has been reported for the syntheses of MIL-101(Cr and Al) and they have been shown to be active as base catalysts for the Knoevenagel reaction.[24] Also, the synthesis of amino-MIL-68(In) demonstrates enhanced adsorption properties of the framework for H_2 and CO_2 compared with the non-functionalised MIL-68(In).[13]

MIL-53 is one of the most widely studied MOFs because of its properties of breathing, characteristics that can make it highly porous and selective for adsorption of gases. MIL-53 has been synthesized with the trivalent metals Cr^{3+}, Al^{3+}, Fe^{3+}, Ga^{3+}, In^{3+} and Sc^{3+}, but the Al^{3+} analogue MIL-53(Al) has been studied in more detail in terms of its amino-functionalisation.[9] Several studies on MIL-53(Al) have reported functionalisation with X-BDC, where X = Cl, Br, Br, CH_3, CH_3, NO_2, NH_2 and OH.[9,25,26]. Amino-functionalisation of MIL-53 with other trivalent metals, In^{3+}, and Ga^{3+} has been reported and compared with the Al^{3+} analogue,[20] for CO_2 adsorption showing that the interaction with their frameworks depends on the electropositivity of the metal, which modulates the flexibility. Hence, the relative stability for amino MIL-53(Ga) and MIL-53(In) in the narrow pore form is higher than for MIL-53(Al).

One of the strategies of interest in this thesis is to prepare functionalised MOF by the mixed ligands approach,[8, 27-30] where two ligands are co-crystallized in the direct synthesis of the same MOF crystals. Horike et al.[31] reported one of the first such syntheses using the mixed ligand approach in which they varied the ratio of the ligands 5-nitroisophthalate (5-NO_2-ip) and 5-methoxyisophthalate (5-MeO-ip). The mixed ligand MOF CID-5/6 $[Zn(5NO_2\text{-ip})_{1-x}(5MeO\text{-ip})_x(bpy)]_n$ resulted. It was confirmed by X-ray diffraction analysis not to be a physical mixture of MOF CID-5 [Zn(5-NO2-ip)(bpy)] and CID-6 [Zn(5-MeO-ip)(bpy)]. On their own, CID-5 is flexible but CID-6 is rigid but porous. By combining both ligands makes the CID-5/6 more selective for gas separation.

Reinsch et al.[28] have reported the use of mixtures of linkers to synthesize a series of MOFs with the CAU-10 topology (CAU = Christian-Albrechts-Universität). This investigation demonstrated that the structure of CAU-10(Br) [Al(OH)(BDC-Br)] is not porous either for H_2 or N_2 but gave a low uptake for CO_2. Adding a second linker (NH_2-BDC, NO_2-BDC and CH_3-BDC, or –H) in the direct synthesis enhanced the adsorption of CO_2 , N_2 and H_2.

The synthesis using mixed ligands in the preparation of MIL-53(Al) has been reported by Marx et al.,[32] in which the terephthalate and the amino-terephthalate groups are present in different proportions in homogeneous materials. More recent studies using the same approach reported adsorption analysis of samples containing 90% of BDC and 10% of NH_2-BDC, in MIL-53(Al),[22] which affects the breathing properties of the material.

The post-synthetic modification (PSM) of MOFs has also been studied by many groups.[5, 6, 33-36] One of the first reports of PSM was performed on the MOF, POST-1[37] [$Zn(\mu_3\text{-}O)(D\text{-}PTT)_6$ D-PTT=(4S,5S)-2,2-dimethyl-5-(pyridine-4-ylcarboxyl)-1,3-dioxolane-4-carboxylate]. The PSM on this MOF involved N-alkylation by pyridyl functionalities with iodo-methane and iodo-hexane to give N-alkylated pyridinum ions decorating the pores. Many subsequent routes to PSM of MOFs have investigated treatments using acids and amines to incorporate functional groups. Cohen's group explored the PSM of IRMOF-3 using acetylation, where the MOF was treated with acetic anhydride to obtain IRMOF-3-AM1[38] which showed comparable crystallinity to IRMOF-3. This strategy aims to tune the pore cavities by introduction of functional groups into the frameworks when these materials are difficult to obtain by direct synthesis. Also, PSM can be achieved by solvent-assisted linker exchange (SALE). [36, 39, 40] Takaishi et al.,[39] have reported the PSM of porphyrinic MOFs using SALE, where varying reaction time under mild conditions gave crystalline materials and linker exchange.

Among the scandium MOFs published by Wright's group, the scandium terephthalates Sc_2BDC_3 and MIL-53(Sc) are materials of interest for their flexibility and adsorption properties. Sc_2BDC_3 was described for first time by Miller et al.,[41] and demonstrated significant porosity for small molecules and high thermal stability. The functionalised $Sc_2(NH_2\text{-}BDC)_3$ has been reported[12] as a microcrystalline powder with impurity of scandium oxide, but nevertheless it shows enhanced CO_2 adsorption at 0 ℃ and low pressures

compared to the non-functionalised material. The functionalised $Sc_2(NO_2\text{-}BDC)_3$ adsorbs less CO_2 due to the bulky NO_2 groups, however these do not block the pores, suggesting that the NO_2 groups can rotate in the framework structure to allow the uptake of adsorbent. Figure 4.1 shows the structures of these MOFs.

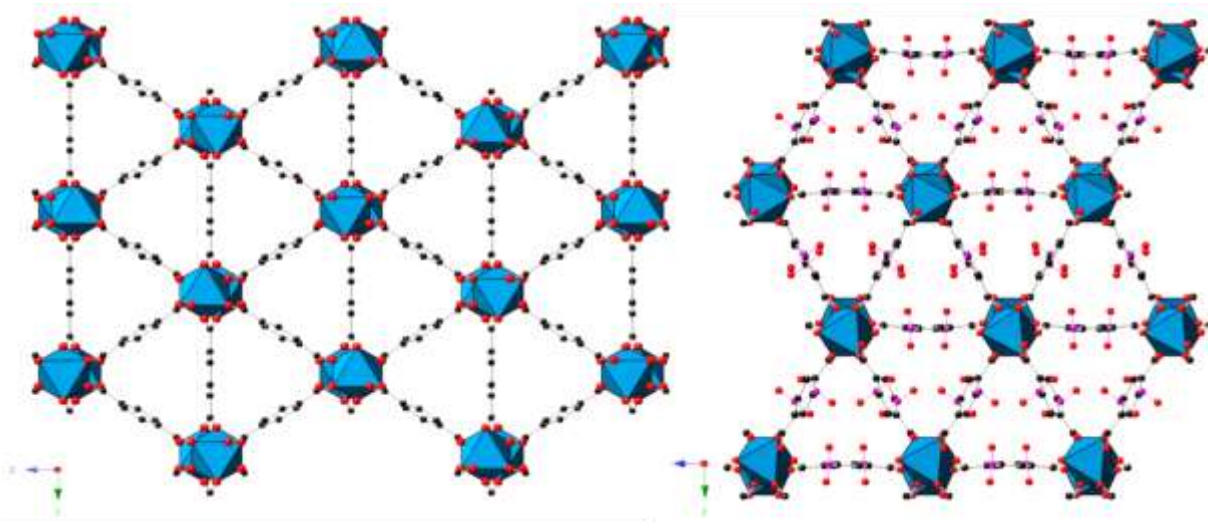

Figure 4.1: Images of the structures of (left) Sc_2BDC_3 and (right) $Sc_2(NO_2\text{-}BDC)_3$ viewed down the channels parallel to the x-axis. ScO_6 octahedra are shown in blue. Black, purple and red spheres represent the carbon, nitrogen and oxygen atoms of the organic linker, respectively. H atoms not shown.

In the terephthalate system Sc_2BDC_3 the synthesis of its pure amino and bromo- derivatives is of interest in this investigation. Previous attempts to prepare the functionalised $Sc_2(Br\text{-}BDC)_3$ were carried out by Mowat[42] but it was not possible to obtain the fully brominated solid. Another area of investigation for this system is the exploration of the post-synthetic surface modification of $Sc_2(NH_2\text{-}BDC)_3$, which might enhance the adsorption behaviour or introduce selectivity for gas separations.

The synthesis of MIL-53 using scandium has been reported along with that of its functionalised nitro- derivative (Figure 4.2).[43] Functionalisation using nitro-groups prevent the framework closing upon desolvation, unlike the non-functionalised MIL-53(Sc). Recently, amino-derivatives of MIL-53 have been reported for In^{3+}, Al^{3+}, Ga^{3+} and their

adsorption properties studied.[20] Synthetic studies on amino-MIL-53(Al) have reported control over its morphology resulting in crystals with different sizes which could be a potential target for post-synthetic modification.[44] Thus it is desirable to synthesize the amino-functionalised MIL-53(Sc) to investigate the effect of the amino-group on the uptake and breathing behaviour, especially for CO_2, and extend our understanding of the role of the metal cation in determining the flexibility of MIL-53.

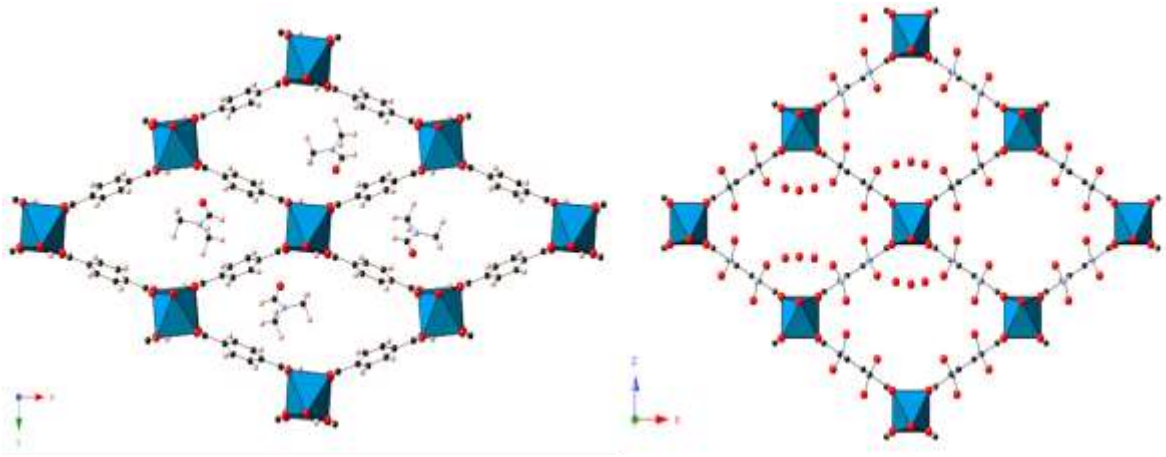

Figure 4.2: Images of the structures of (left) as-prepared MIL-53(Sc)-DMF and (right) functionalised NO_2-MIL-53(Sc).

Moreover the amino-functionalisation of the scandium forms of MIL-101, MIL-88B and MIL-68 has been investigated. Several groups have explored the synthesis of amino MIL-101(Cr, Al, Fe),[18, 26, 45, 46] MIL-88B(Fe)[18] and MIL-68(In, Al).[13,47] These studies have demonstrated that the use of amino groups enhance the properties of these materials for adsorption and catalysis.

4.2 Aims

The main objective of the experiments reported in this chapter is the functionalisation of scandium carboxylate MOFs, in particular with amino groups, by using a novel optimised low temperature/mixed solvent route of synthesis. Some of these MOFs can be suitable

candidates for the separation of small gas molecules. Hence, their adsorptions properties are investigated.

4.3 Experimental

The experimental section is described in two parts, the first one describing the direct synthesis of functionalised scandium carboxylate MOFS by a solvothermal route, involving the use of a mixture of solvents, where shorter reaction times and lower temperatures than those previously described were used. The second part describes the synthesis of amino-MIL-53 by crystallisation using a mixture of ligands including 5-aminoterephthalic acid. This is significant because the use of the 5-aminoterephthalic acid by itself leads to the crystallisation of scandium amino-terephthalates with topologies other than that of MIL-53. A series of experiments were performed, in which a range of carboxylic acids were used. Organic linkers used in the synthesis of functionalised scandium terephthalates are shown in Figure 4.3. All reagents and solvents were purchased commercially and used without further purification. N,N-dimehylformamide (DMF, Acros, 98%) and ethanol (EtOH, VWR, 99.8%). The linkers were; terephthalic acid (BDC, Aldrich 98%), 2-aminoterephthalic acid (NH_2-BDC, Aldrich 99%), (c) 2-nitroterephthalic acid (NO_2-BDC, Aldrich 99%), (d) 2-bromoterephthalic acid (Br-BDC, Aldrich 95%), (e) 2, 5-dihydroxyterephthalic acid ($(OH)_2$-BDC, Aldrich 98%).

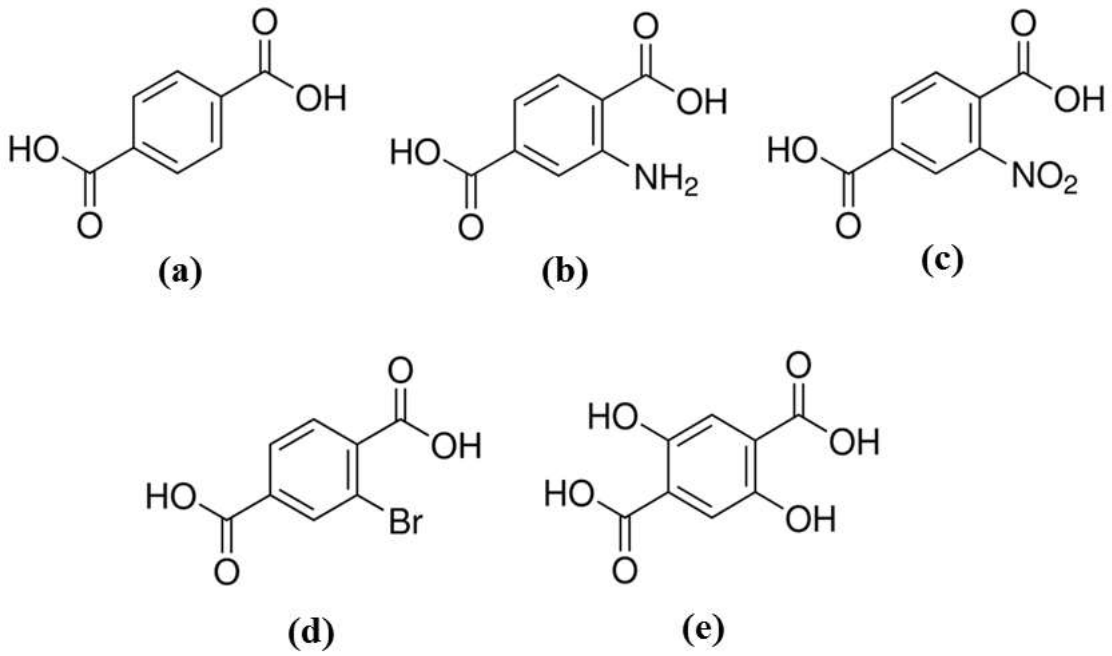

Figure 4.3: Structure of the organic ligands used in the preparation of scandium terephthalates MOFs. (a) terephthalic acid (BDC), (b) 2-aminoterephthalic acid (NH_2-BDC), (c) 2-nitroterephthalic acid (NO_2-BDC), (d) 2-bromoterephthalic acid (Br-BDC), (e) 2, 5-dihydroxyterephthalic acid ($(OH)_2$-BDC).

4.3.1 Synthesis of functionalised Scandium MOFs

A first series of experiments was performed using a mixture of solvents to obtain scandium amino-terephthalates, at lower temperature and shorter times, compared to reaction conditions used previously in the Wright group.[42, 48] The mixture of solvents was similar to those of previous experiments giving scandium carboxylates MOFs described in Chapter 3, where a mixture of DMF, ethanol and water gives the first synthesis of MIL-68(Sc), (whereas the use of DMF and ethanol gives pure MIL-101(Sc)). Thus, the procedure of mixtures of solvents and mild conditions was adopted for the preparation of amino-terephthalate MOFs. Firstly, the synthesis of amino-functionalised MIL-101(Sc), MIL-88B(Sc) and MIL-68(Sc) are discussed and the materials compared to their non-functionalised analogues.

Although the synthesis of $Sc_2(NH_2\text{-}BDC)_3$ has been reported using DMF as solvent[12] the synthetic products are microcrystalline and often of poor crystallinity, and there is often some

linker decomposition at the elevated temperatures (190℃). In this investigation the use of a mixture of solvents (DMF and H_2O) is found to facilitate the synthesis of $Sc_2(NH_2\text{-}BDC)_3$. This new procedure of synthesis involves lower temperatures (120-130 °C) and shorter times of reaction (12 h), whereas the previous method required longer times of reaction (3 days) and higher temperature (190 ^oC). The improved synthetic method yielded $Sc_2(NH_2\text{-}BDC)_3$ crystal of suitable quality for single crystal analysis, *in situ* X-ray diffraction and gas adsorption. In order to put into the context the adsorption properties of $Sc_2(NH_2\text{-}BDC)_3$, the synthesis of $Sc_2(BDC)_3$, $Sc_2(Br\text{-}BDC)_3$, and $Sc_2(NO_2\text{-}BDC)_3$ under the same conditions were also prepared. This is the first time that the $Sc_2(Br\text{-}BDC)_3$ has been prepared. Previous efforts at elevated reaction temperatures led to 'in situ' reaction of the C-Br bond with solvent DMF. Comparison of these functionalised MOFs and the post-synthetically modified $Sc_2(NH_2\text{-}BDC)$ for adsorption of CO_2 has been carried out, and adsorption of methanol and hydrocarbon compounds has also been examined. Table 4.1 lists the reaction conditions and reactant molar ratios for the mixed solvent synthesis.

a) ***NH_2-MIL-101(Sc)***: With formula $Sc_3O(OH)(H_2O)_2(NH_2\text{-}C_8H_3O_4)_3$, synthesis of amino MIL-101(Sc) involved the use of mixed solvent DMF (4 mL) and EtOH (5 mL) and 0.58 mmol of scandium chloride solution (1.45 M) and NH_2-BDC (0.75 mmol) were added into an autoclave and heated at 80 ℃ for 24 h. The solid crystalline as microcrystalline yellow powder which was filtered and washed with ethanol, then the MOF was dried overnight at 60 ℃.
b) ***NH_2-MIL-68(Sc)***: Synthesis of amino MIL-68(Sc), $Sc_3(OH)(NH_2\text{-}C_8H_3O_4)$ was performed using the mixture of solvents include; DMF (1.5 mL), EtOH (2.5 mL) and H_2O (2.5 mL), all together with 0.47 mmol of scandium chloride and 0.41 mmol of NH_2-BDC. The mixture was heated at 90 ℃ for 12 h. After heating time the autoclave

was cooled and the yellow precipitate was filtered, washed with ethanol and dried overnight at 60 ℃.

c) ***NH_2-MIL-88B(Sc)***: Three routes to synthesise NH_2-MIL-88(Sc), formula $Sc_3O(OH)(H_2O)_2(NH_2\text{-}C_8H_3O_4)_3$ were discovered. Firstly, the highly crystalline *"sample 1"*was prepared using scandium chloride (0.47 mmol) and the ligand NH_2-BDC (0.41 mmol), in a mixture of solvents DMF (4 mL) and EtOH (5 mL). The resulting mixture was heated at 80 ℃ for 24 h. Upon cooling, the reaction was filtered and washed with ethanol. The yellow solid was dried at 60 ℃ for 12 h. *"Sample 2"* was also prepared from a solvent mixture containing DMF (3 mL), H_2O (5 mL) and EtOH (5 mL), $ScCl_3$ (0.47 mmol) and the NH_2-BDC(0.41 mmol). The mixture was heated at 90 ℃ for 24 h. After heating time the yellow precipitate was filtered and washed with ethanol. The solid was dried overnight at 60 ℃. The other route involves mixed solvents DMF (1mL) and H_2O (4 mL) and heating at 65 ℃ for 12 h, keeping the same molar ratio Sc:linker, 1:1. The solid crystallised as NH_2-MIL-88(Sc) powder.

d) ***$Sc_2(NH_2\text{-}BDC)_3$*:** The MOF with formula $Sc_2(NH_2\text{-}C_8H_3O_4)_3$ was synthesised by an optimized route using mixed solvents DMF (1mL) and H_2O (4 mL), then 1.2 mmol of $ScCl_3$ and 1 mmol of the NH_2-BDC were added into the autoclave and stirred for 1 h. The mixture was heated at 130 ℃ for 12 h. The yellow precipitate was filtered and washed with water. The solid was dried overnight at 60 ℃ .

e) ***$Sc_2(Br\text{-}BDC)_3$* :** The synthesis of $Sc_2(Br\text{-}C_8H_3O_4)_3$ involves mixed solvents DMF (1 mL) and H_2O (4mL), $ScCl_3$ (1.21 mmol) and Br-BDC (1.14 mmol) the mixture was stirred for 3 h. Then the autoclave was heated at 130℃ for 12 h. After heating time the autoclave was cooled and the yellow precipitate was filtered and washed with water then dried overnight at 60 ℃.

f) ***$Sc_2(BDC)_3$*:** The synthesis of this MOF with formula $Sc_2(C_8H_4O_4)_3$ was performing using the same optimized route for comparison with the other derivatives. Using 0.66 mmol of $ScCl_3$ and 1.10 mmol of BDC were added in a mixture of solvents DMF (1 mL) and H_2O (4mL), then the solution was heated at 130℃ for 12 h. After heating time the autoclave was cooled and the precipitate was filtered and washed with water then dried overnight at 60 ℃.

g) ***$Sc_2(NO_2\text{-}BDC)_3$*: S**ynthesis of $Sc_2(NO_2\text{-}C_8H_3O_4)_3$ is achieved in water (10 mL), $Sc(NO_3)_3$ (0.73 mmol) and NO_2-BDC (1.12 mmol), the resulting mixture was heated at 190 ℃ for 72 h. Following the reaction, sample was filtered and washed with water and dried overnight at 60 ℃.

Table 4.1: Reaction conditions for the preparation of functionalised terephthalates.

Linker (***l***)	**M. R** (***Sc/l***)	**M.R** ***(S/l)***			**Temp.** (***°C***)	**Time** (**h**)	**MOF**
		DMF	EtOH	H_2O			
BDC	0.6	10		200	130	12	**Sc_2BDC_3**
BDC	1.2	10		200	130	12	**Sc_2BDC_3+MIL-53**
NH_2-BDC	0.8	70	120		80	24	**NH_2-MIL-101(Sc)**
NH_2-BDC	1.1	130	210		80	24	**NH_2-MIL-88B(Sc)**
NH_2-BDC	1.1	90	200	600	90	12	**NH_2(MIL-68+ScBDC)**
NH_2-BDC	1.1	90	200	600	90	24	**NH_2-MIL-88B(Sc)**
NH_2-BDC	1.1	45	100	300	90	12	**NH_2-MIL-68(Sc)**
NH_2-BDC	0.6	10		200	120-130	12	**$Sc_2(NH_2\text{-}BDC)_3$**
NH_2-BDC	1.0	10		200	120-130	12	**$Sc_2(NH_2\text{-}BDC)_3$**
NH_2-BDC	0.6	10		200	65	12	**NH_2-MIL-88B(Sc)**
NH_2-BDC	0.6-1	10		200	80-110	16-24	**Mix. of NH_2(Sc_2BDC_3+MIL-88B+MIL-53)**
Br-BDC	1.1	10		200	130	12	**$Sc_2(Br\text{-}BDC)_3$**
NO_2-BDC	0.6	10		200	130	12	**Unknown phase**
NO_2-BDC	0.6			500	190	48	**$Sc_2(NO_2\text{-}BDC)_3$**

The scandium source was $ScCl_3$ solution (1.45 M). M.R is molar ratio, Sc/l is the molar scandium to linker ratio, and the S/l the solvent to linker ratio

4.3.2 Mixed solvents and mixed ligands to synthesize 'amino MIL-53(Sc)'

Attempts to prepare pure NH_2-MIL-53(Sc) were unsuccessful using the general route of synthesis mentioned above and only the aminoterephthalic acid, giving instead mixtures of NH_2-MIL-53(Sc) with $Sc_2(NH_2\text{-}BDC)_3$ or NH_2-MIL-88B, depending on the conditions. Therefore, a second series of experiments was performed. This series followed the same approach of mixed solvents but also a mixture of linkers (Figure 4.4) with NH_2-BDC the major linker. Table 4.2 gives the conditions used in these preparations. The relative amount of two ligands in samples was confirmed post-synthesis by solution phase NMR of the dissolved solids. The samples (4.5 mg) were digested in DMSO-d_6 and 0.3 mL of HNO_3 (0.2 M) followed by sonication for ca. 5 min leading to complete dissolution.

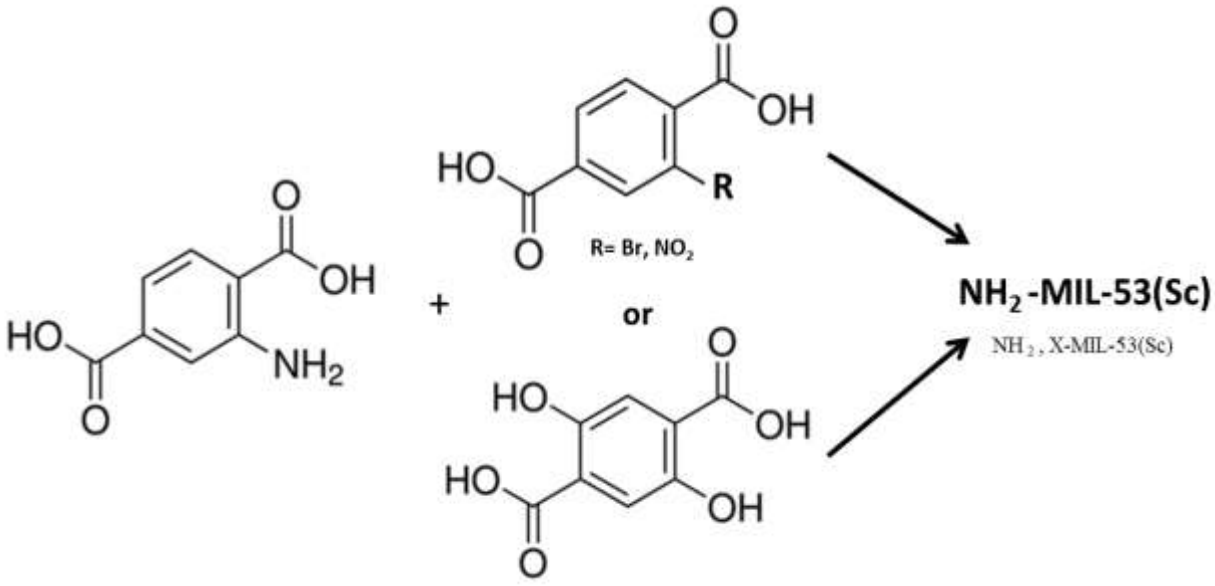

Figure 4.4: Approach of mixed linker synthesis to prepare amino MIL-53(Sc).

a) ***MIL-53(Sc)[NH_2-BDC]$_x$·[NO_2-BDC]y***: To prepare NH_2-MIL-53(Sc) $Sc_3(OH)(NH_2\text{-}C_8H_3O_4)$ with y% of NO_2-BDC, several attempt were made. A typical synthesis for example, the sample prepared with 10% NO_2-BDC was prepared using scandium chloride (1.2 mmol) and linkers NH_2-BDC (0.69 mmol) and NO_2-BDC(0.28 mmol),

all together in mixed solvent DMF (2 mL) and H_2O (8 mL). The mixture was heated at 130 ℃ for 12 h. After heating time the autoclave was cooled and the yellow precipitate filtered and washed with water. The solid was dried overnight at 60℃

b) ***MIL-53(Sc)[NH_2-BDC]$_x$·[$(OH)_2$-BDC]y***: The synthesis contained 20% of $(OH)_2$-BDC was carried out as follows. Mixed solvents DMF (1 mL) and H_2O (4 mL), and $ScCl_3$ (1.2 mmol) and both ligands NH_2-BDC (0.58 mmol) and $(OH)_2$-BDC (0.41 mmol) were added and the and the resulting suspension stirred until homogeneous before being heated for 12 h at 130 ℃. Finally, the yellow precipitate after heating time was filtered and washed with water and drying the solid at 60 ℃.

c) ***MIL-53(Sc)[NH_2-BDC]$_x$·[Br-BDC]y***: Several synthesis in attempts to attempt 'amino-MIL-53(Sc)' with added Br-BDC were explored. This MOF contained 15 % of Br-BDC where $ScCl_3$ (1.2 mmol) and both ligands, NH_2-BDC (0.65 mmol) and Br-BDC (0.35 mmol) in 2 mL of DMF and 8 mL of H_2O were mixed and sealed in an autoclave and heated at 130 ℃ for 12 h. After cooling to room temperature crystalline yellow solid were filtered and washed with water, and dried overnight at 60 ℃.

Table 4.2: Reaction conditions used to prepare 'amino-functionalised MIL-53(Sc)' based on the approach of mixed ligands.

$ScCl_3$ (mmol)	**Ligand 1 NH_2-BDC** (mmol)	**Ligand 2 *X*-BDC**	**Ligand 2** (mmol)	**M.R** (Sc/*l*)	**Solvent** (S/*l*)		**Temp. (^oC)**	**Time (h)**	**Product**
					DMF	H_2O			
0.6-1	0.6-1.0	0	0	0.6-1.0	10	200	120-130	12	$Sc_2(NH_2\text{-BDC})_3$
0.6	0.60	0	0	1.0	20	400	80-100	12-24	NH_2-MIL-88B(Sc)
0.60	0.60	0	0	1.0	20	600	130	12	Mix. $Sc_2(NH_2\text{-BDC})_3$ + NH_2(MIL-53)
0.60	0.60	0	0	1.0	20	400	130	12	Mix. NH_2(MIL-53)+ $Sc_2(NH_2\text{-BDC})_3$
1.2	0.9	NO_2-BDC	0.10	1.1	10	200	130	12	Mix. $Sc_2(NH_2\text{-BDC})_3$ +NH_2-MIL-53(Sc)
1.2	0.85	NO_2-BDC	0.15	1.1	10	200	130	12	Mix. $Sc_2(NH_2\text{-BDC})_3$ +NH_2-MIL-53(Sc)
1.2	0.69	NO_2-BDC	0.28	1.1	10	200	130	12	Mix. $Sc_2(NH_2\text{-BDC})_3$ +NH_2-MIL-53(Sc)
1.2	0.69	NO_2-BDC	0.28	1.1	20	400	130	12	'NH_2-MIL-53(Sc)'(10%NO_2-BDC)
1.2	0.58	$(OH)_2$-BDC	0.41	1.1	10	200	130	12	'NH_2-MIL-53(Sc)'(20%$(OH)_2$-BDC)
1.2	0.90	Br-BDC	0.12	1.1	10	200	130	12	$Sc_2(NH_2\text{-BDC})_3$ + impurity
1.2	0.65	Br-BDC	0.35	1.0	10	200	130	12	Sc_2(Br-BDC)$_3$ + 'NH_2-MIL-53(Sc)'
1.2	0.65	Br-BDC	0.35	1.0	20	400	130	12	'NH_2-MIL-53(Sc)'(15%Br-BDC)
1.2	0.40	Br-BDC	0.65	1.1	20	400	130	12	Sc_2(Br-BDC)$_3$ + impurity

M.R = Molar ratio, Sc/l = scandium to linker molar ratio, where l is the sum of linkers used in the synthesis, and S/l denotes solvent to linker molar ratio.

4.4 Results and Discussions

4.4.1 NH_2-MIL-101(Sc)

The most successful attempts at the synthesis of NH_2-MIL-101(Sc) gave a mixture of this as the majority phase with some impurity NH_2-MIL-88B(Sc) (Figure 4.5). The PXRD pattern of the solid obtained was compared with the as-prepared MIL-101(Sc) and the MIL-88B(Sc) simulated. The sample contained the principal reflection for MIL -101(Sc) and also it is clearly that the sample has some of the MOF amino-MIL-88B(Sc).

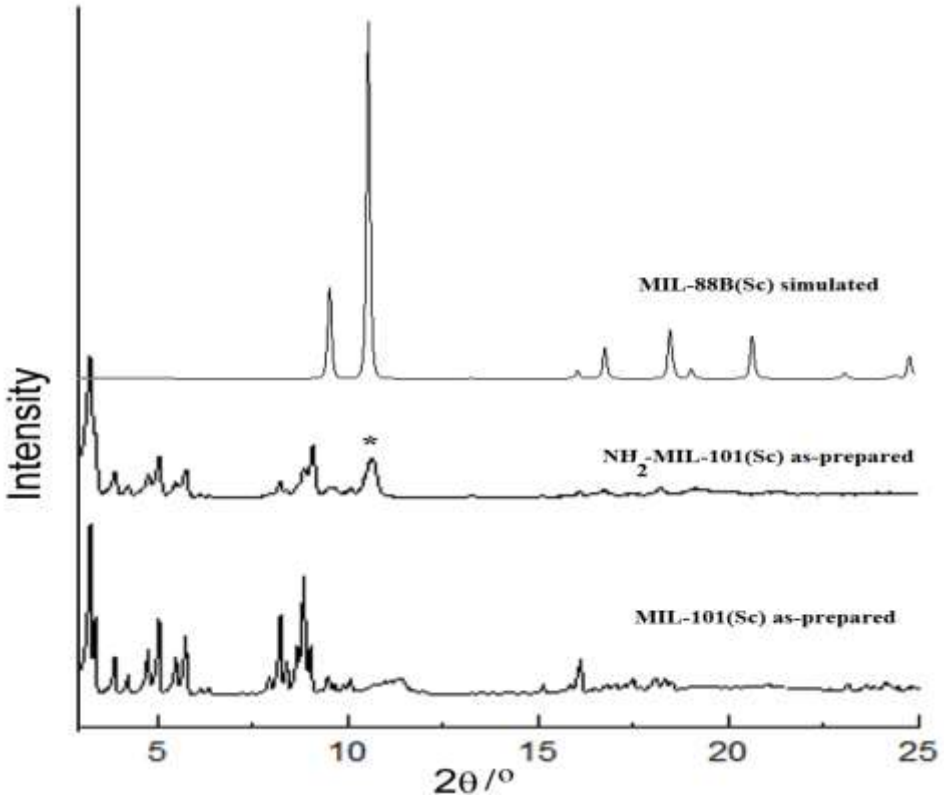

Figure 4.5: PXRD of as-prepared NH_2- MIL-101(Sc) compared to that measured for MIL-101(Sc) and the simulated for MIL-88B(Sc).

TGA of as-synthesised NH_2-MIL-101(Sc) under flowing air (Figure 4.6) shows a weight loss of 14.5% up to 150 °C attributed to the solvent. The amino-functionalised form is thermally less stable than unfunctionalised MIL-101(Sc), starting to collapse at 300 ℃ rather than 450 ℃.

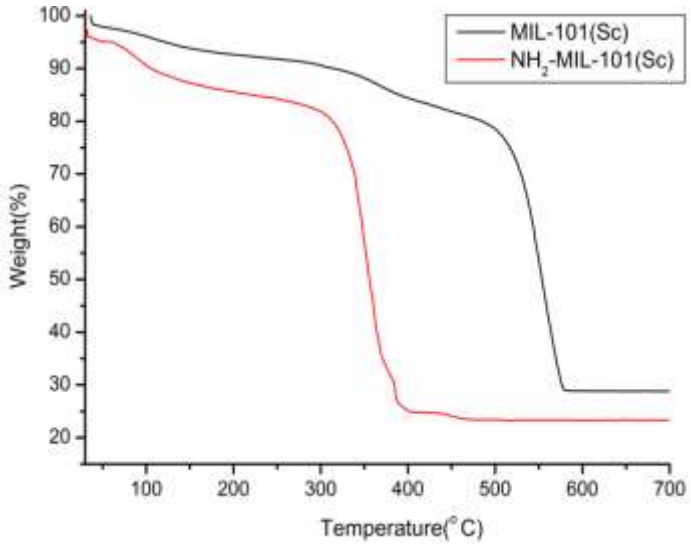

Figure 4.6: Thermogravimetric analysis on MIL-101(Sc) in the as-prepared form (black one) and amino-functionalised MIL-101(Sc) (red one) under flowing air for 12 h.

Activation by heating at 65 - 120 ℃ resulted in recrystallisation to NH_2-MIL-88B(Sc) to a greater or lesser extent (Figure 4.7). Figure 4.8 shows the N_2 adsorption isotherm of a sample heated at 65 ℃ for 4 h. The sample exhibited a surface area of 180 m^2 $g^{-1.}$ The TGA (Figure 4.6) therefore shows that once recrystallized to MIL-88B(Sc), NH_2-MIL-88(B) is less stable than MIL-88B(Sc).

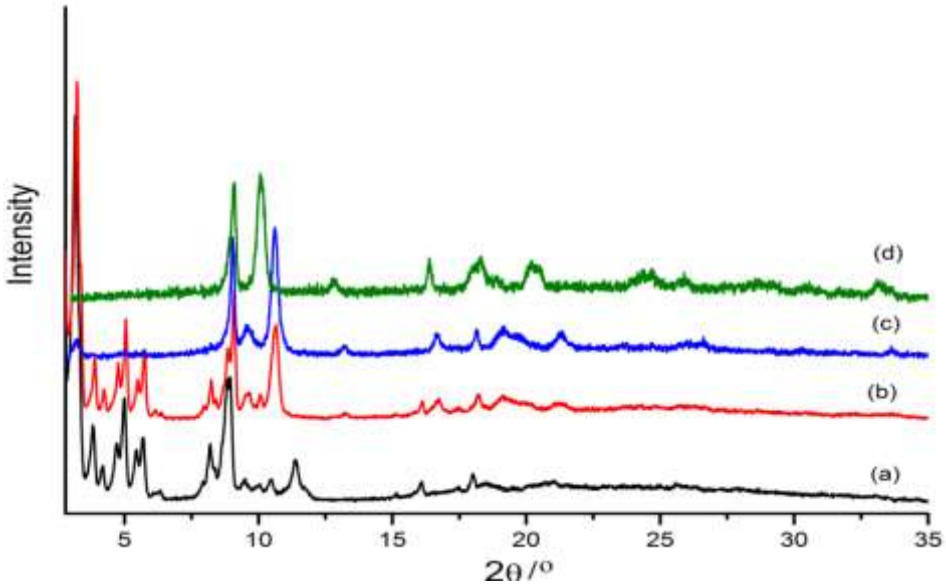

Figure 4.7: PXRD of (a) MIL-101(Sc) as-prepared, (b) NH_2-MIL-101(Sc) as-prepared, (c) and (d) NH_2-MIL-101(Sc) after activation treatment at 65 ℃ and at 80 ℃ respectively, showing the recrystallization into NH_2-MIL-88B.

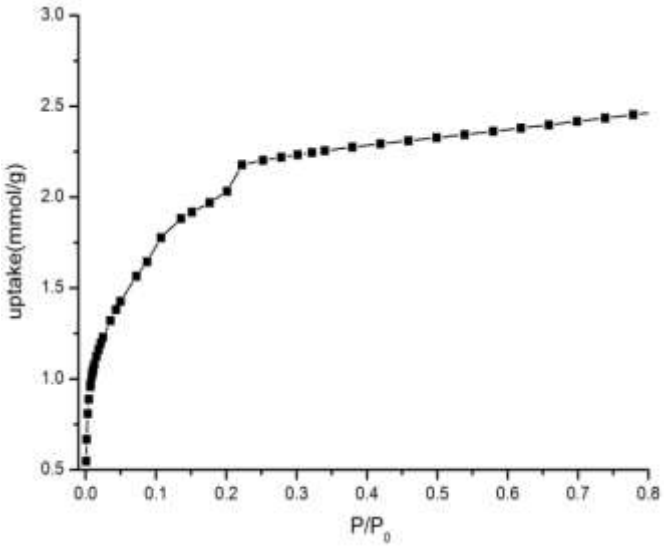

Figure 4.8: Nitrogen adsorption at -196℃ on functionalised NH_2 -MIL-101(Sc)

4.4.2 NH_2-MIL-68(Sc)

Several routes were explored to optimise the pure preparation of NH_2-MIL-68(Sc).The reactions conditions involves scandium chloride (0.47 mmol) and NH_2-BDC (0.41) in a mixture of solvents DMF (1.5 mL), EtOH (2.5 mL) and H_2O (2.5 mL).The PXRD of the solid was obtained and compare with XRD pattern of as-prepared MIL-68(Sc) confirming the pure phase (Figure 4.9).

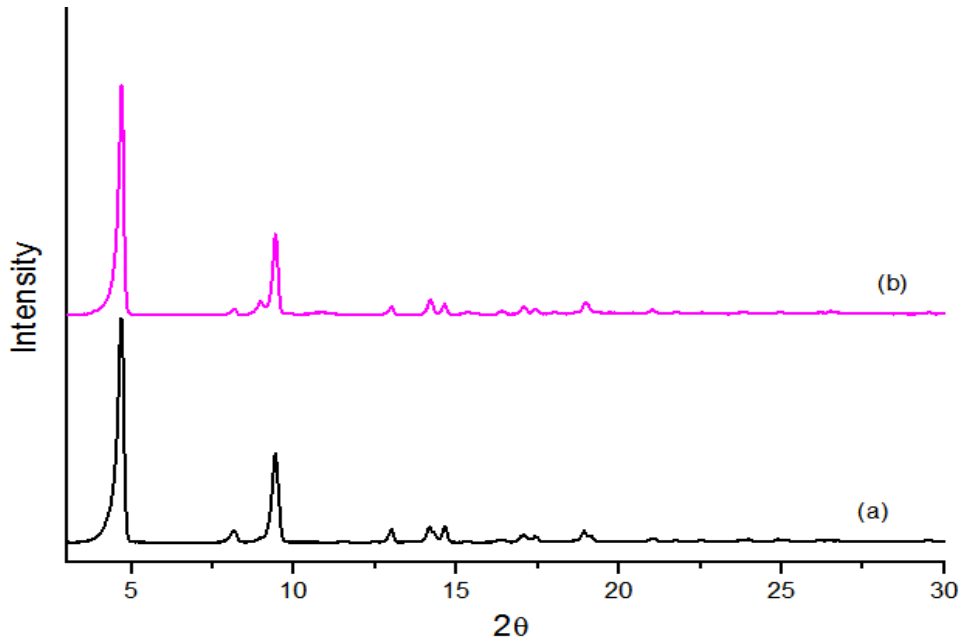

Figure 4.9: PXRD for (a) as-prepared MIL-68(Sc) and (b) as prepared NH_2-MIL-68(Sc).

TGA was performed under flowing air. Figure 4.10 shows 8 wt% loss of solvent by 300 ℃ and framework decomposition beginning at 450 ℃. N_2 and CO_2 adsorption were carried out (Figure 4.11) following activation in a tube furnace under flowing air at 200 ℃ for 12 h and activation under vacuum at 120 ℃ prior to isotherm measurement. N_2 adsorption gave a BET surface are of only 120 m^2g^{-1} (2 mmol g^{-1}), which is very low compared to that obtained for NH_2-MIL-68(In) (1230 m^2 g^{-1}),[13] but close to that obtained for MIL-68(Sc) (200 m^2 $g^{-1,}$ uptake of 3 mmol g^{-1}).[49] As observed in the case of MIL-68(Sc), CO_2 adsorption isotherm was of type IV, with an uptake of 9 mmol g^{-1} measured at –77 °C, which is lower than the uptake obtained for activated unfunctionalised MIL-68(Sc) (20 mmol g^{-1}).

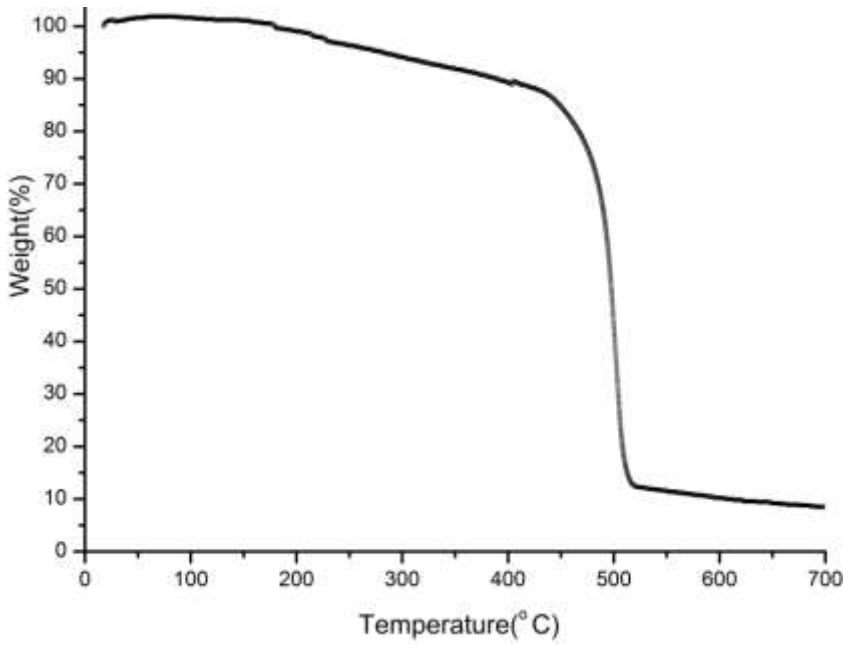

Figure 4.10: Thermogravimetric analysis of NH_2-MIL-68(Sc).

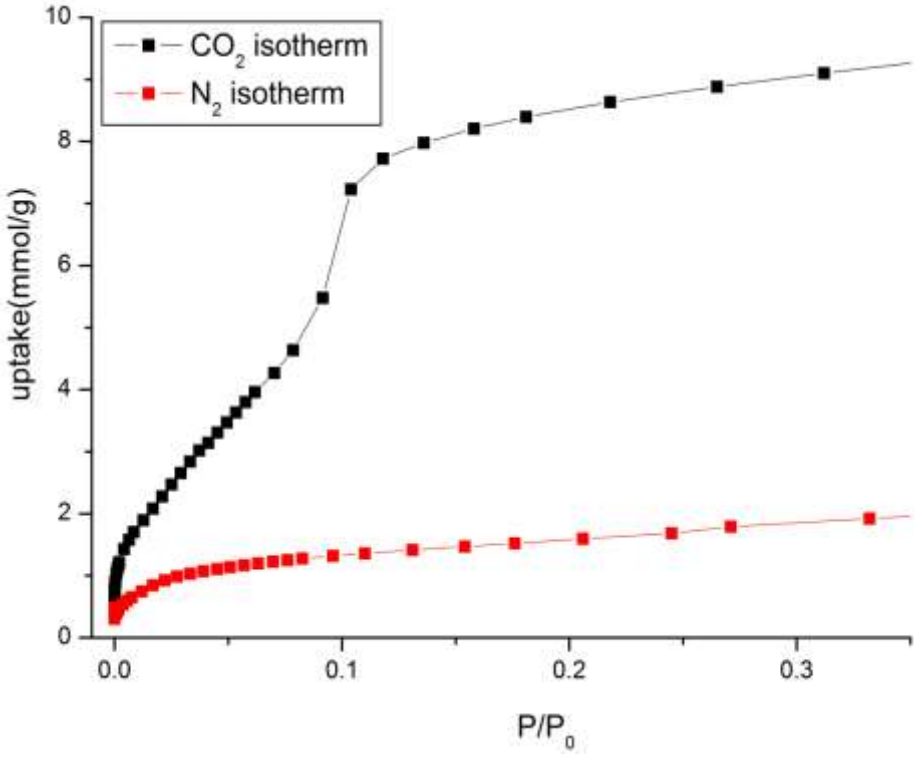

Figure 4.11: CO_2 and N_2 isotherms collected on NH_2-MIL-68(Sc) at –77 °C and -196 ℃ respectively

4.4.3 NH_2-MIL-88B(Sc)

The synthesis of NH_2-MIL-88(Sc) was performed at a temperature range between 65-90 ℃, with short reaction times (12 or 24 h). Figure 4.12 gives the PXRD collected on two samples prepared under different reaction conditions given in Table 4.1, compared with the simulated pattern for MIL-88B(Sc). For "*sample 1",* the powder diffraction pattern was indexed as the hexagonal unit cell ($P\bar{6}2c$) with *a* = 13.1838Å, *c* = 18.603Å, *volume* = 2798.8Å^3. Thermogravimetric analysis (Figure 4.13) shows a weight loss of 10% up to 150 ℃ attributed to loss of solvent and another major weight loss after 400℃ attributed to decomposition. This material was heated at 120 ℃ for 12 h, and changes in the PXRD indicate breathing behaviour, characteristic of this MOF, because the diffraction pattern could be indexed as hexagonal *a* = 11.1610 Å, *c* = 19.4863 Å, *volume* = 2102.4 Å^3 after solvent removal.

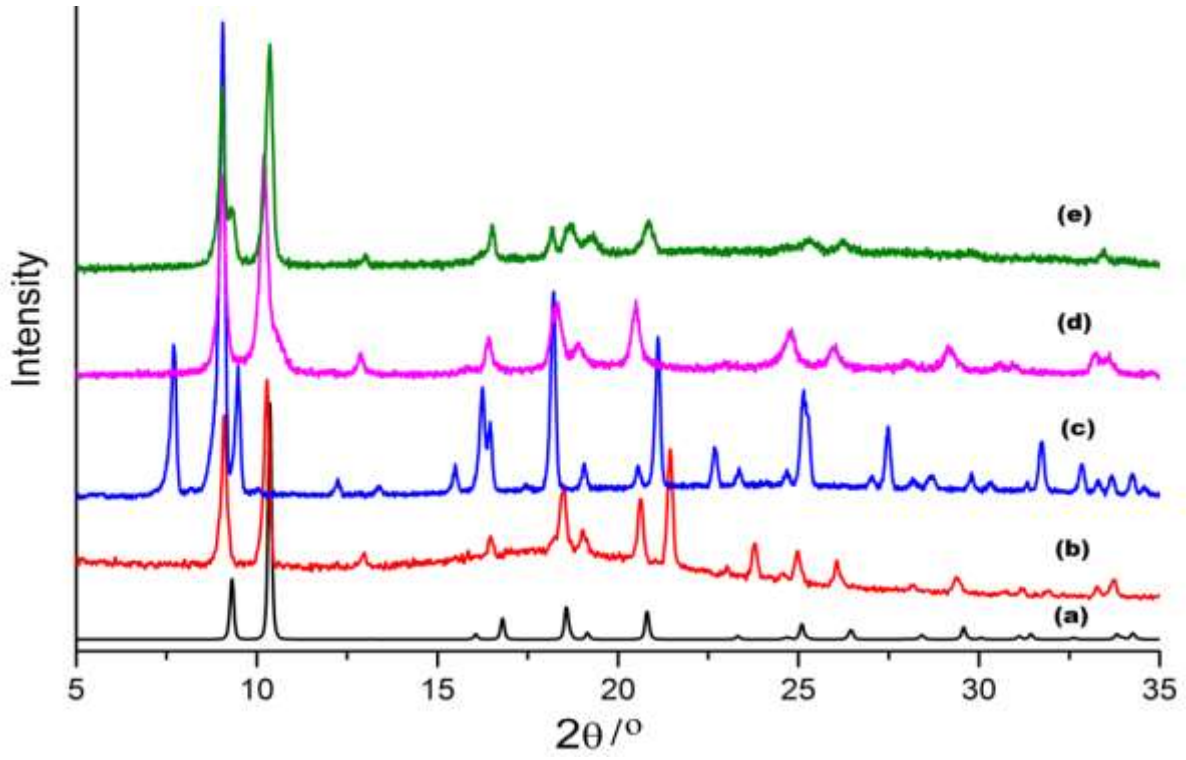

Figure 4.12: PXRD for MIL-88B: (a) simulated for MIL-88B(Sc), (b) as-prepared MIL-88B(Sc), (c) as-prepared NH_2-MIL-88(Sc) *"sample 1"*, (d) dried *"sample 1"* NH_2-MIL-88(Sc), (e) NH_2-MIL-88(Sc) *"sample* 2".

The second sample '2', the diffraction pattern of the as-prepared material was indexed with a hexagonal cell, a = 11.3858 Å, c = 19.681 Å, volume = 2100 $Å^3$ and so shown already to be in the closed form. TGA of this sample showed higher thermal stability than that of *'sample 1'*, with decomposition starting at around 550 ℃ (Figure 4.13). This is probably because the structure remains in the closed form, and air cannot enter to initiate decomposition. The '*sample 2'* was obtained as yellow crystals of NH_2-MIL-88(Sc) crystallising as bipyramidal hexagonal prism-like single crystals ~30-50 μm in length and ~5 μm in width (Figure 4.14). These are similar to those reported by Pham et al.[50] for the synthesis of NH_2-MIL-88B(Fe), but they required Pluronic F127 and acetic acid in the synthesis. Here in this work the same morphology is obtained when the mixed solvents are used in the synthesis without addition of extra acids.

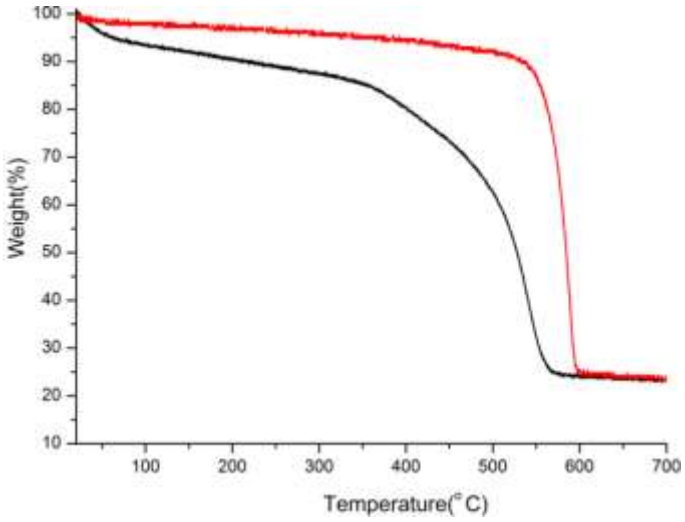

Figure 4.13: Thermogravimetric analysis on NH_2-MIL-88(Sc). as-prepared sample 1 (black) and as-prepared sample 2 (red).

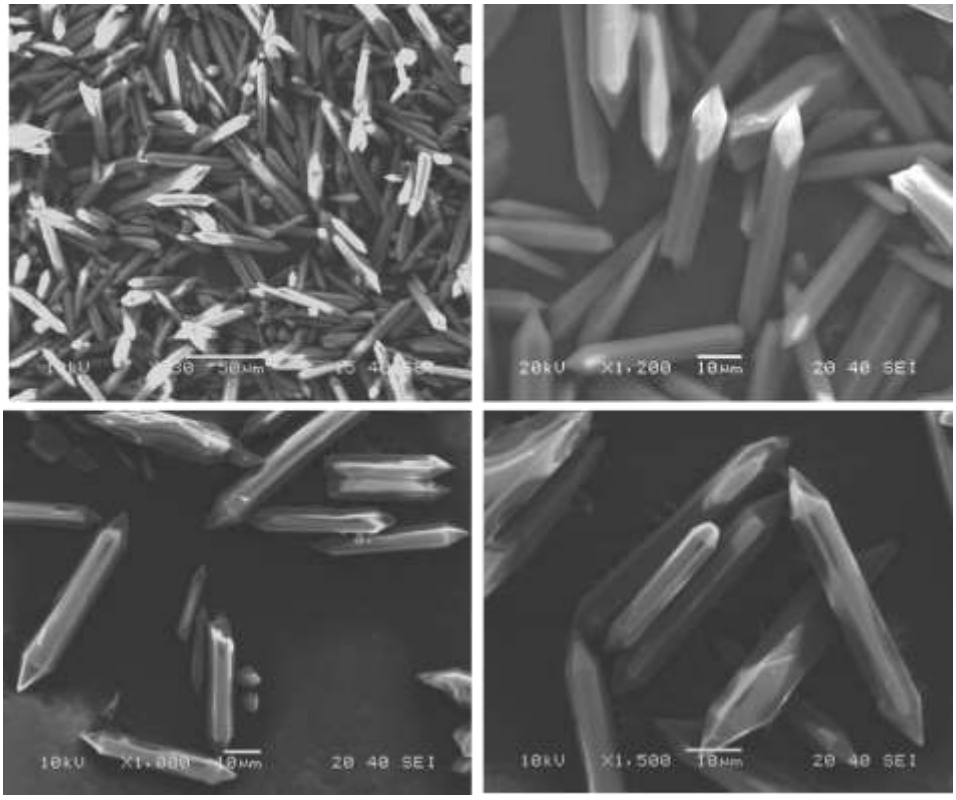

Figure 4.14: SEM images of NH_2-MIL-88(Sc); "sample 2" bipyramidal hexagonal prism-like single crystals (~30-50 μm in length).

Adsorption analysis of N_2 on both samples showed no uptake but CO_2 isotherms at -77 ℃ (Figure 4.15) indicated uptakes of 2.5 mmol g^{-1}, in contrast to the unfunctionalised MIL-88B(Sc), which showed no uptake. The isotherm of NH_2-MIL-88B(Sc) shows gradual

opening structure and demonstrates that the amino-functionalisation enhances CO_2 adsorption.

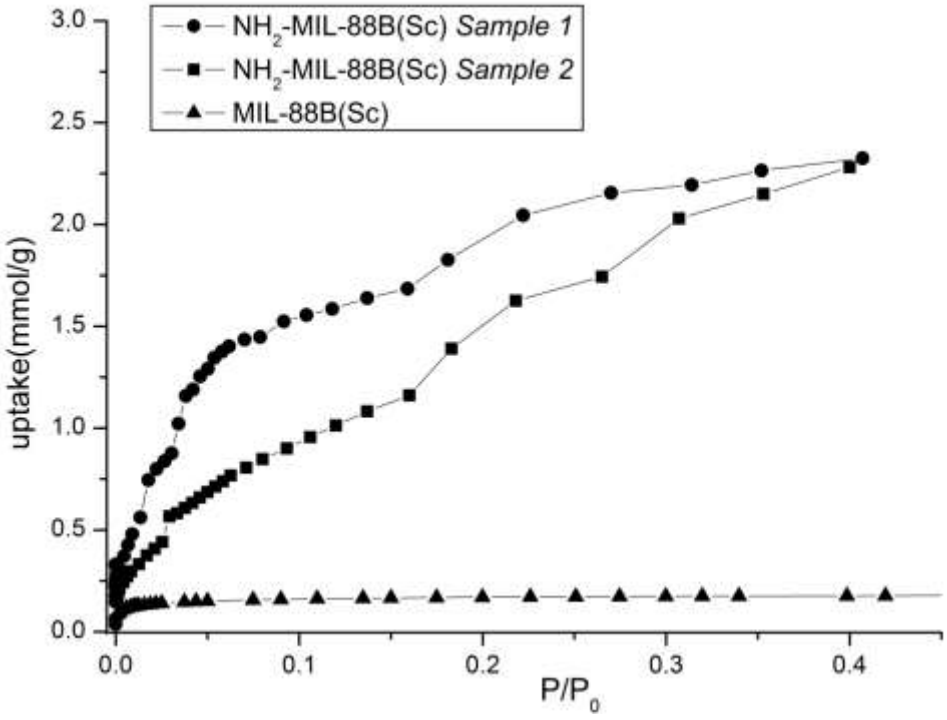

Figure 4.15: CO_2 gas adsorption at -77 ℃ on NH_2-MIL-88(Sc) and MIL-88B(Sc)

4.4.4 $Sc_2(NH_2\text{-}BDC)_3$

4.4.4.1 Synthesis and structural analysis of $Sc_2(NH_2\text{-}BDC)_3$

Following the mixed solvents route, pure $Sc_2(NH_2\text{-}BDC)_3$ was obtained for first time. Previously this material had only been prepared as microcrystalline powder at high temperatures and with Sc_2O_3 impurity.[12] The resulting yellow prismatic crystals of $Sc_2(NH_2\text{-}BDC)_3$ were suitable for single crystal analysis. Powder diffraction data confirms the phase identity and purity when compared with that simulated from the single crystal structure (Figure 4.16). The structure was solved and refined with the Crystals software suite,[51] in the orthorhombic space group *Fddd* .The crystallographic details are given in Table 4.3 and Table 4.4.

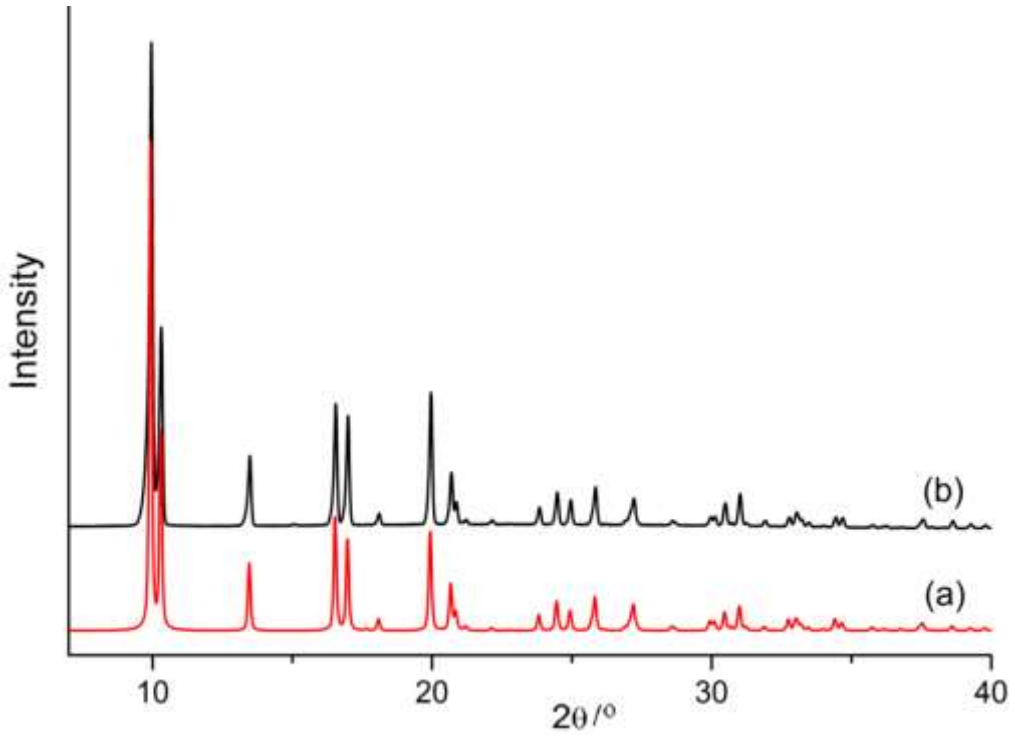

Figure 4.16: Experimental powder diffraction pattern of $Sc_2(NH_2\text{-}BDC)_3$ (b) compared to the pattern simulated from the single crystal model(a).

Table 4.3: Crystallographic data for $Sc_2(NH_2\text{-}BDC)_3$ from SXRD

Structure	**$Sc_2(NH_2\text{-}BDC)_3$**
Formula unit	$Sc_2(C_8H_5NO_4)_3$
Crystal system	Orthorhombic
Space group	*Fddd*
X-ray source	Cu $K\alpha_1$
Diffractometer	
Wavelength (Å)	1.54187
Unit cell (Å)	
a/Å	8.7059(14)
b/Å	20.802(4)
c/Å	34.346(6)
Volume/Å^3	6220.1(11)
R	0.0632
Rw	0.1235

Table 4.4: Atomic positions and occupancies obtained from SXRD of $Sc_2(NH_2\text{-}BDC)_3$

Atom		x	y	z	Atom site Uiso or equiv	Occupancy
Sc1	Sc	0.375	0.375	0.61550(2)	0.0107	1.0000 Uani
O2	O	0.2448(3)	0.41592(14)	0.57058(7)	0.0297	1.0000 Uani
O4	O	0.0066(3)	0.41605(16)	0.59243(8)	0.0395	1.0000 Uani
O9	O	0.5049(3)	0.45799(12)	0.61482(10)	0.0388	1.0000 Uani
C3	C	0.1049(4)	0.43010(19)	0.56720(11)	0.0248	1.0000 Uani
C5	C	0.0542(4)	0.4663(2)	0.53211(11)	0.0299	1.0000 Uani
C6	C	-0.0993(5)	0.4832(3)	0.52898(13)	0.0465	1.0000 Uani
C7	C	-0.1555(5)	0.5166(3)	0.49719(13)	0.0488	1.0000 Uani
C10	C	0.625	0.4865(2)	0.625	0.0245	1.0000 Uani
C11	C	0.625	0.5582(2)	0.625	0.0299	1.0000 Uani
C12	C	0.4922(14)	0.5918(8)	0.6334(4)	0.0449	0.5000 Uani
C13	C	0.4930(13)	0.6588(9)	0.6344(4)	0.0453	0.5000 Uani
N1	N	0.332(4)	0.6839(17)	0.6474(9)	0.145(13)	0.2500 Uiso
N8	N	-0.3158(13)	0.5343(5)	0.4983(3)	0.081(3)	0.5000 Uiso
H81	H	-0.3722	0.524	0.5186	0.0894	0.5000 Uiso
H82	H	-0.3569	0.5555	0.4787	0.0894	0.5000 Uiso
H11	H	0.319	0.7257	0.6495	0.1396	0.2500 Uiso
H12	H	0.2545	0.6576	0.6509	0.1396	0.2500 Uiso
H61	H	-0.1678	0.4716	0.5493	0.056	1.0000 Uiso
H121	H	0.3998	0.5691	0.6384	0.0535	0.5000 Uiso
H71	H	-0.2616	0.5275	0.4955	0.058	0.5000 Uiso
H131	H	0.4026	0.6816	0.6416	0.0545	0.2500 Uiso

Analysis of single-crystal diffraction data collected on a sample gave the position of the N of the $–NH_2$ group in the framework. Figure 4.17 shows the different positions of the $–NH_2$ group, one group 1 and two on group 2 terephthalate (Figure 4.18). (CIF file available, see the Appendix B).

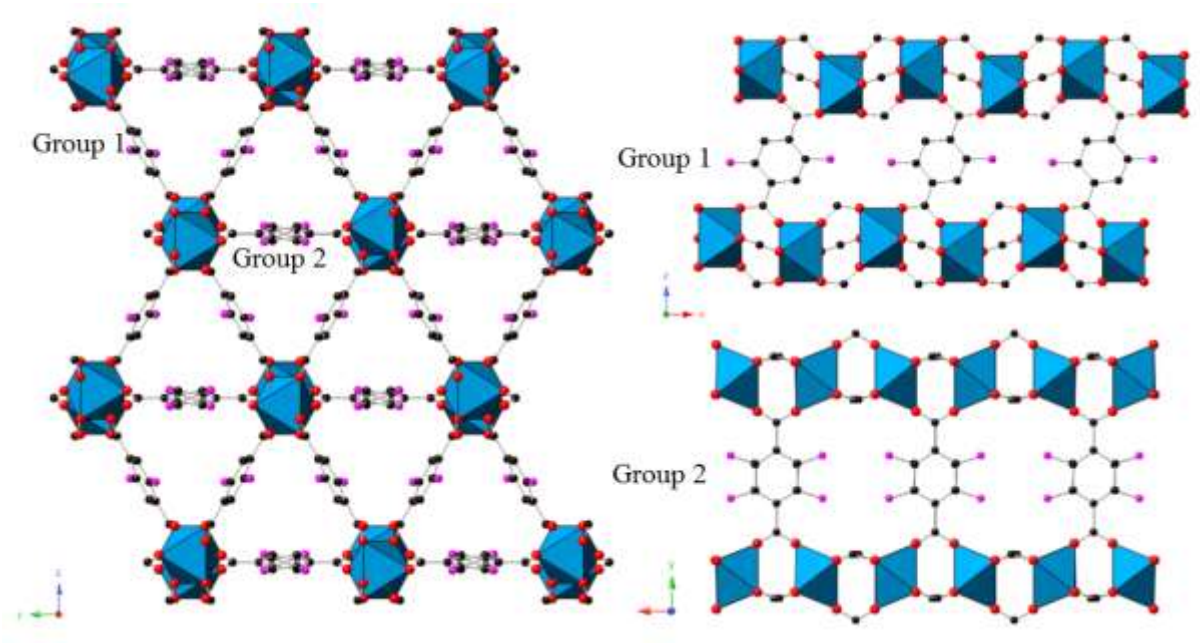

Figure 4.17: View of the structure of $Sc_2(NH_2\text{-}BDC)_3$ down the channels and perpendicular to the two types of terephthalate layers (Group 1(top), Group 2 (middle). ScO_6 octahedra are shown in blue. Black, pink and red spheres represent the carbon, nitrogen and oxygen atoms of the organic linker respectively.

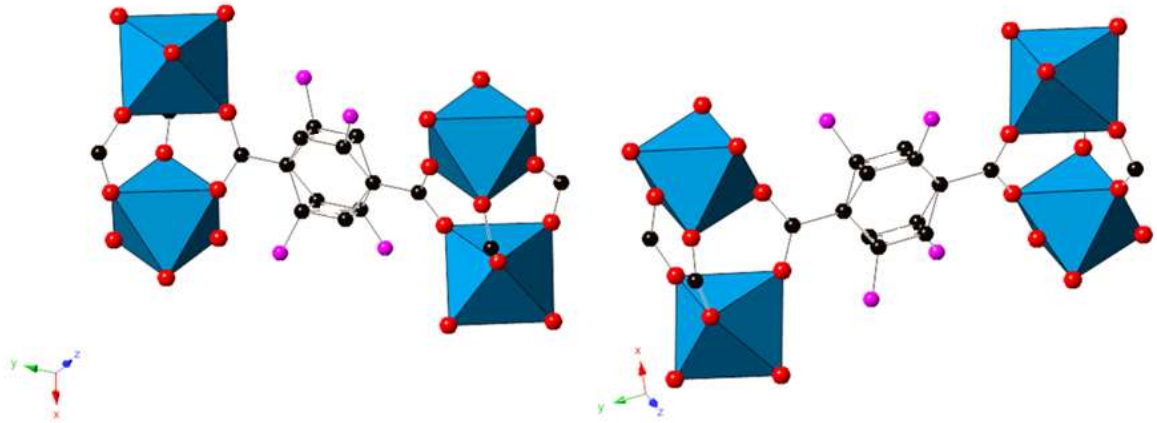

Figure 4.18: Images of disordered, tilted positions of the amino-terephthalate groups in $Sc_2(NH_2\text{-}BDC)_3$.

CHN and EDX analysis give a composition of the MOF as follows, Sc expected 14.3 wt%; 17.7% measured; C expected 45.9 wt%; 44.5 % wt measured, N expected 6.7 wt% measured 7.5 wt. %. Thermogravimetric analysis on $Sc_2(NH_2\text{-}BDC)_3$ in Figure 4.19 exhibits remarkably high thermal stability, with complete decomposition of the framework to Sc_2O_3 at 500℃

under flowing air. Notably no solvent molecules are present in the channels of the MOF after synthesis.

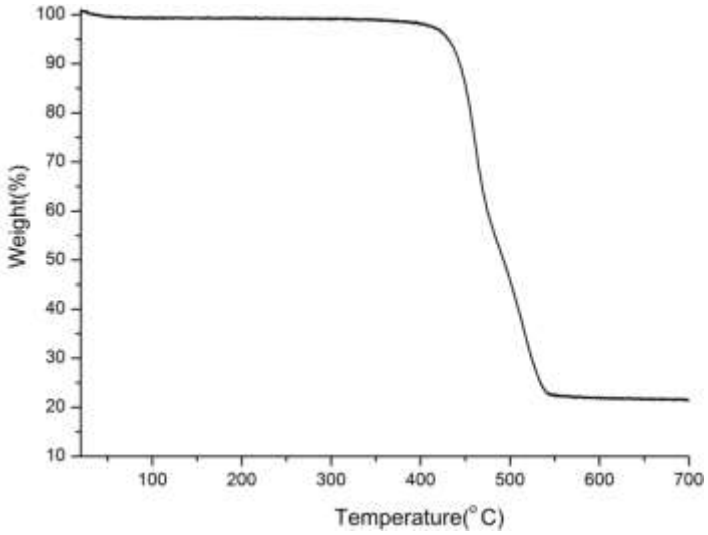

Figure 4.19: Thermogravimetric analysis on $Sc_2(NH_2\text{-}BDC)_3$.

Figure 4.20 shows SEM images of the prism-like crystals of two of the $Sc_2(NH_2\text{-}BDC)_3$ samples prepared. The size of the crystals is fairly uniform, with typical crystals having dimensions of 20 - 30 μm in width (across cross section) and 60 - 110 μm in length and showed show that the crystals exhibit a well-defined and clearly identifiable anisotropic morphology with a single long axis and a pseudohexagonal cross section.

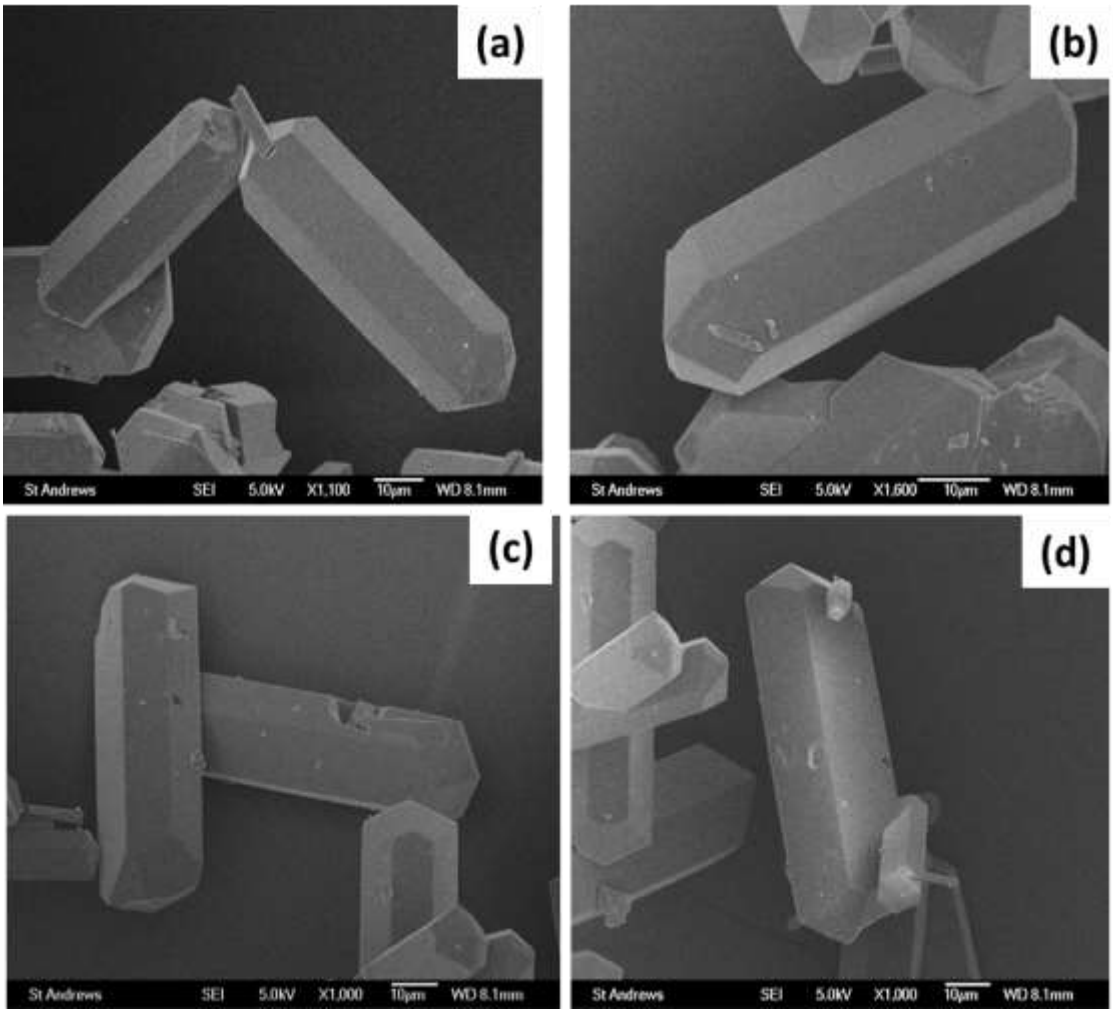

Figure 4.20: SEM secondary electron micrographs of samples of as-prepared $Sc_2(NH_2\text{-}BDC)_3$

Face indexing was performed on several crystals of $Sc_2(NH_2\text{-}BDC)_3$ in collaboration with J. Sotelo and S. Moggach (at the University of Edinburgh). Analysis of the crystals by face indexing of the as-prepared solid was used to establish the orientation of the crystallographic unit cell relative to the physical morphology of the crystal. Face indexing shows the longest (in microns) morphological direction of the crystals is parallel to the *a* axis (channel) of the crystallographic unit cell. Face indexing also reveals that the crystals have a regular morphology, with planes parallel to the long axis expressing the {001} and the {011} planes giving a pseudohexagonal cross section (Figures 4.21).

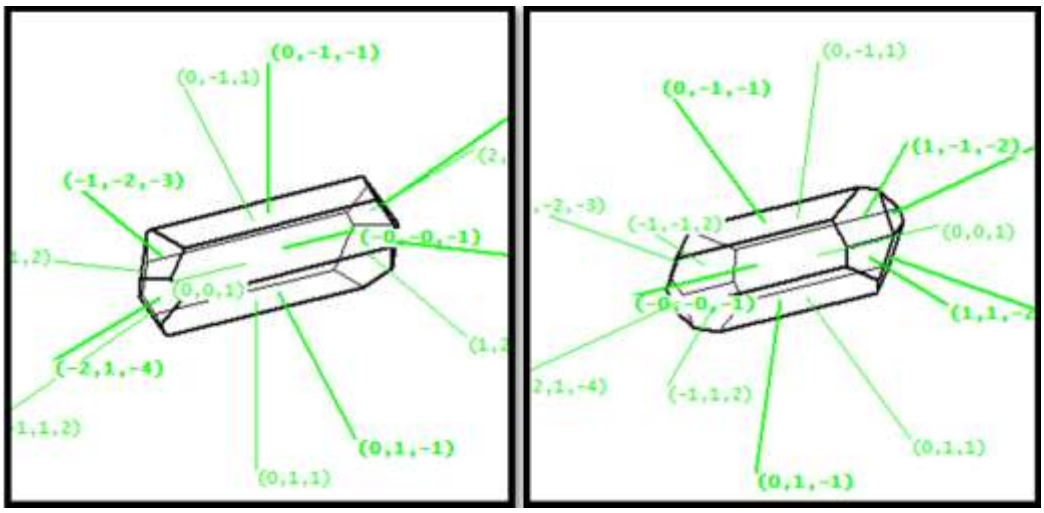

Figure 4.21: Dramatic representation of single crystals of $Sc_2(NH_2\text{-}BDC)_3$, showing the faces normal. Note the main six faces parallel to the longest axis are (0 0 1), (0 0 -1), (0 1 1), (0 -1 1), (0 1 -1) and (0 -1 -1).

Solid state MAS NMR of ^{1}H, ^{13}C and ^{45}Sc was performed. The spectra are shown in Figure 4.23. The ^{1}H MAS NMR spectrum (Figure 4.22a) shows peaks at chemical shift (7.2 and 7.7 ppm) typical of aromatic protons, the other peak at 5 ppm is assigned to NH_2 protons. The ^{13}C MAS NMR is consistent with that of the linker molecule, with a chemical shift (~150 ppm) characteristic of the aromatic carbon attached to the NH_2-group (Figure 4.22 (b and c)). The spectrum for ^{45}Sc MAS NMR spectra for the as-prepared $Sc_2(NH_2\text{-}BDC)_3$ is shown in Figure 4.22(e) and, expanded in Figure 4.22(f), and show a smooth featureless lineshapes with characteristic 'tails' at low frequency, indicating little disorder. Also, Figure 4.22(d) shows the ^{13}C MAS NMR spectra with the variable contact time. The resonance corresponding to the C1 site is shifted downfield owing to the electron withdrawing NH_2-group.

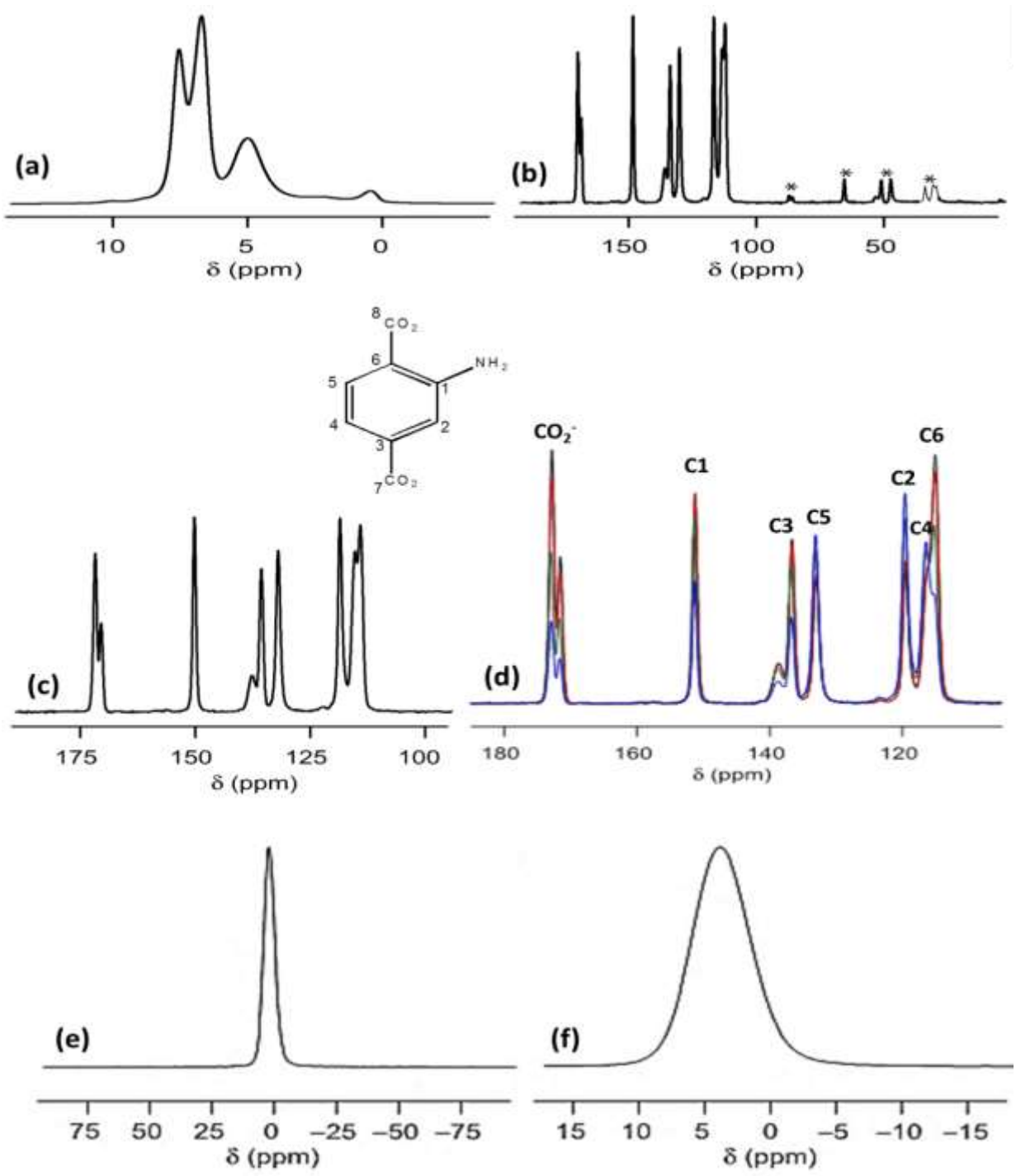

Figure 4.22: NMR Spectra collected on $Sc_2(NH_2\text{-}BDC)_3$; (a) ^{1}H and (b, c, d) ^{13}C spectra (14.1 T) where (c) and (d) are expanded carboxylate and aromatic regions of variable-contact time; and (e, f) ^{45}Sc spectra. The MAS rate was 40 kHz, 12.5 kHz and 40 kHz for ^{1}H, ^{13}C and ^{45}Sc, respectively. The contact times were 5 ms (blue), 10 ms (green), 25 ms (red) and 20 ms (black).* Indicate the spinning sidebands .

4.4.4.2 Adsorption properties of $Sc_2(NH_2\text{-}BDC)_3$

(a) N_2 adsorption on $Sc_2(NH_2\text{-}BDC)_3$.

Nitrogen adsorption experiments on $Sc_2(BDC\text{-}NH_2)_3$ were carried out after outgassing at 130°C under vacuum for 12 h. The uptake on this sample is 4 mmol g^{-1} (pore volume 0.138 $cm^3\ g^{-1}$) (Figure 4.23), which is similar to the pore volume obtained for the microcrystalline powder $Sc_2(BDC\text{-}NH_2)_3$ (0.148 $cm^3\ g^{-1}$) and lower than the non-functionalised Sc_2BDC_3 (0.263 $cm^3\ g^{-1}$) due to the presence of the bulky -NH_2 groups in the framework.

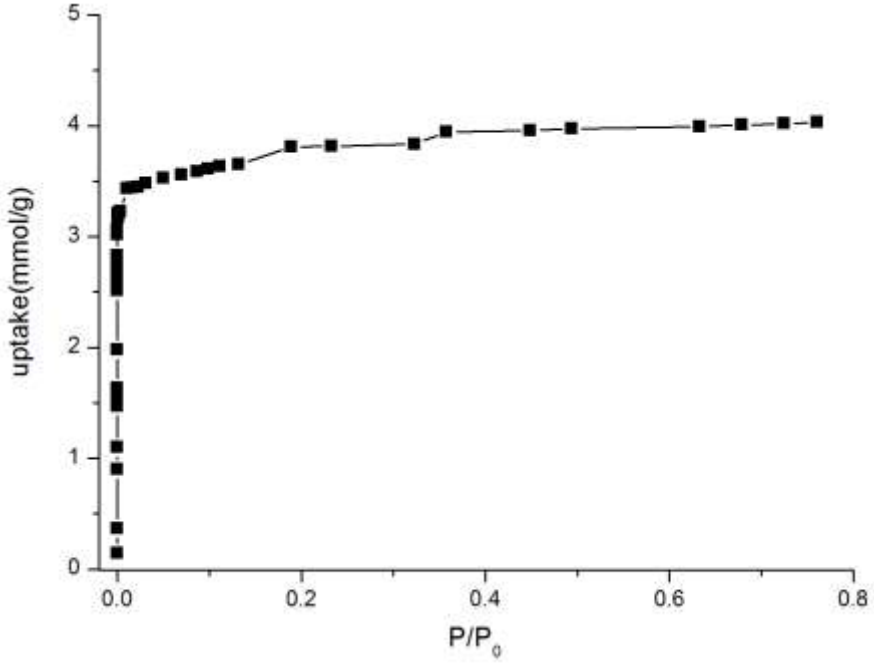

Figure 4.23: Nitrogen adsorption isotherm at -196 ℃ on $Sc_2(NH_2\text{-}BDC)_3$.

(b) CO_2 adsorption on $Sc_2(NH_2\text{-}BDC)_3$ and Isosteric Heat of Adsorption

Prior to adsorption of CO_2 the samples were heated at 130℃ under a vacuum of 3 x 10^{-10} bar for 12h. During this degassing period samples lost very little mass as expected from TGA analysis (< 2%). Carbon dioxide adsorption analysis was investigated at different temperatures. The CO_2 isotherms for functionalised $Sc_2(NH_2\text{-}BDC)_3$ were collected up to 1 bar at a range of temperatures including 30, 20, 15, 10, 0 and -77℃ (using a Grant GR150

thermostatic refrigerated bath for temperature control) using a Hiden IGA automatic gravimetric porosimeter. The adsorption at each pressure point was taken at a value predicted to be 98% of its increase in uptake towards equilibrium, up to a maximum wait time of 120 minutes. The isotherms are shown in Figure 4.24.

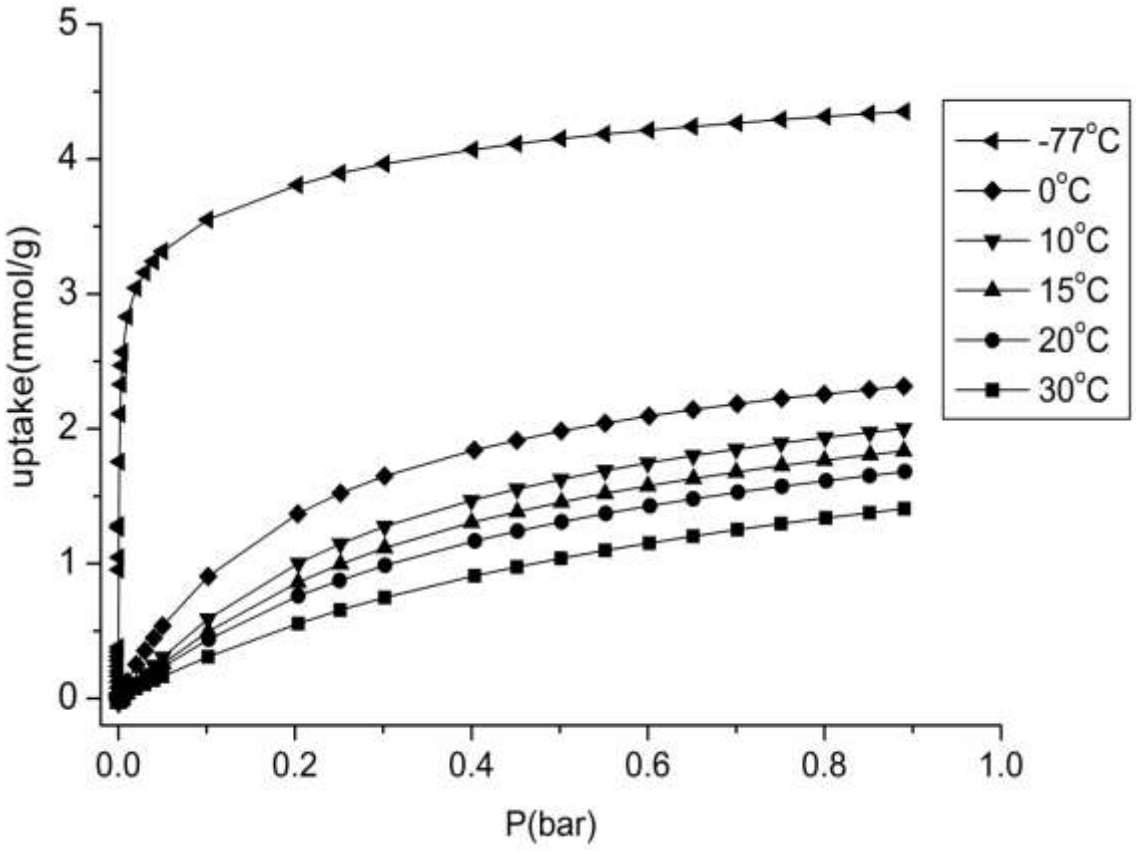

Figure 4.24: Carbon dioxide adsorption data on functionalised $Sc_2(NH_2\text{-}BDC)_3$ measured at -77, 0, 15, 15, 20 and 30℃.

Estimation of heat of adsorption of CO_2 was calculated by fitting the adsorption isotherms at 0, 10, 15, 20 and 30℃ using polynomial functions and from these equations values of pressure could be calculated for fixed coverage (uptake). A van't Hoff equation (Equation 5.1) was used to calculate the isosteric heat of adsorption. The isosteric heat (Q_{st}) is defined by Equation 5.2, where R is the universal gas constant (8.314 J mol^{-1} K^{-1}), and n_a is the adsorbed amount. In the Figure 4.25 the van't Hoff plot of lnP vs 1 /T is shown.

$$\Delta H_{ads}(n_a) = R\left(\frac{d\ln P}{d\left(\frac{1}{T}\right)}\right)_{n_a} \quad 5.1$$

$$Q_{st} = -\Delta H_{ads}(n_a) = -R\left(\frac{d\ln P}{d\left(\frac{1}{T}\right)}\right)_{n_a} > 0 \quad 5.2$$

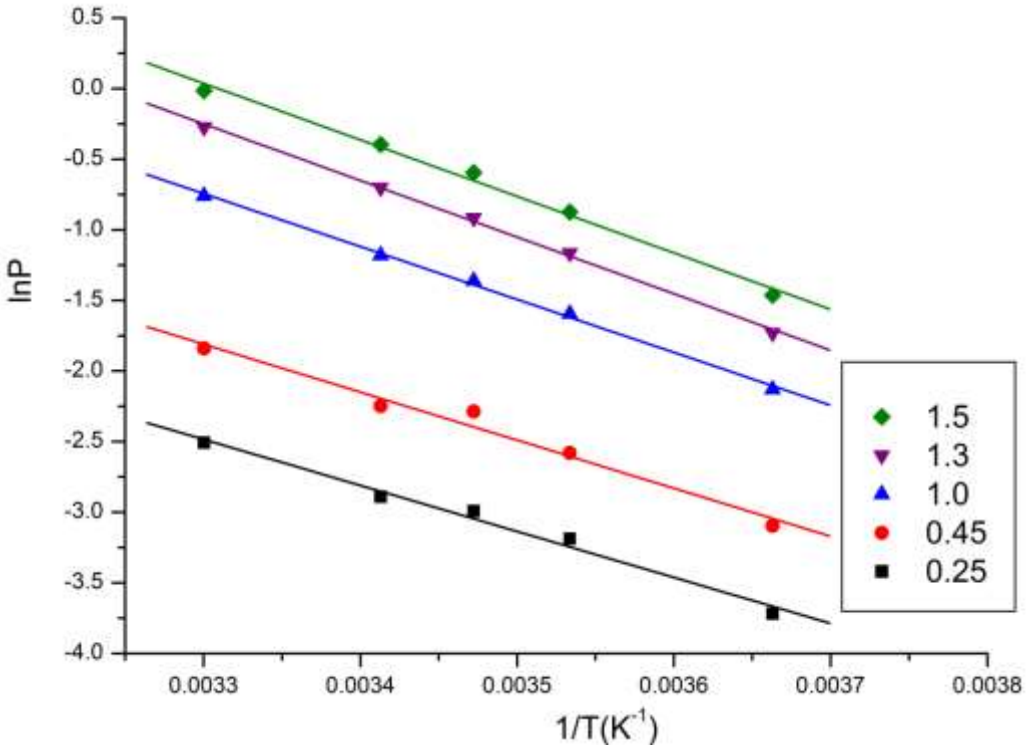

Figure 4.25: A van't Hoff plot of lnP vs 1 /T was used to calculate the isosteric heat of adsorption at various loadings.

The calculated heats of adsorption are listed in Table 4.5; the average value for the isosteric heat of adsorption is 30.9 ± 2.9 kJ mol^{-1}. The Qst values obtained for the functionalised $Sc_2(NH_2\text{-}BDC)_3$ are higher than those reported previously for Sc_2BDC_3 (23 kJ mol^{-1}).[52] This is the result of interaction of CO_2 with the NH_2 groups.

Table 4.5: Qst values of the CO_2 adsorption in the $Sc_2(NH_2\text{-}BDC)_3$.

Uptake (mmol g^{-1})	Slope	Intercept	σ (slope)	Qst (kJ mol^{-1})
0.25	-3281.000	8.340	0.07	27 ± 2
0.45	-3425.000	9.500	0.09	29 ± 2
1	-3774.300	11.710	0.03	31.4 ± 0.9
1.3	-4038.600	13.073	0.02	33.6 ± 0.8
1.5	-4032.200	13.340	0.05	33.5 ± 1.7

(c) In situ gas adsorption and XRD on $Sc_2(NH_2\text{-}BDC)_3$

In situ gas adsorption variable temperature powder X-ray diffraction data was collected at beamline I-11 of the Diamond Light Source (DLS, (UK synchrotron). A sample of $Sc_2(NH_2\text{-}BDC)_3$ was ground and packed into a 0.7 mm quartz glass capillary and held in place by a quartz glass plug The capillary was attached to a goniometer head that could be rocked by +/- 40° to improve powder averaging on the I11 beamline at Diamond Light Source. The sample was evacuated and heated to 130℃ for 30 minutes. The activated sample was then allowed to attain 25℃ over approximately 20 minutes. The sample was dosed to 0.1 bar of CO_2 and allowed to equilibrate. A variable temperature experiment was conducted by using the cryostat probe available at I11 to control the temperature. The temperature was raised from 25℃ to 130℃ at 1 ℃ per minute and diffraction patterns were collected at 10 ℃ steps throughout the experiment (27 - 130℃) The XRD pattern (Figure 4.26) was measured using monochromated X-rays of wavelength 0.826956 Å using the Mythen position sensitive detector on the I11 beamline: 10 second scans were used to collect the diffraction patterns. Analysis of the diffraction patterns collected shows that the structure of $Sc_2(BDC\text{-}NH_2)_3$ is orthorhombic *Fddd* as shown by single crystal diffraction and does not undergo any phase changes or breathing effects over the range of temperatures tested.

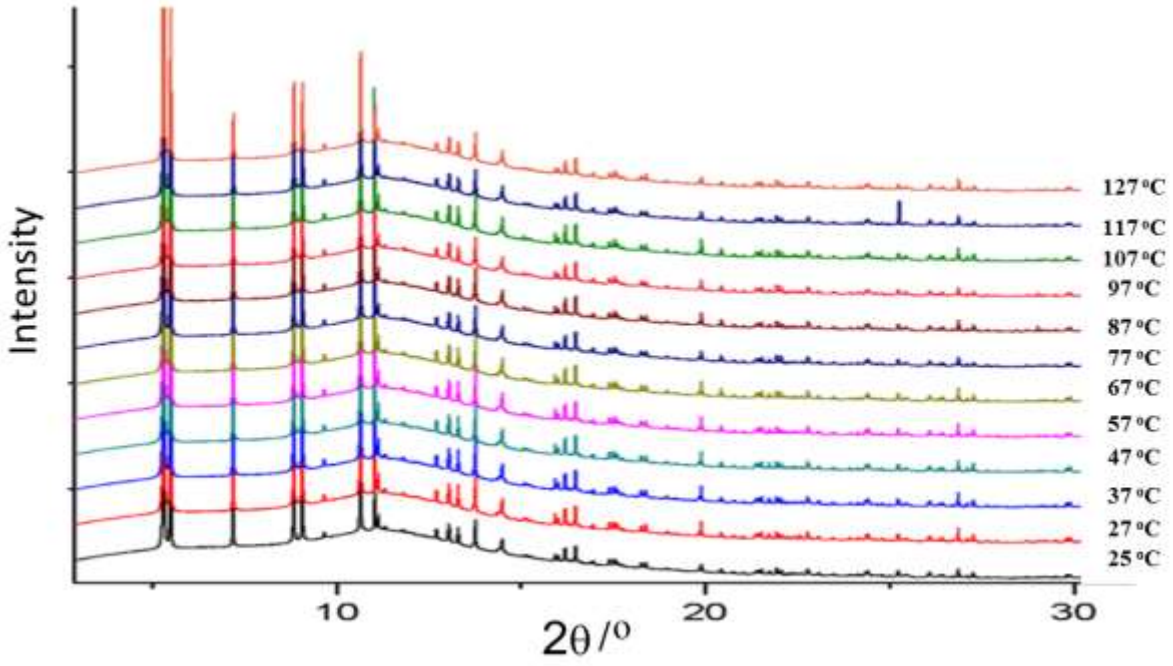

Figure 4.26: PXRD (λ = 0.826956 Å) of $Sc_2(BDC\text{-}NH_2)_3$ in contact with 0.1 bar CO_2.

The properties of $Sc_2(BDC\text{-}NH_2)_3$ crystals, including well-defined morphology, hydrophobicity, strong adsorption of CO_2, and the presence of the NH_2-bonds in the framework made them ideal candidate for synchrotron IR microcrystal spectroscopy investigation under flowing CO_2. The results of his work have been published in Angewandte Chemistry.

In situ synchrotron IR microspectroscopy of CO_2 adsorption on single crystals of the functionalised MOF, $Sc_2(BDC\text{-}NH_2)_3$: A technique to analyse carbon capture sorbents

Alex Greenaway, Berenice Gonzalez-Santiago, Paul M. Donaldson, Mark D. Frogley, Gianfelice Cinque, Jorge Sotelo, Stephen Moggach, Eleni Shiko, Stefano Brandani, Russell F. Howe and Paul A. Wright.

Angew. Chem. Int. Ed., 2014, 53, 13483–13487. DOI: 10.1002/anie.201408369

4.4.5. Sc_2(Br-BDC)$_3$

Following the success of the mixed solvents and low temperature synthetic approach for $Sc_2(NH_2\text{-}BDC)_3$, it was applied to synthesis of the bromo-derivative, which had not previously been synthesized due to reactivity of the C-Br bond at higher temperature. The solvothermal synthesis yielded yellow needle-shaped crystals of sufficient quality to be analysed by single crystal X-ray diffraction. Figure 4.27 shows the patterns of the as-prepared sample compared with the simulated pattern from single crystal analysis. (CIF file available see the Appendix B)

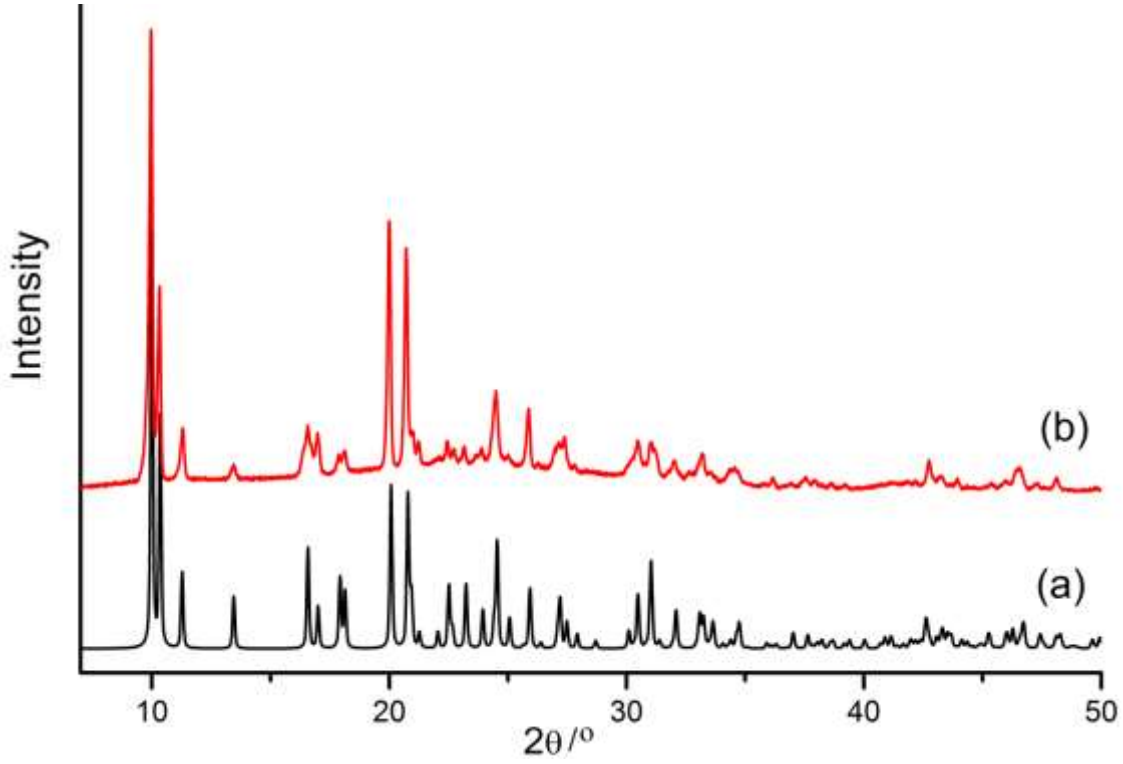

Figure 4.27: Experimental powder diffraction pattern of $Sc_2(Br\text{-}BDC)_3$ (b) compared to the pattern simulated from the single crystal model(a).

The structure was solved and refined using the Crystals software suite.[51] The bromine atoms group were located and the occupancy fixed to one Br per terephthalate group. Thus, in the framework there are three unique terephthalates and six crystallographically-distinct carbon sites where the -Br groups can be located resulting in considerable distortion in the structure

(Figure 4.28). In the orthorhombic structure, the three crystallographic carbon positions for the –Br group are allocated one on the group 1 and two on the group 2 (groups 2a and 2b). Table 4.6 gives the crystallographic details of the solved structure. Unlike the amino-form, the bromo form crystallize in the *Fdd2* space group, due to the additional ordering of the functional groups and the tilting of the structure

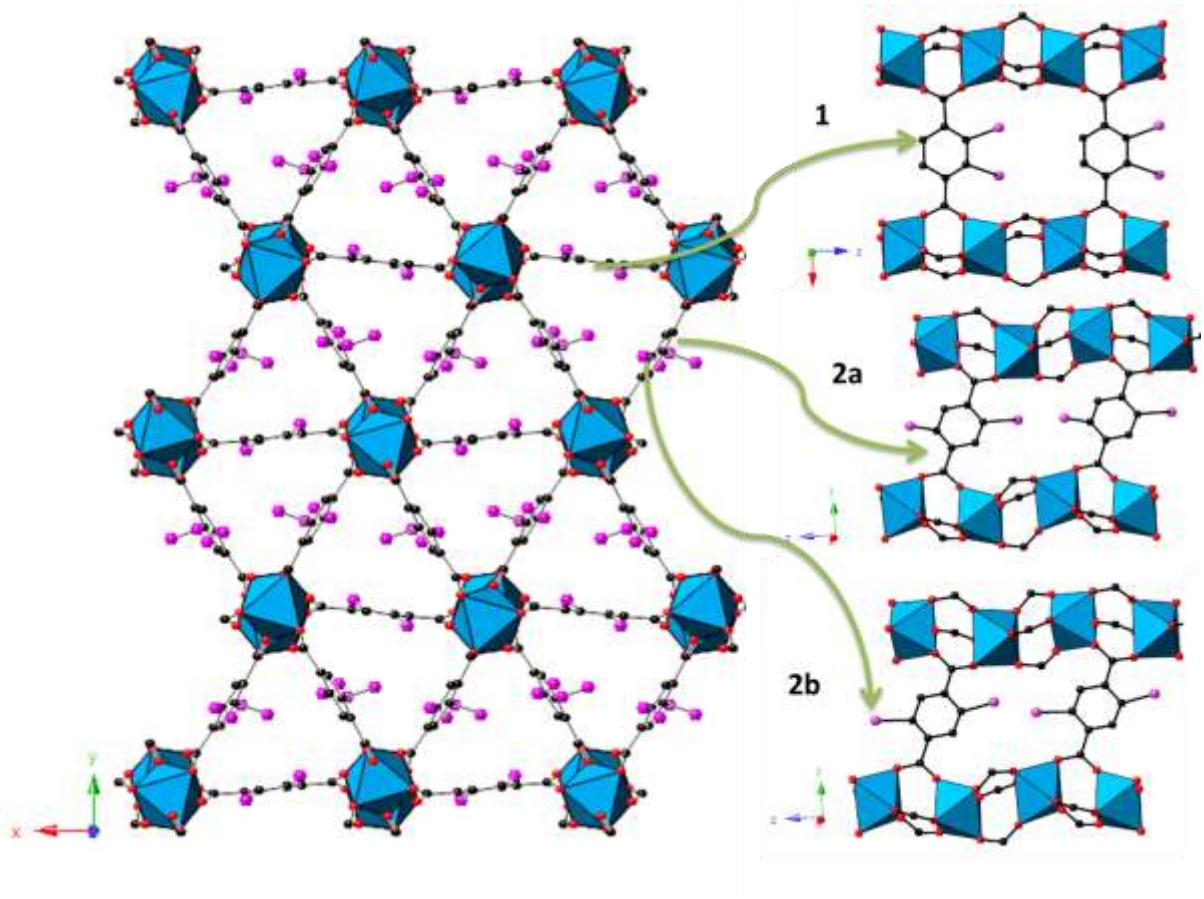

Figure 4.28: View along the channels and perpendicular to the three types of terephthalate layers of the structure of $Sc_2(Br\text{-}BDC)_3$. The framework structure exhibits distortion to accommodate the –Br group in the framework.. Scandium octahedra are shown in blue. Black, purple and red spheres represent the carbon, bromine and oxygen atoms of the organic linker respectively.

Table 4. 6: Crystallographic data for $Sc_2(Br\text{-}BDC)_3$ from single crystal diffraction data

Structure	$Sc_2(Br\text{-}BDC)_3$
Formula unit	$Sc_2(C_8H_3O_4Br)_3$
Crystal system	Orthorhombic
Space group	*Fdd2*
X-ray source	Mo Kα
Diffractometer	
Wavelength (Å)	0.71073
Unit cell (Å)	
a/Å	20.6587(6)
b/Å	34.1623(9)
c/Å	8.7488(3)
β/°	113.755(5)
Volume/$Å^3$	6174.45
R	0.0592
R_w	0.124

The SEM micrographs indicate that synthesis gave $Sc_2(Br\text{-}BDC)_3$ as yellow solid comprising needle-shaped crystals, 50 -60 µm in size (Figure 4.29a-c). EDX analysis confirms the molar ratio between Sc/Br to be 0.60, close to that expected from structural formula. Elemental analysis measured (expected) on this sample gives: 35.32 wt % (35.2 wt %), H 1.05 wt % (1.1 wt %) . EDX analysis is shown in Figure 4.29(d).

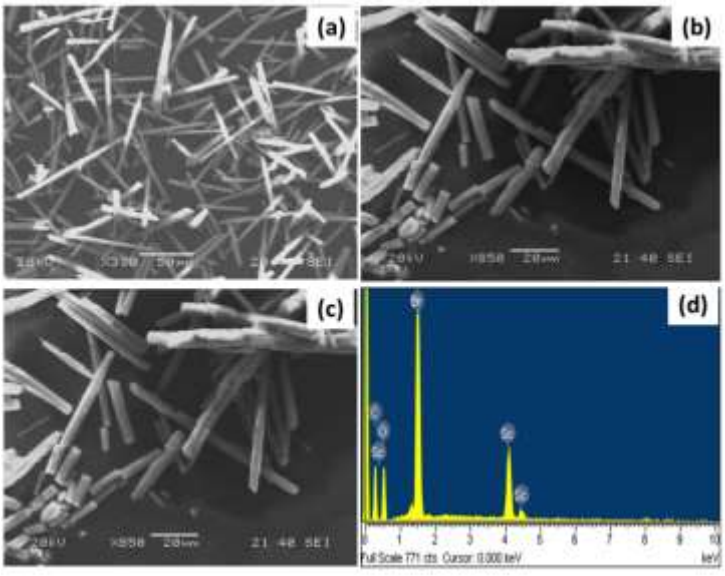

Figure 4.29: Images of SEM (a-c) and EDX analysis (d) of $Sc_2(Br\text{-}BDC)_3$

The TGA plot is shown in the Figure 4.30. This indicates that as-synthesized $Sc_2(Br\text{-}BDC)_3$ is thermally stable in flowing air up to 450 ℃. Gas adsorption studies on the material activated at 130°C for 4 h under vacuum indicated the MOF had no porosity for nitrogen gas (Figure 4.31). In contrast the uptake of CO_2 measured at -77 ℃ gives an uptake of 2.5 mmol g^{-1} (Figure 4.31).

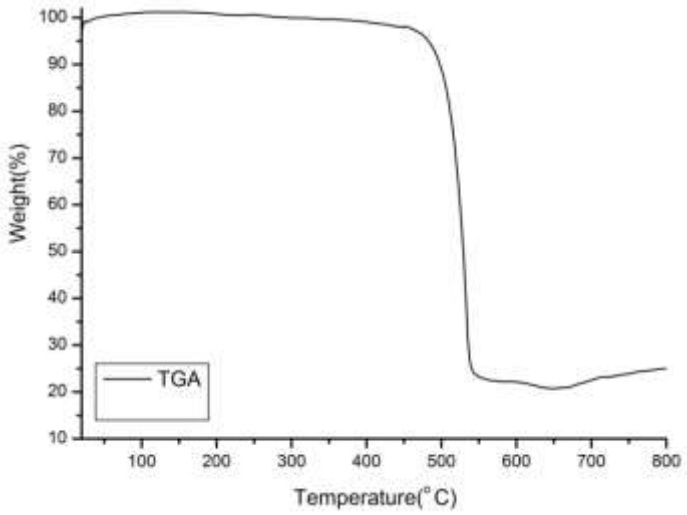

Figure 4.30: Thermogravimetric analysis on $Sc_2(Br\text{-}BDC)_3$ under flowing air.

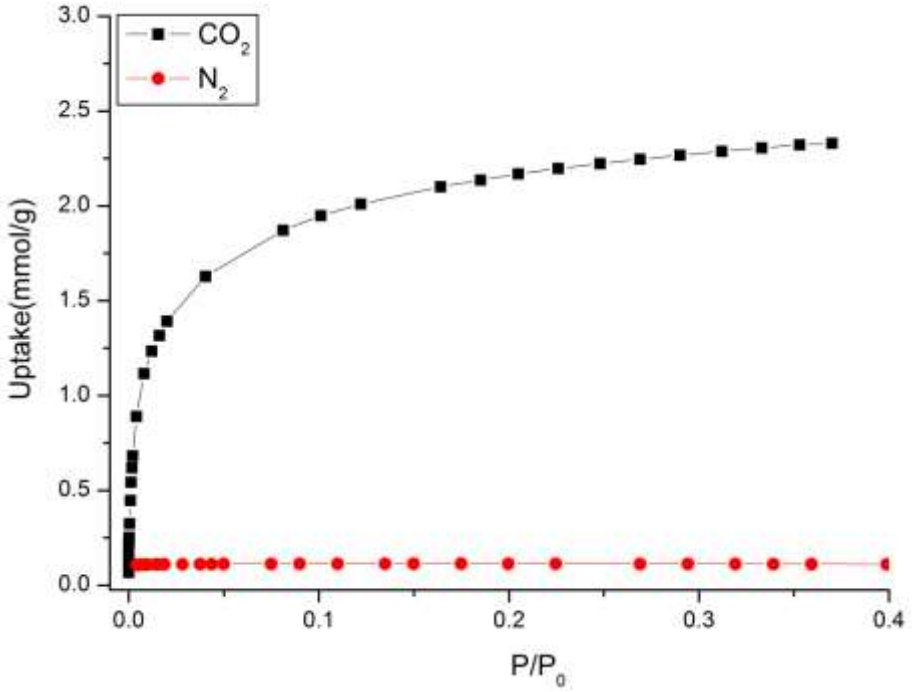

Figure 4.31: CO_2 and N_2 Adsorption isotherms measured at -77 ℃ and -196 ℃ respectively, collected on $Sc_2(Br\text{-}BDC)_3$

The CO_2 isotherm shows that the Br-functionalised MOF has the same uptake (2.5 mmol g^{-1}) as that reported for the nitro-functionalised Sc_2BDC_3, but is lower in comparison with the non-functionalised solid, which is 6 mmol g^{-1} (Table 4.7). Neither nitro-or bromo-forms adsorbs N_2 at -196℃, because the bulky substituents block the pores and these temperatures the aromatic ring cannot rotate enough to permit N_2 diffusion

Table 4.7: Comparison of uptakes of N_2 and CO_2 gas adsorption of Sc_2BDC_3 and its derivatives

MOF	N_2 Uptake (mmol g^{-1})	CO_2 Uptake (mmol g^{-1})(at -77℃)	Pore volume (cm^3 g-1)
Sc_2BDC_3	6.5	6	0.263
$Sc_2(NH_2\text{-}BDC)_3$	4	4	0.148
Sc_2(Br-BDC)$_3$	0	2.5	0.086
$Sc_2(NO_2\text{-}BDC)_3$	0	2.5	0.086

Studies of solid state NMR on Sc_2(Br-BDC)$_3$ for ^{1}H, ^{13}C and ^{45}Sc are shown in Figure 4.32. The ^{1}H MAS NMR spectrum (Figure 4.32a) shows a broad peak at a chemical shift 7.7 ppm, typical of aromatic protons of the linker. The ^{13}C MAS NMR showed broader peaks (Figure 4.32 "b and c (expanded)") suggested a more disordered environment than observed for the Sc_2 (NH_2-BDC)$_3$ framework. Figure 4.32(d) shows the ^{13}C MAS NMR spectra in the variable-contact time experiment. The resonances from all carbon sites are shifted downfield owing to the electron-withdrawing, bromo-group. Also, the spectrum for ^{45}Sc MAS NMR showed a broad peak in agreement with the positional disorder of the Br group. Figure 4.32(e) and (f) show the spectrum, expanded.

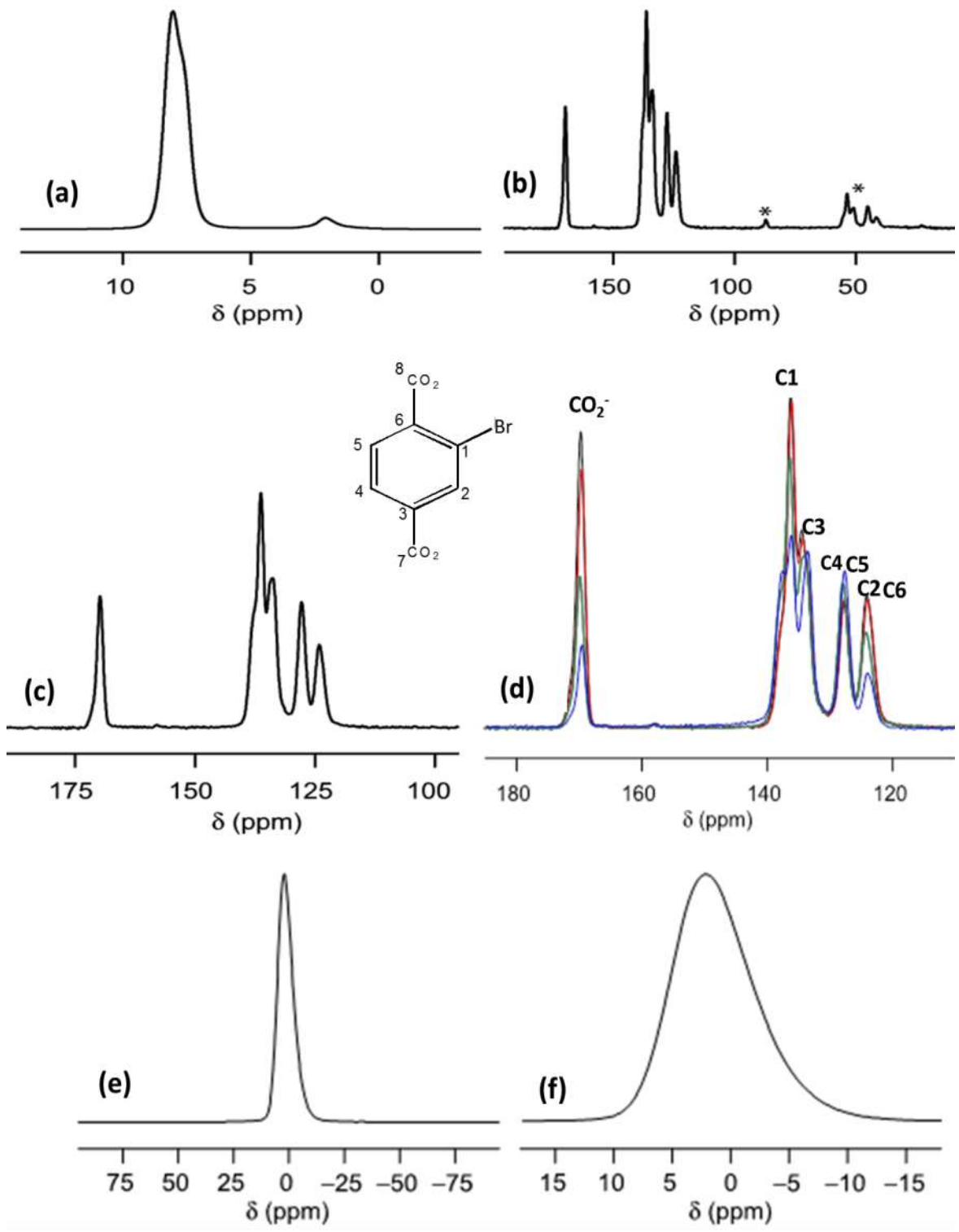

Figure 4.32: NMR Spectra collected on Sc_2(Br-BDC)$_3$; (a) ^{1}H and (b, c, d) ^{13}C spectra (14.1 T) where c and d expanded carboxylate and aromatic regions of variable-contact time, (e, f) ^{45}Sc spectra where (f) expanded Figure. The MAS rate was 40 kHz, 12.5 kHz and 40 kHz for ^{1}H, ^{13}C and ^{45}Sc, respectively. The contact times were 5 ms (blue), 10 ms (green), 25 ms (red) and 20 ms (black). *Indicate the spinning sidebands.

In order to accommodate the Br-groups in the framework and control the distortion observed in the framework, attempts to introduce BDC linker in the direct synthesis of the MOF was carried out. However the syntheses yielded microcrystalline powder. PXRD are given in Figure 4.33. An additional reflection appears at 18^{o} 2θ, with increase in content of the bromo terephthalic acid in the synthesis, but this aside, there is a gradual charge of intensities. EDX in Figure 4.34 suggested an even distribution of Br over the powder but it was not possible to distinguish between a physical mixture or a solid solution.

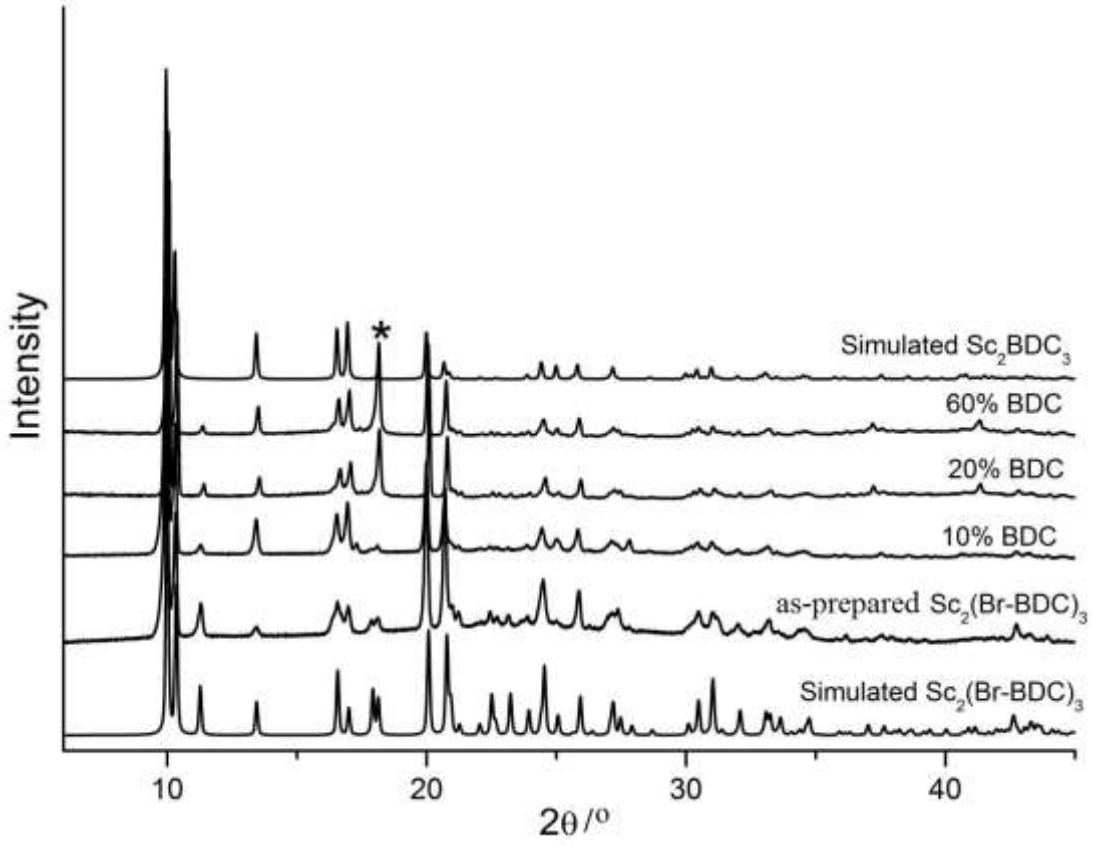

Figure 4.33: Powder diffraction pattern of as prepared $Sc_2(NH_2\text{-}BDC)_3$ compared to the patterns of the samples obtained by PSM with 10, 25 and 60% of BDC in the framework .* show the appearance of single reflections on samples with 25 and 60% on BDC.

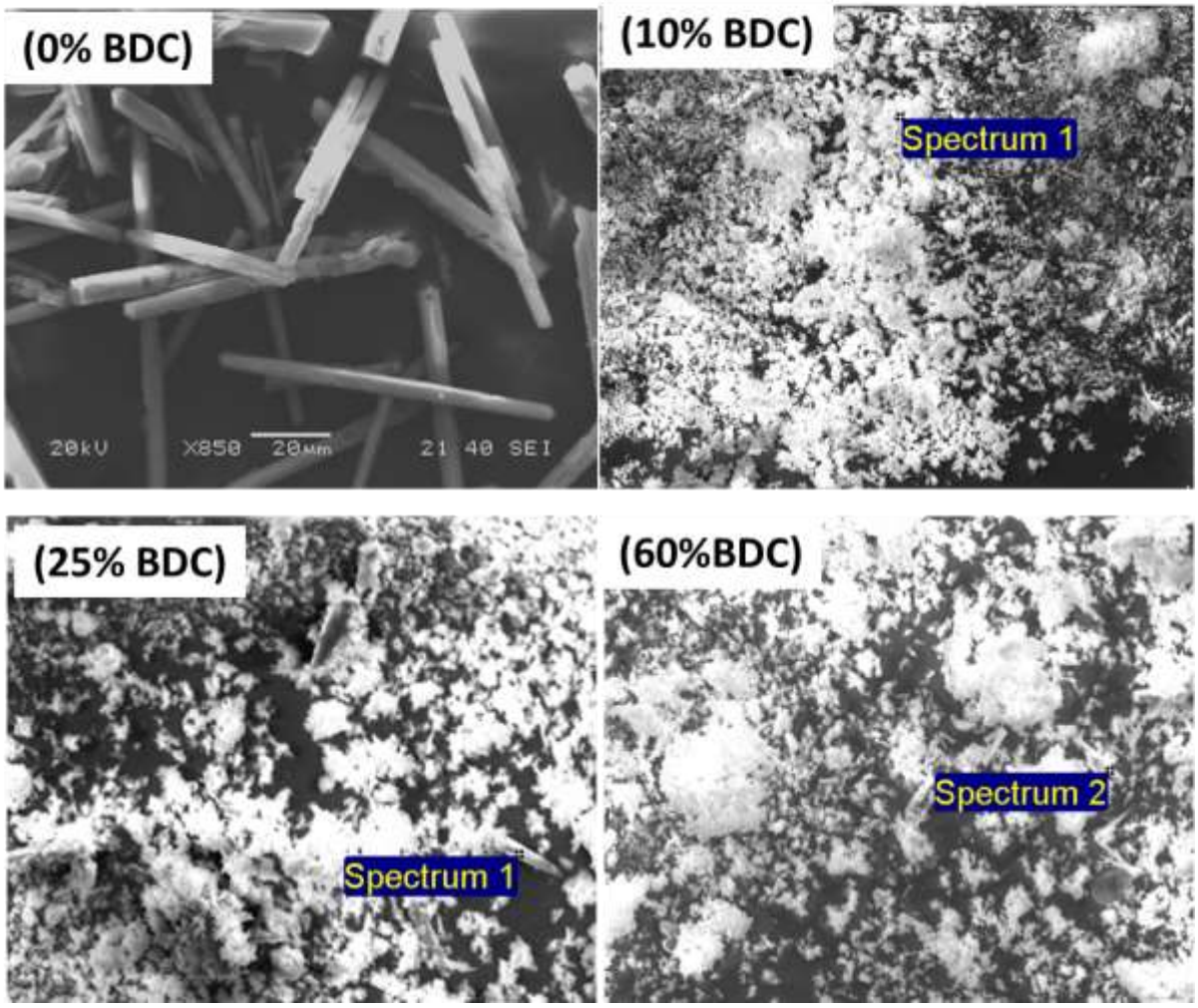

Figure 4.34: Images of SEM of the post-modified samples with 10, 25 and 60% BDC

4.4.6 Post-synthetic modification (PSM) of $Sc_2(NH_2\text{-}BDC)_3$

The ability of the nitro-form, $Sc_2(NO_2\text{-}BDC)_3$ [43] to adsorb CO_2 at 0 ℃ but no N_2 at -196 ℃, suggested that a core-shell Sc_2BDC_3 structure of ($-NH_2$ /$-NO_2$) might absorb CO_2 strongly but exclude bulkier molecules. Thus, emerged the idea for post-synthetic modification (PSM) of the amino-derivative $Sc_2(NH_2\text{-}BDC)_3$. The post-synthetic modification (PSM) of $Sc(NH_2\text{-}BDC)_3$ was explored using a solution of NO_2-BDC under mild conditions. Firstly the ligand NO_2-BDC (0.2 mmol) was immersed in water (10 mL) or mixed solvents, DMF (1 mL) and water (9 mL) followed by sonication to dissolve the ligand. When the ligand was dissolved

MOF (0.6 mmol) was added and the mixtures left for different reaction times as outlined in Table 4.5. Characterisation of the samples was carried out by SEM and PXRD (Figure 4.35 and 4.36). The samples remain crystalline and for those samples left for longer time of reaction (four days), some impurities appear, probably due to dissolution of the MOF crystals. However, these reflections do not match with the characteristic peaks of the linker.

Table 4.8: Recovered yields (%) for PSM $Sc(NH_2\text{-}BDC)_3$.

Sample	Time(day)	Yield
PSM-1	1	60
PSM-2	1*	50
PSM-3	2	50
PSM-4	2*	50
PSM-5	4	40
PSM-6	4*	30

PSM was in water unless asterisked, in which case DMF/H_2O was used as solvent, as described in the text.

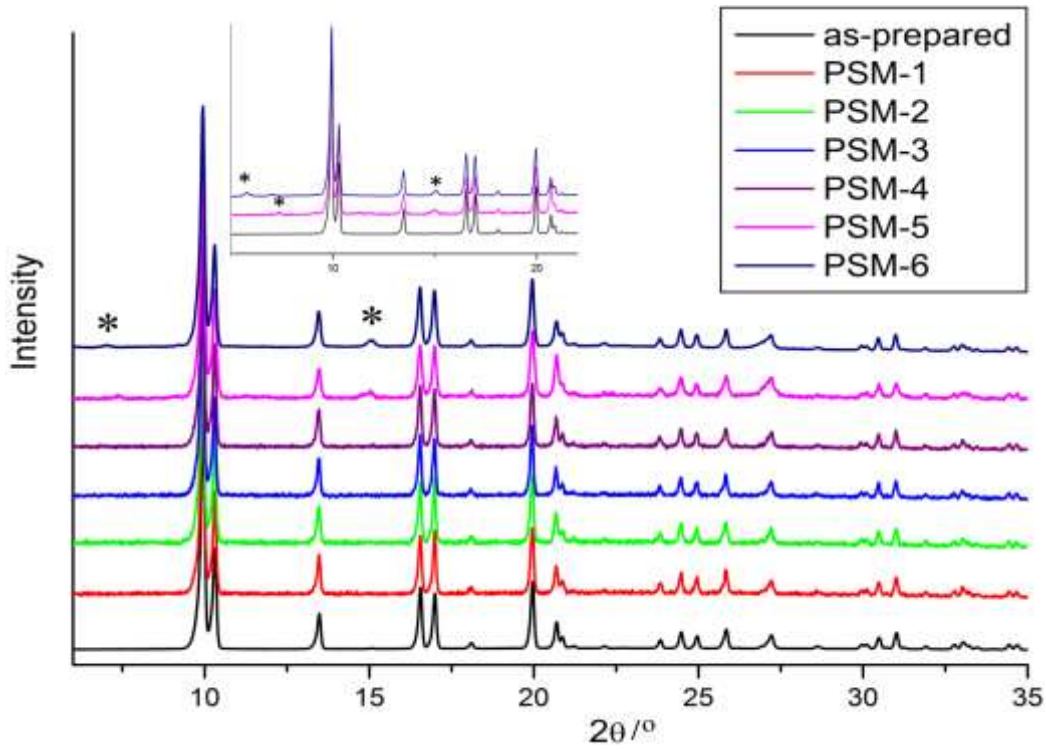

Figure 4.35: Powder diffraction pattern of as prepared $Sc_2(NH_2\text{-}BDC)_3$ compared to the patterns of the samples obtained by PSM. * Impurities.

SEM micrographs of the post-synthetically modified samples are shown in Figure 4.36. These images exhibit equatorial cracking on the crystals and this increased when the crystals were kept for long periods of time such as 4 days. The use of mixed solvents DMF and H_2O accelerated the equatorial cracking. To check if this phenomenon was due to the addition of the ligand NO_2-BDC or just because of the immersion in solvents, the MOF was put in mixed solvents, or just water, but in both cases the equatorial cracking was not observed.

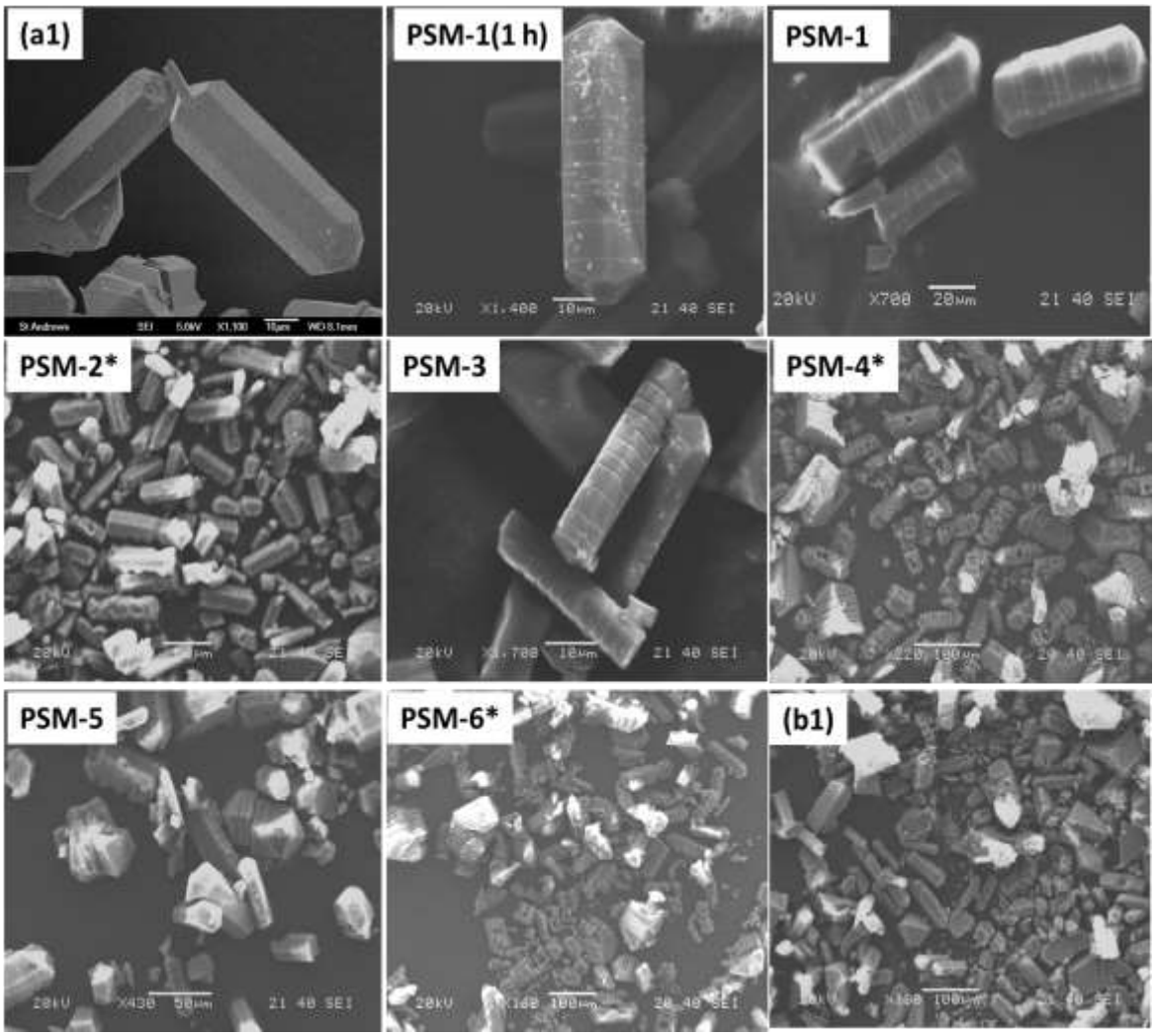

Figure 4.36: SEM images of $Sc_2(NH_2\text{-BDC})_3$; (a1) as-prepared $Sc_2(NH_2\text{-BDC})_3$, (b1) as-prepared $Sc_2(NH_2\text{-BDC})_3$ without immersion in nitro-terephthalic acid solution, but only in mixed solvents (DMF and H_2O) and PSM1-PSM-6 samples prepared by PSM using NO_2-BDC. * Samples using mixed solvents (DMF and H_2O).

Sample PSM-3 was selected for further studies because the crystals remained intact and can be compared with the unmodified $Sc_2(NH_2\text{-}BDC)_3$ for analysis of adsorption properties. The presence of NO_2-BDC on post-synthetically modified sample PSM-3 was confirmed by solution phase NMR (Figure 4.37). The sample was digested in DMSO-d_6 and 0.3 mL of HNO_3 (0.2 M) followed by sonication ca. for 5 min leading to complete dissolution. Results of this analysis confirm ca. 8% of NO_2-BDC in the post-synthetically modified sample PSM-3.

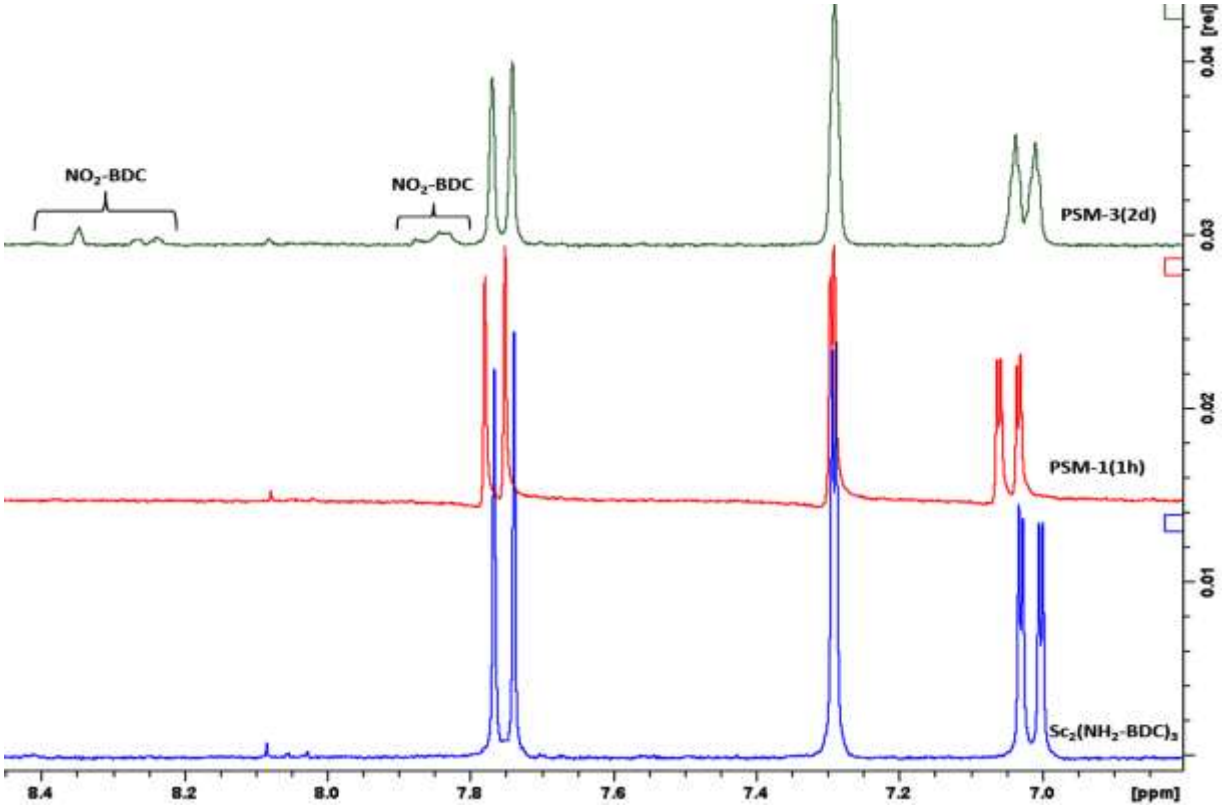

Figure 4.37: ^{H}NMR of dissolved, as-prepared $Sc_2(NH_2\text{-}BDC)_3$ the PSM-3. The resonances of the ligand NO_2-BDC are on 7.8, 8.200, 8.248 and 8.358 ppm.

In terms of adsorption for the post-synthetically modified material PSM-3, analysis of N_2 and CO_2 adsorption using was investigated (Figure 4.38). Prior to analysis the sample was heated at 130 ℃ under vacuum for 4 h and the uptake is 4 mmol g^{-1}, the same uptake as obtained for

the as-prepared $Sc_2(NH_2\text{-}BDC)_3$, while N_2 adsorption resulted in an uptake of 1.5 mmol g^{-1} compared to 4 mmol g^{-1} for $Sc_2(NH_2\text{-}BDC)_3$. This indicated partial blockage of the structure.

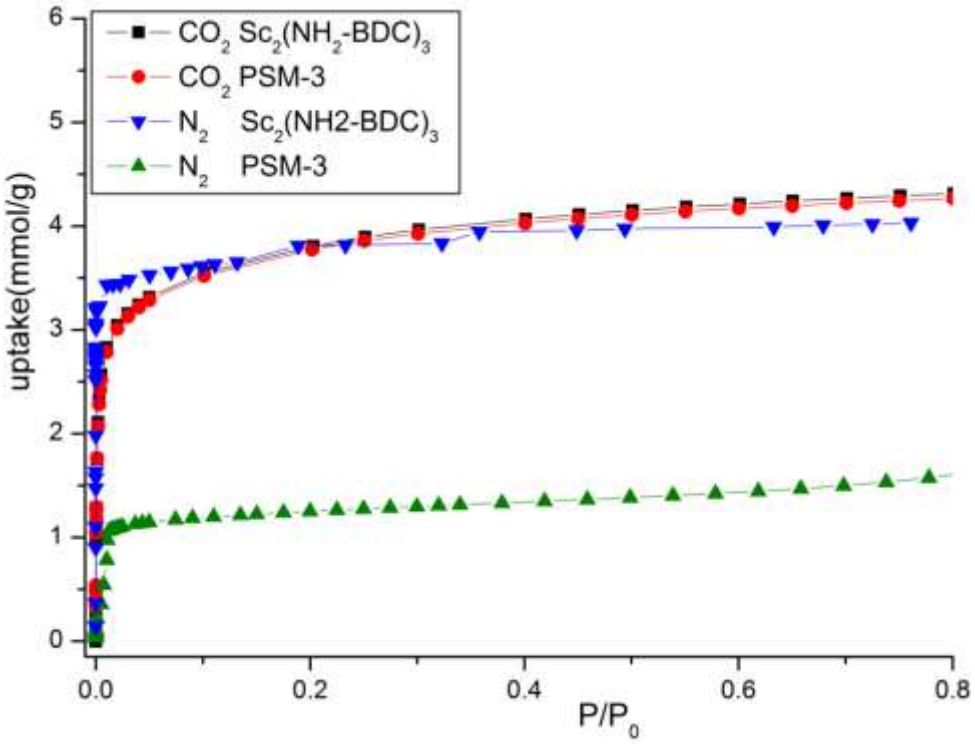

Figure 4.38: CO_2 and N_2 adsorption measured at -77℃ and -196 ℃ on the PSM-3 sample compared to the as-prepared $Sc_2(NH_2\text{-}BDC)_3$

TGA of modified sample PSM-3 is shown in Figure 4.39. The TGA plot shows a weight loss at around 300℃ attributed to loss of the ligand NO_2-BDC. The rest of the framework starts to collapse at 400℃. The percent of NO_2-BDC by calculating the residual mass in the TGA gives a value of 7%, which is close to the 8% calculated by solution phase NMR.

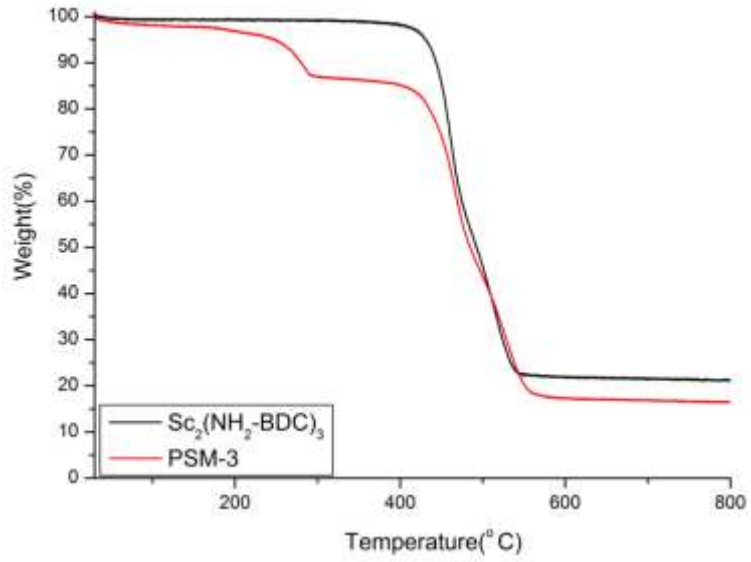

Figure 4.39: Thermogravimetric analysis on unmodified $Sc_2(NH_2\text{-}BDC)_3$ (black one) and the PSM-3 (red one) under flowing air.

4.4.7 $Sc_2(BDC)_3$ and $Sc_2(NO_2\text{-}BDC)_3$

$Sc_2(BDC)_3$ and $Sc_2(NO_2\text{-}BDC)_3$ were prepared separately using the approach of mixed solvents at low temperature to compare their adsorption properties with post- synthesis modified $Sc_2(NH_2\text{-}BDC)_3$. Results are discussed below.

4.4.7.1 Sc_2BDC_3

A mixture of solvents involves DMF (1 mL) and water (4 mL) was used to synthesize Sc_2BDC_3, however it was within mixtures wit recrystallised ligand. To remove the unreacted terephthalic acid from the framework, the sample was immersed in DMF and sonicated at 60^oC for 1 h. The purified sample was identified by comparison with a simulated pattern reported previously (Figure 4.40).

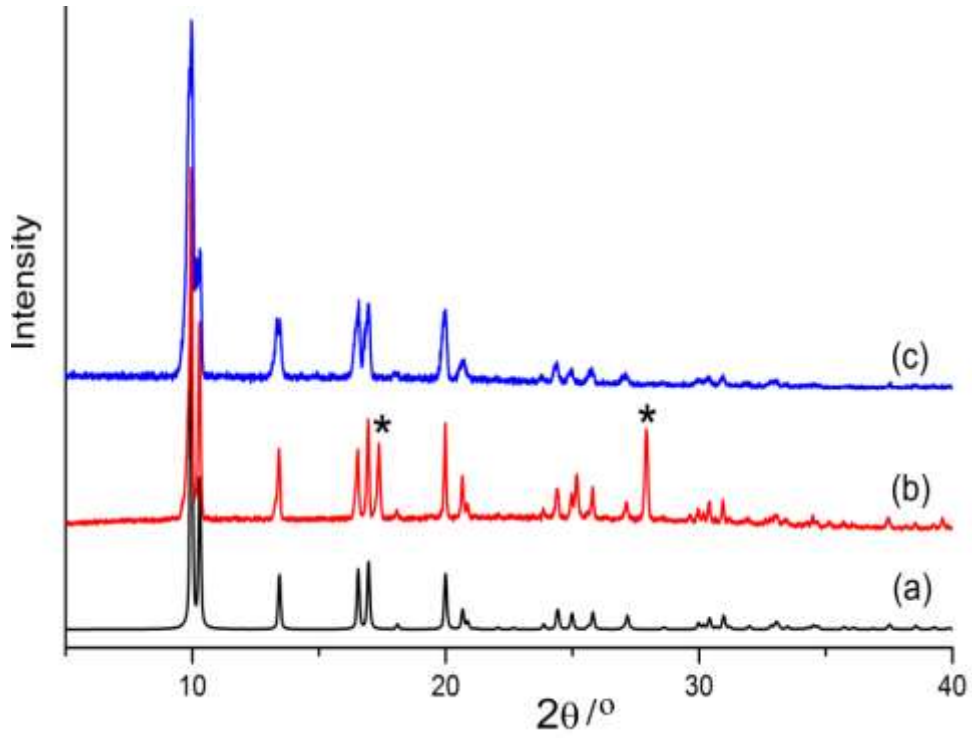

Figure 4.40: Powder diffraction pattern of Sc_2BDC_3; (a) pattern simulated from the single crystal model, (b) as-prepared and (c) after sonication.*Peaks related to impurity of terephthalic acid.

Figure 4.41 shows the TGA and the isotherm for N_2. Sc_2BDC_3 has a thermal stability, over 450°C under flowing air. Nitrogen adsorption experiments were carrying out on the purified sample giving an uptake of 5 mmol g^{-1}. This value is close to those reported by Mowat et al,[12] which was 6 mmol g^{-1}.

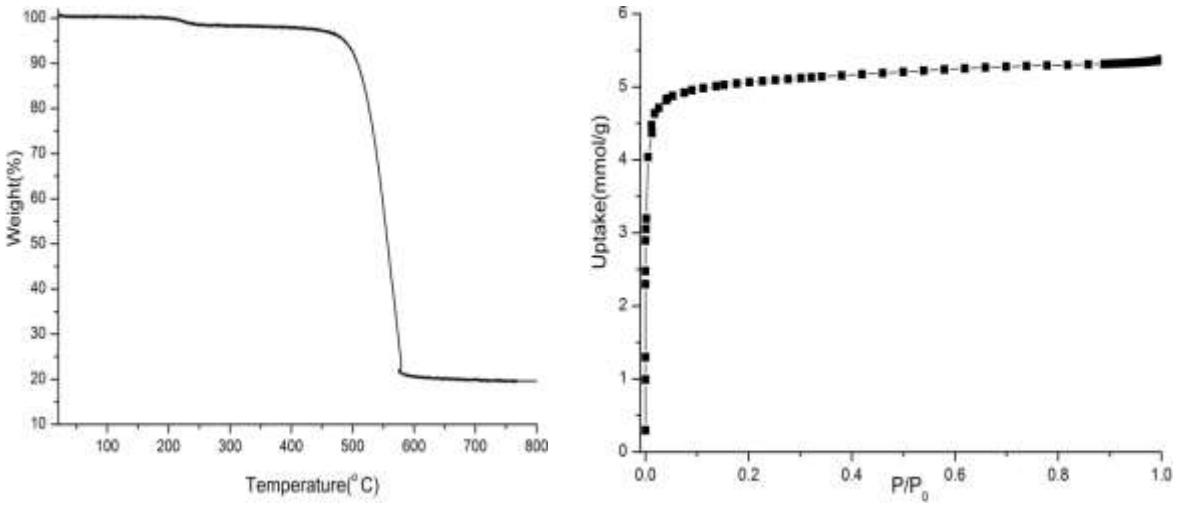

Figure 4.41: (Left) Thermogravimetric analysis on Sc_2BDC_3 and (right) N_2 adsorption measured at -196℃.

4.4.7.2 $Sc_2(NO_2\text{-}BDC)_3$

The $Sc_2(NO_2\text{-}BDC)_3$ was synthesized following the procedure published elsewhere,[12] using scandium chloride solution. Figure 4.42 shows the diffraction pattern collected for this MOF compared with the simulated diffraction patterns from the literature.[12] TGA of the sample indicated that the solid is thermally stable (Figure 4.43).

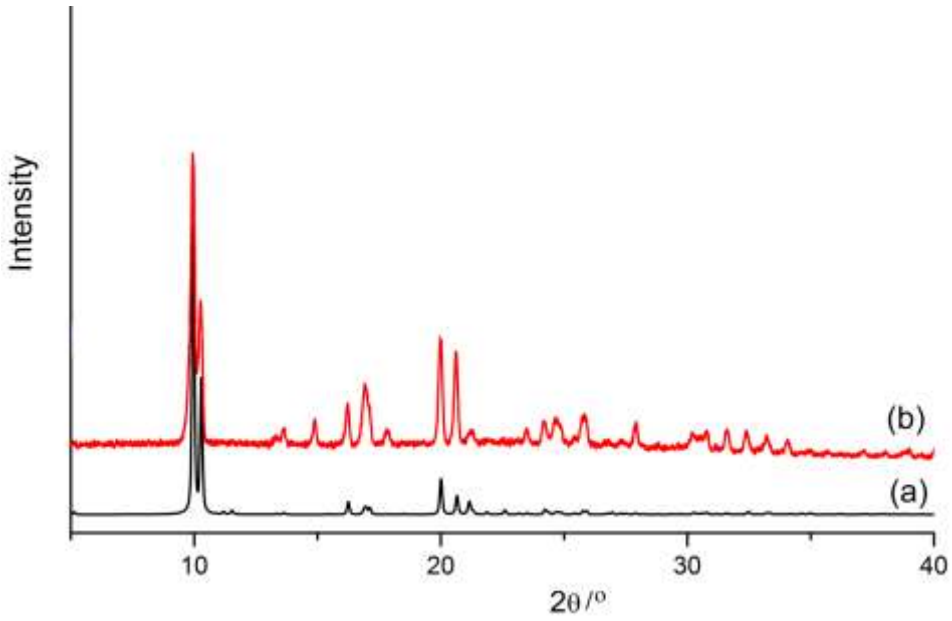

Figure 4.42: PXRD of $Sc_2(NO_2\text{-}BDC)_3$ (a) simulated from the single crystal model (a), (b) as-prepared.

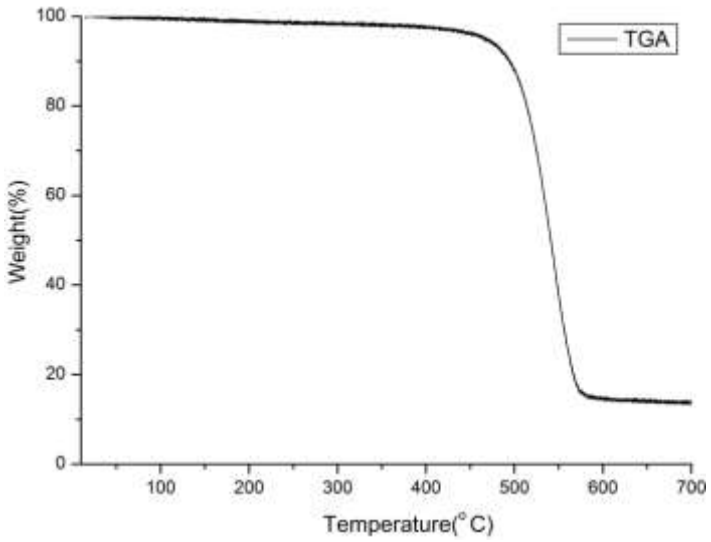

Figure 4.43: Thermogravimetric analysis on $Sc_2(NO_2\text{-}BDC)_3$ under flowing air.

4.4.8 Adsorption studies of organic molecules on Sc_2BDC_3 and its derivatives

Further adsorption studies using organic molecules such as methanol and hydrocarbons were performed on $Sc_2(NH_2\text{-}BDC)_3$ and compared to Sc_2BDC_3 and its other functionalised derivatives $Sc_2(Br\text{-}BDC)_3$ and $Sc_2(NO_2\text{-}BDC)_3$ and the post-synthetically modified solid PSM-3. The aim of this part is to analyze the adsorption of hydrocarbons on MOFs. In order to enhance the analysis of the adsorption properties of functionalised MOFs prepared in this chapter, we have chosen for this purpose the different adsorbates methanol, alkanes and branched-chain alkanes (Figure 4.44). A series of gas isotherms were collected at 25 ℃ testing the organic molecules as adsorbates on the MOFs by using a manually assembled porosimeter (Figure 4.45).

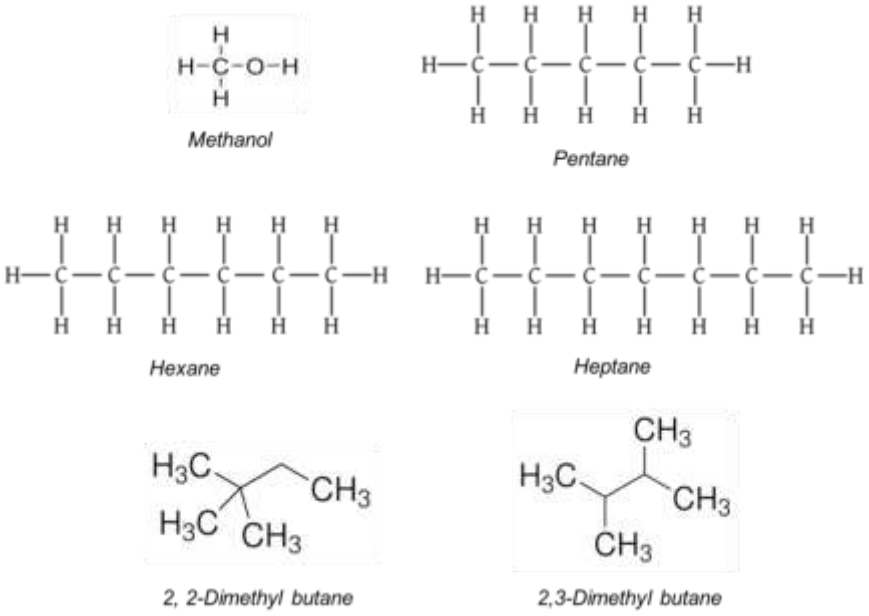

Figure 4.44: Organic molecules used as adsorbates in gas adsorption

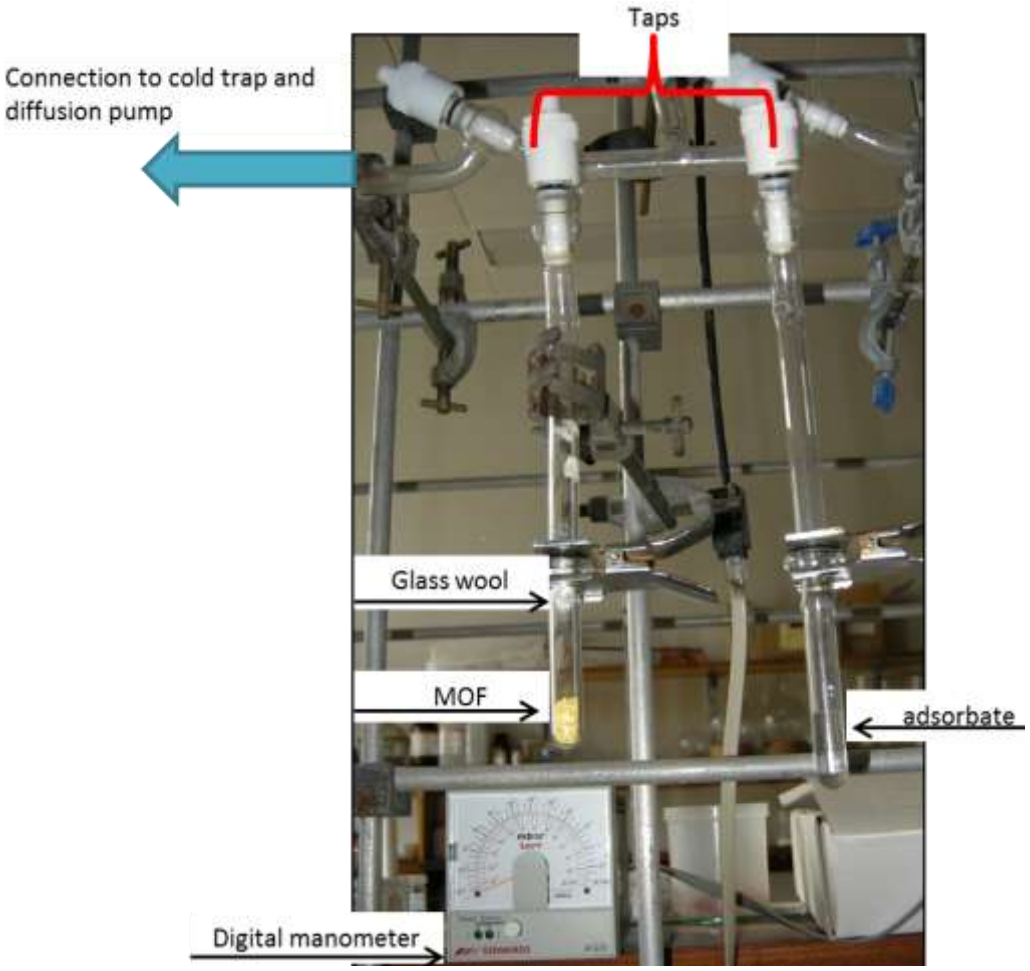

Figure 4.45: Assembled porosimeter based on vacuum line.

Prior to adsorption of the indicated adsorbates the MOFs were degassed at 150 ℃ under vacuum for 2 h. The solvent was degassed by a freeze-thaw process in which the adsorbate was frozen in liquid nitrogen and then exposed to vacuum as it thawed removing any gaseous species dissolved in the adsorbate. Collection of the data was carried out by analysing the dosing area. To collect the isotherms the tap of the dosing area was manually dosed with an amount of adsorbate, the pressure recorded and the quantity of adsorbate in the dose calculated. The dosing area was then opened to the sample area and allowed to equilibrate with the sample and the pressure recorded. This value was used to calculate the quantity of sample adsorbed during each dose. The dosing area was then exposed to a higher pressure of adsorbate and the process repeated. The quantities adsorbed were then summed and plotted against the equilibration pressure. Adsorption isotherms for methanol, pentane, hexane,

pentane, 2,2-dimethylbutane (2,2-DMB) and 2,3-dimethylbutane (2,3-DMB) collected in a series of MOFs are shown in Figure 4.46. Table 4.9 summarizes the adsorbed quantities on each MOF tested; Sc_2BDC_3 and its functionalised derivatives, and the PSM-3 sample.

Table 4.9: Maximum adsorbed quantities for the different adsorbates tested in this adsorption analysis on MOFs.

	Adsorbates				
MOF	**Methanol** *uptake (mmol g^{-1})*	**Pentane** *uptake (mmol g^{-1})*	**Hexane** *uptake (mmol g^{-1})*	**Heptane** *uptake (mmol g^{-1})*	**2,3-DMB** *uptake (mmol g^{-1})*
Sc_2BDC_3	2.8	0.42	0.38	0.24	0.14
$Sc_2(NH_2\text{-}BDC)_3$	2.3	0.7	0.8	0.25	0.10
PSM-3	1.5	0.34	0.41	0.12	0.08
$Sc_2(Br\text{-}BDC)_3$	1.1	0.24	0.31	0.11	0.03
$Sc_2(NO_2\text{-}BDC)_3$	1.2	0.27	0.27	0.10	0.03

The Sc_2BDC_3-based materials show significant variations in uptakes of the vapours, expressed in terms of mmol g^{-1} (Figure 4.46).

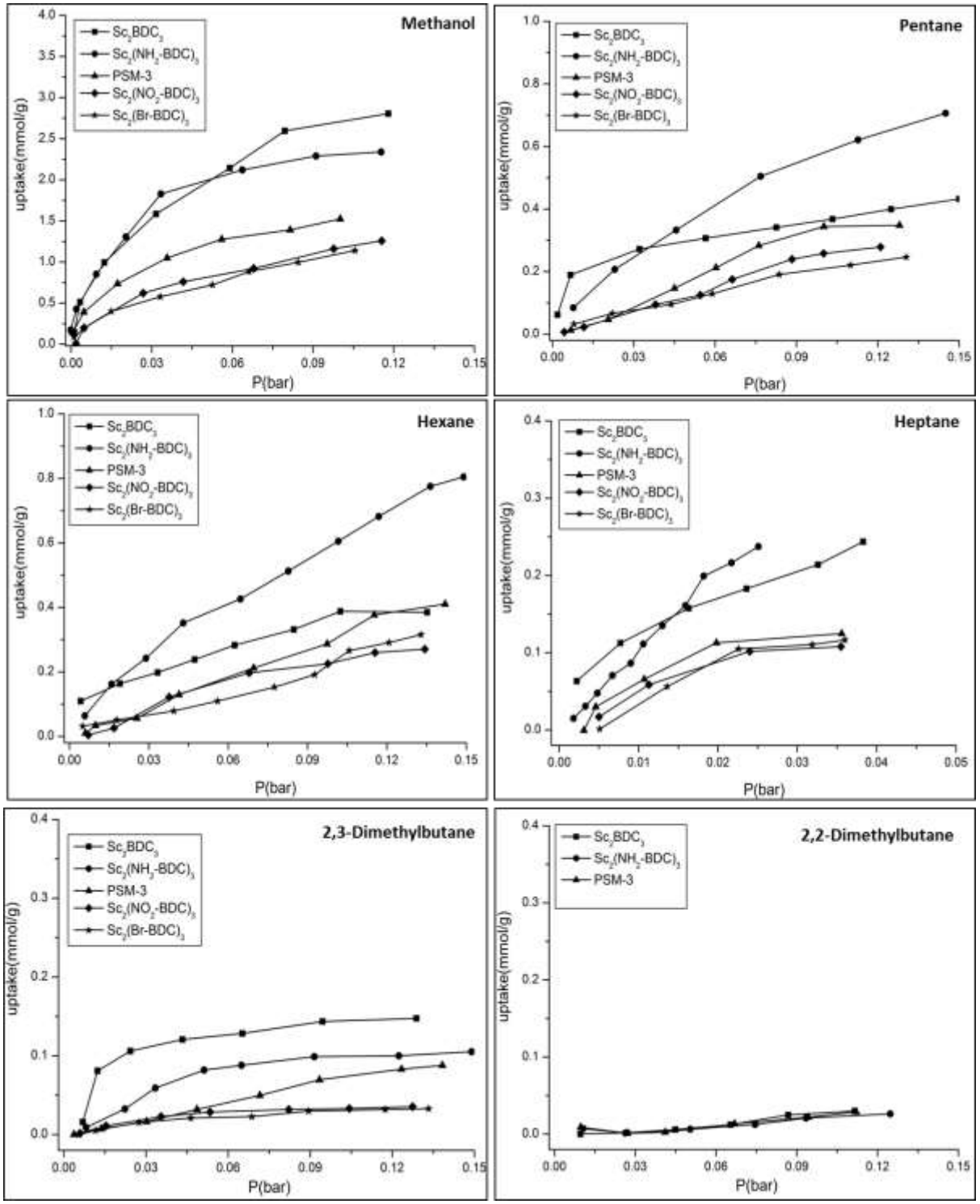

Figure 4.46: Adsorption isotherms of methanol, pentane, hexane, heptane, 2,2-dimethylbutane and 2,3-dimethylbutane collected on a series of MOFs.

In general, where molecules are adsorbed, the amino-and non-functionalised forms show the largest (and similar) uptakes, while the nitro-and bromo-functionalised forms take up similar,

significantly lower, amounts. This can be expected partly because the bulky groups NO_2 and Br-groups take up pore space, partly because of the structure distortion from maximum volume orthorhombic *Fddd* (Sc_2BDC_3 and amino-functionalised) to lower symmetry, lower volume monoclinic *C2/c* (NO_2- form) or orthorhombic *Fdd2* (Br-form) and also because the Br-and NO_2- groups are heavier than H- and NH_2-groups (Figure 4.47).

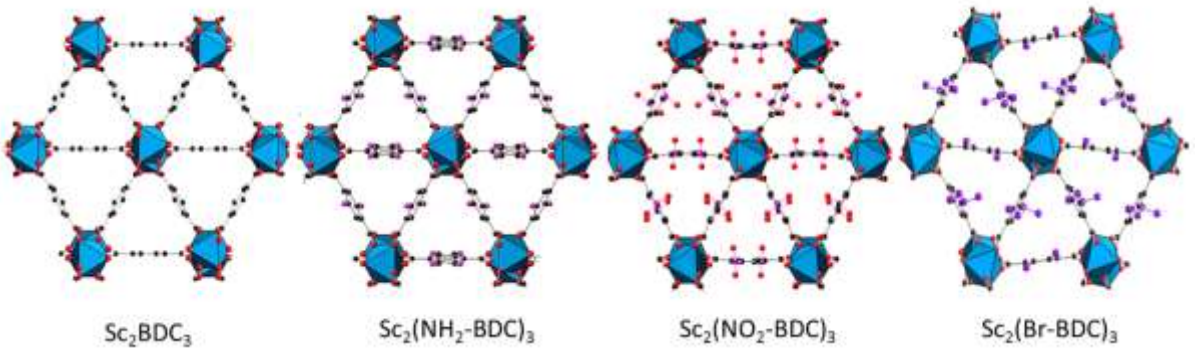

Figure 4.47: Images of the structure of Sc_2BDC_3 and its amino, nitro, and bromo derivatives.

The molar uptakes of methanol are the highest observed (up to 2.8 mmol g^{-1} in Sc_2BDC_3), because the small molecule can pack efficiently. Recent studies have shown how the MeOH molecule is located within the triangular channels.[53] Uptake on the nitro-and bromo-forms is less than half this value, but the fact that adsorption occurs at all suggested considerable rotation of the terephthalate linkers is possible.

For the n-alkanes pentane, hexane and heptane the amino-form shows the highest uptakes, possibly because of greater dispersive interactions, but all forms can adsorb the n-alkanes, which have a cross sectional diameter of 3 Å. Among the branched alkanes, the 2,3 –dimethyl butane is taken up at vapour pressures of around 0.1 bar on the amino and non-functionalised forms, but is excluded from the bromo-and nitro-functionalised forms, showing that the molecular sieving potential is modified by functional groups. All forms of Sc_2BDC_3 excluded

2,2- dimethyl butane, which is a bulkier molecule. The different form of Sc_2BDC_3, therefore show different molecular sieving behaviour towards branched hydrocarbons.

Following the results, a sample of $Sc_2(NH_2\text{-}DC)_3$ that had been modified by solvent-assisted ligand exchange (PSM-3) with NO_2-BDC (nitro-terephthalic acid) was investigated to see if its adsorption selectivity could be controlled by the surface rather than the bulk. Close inspection of the results show that the adsorption properties have been modified so that the uptake has been reduce to be closer to the NO_2 and Br-form. However, a complete core- shell structure is not supported by the adsorption data for 2,3 dimethyl butane, where some uptake is observed at 0.13 bar, where none would be expected if an intact layer of NO_2-BDC were present. It may be that whereas some parts of the crystals exterior are covered, other are not, permitting adsorption through the surface in 'uncovered' places.

4.4.9 NH_2-MIL-53(Sc)

4.4.9.1 Introduction

The aim of this work was to prepare amino-MIL-53(Sc) for the first time. Earlier preparations with amino-terephthalic acid gave NH_2(MIL-88B(Sc) or $Sc_2(NH_2\text{-}BDC)_3$. First attempts with the solvent mixture gave only mixed phase products, but addition of a second linker was found to favour formation of NH_2-MIL-53(Sc). Three additional functionalised linkers were used, X-BDC, where X= $(OH)_2$, NO_2 and Br. The variation in the structure of MIL-53 due to its breathing behaviour made identification of NH_2-MIL-53(Sc) problematical, due to variability of the corresponding powder pattern. However, partial structure solution from single crystal data did identify MIL-53 phases, even if the solvent content and structural disorder resulted in structure solution of low quality. This information was used to index the observed powder pattern of NH_2-MIL-53(Sc) and confirm that its amino-form had been produced albeit with minor amounts of impurity. It was therefore possible to measure the

carbon dioxide (CO_2) adsorption properties, and compare them with those previously measured at -77 ^{0}C for MIL-53(Sc) and its nitro-derivative.

4.4.9.2 Attempts to prepare pure NH_2-MIL-53(Sc)

Attempts to prepare the NH_2-MIL-53(Sc) for the first time were initially made using the amino-terephthalate (NH_2-BDC) linker and scandium chloride solution and mixed solvents (DMF and H_2O), using the synthetic conditions given in Table 4.2. Figure 4.48 shows the PXRD of the syntheses prepared. Those syntheses with a molar ratio (Sc/L) from 0.6 to 1.1, DMF:H_2O (1:20) and performed at 130 ℃ did give $Sc_2(NH_2\text{-}BDC)_3$, but not pure. Doubling the amount of solvent gave the product with the lowest impurity (Figure 4.48e). Other preparations at lower temperatures gave the formation of the amino-functionalised MIL-88B(Sc) or mixture of both amino-$Sc_2(BDC)_3$ and MIL-88B(Sc).

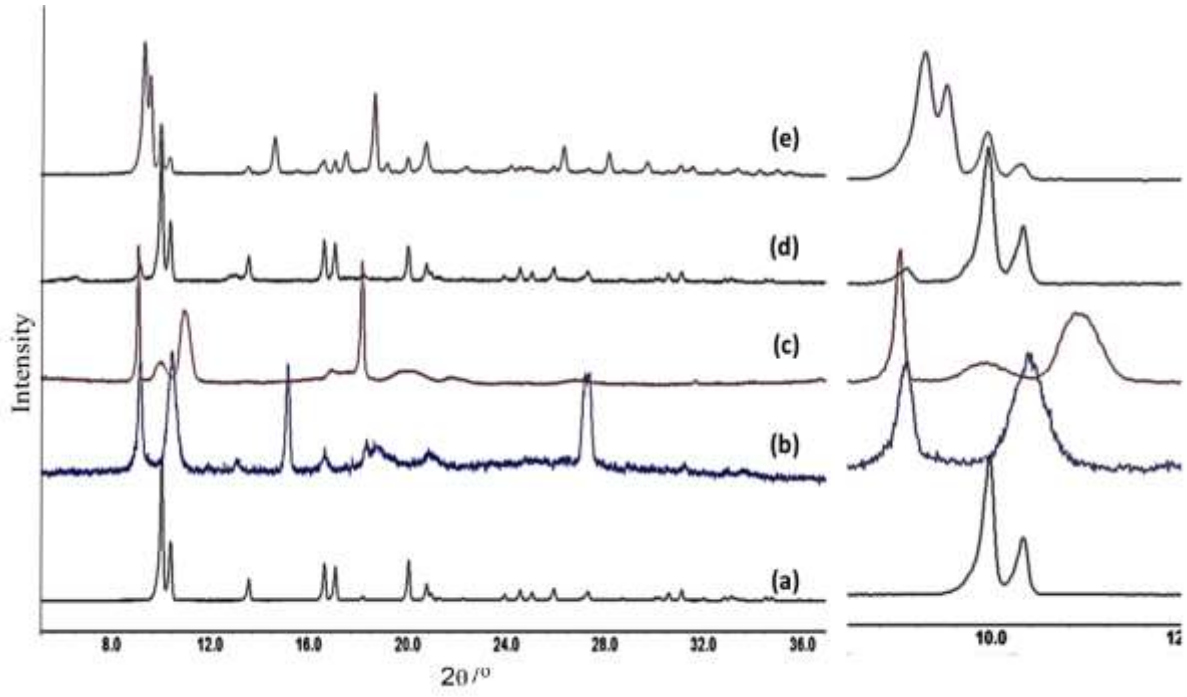

Figure 4.48: PXRD patterns of attempts to prepare amino-MIL-53(Sc): (a) prepared with Sc/L(0.6 or 1.0) in DMF:H_2O (10:200) at 130 ℃, (b) Sc/L= 0.6 in DMF:H_2O (20:400) at temperature range 80 ℃, (c and d) Sc/L= 1.0 in DMF:H_2O (20:600) at 100 or 130℃, respectively, and (e) Sc/L=1.0 in DMF:H_2O (20:400) at 130 ℃.

Addition of a second ligand in to the synthesis using the approach of mixed solvents and low temperature was later found to yield pure MIL-53(Sc), predominantly as the amino-terephthalate, but with some mixed linker. In these experiments, the amount of the second ligand, such as NO_2-BDC, $(OH)_2$-BDC or Br-BDC, was explored in a range between 10-60% of the total carboxylic acid, keeping the gel composition the same in other variables. Analyses of each set of reactions are discussed below.

4.4.9.3 MIL-53(Sc)[NH_2-BDC]$_x$[NO_2-BDC]$_y$

A series of syntheses varying the molar ratio of two ligands in the mixtures was explored from input levels between 10-60% of NO_2-BDC, mixed solvent DMF (2 mL) and H_2O (8 mL), scandium to ligand ratio ca. 1:1 at 130℃ for 12 h. Using solution ^{1}H NMR the percent of the second ligand is confirmed to be lower than that present in the reactant mix. Adding 10% of NO_2-BDC (0.03 mmol) in experimental conditions given above yields a mixture of NH_2-MIL-53(Sc), $Sc_2(NH_2\text{-BDC})_3$ and other impurities. Further exploration of the synthesis conditions gave an improved route, in which the volume of solvents was doubled, keeping all other ratios constant. Table 4.10 lists the percent of NO_2-BDC present in the samples confirmed by solution.

Table 4.10: Percent of NO_2-BDC used in attempts to prepare NH_2-MIL-53(Sc). *Synthesis made in DMF and H_2O, 2 and 8 mL respectively.

Ligand 1	**Ligand 2**	**Ligand 2** *Theoretical*	**Ligand 2** *% by solution NMR*	**Sample**
NH_2-BDC	NO_2-BDC	10	3	843
NH_2-BDC	NO_2-BDC	15	5	843B
NH_2-BDC	NO_2-BDC	30	10	843C
NH_2-BDC	NO_2-BDC	30*	10*	843D

Solution ^{1}H NMR gave the final percentage of the two terephthalates in the solid. For the preparation with 30% of NO_2-BDC, the resulting solid contained just 10% of this linker as % of the total number of terephthalate groups. Indeed, all solids contained a lower ratio of the second linker than their parent synthesis mixtures.

Figure 4.49 shows the PXRD patterns of the samples prepared with different amounts of the second linker, nitro-terephthalate. The sample closest to a single, mixed linker, MIL-53(Sc) is sample 843D, with 10% NO_2-BDC and 90% NH_2-BDC. The solution phase ^{1}H NMR of this sample, once digested, is given in Figure 4.50.

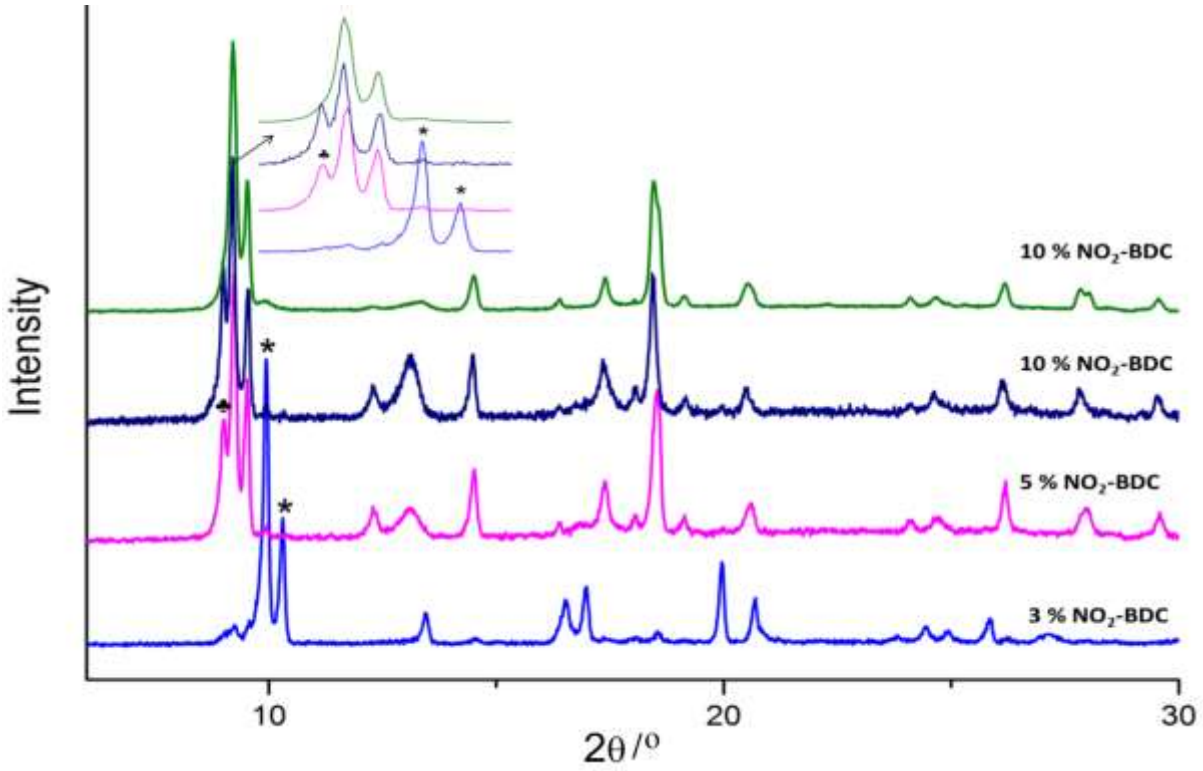

Figure 4.49: PXRD patterns as in attempts to prepare NH_2-MIL-53(Sc) with 3, 5 and 10 % of NO_2-BDC). Green PXRD, synthesis carried out in molar ratio DMF:H_2O (40:600), sample named 843D. Using 3% of the second ligand gave the MOF $Sc_2(BDC)_3$. ♣ Other impurity.

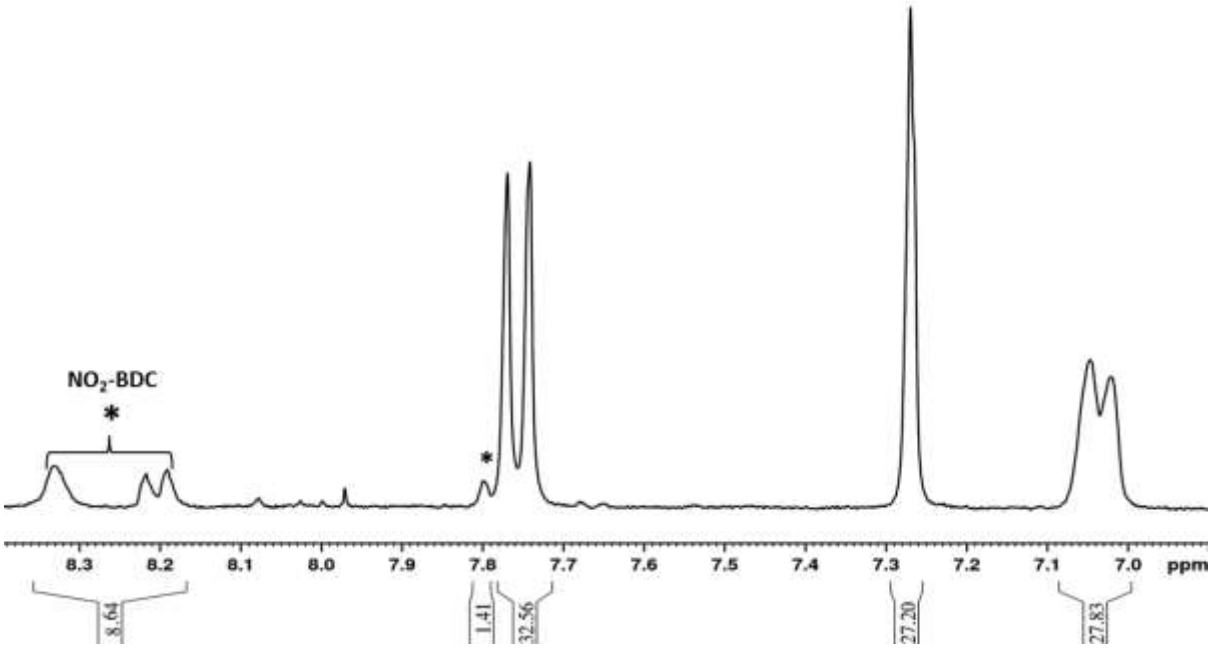

Figure 4.50: ^{1}H NMR of the digested NH_2-MIL-53(Sc-10% NO_2-BDC). *Signal attributed to the linker NO_2-BDC located in 7.80, 8.20, 8.25 and 8.36 ppm.

Experiment yielded NH_2-MIL-53(Sc-10% NO_2-BDC), as large crystal with rectangular shape and length of *ca.* 60µm. It is known that this material shows drastic changes upon drying or hydration treatment. Figure 4.51 shows images of the crystals using SEM microscopy and optical microscope, these images showed that the crystals that have started to deform and fracture. This phenomenon was previously observed on MIL-53(Sc) upon drying.[42]

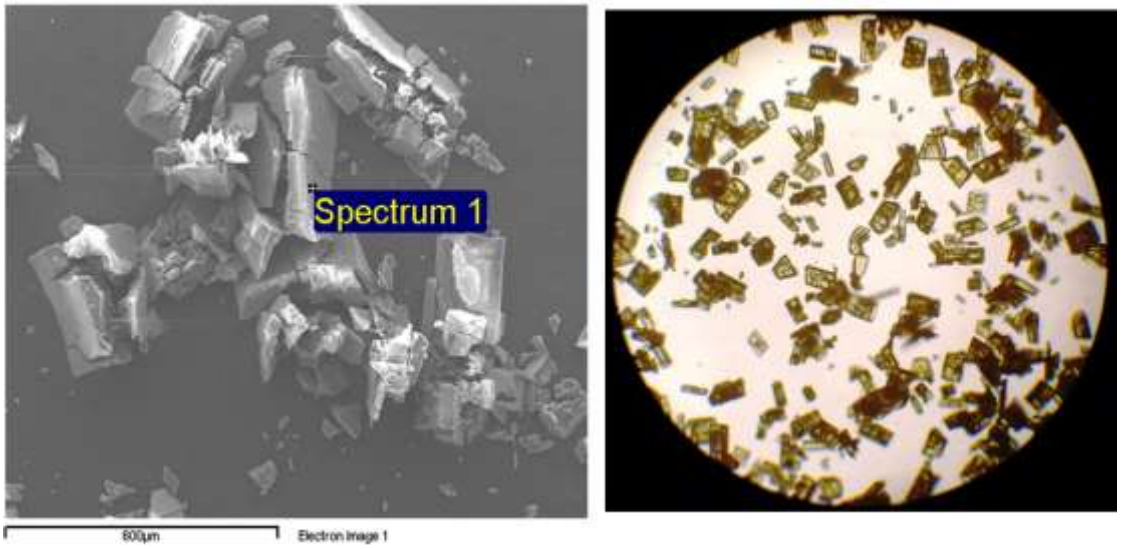

Figure 4.51: SEM and optical microscopy images of sample NH_2-MIL-53(Sc)·10% of NO_2-BDC.

Single crystal analysis of crystals from a batch of NH_2-MIL-53(Sc)(10% NO_2-BDC) was performed at -148 °C. The structure was solved using the Crystal software[51] using direct methods. It was found to possess orthorhombic symmetry, with space group *Imcm*, a = 7.289 (0.003) Å, b = 11.017 (0.005) Å, c = 18.625 (0.008) Å, but the fit had high residuals (Rp = 0.16, wR= 0.52) (CIF file available see the Appendix B).

The observed powder diffraction patterns (collected at room temperature upon standing in air) were not matched by that simulated from the single crystal structure. This was attributed to the well documented breathing type behaviour of MIL-53 samples. In fact, a closer (but not perfect) match was achieved between the simulated pattern from the SXRD of NH_2-MIL-53(Sc) in this work with that simulated using a model for MIL-53 in the narrow pore form, as taken from the literature[43], even though there are differences in the unit cells (Figure 4.52).

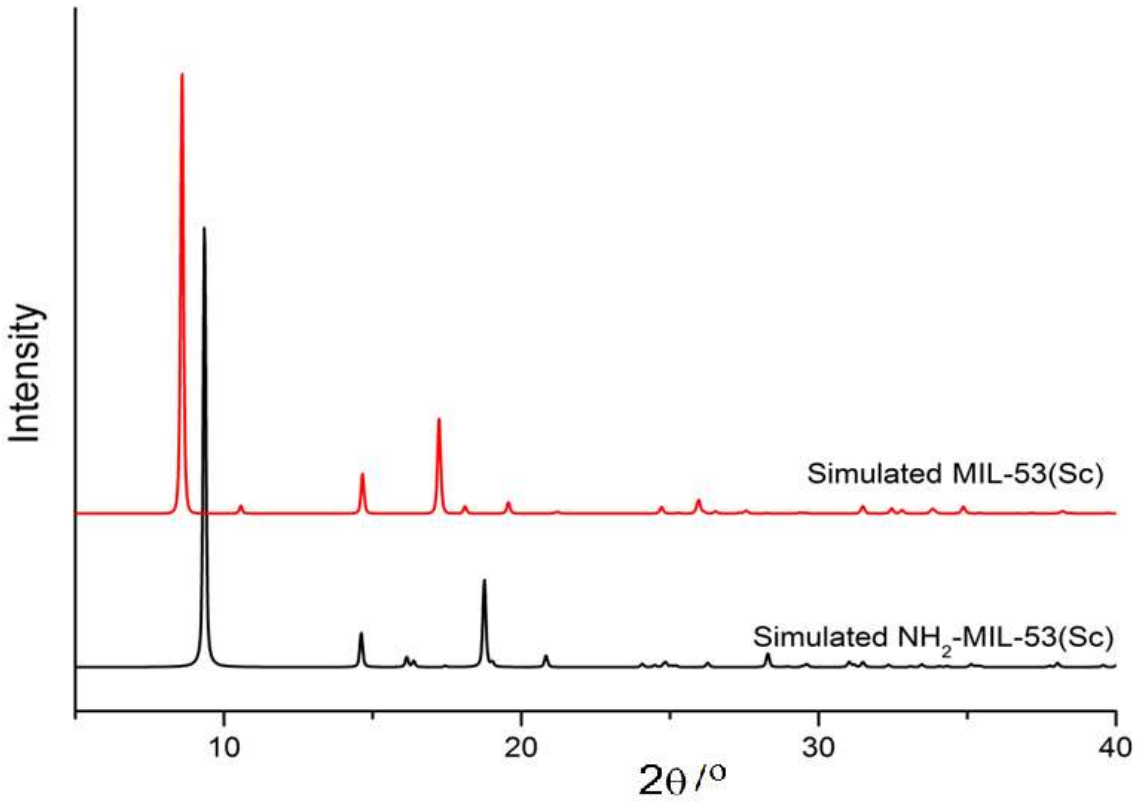

Figure 4.52: Simulated pattern of MIL-53(Sc)[43] and its amino derivative on the narrow pore (*np*) form obtained by single crystal diffraction analysis.

Figure 4.53 shows the structure of NH_2-MIL-53(Sc)(10%NO_2-BDC), as determined by direct methods from single crystal diffraction data and neglecting the presence of nitro groups. It is similar to that measured previously for the nitro-form[43] and is isostructural with other MIL-53 materials. The framework comprises infinite, corner-sharing $ScO_4(OH)_2$ chains bridging through μ_2O(H) species. These chains are linked by terephthalate groups. Each ring has just one $–NH_2$ group, distributed over the different C atoms with fractional occupancy 0.25.

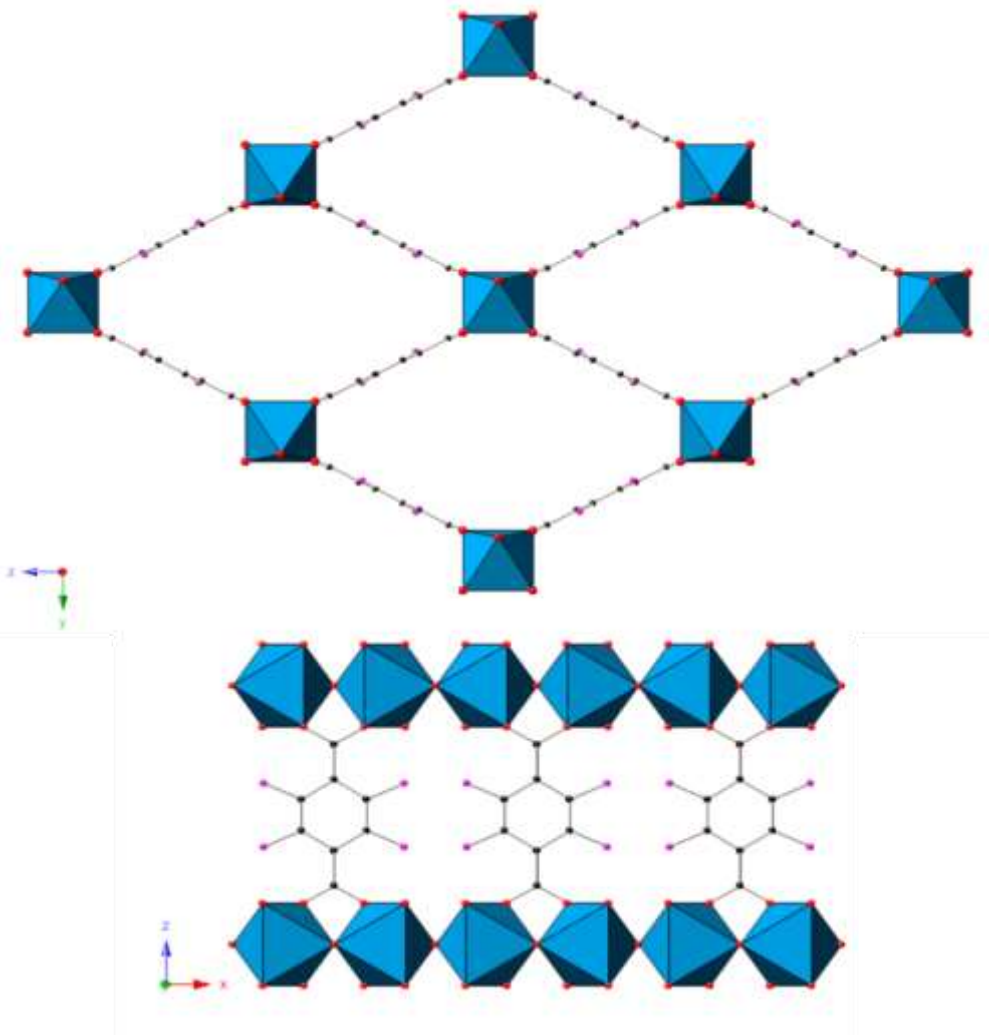

Figure 4.53: Structure of NH_2-MIL-53(Sc) (10%NO_2-BDC) in an partial open configuration viewed down the channels parallel to the x-axis (top) and the layers of amino-terephthalates connecting the chains (bottom). ScO_6 octahedra are shown in blue. Black, red and magenta spheres represent the carbon, oxygen and nitrogen atoms of the organic linker respectively.

In order to determine the unit cell of the as-prepared NH_2-MIL-53(Sc)(10%NO_2-BDC) at room temperature, the PXRD pattern was indexed using the DICVOL method in the FullProf software. This analysis yielded an orthorhombic lattice with a = 18.4297Å, b = 11.5012 Å, c = 7.2767Å. Then a model was constructed from the MIL-53(Sc)·DMF structure reported by Mowat et al[43]. To prepare the model, the unit cell from the indexed pattern and the space group and atom positions from the reported MIL-53(Sc)·DMF, $Pna2_1$, were taken and the amino N atoms were placed on all possible C atoms of the terephthalate phenyl groups with 0.25 occupancy (Figure 4.54).

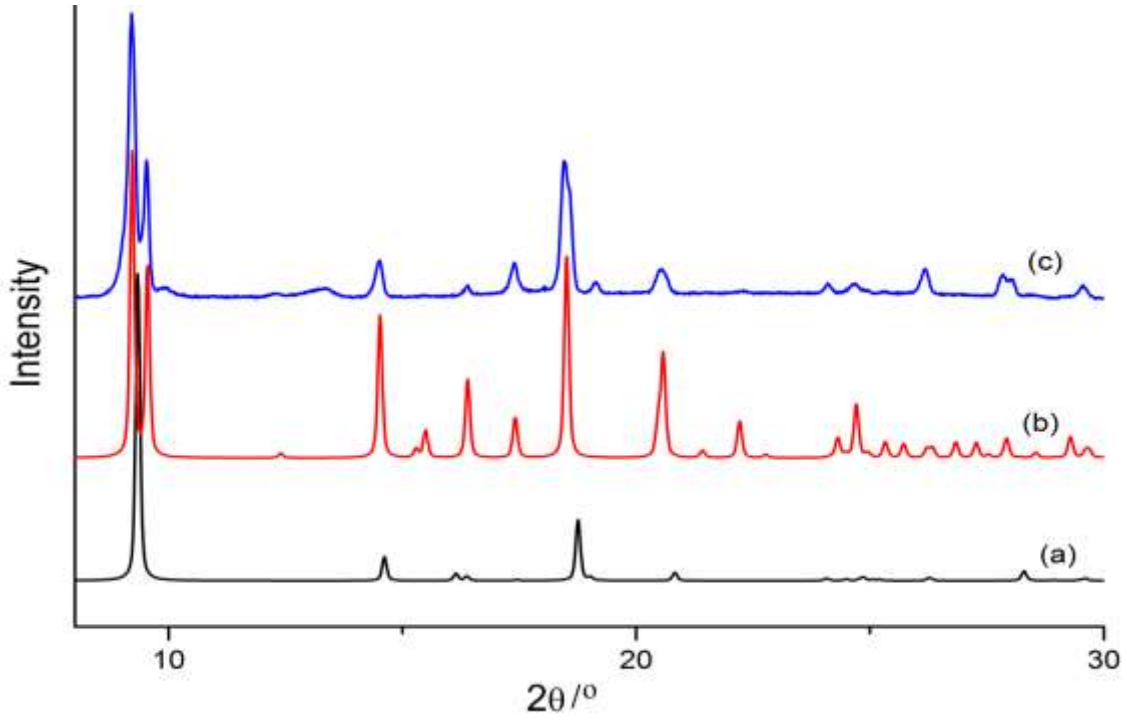

Figure 4.54: Diffraction pattern of NH_2-MIL-53(Sc); (a) and (b) simulated X-ray obtained by single crystal diffraction and constructed from structure of Mowat [43] respectively, and (c) as-prepared NH_2-MIL-53(Sc)·10% of NO_2-BDC)

The Le Bail method was used to determine unit cell parameters. The unit cell and symmetry determined from single crystals at -148 °C and from powder data at room temperature are compared in Table 4.11 and Figure 4.55 shows the Le Bail refinement. Ignoring the different

settings of the space group, the unit cells are observed to be quite close, so that the structural change is subtle, and is likely to involve small tilts rather than strong structural distortions.

Table 4.11: Comparison of the Lattice Parameters of NH_2-MIL-53(Sc), as-prepared NH_2-MIL-53(Sc)(10%NO_2-BDC) (at room temperature) and solved using single crystal X-ray diffraction (SXRD) (at -148 ℃)

	Unit cell				Space group
NH_2-MIL-53(Sc)	a/Å	b/Å	c/Å	% R	
SXRD	7.289	11.017	18.625	0.16	*I m c m*
As-prepared 843D	18.5056	11.1771	7.269		*P n a* 2_1

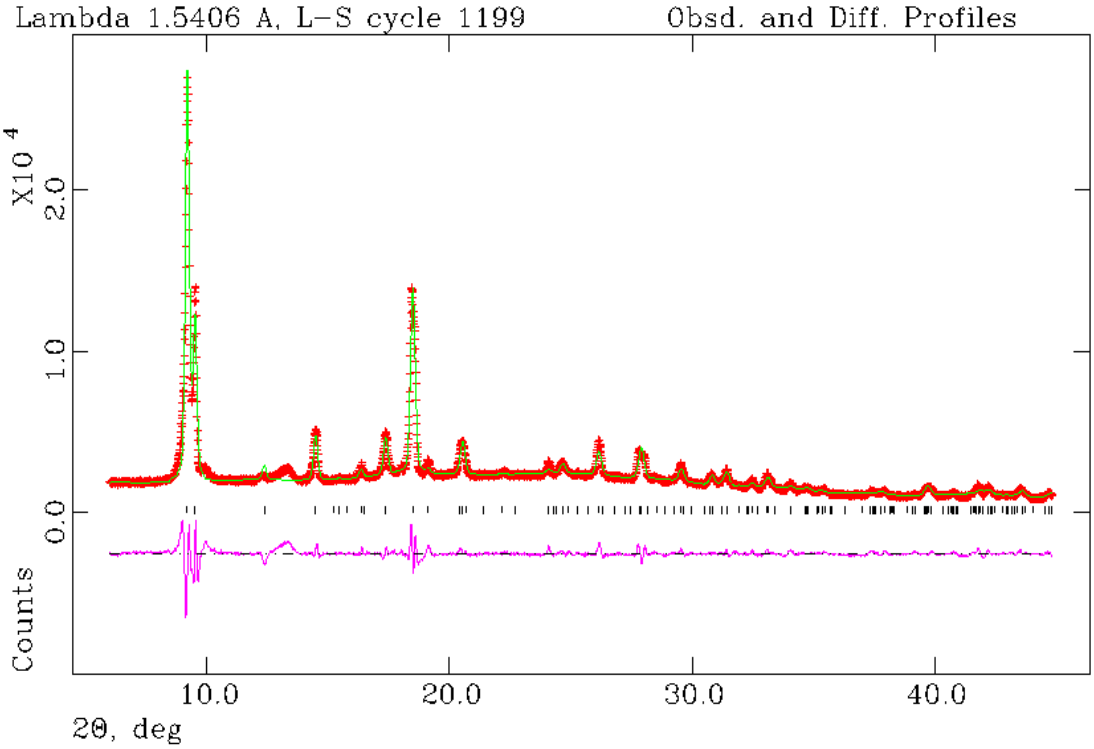

Figure 4.55: Le Bail plot for the unit cell refinement on NH_2-MIL-53(Sc)(10%NO_2-BDC) sample.

TGA for the as-prepared NH_2-MIL-53(Sc)(10%NO_2-BDC) gives a 13.5% loss solvent at 120 ℃ and the framework start to collapse at 400 ℃ (Figure 4.56, red trace). The complete

removal of solvent was proven by TGA data collected after heating the sample at 150 ℃ for 6 h (Figure 4.56, black trace).

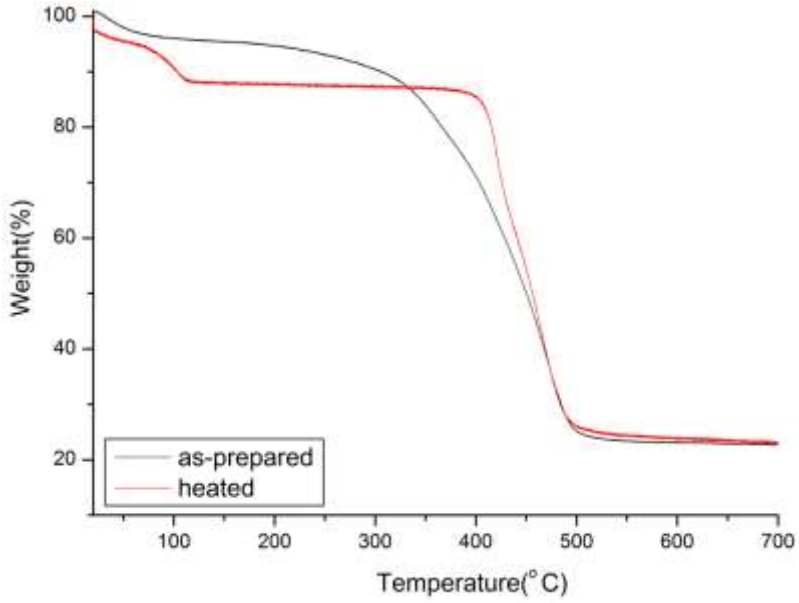

Figure 4.56: Thermogravimetric analysis on NH_2-MIL-53(Sc) collected on sample with 10% of NO_2-BDC as- prepared (red trace) and heated at 150 ℃ (black trace).

The behaviour of NH_2-MIL-53(M), M=Al, Cr, Ga, etc. with heating and cooling, and upon CO_2 adsorption, has been examined previously.[20] For this new as-prepared NH_2-MIL-52(Sc)(10% NO_2-BDC), in situ PXRD was used to investigate its response to heating and cooling cycles. This was performed using the STOE STADIP diffractometer, primary beam monochromator (Cu Kα) in the capillary mode, which is equipped with permanently mounted Cobra Plus liquid-nitrogen cryostream (Oxford Cryosystems) to explore the thermal response of the amino-functionalised MIL-53(Sc). PXRD patterns were obtained in Debye-Scherrer geometry within a sealed 0.7 mm quartz capillary, the measurements were performed over a range of temperatures from -73 ℃ to 225 ℃ and to prove if the material show the reversibility then cooling down to 25 ℃. The temperature was held for 10 minutes before each run. Figure 4.57 shows the series of PXRD patterns collected.

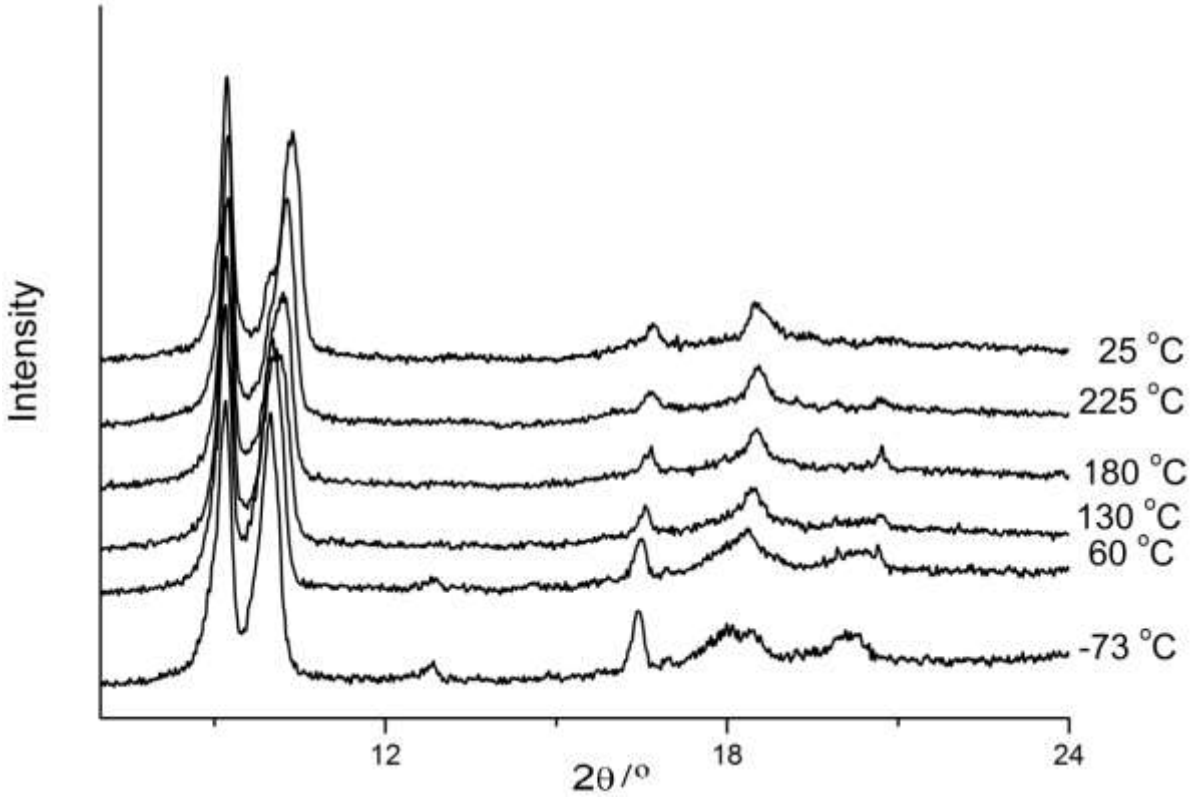

Figure 4.57: *In situ* PXRD patterns collected on the as-prepared NH_2-MIL-53(Sc)(10% NO_2-BDC).

This experiment revealed only small changes in the powder patterns upon cooling and heating; the structure does not change significantly. It might be due to the presence of the NH_2 and NO_2-groups within the framework preventing closure of the structure. To understand the desolvation of amino- functionalised MIL-53(Sc), the as-prepared sample NH_2-MIL-53(Sc)(10% NO_2-BDC) was loaded in a capillary which was dehydrated at 200 ^oC for 12 h in *vacuo* at 10–5 mbar on a glass line and then flame sealed. The pattern was collected and the same capillary was broken up and exposed to air for 96 h to allow hydration. The diffraction shows that the structure loses long range order upon desolvation, but recovers much of this upon rehydration in most air. Comparison of the powder diffraction patterns of the materials are shown in Figure 4.58.

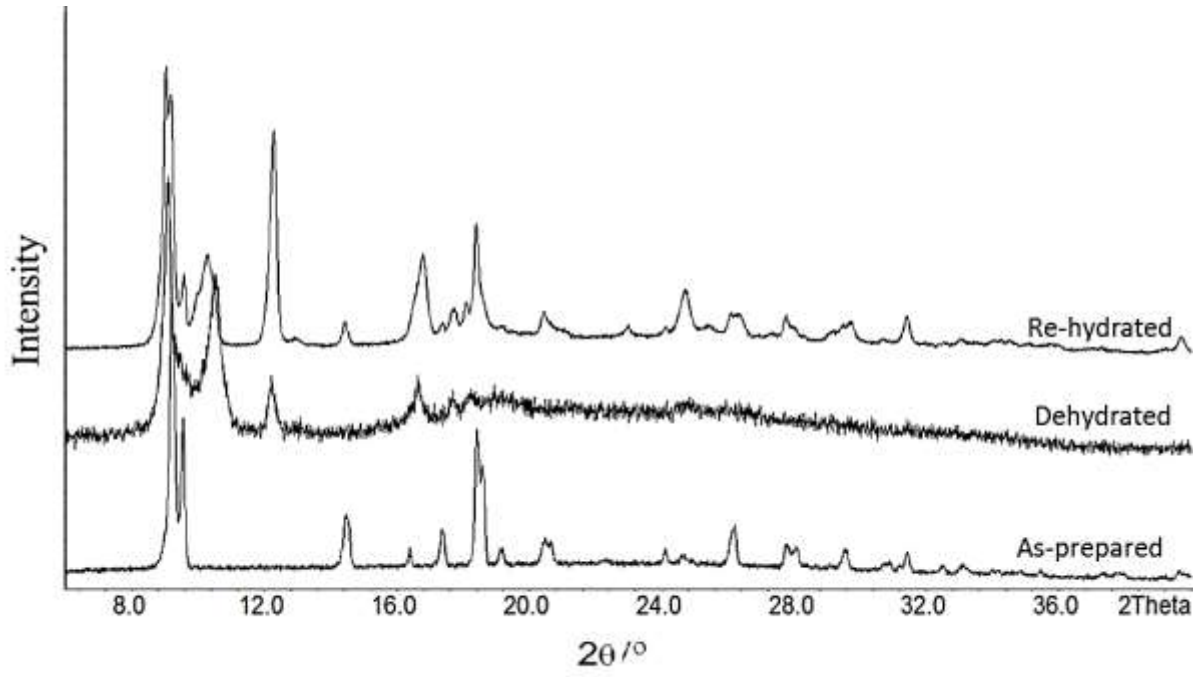

Figure 4.58: PXRD of NH_2-MIL-53(Sc)(10% NO_2-BDC) in as-prepared, thermally desolvated and rehydrated forms, showing the loss and partial recovery of long range structural order.

4.4.9.4 MIL-53(Sc)[NH_2-BDC]$_x$[$(OH)_2$-BDC]$_y$

In the case of the synthesis involving dihydroxyterephthalate as the dopant linker, the first attempt to prepare amazed linker, 'pure' amino MIL-53(Sc) was successful. This was prepared by using an input 40% percent of $(OH)_2$-BDC (0.41 mmol), and 60% of NH_2-BDC (0.58 mmol), in a autoclave with scandium chloride solution (0.83 mmol) in mixed solvents DMF (1 mL) and H_2O (4 mL) heated at 130℃ for 12 h. Hereafter the sample is named as 844. Synthesis of 844 yielded yellow block crystals and characterisation by SEM microscopy and optical microscope are shown in Figure 4.59. These images exhibit deformation of the crystal upon characterisation by SEM, while in the optical microscope in a drop of water they remained as intact blocks. Using solution state ^{1}H NMR, the percent of the second ligand is confirmed to be 20% of the theoretical. Figure 4.60 shows the presence of both ligands used in the synthesis by using solution ^{1}H NMR spectra of sample 844.

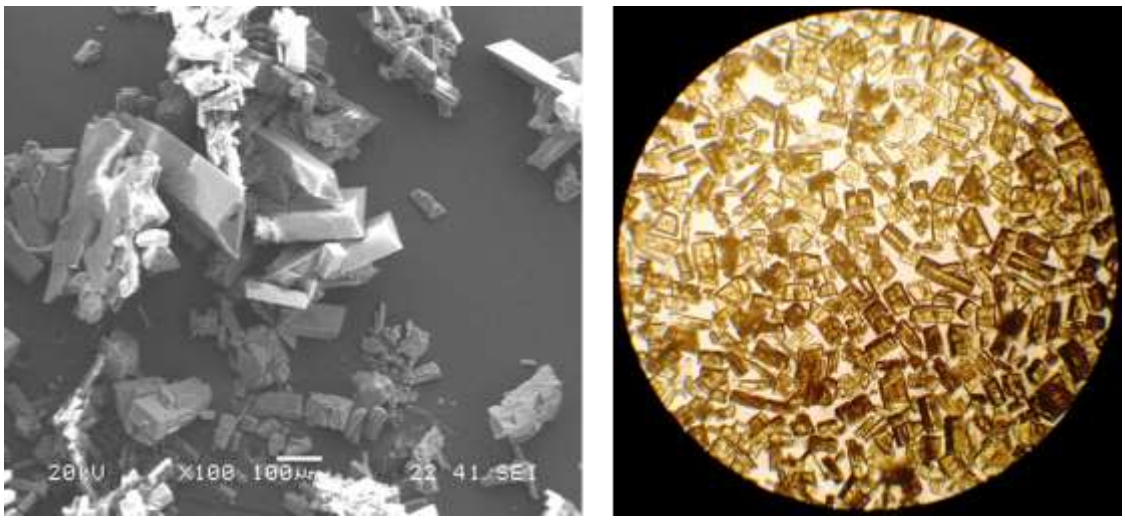

Figure 4.59: SEM and optical microscopy images of sample 844, NH_2-MIL-53(Sc)(20% $(OH)_2$-BDC)) crystals, 60 -200 µm in length.

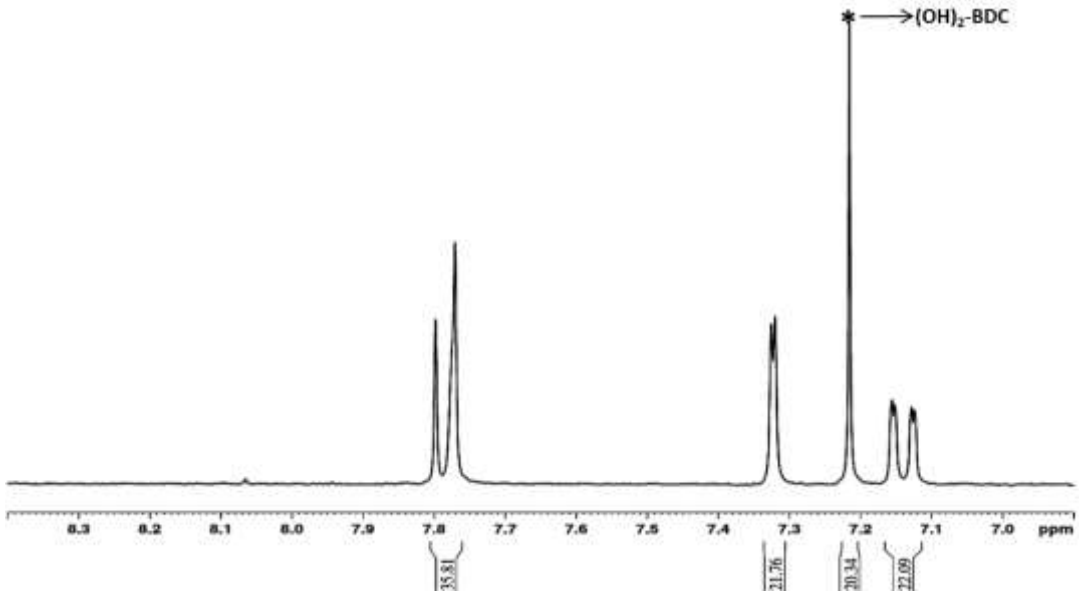

Figure 4.60: ^{1}H NMR of the digested sample NH_2-MIL-53(Sc)(20% $(OH)_2$-BDC)), showing the resonances (7.210 ppm) for the second ligand present in the amino MIL-53(Sc).

Crystals were suitable for SXRD analysis (performed at -148 ℃) and this confirmed the material was MIL-53. The simulated PXRD pattern from the SXRD structure is compared with the room temperature PXRD data of as-prepared sample 844 (NH_2-MIL-53(Sc)(20%-$(OH)_2$-BDC)) in Figure 4.61. The PXRD patterns are similar, with small changes in peak positions that may be attributed to the analyses being performed at different temperatures.

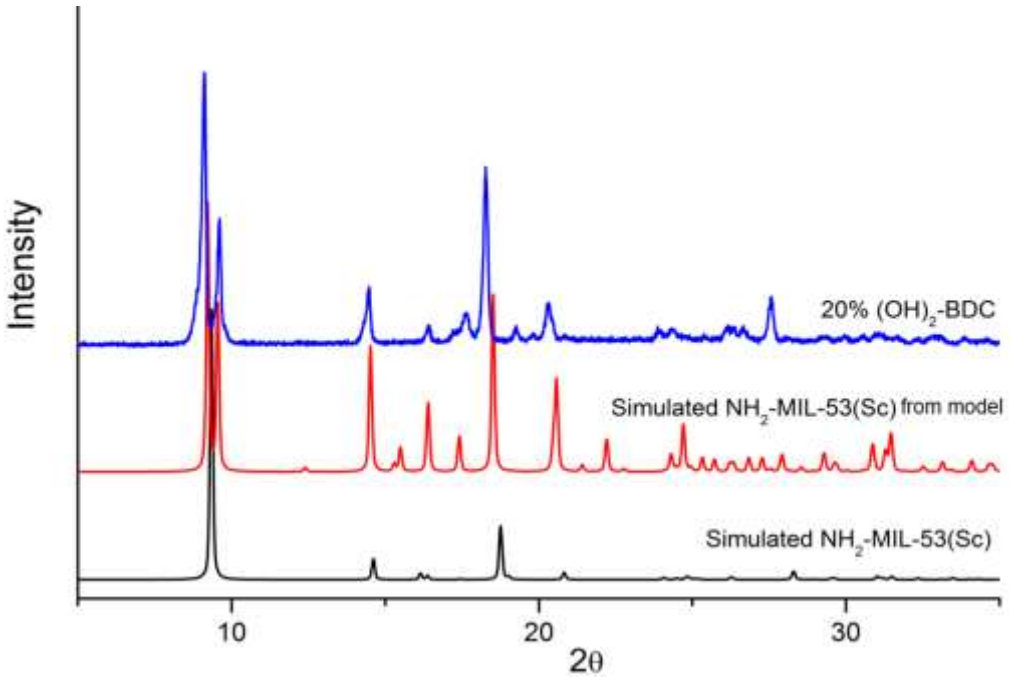

Figure 4.61: Diffraction pattern of as-prepared 844 (NH_2-MIL-53(Sc) with 20% of $(OH)_2$-BDC compared with the pattern simulated from the SXRD and the constructed model.

The structure of this solid was the same as the model described above, a framework composed of infinite, corner sharing, $ScO_4(OH)_2$ that are connected by terephthalate linkers , forming one dimensional channels with a rhombic cross-section. This is shown in Figure 4.62.

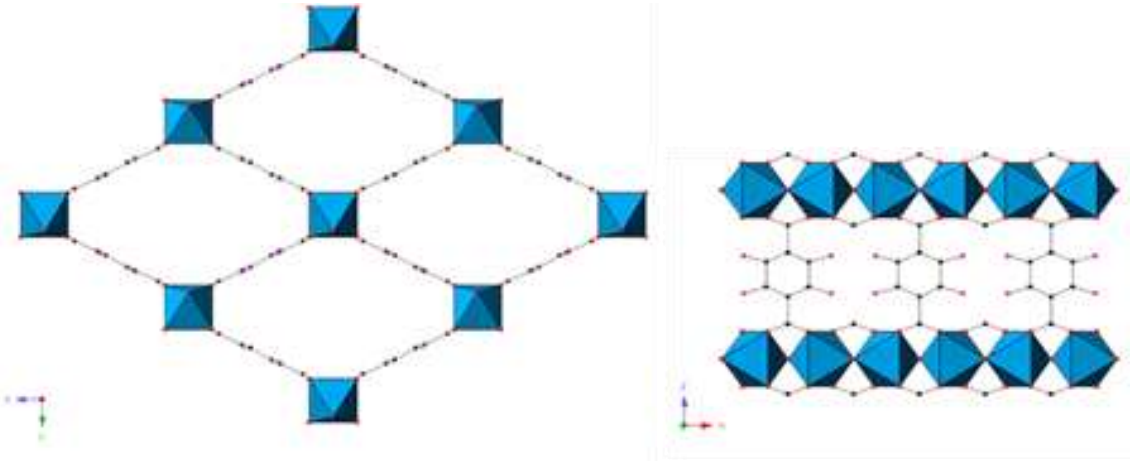

Figure 4.62: Structure of NH_2-MIL-53(Sc)(20% $(OH)_2$-BDC) in an partial open configuration viewed down the channels parallel to the x-axis (top) and the layers of amino-terephthalates connecting the chains (bottom).

Le Bail method was used to refine the unit cell parameters of the as-prepared 844. Le Bail refinement of the unit cell was performed against laboratory PXRD data (Figure 4.63). The unit cell parameters determined from SXRD and PXRD are similar, although the space groups used were different (Table 4.12).

Table 4.12: Comparison of the Lattice Parameters of NH_2-MIL-53(Sc)(20% $(OH)_2$-BDC) in as-prepared and solved using single crystal X-ray diffraction (SXRD).

	Unit cell				Space group
NH_2-MIL-53(Sc)	a/Å	b/Å	c/Å	% R	
SXRD	7.263	10.970	18.647	0.28	*I m c m*
As-prepared 844	18.5290	11.969	7.283		*P n a* 2_1

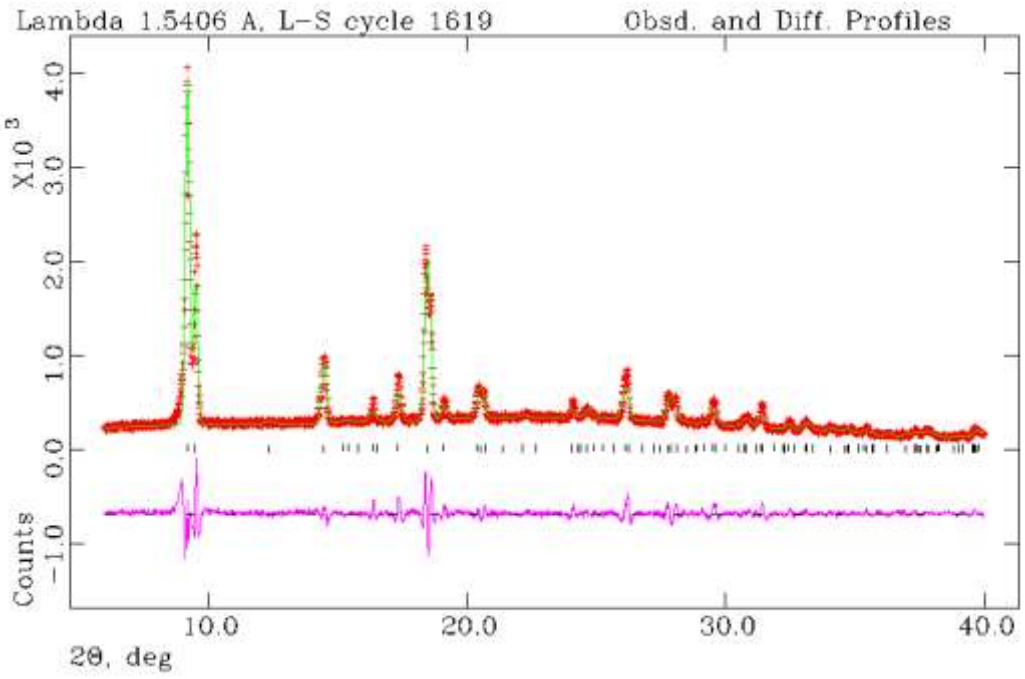

Figure 4.63: Le Bail plot for the unit cell refinement on NH_2-MIL-53(Sc) sample 844.

TGA of the as-prepared 844, exhibits a 13.5% of loss solvent at 180 ℃ and the framework start to collapse at 350 ℃ (Figure 4.64). The sample was heated at 200 ℃ to remove any solvent, however, upon heating there is 5% loss weight at 250 ℃, which could be attributed to residual ligand into the framework.

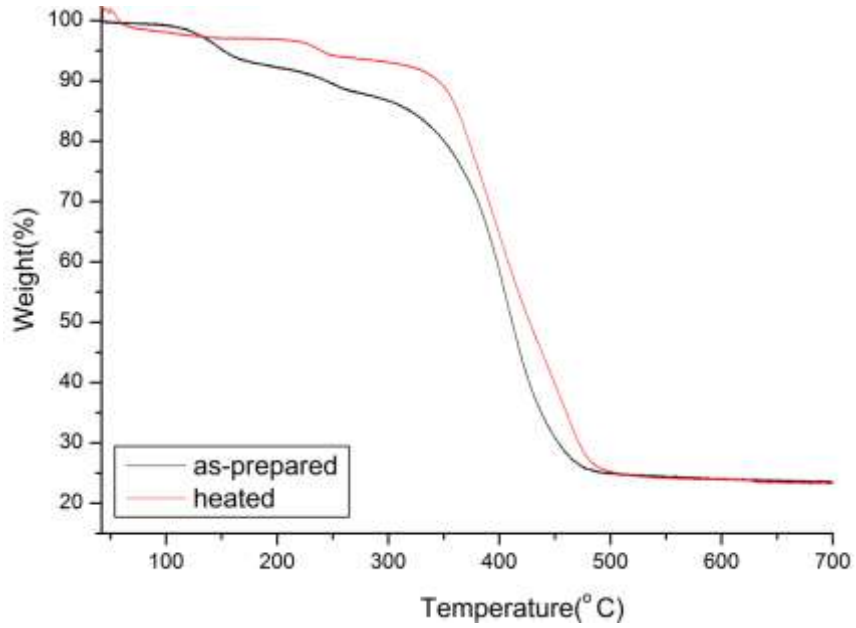

Figure 4.64: Thermogravimetric analysis on NH_2-MIL-53(Sc) collected on sample 844 prepared with 20% of $(OH)_2$-BDC.

In situ variable temperature diffraction X-ray of the sample was performed at St Andrews, using the diffractometer described earlier. The sample shows some minor changes upon heating to 225 °C and a more noticeable one upon cooling to room temperature, once the solvent has been removed. The change is more significant than for the sample containing NO_2- groups, possibly because the terephthalate -OH groups are less bulky and allow greater structural readjustment of the desolvated material (Figure 4.65).

In a second experiment, an as-prepared sample was degassed in a glass capillary at 250 °C for 12 h in a vacuum to remove solvent, before being sealed and an XRD pattern run. This resulted in a less crystalline solid. The capillary was then broken and the sample allowed to hydrate, resulting in partial hydration and an increase in order (Figure 4.66).

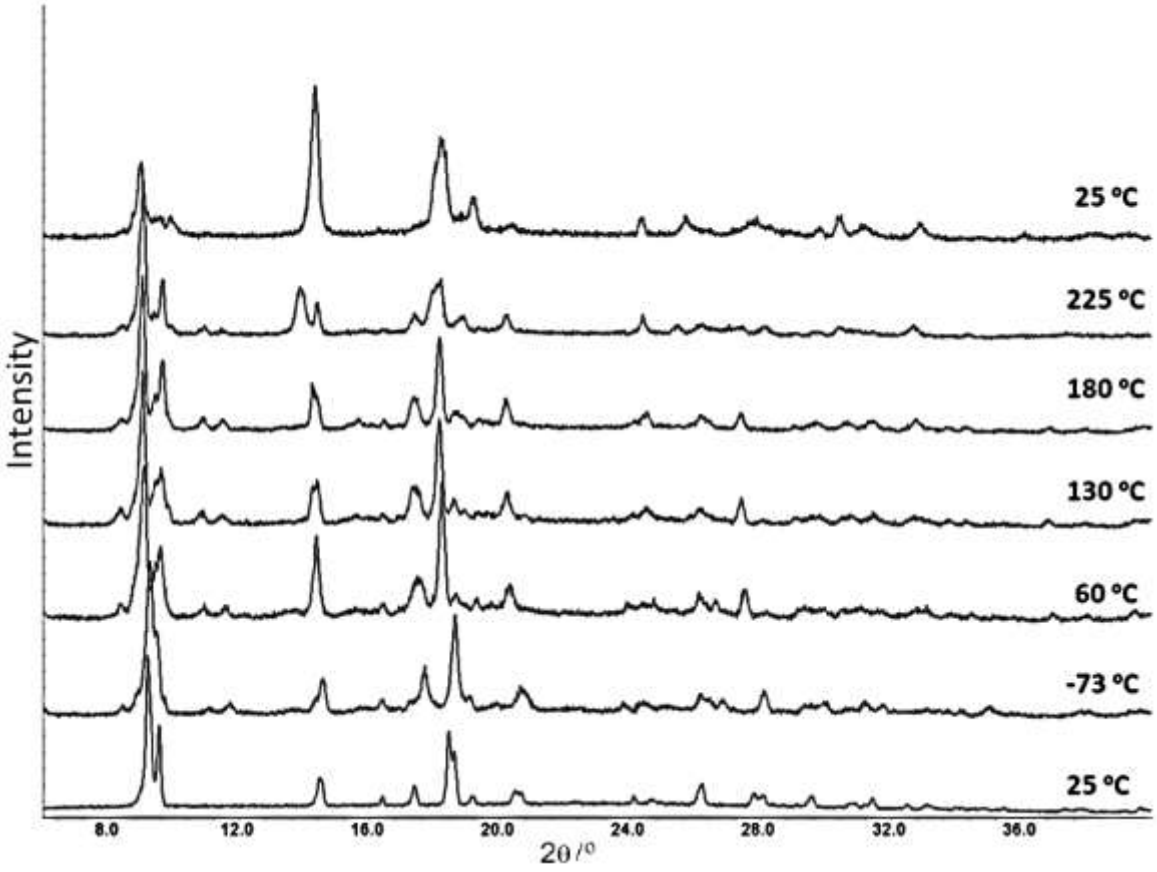

Figure 4.65: In situ PXRD patterns of NH_2-MIL-53(Sc)(20%-$(OH)_2$-BDC) during heating and cooling.

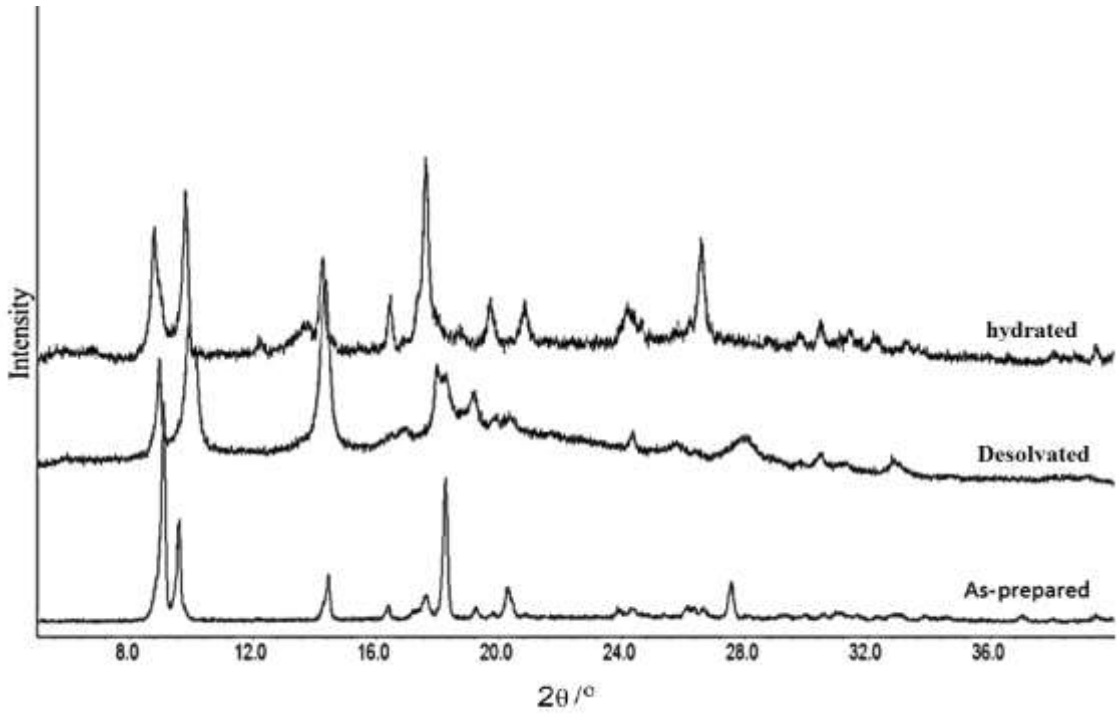

Figure 4.66: PXRD of NH_2-MIL-53(Sc)(20%-$(OH)_2$-BDC) upon desolvation and hydration.

4.4.9.5 MIL-53(Sc)[NH_2-BDC]$_x$[Br-BDC]$_y$

A series of syntheses varying the molar ratio between NH_2-BDC and Br-BDC was performed. The percentage of Br-BDC in the total terephthalic acid content was varied between 10 and 60%, and the preparations were performed in mixed solvent (1 mL DMF and 4 mL H_2O) at 130 ℃ for 12 h. The Sc/linker molar ratio was 1.0. The amount of $ScCl_3$ used in each preparation was 1.2 mmol (1.45 M). The first attempts yielded mixtures of MOFs so this addressed to increase the volume of solvents to 2 mL of DMF and 8 mL H_2O, which gave the "most pure solid", when 15% of the Br-BDC was used. Table 4.13 are listed the percent of Br-BDC confirmed by solution state ^{1}H NMR (Figure 4.67).

Table 4.13: Samples of NH_2-MIL-53(Sc), prepared with different percent of Br_2-BDC. Synthesis achieved in DMF (2 mL) and H_2O (8 mL) asterisked.

Ligand 1	Ligand 2	Ligand 2 Molar % in reaction mixture	Ligand 2 % by solution state ^{1}H NMR	Sample
NH_2-BDC	Br-BDC	10	5	845
NH_2-BDC	Br-BDC	30	15	845C
NH_2-BDC	Br-BDC	30	15*	845D
NH_2-BDC	Br-BDC	60	30*	845E

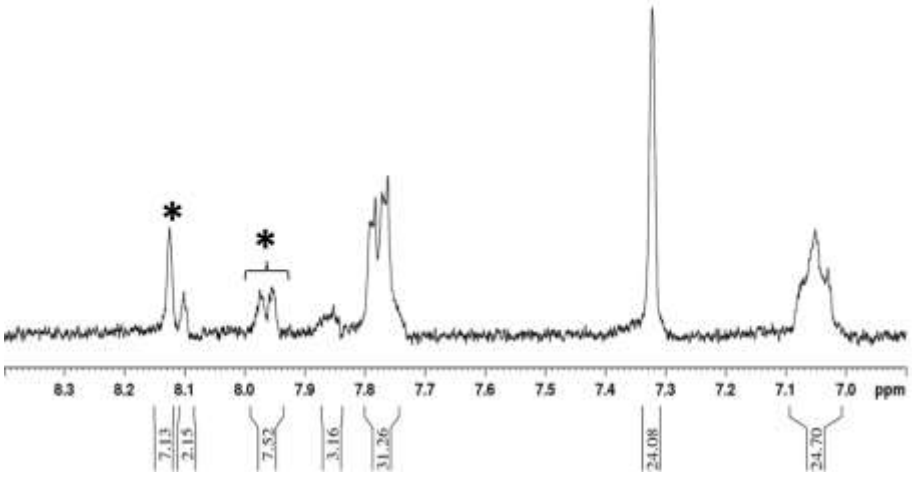

Figure 4.67: ^{1}H NMR of the digested sample of NH_2-MIL-53(Sc)(15% Br-BDC) (845D) , showing the resonances (located at 7.98 and 8.12 ppm) for the second ligand present in the sample.

PXRD (Figure 4.68) showed that at low concentrations of Br-BDC the Sc_2BDC_3 phase forms, but when the preparation was performed under 'dilute' conditions with 15% of included Br-BDC the main phase was MIL-53(Sc). Further increase of the ligand gave mixtures where the main phase was $Sc_2(Br\text{-}BDC)_3$ No recrystallised ligand was apparent.

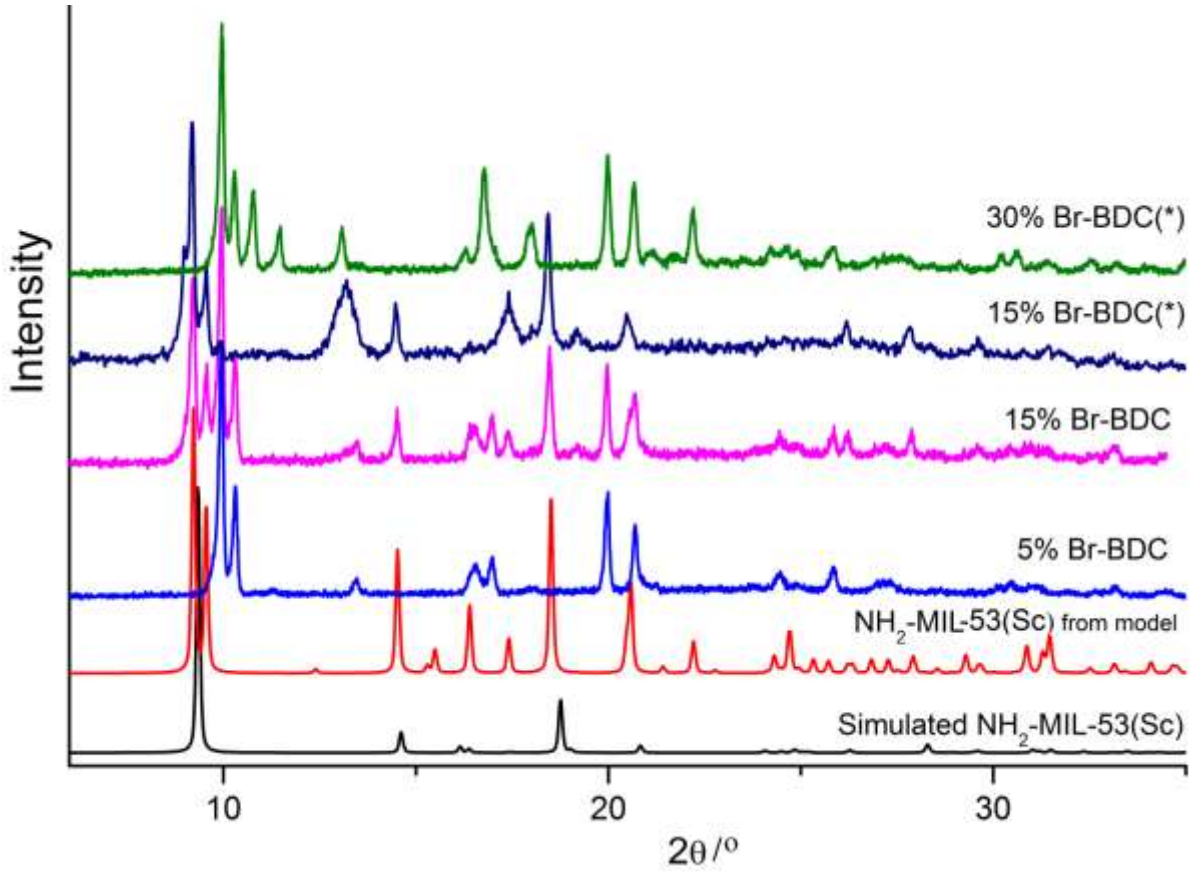

Figure 4.68: PXRD patterns of mixed linker NH_2-BDC/Br-BDC preparations, as described in Tables 4.2 and 4.13 and in the text .

SEM (Figure 4.69) of the sample with most MIL-53 (845D) showed a mixture of tabular crystals NH_2-MIL-53(Sc)(15%Br-BDC) with some microcrystalline unidentified and poorly crystalline powder.

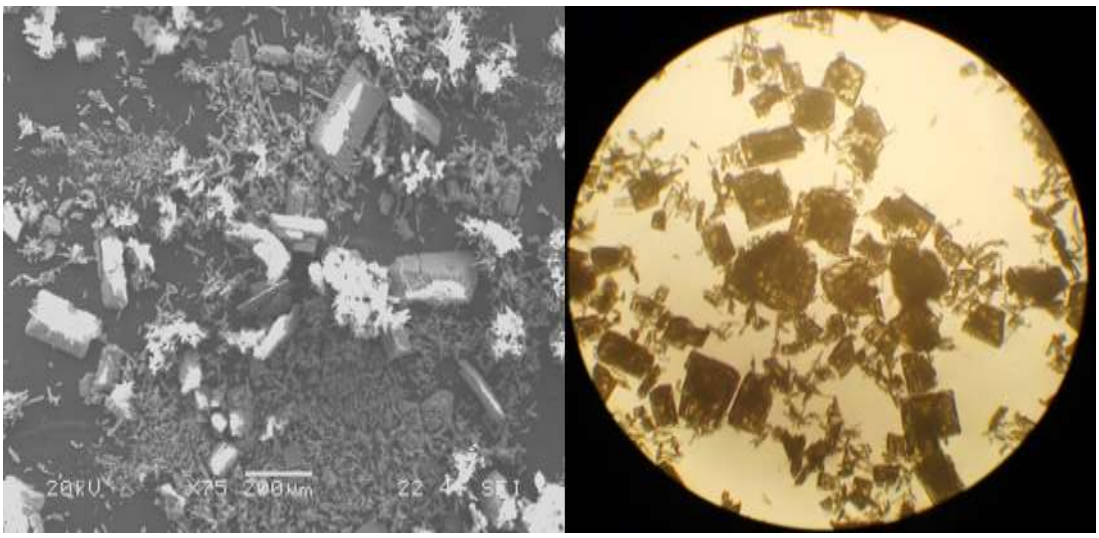

Figure 4.69: SEM micrograph of sample NH_2-MIL-53(Sc)(15%Br-BDC) and photo taken using the optical microscope.

The unit cell of the major 'MIL-53' phase in sample 845D could be indexed with an orthorhombic unit cell, a = 18.517 Å, b = 11.306 Å, c = 7.262 Å). Figure 4.70 shows the plot for the unit cell refinement of sample 845D. TGA shows the material has a 7% of loss solvent at 100 ℃ and the framework started to collapse at 430 ℃ (Figure 4.71).

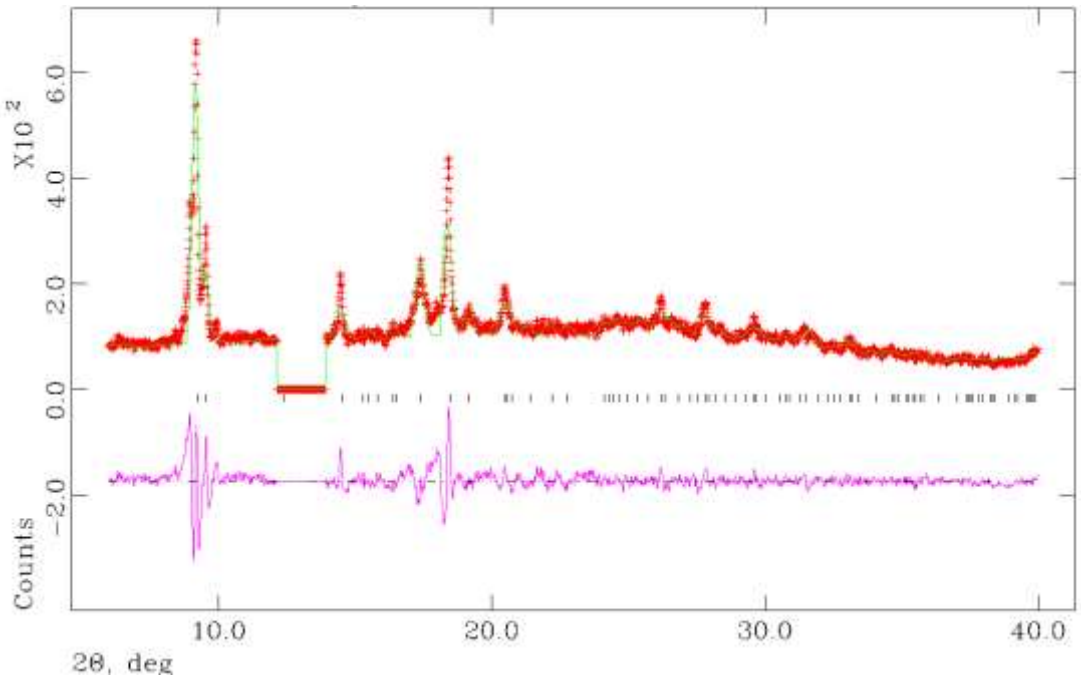

Figure 4.70: Le Bail plot for the unit cell refinement on NH_2-MIL-53(Sc) sample 845D.

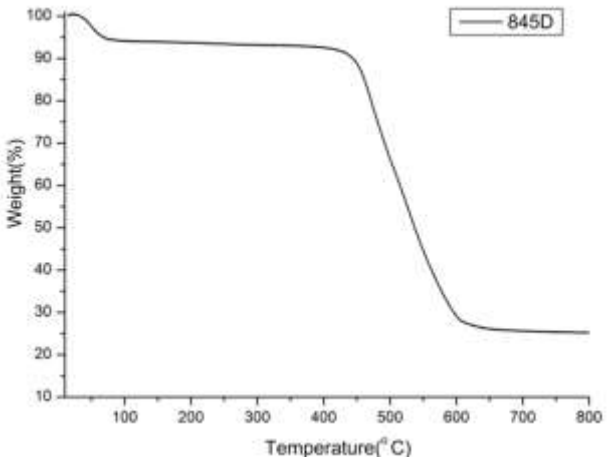

Figure 4.71: Thermogravimetric analysis on NH_2-MIL-53(Sc) collected on sample 845D prepared with 15% of Br-BDC.

4.4.9.6 Adsorption properties of MIL-53(Sc)[NH_2-BDC]$_x$· [R-BDC]$_y$

Figure 4.72 gives the PXRD patterns of samples in which the major phase is a mixed linker MIL-53(Sc) where the major linker is amino-terephthalate and the minor linker is one of NO_2-BDC, $(OH)_2$-BDC or Br-BDC. Of these, the first two are nearly all MIL-53, whereas the last has a considerable amount of an impurity.

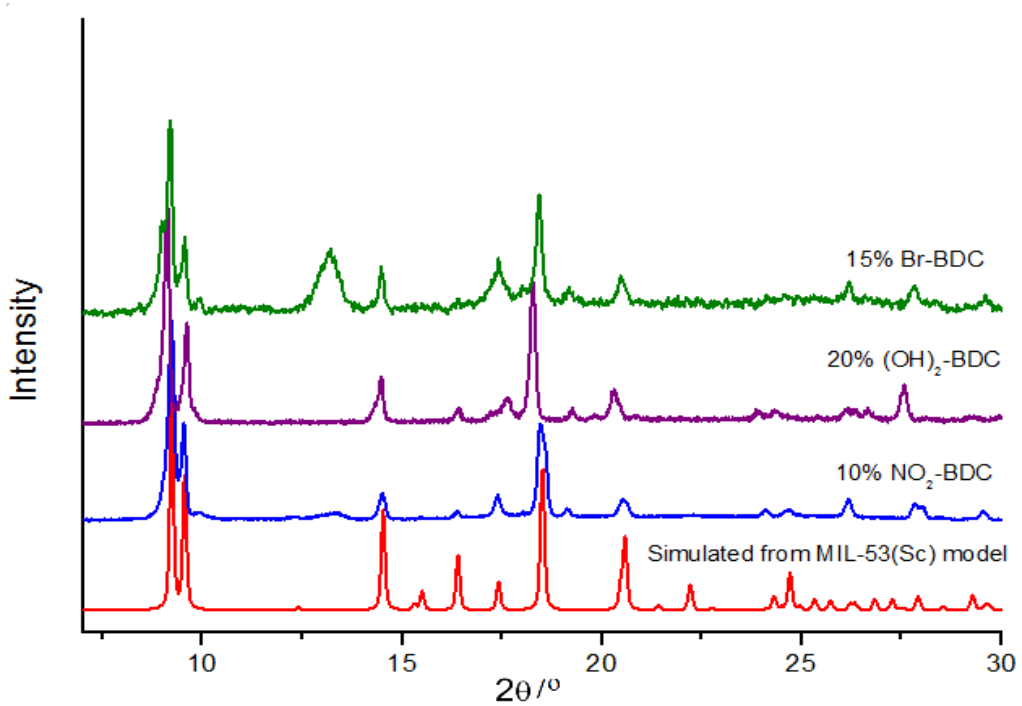

Figure 4.72: Summarised PXRD patterns of NH_2-MIL-53(Sc) with 10, 20 and 15 % second ligand; NO_2-BDC, $(OH)_2$-BDC and Br-BDC respectively.

These three samples were characterised by adsorption of N_2 and CO_2. None of these MIL-53(Sc) samples adsorb N_2 at -196 °C, because the structure closes completely and N_2 does not interact strongly. These materials did not absorb nitrogen, this is because MIL-53(Sc)[42,43] has the narrower channel compare to other MIL-53 reported, situation that make it not big enough to adsorb large molecules, whereas CO_2 was adsorbed. CO_2 adsorption was investigated at 0, -10 and -77 °C. Prior to adsorption the amino-MIL-53(Sc) samples with NO_2- and Br-BDC were activated at 120 °C whereas that with doped $(OH)_2$-BDC was activated at 260 °C, all under vacuum for 4 h, conditions tailored according to the measured TGAs. Figure 4.73 shows the isotherms of the CO_2 isotherms at -10 and 0 °C.

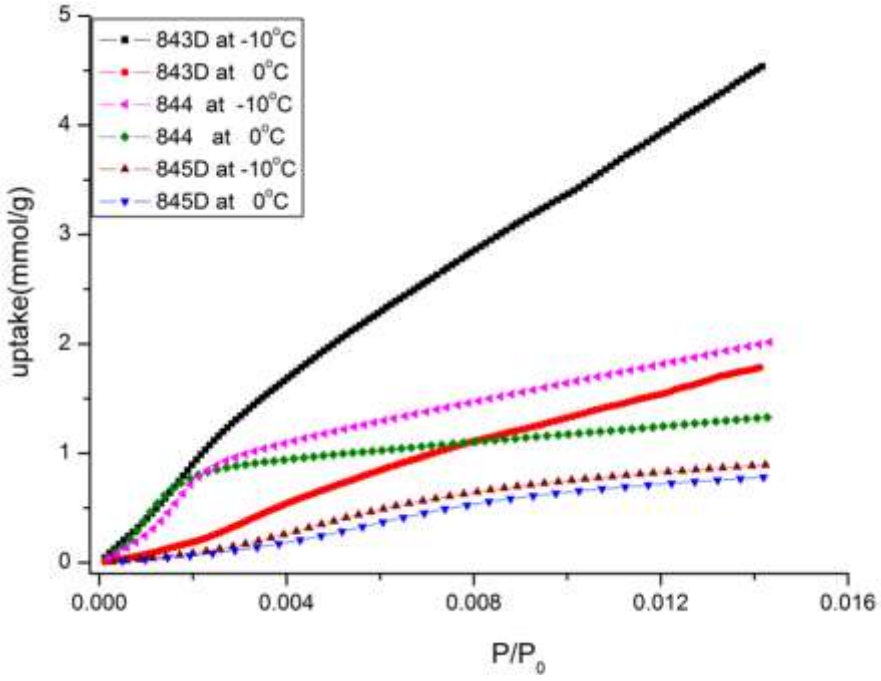

Figure 4.73: CO_2 adsorption data on NH_2-MIL-53(Sc) prepared doped with NO_2-, $(OH)_2$- and Br-terephthalates, samples 843D, 844 and 845D, respectively, measured at -10 and 0 °C.

Figure 4.73 shows the isotherms of CO_2 at -10 and 0 °C on the different samples of NH_2-MIL-53(Sc), with additional, minority, functionalised linkers. It should be noted that previous studies showed that under these conditions the unfunctionalised MIL-53(Sc) does not take up CO_2 (uptake < 0.5 mmol g^{-1}) while the pure NO_2-MIL-53(Sc) shows type I behaviour, with

uptake of ca. 2 mmol g-1, indicating it was held in the narrow pore configuration by the bulky NO_2 groups.[43]

For the NH_2-MIL-53(Sc)(15%Br-BDC), sample 845D, the structure appears to be closed initially, and to show very little uptake, whereas the other two samples show higher uptake at P/Po = 0.02, suggesting at least some of the pores are open. They both show uptakes that show strong increase with increasing partial pressure, and in particular the NH_2-MIL-53(Sc)(15%$(OH)_2$-BDC), sample 843D, shows strong uptake, indicative of pore opening to the large pore form, similar to that observed on NO_2-MIL-53(Sc).

Adsorption of CO_2 at -77 °C (Figure 4.74) showed a range of behaviour for the doped NH_2-MIL-53(Sc) samples (and the mixed NH_2-MIL-53(Sc)/Sc_2(NH_2-BDC)$_3$ sample) that can be compared with the behaviour observed previously for MIL-53(Sc) and NO_2-MIL-53(Sc).[43] MIL-53(Sc) is initially closed then opens via a two-step process to np at P/Po = 0.04, and to lp at P/Po=0.4, whereas NO_2-MIL-53(Sc) is initially in the lp configuration and opens to the lp configuration at P/Po= 0.15.

Of the samples of this thesis, the NH_2-MIL-53(Sc)(10%NO_2-BDC) material shows clear opening behaviour, similar to the reported NO_2-MIL-53(Sc), giving two step adsorption, with uptake typical of the large pore structure via a step beginning at P/Po=0.2. There is a step at P/Po=0.45 for the NH_2-MIL-53(Sc) containing mixture, suggesting that the amino-groups tend to make opening of the structure more difficult than for the unfunctionalised MIL-53(Sc). Neither the $(OH)_2$-BDC or the (Br-BDC) doped solid shows opening to the large pore material, suggesting that there are steric effects that inhibit this. Table 4.14 summarises the uptakes at 1 bar at -77 °C.

This work demonstrates the effects that functionalisation and also double functionalisation have on the adsorption behaviour of MIL-53(Sc) for CO_2 at pressures up to 1 bar. The ease of

opening of MIL-53(Sc) decreases for functional groups in the order NO_2>unfunctionalised>NH_2>Br,$(OH)_2$.

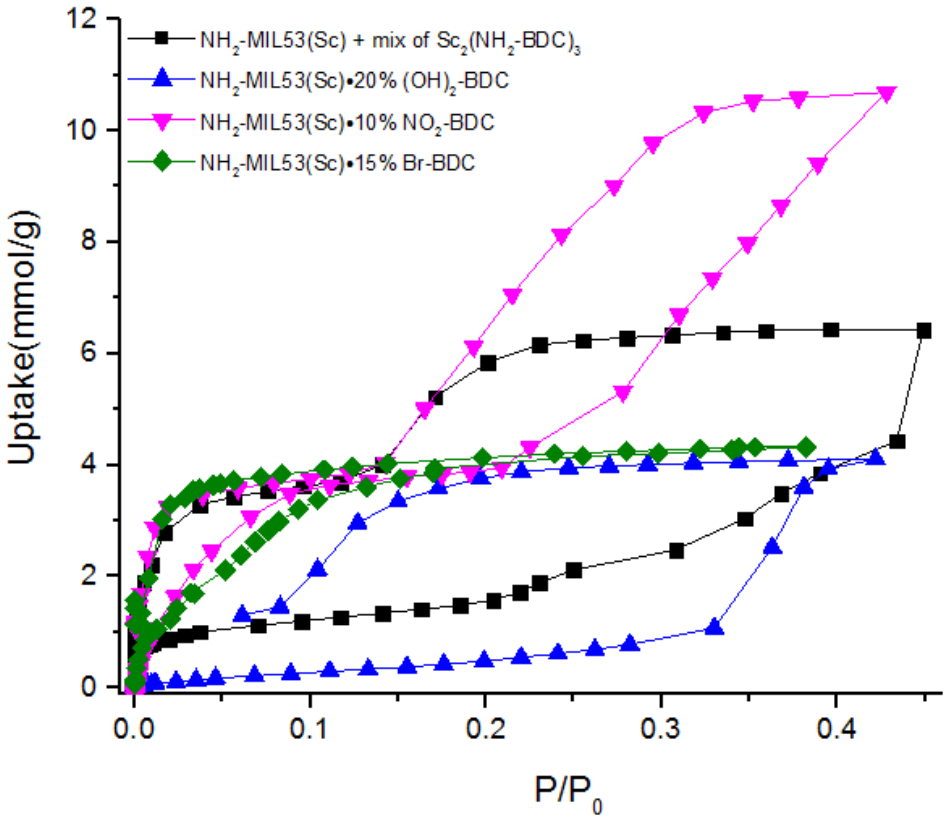

Figure 4.74: CO_2 isotherms measured at -77 ℃ over samples; 843D, 844 and 845D.

Table 4.14: Summarised data of CO_2 adsorption at -77 ℃ over NH_2-MIL-53(Sc)·*y*% of R-BDC.

Sample	Uptake CO_2 -77 ^{o}C mmol g^{-1}
843D(10 % NO_2-BDC)	10.70
844 (20 % $(HO)_2$-BDC)	4.5
845D (15 % Br_2-BDC)	4.5
NH_2-MIL-53(Sc)	6.0

4.5 Conclusion

The successful preparation of NH_2-functionalised scandium terephthalate MOFs was achieved in this chapter. It was possible to prepare four such MOFs for the first time: NH_2-MIL-101(Sc), NH_2-MIL-88B(Sc), NH_2-MIL-68(Sc) and NH_2-MIL-53(Sc), and an improved route to $Sc_2(NH_2\text{-}BDC)_3$ was also discovered. Figure 4.75 shows the amino-functionalised scandium MOFs prepared, as described in this chapter. Also, the Br-functionalised MOF $Sc_2(Br\text{-}BDC)_3$ was prepared for the first time by using a low temperature solvothermal method. All these syntheses were performed in mixed solvents, such as DMF and water.

NH_2-MIL-101(Sc) was prepared and characterized by PXRD, thermal analysis and gas adsorption. For studies of gas adsorption the sample was activated by heating, however recrystallization into NH_2-MIL-88B(Sc) occurs. It was not possible compare its adsorption properties with MIL-101(Sc). The synthesis of NH_2-MIL-88B(Sc) was achieved by several routes and one of those yielded bipyramidal hexagonal prism-like single crystals. In contrast to unfunctionalised MIL-88B(Sc), the solid adsorb CO_2 at -77 ℃, so in this case the amino groups enhance the adsorption properties. In contrast, the measured CO_2 uptake on NH_2-MIL-68(Sc) was reduced by amino-functionalisation (to 9 mmol g^{-1}).

$Sc_2(BDC)_3$ and its derivatives were prepared and their adsorption properties compared. Firstly, $Sc_2(NH_2\text{-}BDC)_3$ and $Sc_2(Br\text{-}BDC)_3$ were synthesized for first time using a optimized solvothermal route and the resulting solids crystallised as large crystals. These were analysed by single crystal diffraction, in both cases in the orthorhombic system: space group *Fddd* for $Sc_2(NH_2\text{-}BDC)_3$ and *Fdd*2 for $Sc_2(Br\text{-}BDC)_3$. Furthermore, post-synthetic modification of $Sc_2(NH_2\text{-}BDC)_3$ was performed by incorporation of nitro-terephthalate groups into the framework using mild conditions at room temperature in water or mixed solvents. Solution

state ^{1}H NMR suggested the presence of both linkers in the final solid, including around a maximum of 7% of the NO_2-BDC linker.

From this study, Sc_2BDC_3 was shown to have the highest uptake of N_2 whereas the amino-functionalisation increases the uptake of CO_2 at lower partial pressures at -77 °C. The N_2 adsorption is affected by the post-synthetic modification of $Sc_2(NH_2\text{-BDC})_3$ because in the framework containing NO_2 groups there is not enough space to allow access to N_2 whereas the CO_2 adsorption does not change (4 mmol g^{-1}). The adsorption of methanol and hydrocarbons was analysed as well, indicating that Sc_2BDC_3 and $Sc_2(NH_2\text{-BDC})_3$ have the highest uptakes for methanol, while $Sc_2(Br\text{-BDC})_3$ and $Sc_2(NO_2\text{-BDC})_3$ have lower uptakes due to the presence of bulky NO_2- and Br-groups. For the hydrocarbons, the NO_2- and Br-forms were selective for n-alkanes over iso-alkanes, indicating shape selectivity was introduced by the presence of the bulky groups.

Finally, attempts were made to prepare amino-functionalised MIL-53(Sc), to compare its CO_2 adsorption with that of other amino-forms of MIL-53. All attempts to prepare pure NH_2-MIL-53(Sc) were unsuccessful, however, and resulted in mixtures of the desired phase with NH_2-MIL-88B(Sc) or $Sc_2(NH_2\text{-BDC})_3$. Nevertheless, pure or largely pure MIL-53-type solids could be prepared by the additional of a second linker, X-BDC, to the preparation (where X=NO_2, $(OH)_2$ or Br). Single crystal XRD confirmed that the phase was 'MIL-53', although the data was not of sufficiently high quality to yield complete solutions, presumably because of structural disorder as solvent was lost upon standing. The presence of the second linker in the final product, as well as the NH_2-BDC, was demonstrated by ^{1}H NMR of the dissolved crystals. CO_2 adsorption at -77 °C showed, among other features, that all adsorbed CO_2 but that the opening up to the large pore form (with uptakes in excess of 10 mmol g^{-1}, was only fully observed for NH_2-MIL-53(Sc)(10%NO_2-BDC), indicating that the presence of amino-groups made the opening more difficult.

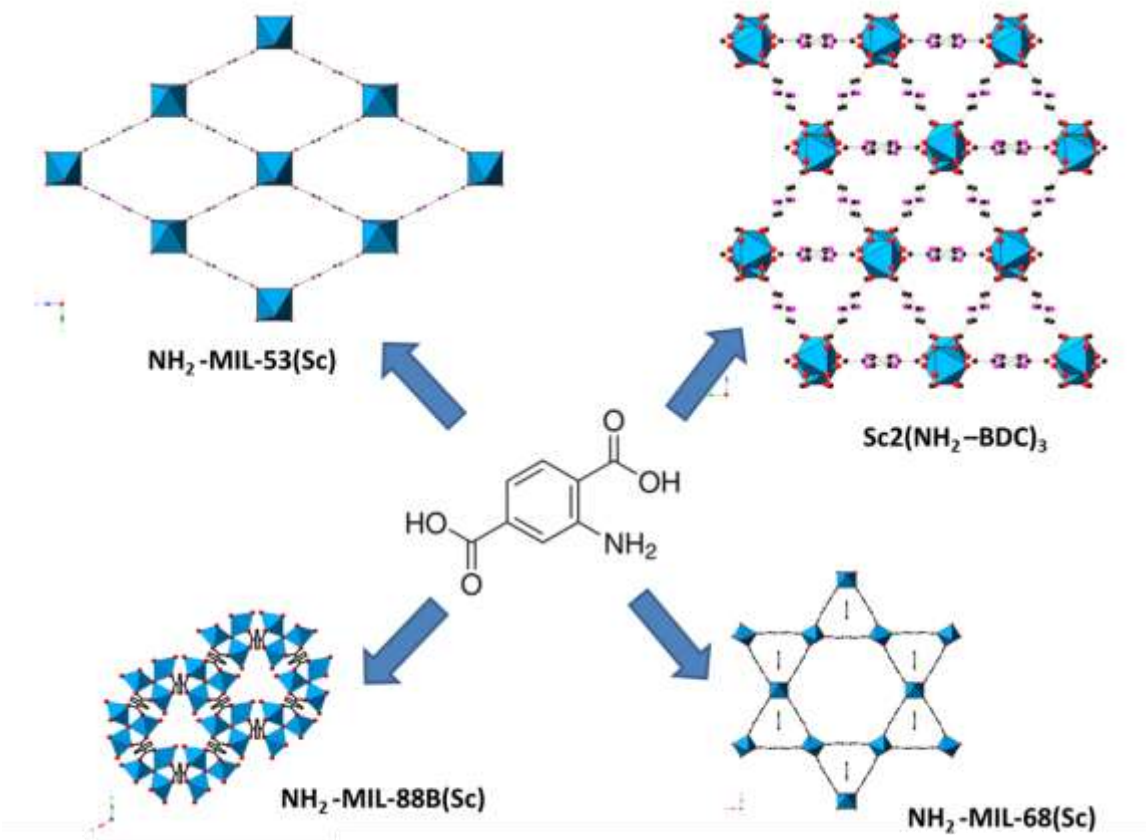

Figure 4.75: Amino-terephthalate scandium MOFs prepared in this chapter.

4.6 References

1. K. K. Tanabe and S. M. Cohen, 2010, 49, 6766-6774.

2. M. Kim, J. A. Boissonnault, C. A. Allen, P. V. Dau and S. M. Cohen, *Dalton Trans.*, 2012, 41, 6277-6282.

3. G. E. Cmarik, M. Kim, S. M. Cohen and K. S. Walton, *Langmuir*, 28, 15606-15613.

4. J. L. C. Rowsell and O. M. Yaghi, *J. Am. Chem. Soc.*, 2006, 128, 1304-1315.

5. K. K. Tanabe, Z. Wang and S. M. Cohen, *J. Am. Chem. Soc.*, 2008, 130, 8508-8517.

6. S. M. Cohen, *Chem. Rev.*, 2011, 112, 970-1000.

7. T. Devic, F. Salles, S. Bourrelly, B. Moulin, G. Maurin, P. Horcajada, C. Serre, A. Vimont, J.-C. Lavalley, H. Leclerc, G. Clet, M. Daturi, P. L. Llewellyn, Y. Filinchuk and G. Ferey, *J Mater Chem*, 2012, 22, 10266-10273.

8. W. Kleist, F. Jutz, M. Maciejewski and A. Baiker, *Eur. J. Inorg. Chem.*, 2009, 3552-3561.

9. S. Couck, J. F. M. Denayer, G. V. Baron, T. Rémy, J. Gascon and F. Kapteijn, *J. Am. Chem. Soc.*, 2009, 131, 6326-6327.

10. S. Couck, J. F. Denayer, G. V. Baron, T. Remy, J. Gascon and F. Kapteijn, *J. Am. Chem. Soc.*, 2009, 131, 6326-6327.

11. D. Sarma, K. V. Ramanujachary, S. E. Lofland, T. Magdaleno and S. Natarajan, *Inorg. Chem.*, 2009, 48, 11660-11676.

12. J. P. S. Mowat, S. R. Miller, J. M. Griffin, V. R. Seymour, S. E. Ashbrook, S. P. Thompson, D. Fairen-Jimenez, A.-M. Banu, T. Düren and P. A. Wright, *Inorg. Chem.*, 2011, 50, 10844-10858.

13. L. Wu, M. Xue, S.-L. Qiu, G. r. Chaplais, A. l. Simon-Masseron and J. l. Patarin, *Micropor. Mesopor. Mat.*, 2011, 157, 75-81.

14. E. Stavitski, E. A. Pidko, S. Couck, T. Remy, E. J. Hensen, B. M. Weckhuysen, J. Denayer, J. Gascon and F. Kapteijn, *Langmuir*, 2012, 27, 3970-3976.

15. M. Eddaoudi, J. Kim, N. Rosi, D. Vodak, J. Wachter, M. O'Keeffe and O. M. Yaghi, *Science*, 2002, 295, 469-472.

16. G. Ferey, *Chem. Soc. Rev.*, 2008, 37, 191-214.

17. S. Bauer, C. Serre, T. Devic, P. Horcajada, J. Marrot, G. Férey and N. Stock, *Inorg. Chem.*, 2008, 47, 7568-7576.

18. S. Bauer, C. Serre, T. Devic, P. Horcajada, J. Marrot, G. Ferey and N. Stock, *Inorg Chem*, 2008, 47, 7568-7576.

19. S. Couck, T. Remy, G. V. Baron, J. Gascon, F. Kapteijn and J. F. Denayer, *Phys. Chem. Chem. Phys.*, 2010, 12, 9413-9418.

20. P. Serra-Crespo, E. Gobechiya, E. V. Ramos-Fernandez, J. Juan-Alcaniz, A. Martinez-Joaristi, E. Stavitski, C. E. Kirschhock, J. A. Martens, F. Kapteijn and J. Gascon, *Langmuir*, 2012, 28, 12916-12922.

21. S. Couck, E. Gobechiya, C. E. Kirschhock, P. Serra-Crespo, J. Juan-Alcaniz, A. Martinez Joaristi, E. Stavitski, J. Gascon, F. Kapteijn, G. V. Baron and J. F. Denayer, *ChemSusChem*, 2012, 5, 740-750.

22. T. Lescouet, E. Kockrick, G. Bergeret, M. Pera-Titus, S. Aguado and D. Farrusseng, *J Mater Chem*, 2012, 22, 10287-10293.

23. C. Scherb, J. J. Williams, F. Hinterholzinger, S. Bauer, N. Stock and T. Bein, *J Mater Chem*, 2011, 21, 14849-14856.

24. J. Juan-Alcaniz, M. Goesten, A. Martinez-Joaristi, E. Stavitski, A. V. Petukhov, J. Gascon and F. Kapteijn, *Chem. Commun.* , 2011, 47, 8578-8580.

25. S. Biswas, T. Ahnfeldt and N. Stock, *Inorg. Chem.*, 2011, 50, 9518-9526.

26. P. Serra-Crespo, E. V. Ramos-Fernandez, J. Gascon and F. Kapteijn, *Chem. Mat.*, 2011, 23, 2565-2572.

27. W. Kleist, M. Maciejewski and A. Baiker, *Thermochim. Acta*, 2010, 499, 71-78.

28. H. Reinsch, S. Waitschat and N. Stock, *Dalton Trans.*, 2013, 42, 4840-4847.

29. S. M. Chavan, G. C. Shearer, S. Svelle, U. Olsbye, F. Bonino, J. Ethiraj, K. P. Lillerud and S. Bordiga, *Inorg. Chem.*, 2014, DOI: 10.1021/ic500607a.

30. M. Lammert, S. Bernt, F. Vermoortele, D. E. De Vos and N. Stock, *Inorg. Chem.*, 2014, 52, 8521-8528.

31. S. Horike, Y. Inubushi, T. Hori, T. Fukushima and S. Kitagawa, *Chemical Science*, 2012, 3, 116-120.

32. S. Marx, W. Kleist, J. Huang, M. Maciejewski and A. Baiker, *Dalton Trans.*, 2010, 39, 3795-3798.

33. S. J. Garibay, Z. Wang and S. M. Cohen, *Inorg. Chem.*, 2010, 49, 8086-8091.

34. Y.-F. Song and L. Cronin, *Angew. Chem. Int. Ed.*, 2008, 47, 4635-4637.

35. M. Savonnet, D. Bazer-Bachi, N. Bats, J. Perez-Pellitero, E. Jeanneau, V. Lecocq, C. Pinel and D. Farrusseng, *J. Am. Chem. Soc.*, 2010, 132, 4518-4519.

36. A. M. Shultz, A. A. Sarjeant, O. K. Farha, J. T. Hupp and S. T. Nguyen, *J. Am. Chem. Soc.*, 2011, 133, 13252-13255.

37. J. S. Seo, D. Whang, H. Lee, S. I. Jun, J. Oh, Y. J. Jeon and K. Kim, *Nature*, 2000, 404, 982-986.

38. Z. Wang and S. M. Cohen, *J. Am. Chem. Soc.*, 2007, 129, 12368-12369.

39. S. Takaishi, E. J. DeMarco, M. J. Pellin, O. K. Farha and J. T. Hupp, *Chem. Sci.*, 2013, 4, 1509-1513.

40. O. Karagiaridi, W. Bury, J. E. Mondloch, J. T. Hupp and O. K. Farha, *Angew. Chem. Int. Ed.*, 2014, 53, 4530-4540.

41. S. R. Miller, P. A. Wright, C. Serre, T. Loiseau, J. Marrot and G. Férey, *Chem. Commun.* , 2005, 3850-3852.

42. J. P. S. Mowat, PhD Thesis,University of St Andrews, 2012.

43. J. P. S. Mowat, V. R. Seymour, J. M. Griffin, S. P. Thompson, A. M. Z. Slawin, D. Fairen-Jimenez, T. Duren, S. E. Ashbrook and P. A. Wright, *Dalton Trans.*, 2012, 41, 3937-3941.

44. X. Cheng, A. Zhang, K. Hou, M. Liu, Y. Wang, C. Song, G. Zhang and X. Guo, *Dalton Trans.*, 2013, 42, 13698-13705.

45. A. Herbst, A. Khutia and C. Janiak, *Inorg. Chem.*, 2014, 53, 7319-7333.

46. L. Gao, C. Y. Li, H. Yung and K. Y. Chan, *Chem. Commun.* , 49, 10629-10631.

47. Q. Y. Yang, S. Vaesen, M. Vishnuvarthan, F. Ragon, C. Serre, A. Vimont, M. Daturi, G. De Weireld and G. Maurin, *J Mater Chem*, 2012, 22, 10210-10220.

48. S. R. Miller, PhD Thesis, University of St. Andrews, 2007.

49. L. Mitchell, B. Gonzalez-Santiago, J. P. S. Mowat, M. E. Gunn, P. Williamson, N. Acerbi, M. L. Clarke and P. A. Wright, *Cat. Sci. Tech.*, 2013, 3, 606-617.

50. M.-H. Pham, G.-T. Vuong, A.-T. Vu and T.-O. Do, *Langmuir*, 2011, 27, 15261-15267.

51. P. W. Betteridge, J. R. Carruthers, R. I. Cooper, K. Prout and D. J. Watkin, *J. Appl. Crystallogr.*, 2003, 36, 1487.

52. S. R. Miller, P. A. Wright, T. Devic, C. Serre, G. Ferey, P. L. Llewellyn, R. Denoyel, L. Gaberova and Y. Filinchuk, *Langmuir*, 2009, 25, 3618-3626.

53. A. J. Graham, A.-M. Banu, T. Düren, A. Greenaway, S. C. McKellar, J. P. S. Mowat, K. Ward, P. A. Wright and S. A. Moggach, *J. Am. Chem. Soc.*, 2014, 136, 8606-8613.

Chapter 5: Novel scandium carboxylate MOFs

5.1 Introduction

Metal organic frameworks (MOFs) have been studied widely for applications including storage of gases, hydrogen storage, separations and catalysis. Among the many trivalent metals used in the synthesis of MOFs, it has been shown that scandium gives a range of stable materials using trimesic acid as a source of carboxylate ligand to give the well-known MIL-100, 4,4′-biphenyldicarboxylic acid gives MIL-88(D) and the most used terephthalic acid linker to construct a large number of compounds including MIL-53, $Sc_2(BDC)_3$, MIL-88(B), MIL-101 and MIL-68, with attractive properties in gas adsorption and also in catalysis.[1-5] There is an interest to explore the synthesis of novel scandium MOFs with other carboxylate linkers using acids such as isophthalic acid (IA) and 2,5-furandicarboxylic acid (FDA), and *meso* tetrakis(4-carboxyphenyl)porphyrin [TCPP] because of their availability. It has been possible to prepare crystalline porous solids of these linkers with di- and trivalent metals. The linker isophthalic acid (IA=1,3-benzene dicarboxylic acid) has been reported for several 3D MOFs.[6-9] One of the first reports based on this ligand was published by Barthelet et al.,[6] synthesizing the MOF known as MIL-59, which is a 3D framework built up from trimers of octahedrally-coordinated vanadium linked via isophthalate groups.

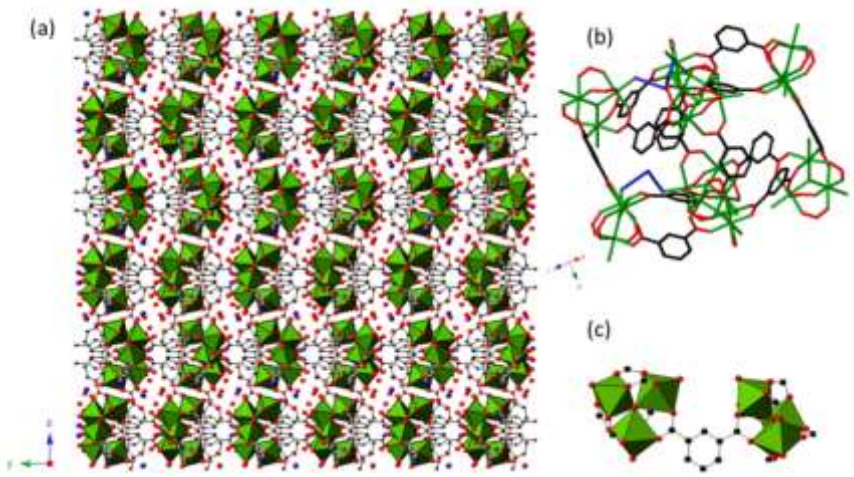

Figure 5.1: Structure of MIL-59, (a) framework, (b) unit cell stick model, (c) trimers coordinated to isophthalate linker. Vanadium polyhedra are shown in green. Carbon, chlorine and oxygen atoms shown as black, blue and red spheres

Previously in the Wright group the use of isophthalic acid was investigated by Miller[10] under hydrothermal conditions with scandium. The use of this linker and scandium gave the structure $Sc_2(O_2CC_6H_4CO_2)_3$ which crystallized in the cubic space group $P2_13$, a = 13.345 Å. There are two crystallographically-distinct scandium sites in the structure, each of which is coordinated to six oxygen atoms. Adsorption studies on the structure indicated no porosity for nitrogen or CO_2 owing to the lack of accessible free space.

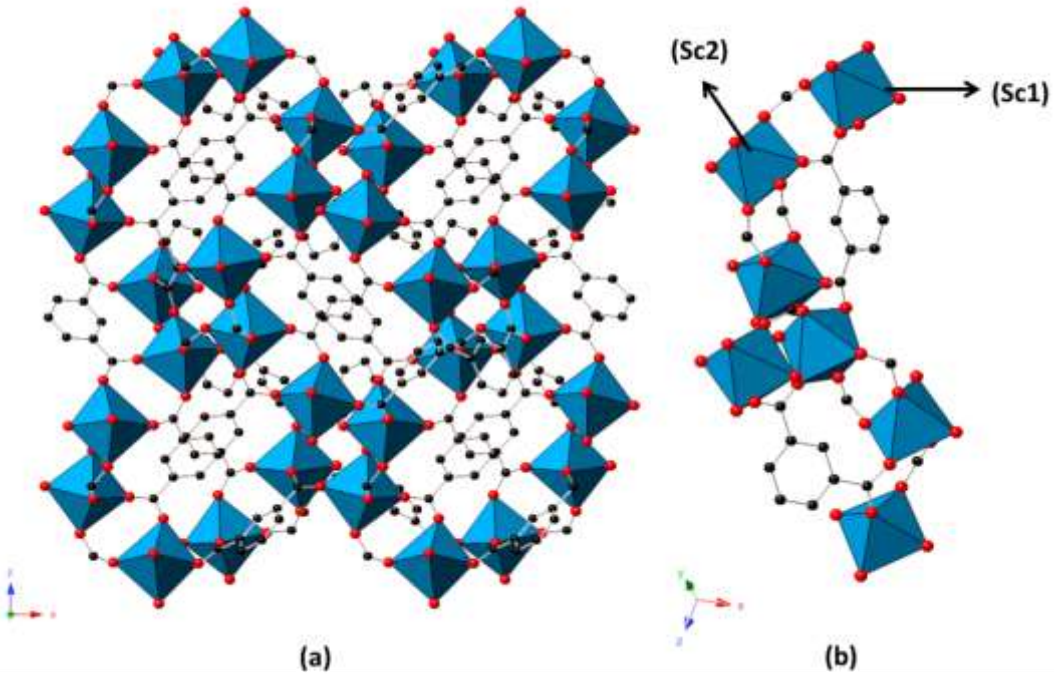

Figure 5.2: Images of the structure $Sc_2(O_2CC_6H_4CO_2)_3$: (a) view of unit cell along the y axis. (b) View of structure showing the two scandium sites in the framework. ScO_6 octahedra are shown in blue. Black and red spheres represent the carbon and oxygen atoms of the organic linker.

Recent studies of MOFs based on the isophthalate linker and aluminium (Al^{3+}) were reported by Reinsch et al.[7] The MOFs based on the X-IA (where X = functional group in 5-position of the aromatic ring; X = H, CH_3, OCH_3, NO_2, NH_2, or OH) crystallized with the CAU-10-X topology, (CAU = Christian-Albrechts-University). These materials contain a similar V-shaped assembly to that observed for the MOF NOTT-401,[11] which was prepared with the geometrically-similar thiophene-2,5-dicarboxylic acid (H_2TDA) and scandium. Figure 5.3

shows the structures obtained with aluminium, the CAU-10(OCH_3), and NOTT-401[$Sc(C_6H_2O_4S)(OH)$]. The distance between the oxygen-atoms of the functional groups in CAU-10(OCH_3) is 6.4 Å centre to centre (Figure 5.3a). Both frameworks are permanently porous. Ji et al.,[9] also have reported the use of IA with indium (In^{3+}) and the framework of that structure $H_2In_3O(OH)_3(1,3\text{-}BDC)_3$ is built up of trimers similar to those in MIL-59. Studies of adsorption properties of this In-IA MOF gave no uptake for N_2 or CO_2 gas.

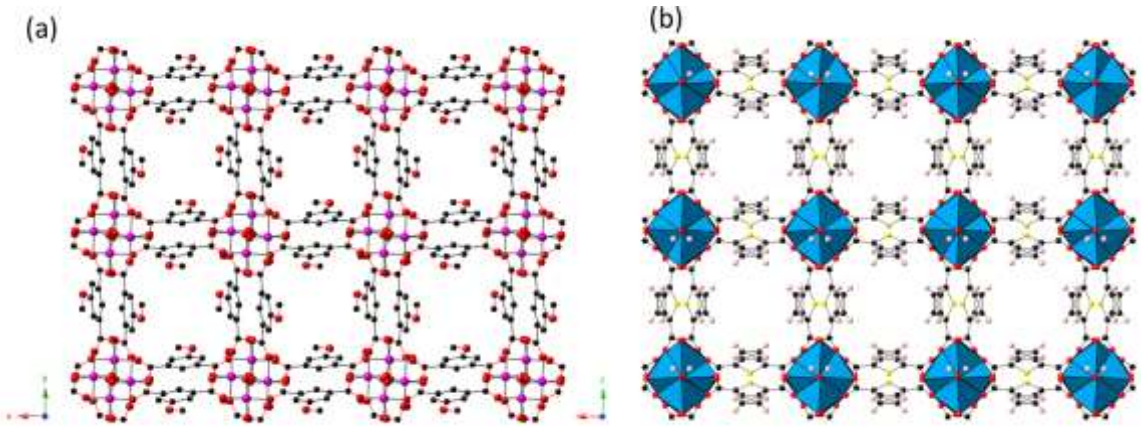

Figure 5.3: Images of the structures of (a) CAU-10(OCH_3), and (b) NOTT-401

2, 5-Furandicarboxylic acid (FDA), is commonly available due to its origin in biomass, and also has been used in the synthesis of MOFs with linear homo/heterotrinuclear cluster containing cobalt (Co^{2+}), gadolinium (Gd^{3+}) and dysprosium (Dy^{3+}), so that the solids showed interesting luminescent and ferromagnetic properties.[12] Also, the synthesis with europium (Eu^{3+}), FDA and oxalic acid yielded 3D coordination polymers,[13] where the oxalate anion serves as a tetra-dentate ligand chelating asymmetric units in a dimer assembly resulting in 3D frameworks formed via covalent bonds between the ligand and metal. To date no reports are found using only FDA and one metal.

The use of large organic molecules is of current interest in the assembly of MOFs. [14] The large tetrakis (4-carboxyphenyl) porphyrin [TCPP] molecule is a potential linker in this

investigation because of its well-defined geometry. Porphyrins are conjugated tetrapyrrolic macrocycles with structures that possess rigid planar geometry, and high photochemical stability. These materials have many applications in different fields, for example in the medical topic of photodynamic therapy, molecular electronics, in solar cells and in catalysis.[15] All these properties made them attractive candidates for their use as a ligand in the synthesis of MOFs. Here in this investigation the use of TCPP with scandium is reported.

The TCPP has four *meso* positions occupied by 4-carboxyphenyl groups in square planar geometry and its use as a linker has been reported to synthesize coordination polymer networks with divalent and trivalent metal cation.[14, 16-21] Kosal et al.[16] reported the use of TCPP and cobalt (II) to give $TCPPCo_{2.5}$ also named PIZA-1 'porphyrinic Illinois zeolite analogue no. 1' in the monoclinic crystal system with space group $P2_1/n$. Adsorption analysis showed that the solid was porous to water, amines and alcohols. However, the adsorption of nitrogen at -196 ℃ gave a BET surface area of the evacuated framework of only 125 $m^2 g^{-1}$.

Lipstman et al.[17] reported two-or three dimensional lanthanide frameworks with metallic cations such as dysprosium (Dy), samarium (Sm), praseodymium **(**Pr), gadolinium (Gd), ytterbium(Yb), europium (Eu) and erbium (Er). However the crystalline solids did not show porosity. Fateeva et al.,[18] reported the synthesis of 3-D coordination polymers based on iron (Fe^{3+}) and nickel (Ni^{2+}) tetracarboxylate porphyrin (Ni-TCPP) namely MIL-141(A) (Figure 5.4) with entrapped cations inside the pores, formula $Fe(Ni\text{-}TCPP)A\bullet(DMF)_3$, (A = Li^+, Na^+, K^+, Rb^+ or Cs^+) which networks showed better porosity than PIZA-1. Table 5.1 shows the adsorption data from N_2 isotherms measured at -196 ^oC for different solids of the MIL-141 type. Morris et al.[22] also reported the use of the TCPP as linker with zirconium (Zr^{4+}) to prepare the MOFs -525 and -545, which are chemically stable. Analysis of their adsorption

properties gave BET surface areas of 2620 and 2260 m^2g^{-1}, respectively. These results encouraged investigation in the Sc^{3+} TCPP system.

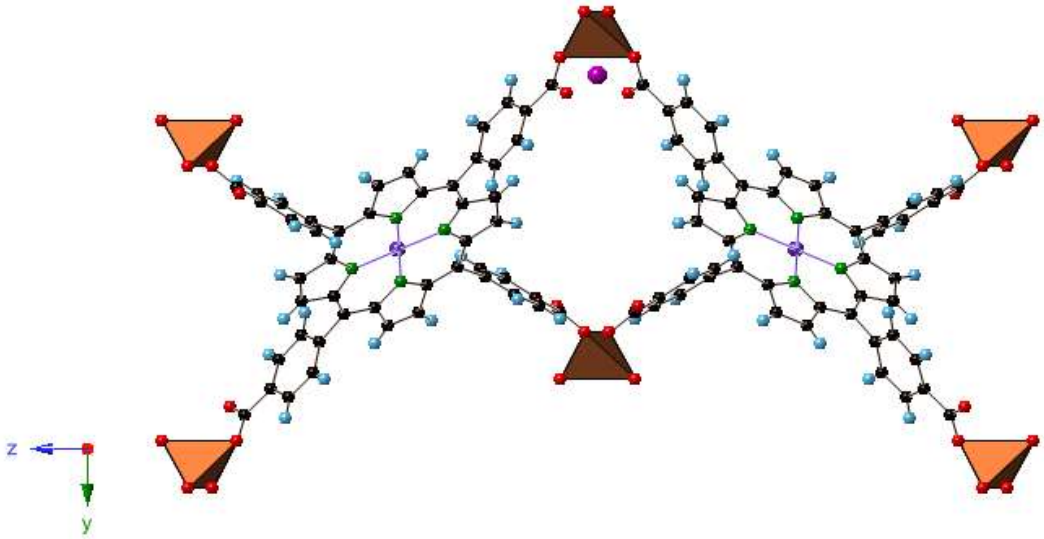

Figure 5.4: Framework of MIL-141(Li) viewed down to the *x*-axis; $Fe(O)_4$ tetrahedral iron and Li+ cation are shown in orange and magenta, respectively. Black, green, purple, red and blue spheres represent the C, N, Ni, O and H atoms.[18]

Table 5.1: Summarised data from N_2 isotherms of MIL-141(A): BET surface areas and micropore volumes measured at -196℃. [18]

A	BET surface area (m^2 g^{-1})	Micropore volume (cm^3 g^{-1})
Li	635	0.27
Na	510	0.23
K	810	0.32
Rb	820	0.36
Cs	860	0.34

5.2 Aims

The aim of this chapter is to investigate the synthesis of novel MOFs using scandium as the framework metal cation and different carboxylate linkers.

5.3 Experimental

A series of experiments was performed using the ligands shown in Figure 5.5. All reagents and solvents were purchased commercially and used without further purification. Two scandium sources were used in this chapter, scandium oxide (Sc_2O_3, 99.999%, Stanford Materials Corporation) and scandium chloride prepared by dissolving scandium oxide (Sc_2O_3, 75 mmol) in 18.6 mL hydrochloric acid (HCl, Fischer Scientific; 38%) to produce $ScCl_3$ 1.45 M ((M=mol l^{-1}) with heating. Solvents used in this syntheses described in this chapter included N,N-dimethylformamide (DMF, Acros, 98%), ethanol (EtOH, VWR, 99.8%) and distilled water. Linkers were purchased from commercial suppliers such as Aldrich and Frontier Scientific. In each experimental section details is given.

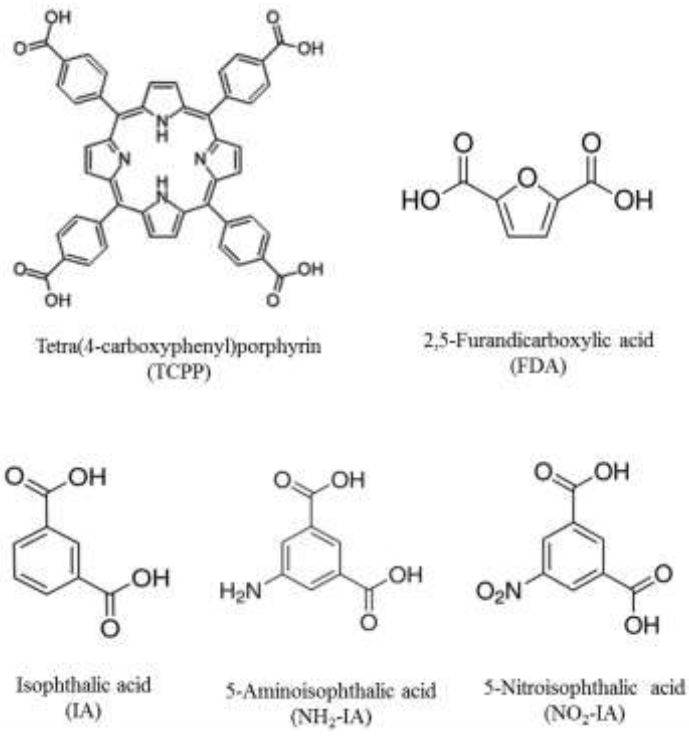

Figure 5.5: Structure of the organic ligands used in the preparation of novel scandium MOF.

5.3.1 Synthesis of scandium isophthalates

A series of experiments was performed using a mixture of solvents DMF and H_2O using as ligands 1,3-benzene dicarboxylic acid (IA=isophthalic acid, Aldrich 99%), 5-aminoisophthalic acid (NH_2-IA, Aldrich 94%) and 5-nitroisophthalic acid (NO_2-IA, Aldrich 98%). Table 5.2 lists the reaction mixtures and conditions used, and gives the final product that was obtained.

Table 5.2: Reaction conditions of synthesis of scandium isophthalate and its amino and nitro-functionalised derivatives. Molar ratio=M. R, then scandium to ligand ratio is defined as Sc/*l*.

Linker (*l*)	**M. R (*Sc/l*)**	**Solvent DMF**	**Solvent H_2O**	**Temp. (^oC)**	**Time (h)**	**MOF**
IA	1	1	4	110-130	12	Sc(IA)-1
IA	0.5	0	10	220	48	Sc(IA)-2
NH_2- IA	0.5	2	8	160	12	$Sc_2(NH_2\text{-IA})_3$
NH_2- IA	0.5-1.0	0	10	110-160	12	Recryst. NH_2- IA
NO_2- IA	0.5	2	8	120	12	Unknown-1
NO_2- IA	1.0	1	4	190	24	Unknown-2
NO_2- IA	1.0	0	10	190	24	Unknown-2

5.3.1.1 Sc(IA)-1

The sample *Sc(IA)-1* was prepared by reaction of scandium chloride (1.16 mmol, 1.45 M aqueous solution) and isophthalic acid (1.20 mmol) in DMF (1 mL) and H_2O (4 mL) transferred into a Teflon-lined steel autoclave and heated at 130 °C for 12 h. After heating, the autoclave was cooled and the mixture filtered. The resulting solid yielded colourless cube-shape crystals, the product was washed with water and dried at 60°C overnight.

5.3.1.2 Sc(IA)-2

This material was prepared following the conditions established by Miller,[10] to compare its properties with the synthesis described above. The sample *Sc(IA)-2* was synthesized using scandium oxide (Sc_2O_3, 0.32 mmol, 99.999%, Stanford Materials Corporation) and isophthalic acid (0.65 mmol) with H_2O (10 mmol) and heated in a Teflon-lined steel autoclave at 220 ℃ for 48 h. The resulting solid was washed with water and dried overnight at 60 °C.

5.3.1.3 Sc(NH_2-IA)

Sample Sc(NH_2-IA) was prepared by reaction of scandium chloride (0.65 mmol, 1.45 M aqueous solution) and 5-aminoisophthalic acid (1.26 mmol) in DMF (2 mL) and H_2O (8 mL) and transferred into an autoclave and heated at 160 °C for 12 h. After heating, the autoclave was cooled and the mixture filtered. The synthesis yielded red cubic crystals which were washed with water and dried overnight at 60 °C.

5.3.1.4 Sc (NO_2-IA)

A series of reactions were performed varying the molar ratio of Sc/L and solvents

Sample (1) was prepared by reaction of scandium chloride (0.65 mmol, 1.45 M aqueous solution) and 5-nitroisophthalic acid (1.26 mmol) in DMF (2 mL) and H_2O (8 mL) heated at 120 °C for 12 h in a Teflon-lined Parr autoclave. After heating, the autoclave was cooled and the mixture filtered, washed with water and dried at 60 °C overnight.

Sample (2): Synthesis was made using scandium chloride (1.16 mmol) and 5-nitroisophthalic acid (1.20 mmol) in DMF (1 mL) and H_2O (4 mL) heated at 160 °C for 24 h in a Teflon-lined Parr autoclave. After heating, the autoclave was cooled and the mixture filtered, washed with water and dried at 60 °C overnight. Under the same reaction conditions but using just water (10 mL) in the synthesis yielded a similar yellow polycrystalline powder.

5.3.2 Synthesis of scandium furandicarboxylates

Syntheses of samples with 2,5-furandicarboxylic acid (FDA) were prepared, using the conditions in Table 5.3. The molar ratios Sc/FDA (FDA= 2,5-furandicarboxylic acid, Aldrich, 99%) were varied, and the reaction mixtures treated solvothermally for 24 - 48 h at a temperature between 120 and 190 ^{o}C.

Table 5.3: Synthetic conditions in the synthesis of scandium with ligand 2, 5 furandicarboxylate. Molar ratio=M. R, then scandium to ligand ratio is defined as Sc/FDA. temperature (Temp.) and time in hours (h).

M. R (Sc/FDA)	Solvent DMF (mL)	Solvent EtOH (mL)	Solvent H_2O (mL)	Temp. (^{o}C)	Time (h)	MOF
1	5			120	48	Amorphous
2	5	2	3	120	48	Triclinic
2	5			160-190	24	unknown

5.3.2.1 Sc(FDA)-1

The preparation of the first compound prepared in the furandicarboxylate system, labelled 'Sc-FDA(1)', was achieved by using mixed solvents DMF (5 mL), EtOH(2 mL) and H_2O (3 mL), scandium chloride (0.625 mmol) and FDA (0.325 mmol). The reaction mixture was transferred in a Teflon-lined steel autoclave and heated for 48 h at 120 ℃. The solid was yielded as colourless crystals, which were washed with water and dried overnight at 60 ℃ .

5.3.2.2 Sc(FDA)-2

The second compound was prepared by varying the solvent, just in DMF (10 mlL) and scandium chloride (0.625 mmol) and FDA (0.325 mmol). The mixture was sealed in a Teflon-lined steel autoclave and heated for 48 h at 160 ℃ or 190 ℃. After the cooling the solid polycrystalline powder was washed with water and dried overnight at 60 ℃ .

5.3.3 Synthesis of scandium TCPP

Solvothermal syntheses of Sc-TCPP were carried out using the 40 mL Teflon-lined Parr autoclave. Scandium chloride was used as the scandium source and TCPP (Frontier Scientific, 97%) in DMF or mixed solvents (DMF and H_2O) was added to investigate the possibility of assembling a scandium carboxylate MOF using the square planar macrocyclic carboxylate. As the TCPP has 4 CO_2-groups that can react with a Sc^{3+} cation it might be 4 Sc cations for each TCPP molecule to form the metal-carboxylate cluster, but this hypothesis yielded amorphous phase, so that several molar ratios were explored. Different molar ratios (Sc/TCPP), solvent, temperature and time of reaction were explored. The reaction conditions are presented in Table 5.4.

Table 5.4: Reaction conditions of synthesis of Sc-TCCP in 10 mL of DMF. Molar ratio=M. R, then scandium to ligand ratio is defined as Sc/TCPP). * Synthesis made in mixed solvents DMF (5mL) and H_2O (3 mL).

M. R (Sc/TCPP)	Solvent DMF (mL)	Time (days)	Temp. (^oC)	Solid
4.6	10	1	70	amorphous
6.9	10	1	70	S2
9.2	10	1	70	S3
4.5	10	2	70	S4
6.9	10	2	70	S5
4.6	10	3	70	S6
4.6	10	5	70	S7
4.6	10	3	110	S8
4.6	10	5	110	S9
2.3	10	5	110	S10
4.6	*	3	70	S11

5.4 Results and discussion

5.4.1 Scandium isophthalate MOFs

5.4.1.1 MOFs: Sc(IA)-1 and 2

The materials obtained with isophthalic acid were characterized by single crystal analysis and their structure solved or compared to that reported. Sc(IA)-1 with formula $Sc_3O(OH)(H_2O)_2(C_8H_4O_4)_3$ and the Sc(IA)-2 obtained hydrothermally $Sc_2(C_8H_4O_4)_3$ are discussed below.

a) Structural analysis of Sc(IA)-1, $[Sc_3O(OH)(H_2O)_2(C_8H_4O_4)_3]$

Figure 5.6 shows the cube-shape crystals obtained, which were suitable for single crystal analysis. Single crystal analysis was performed with CRYSTALS suite programs[23] using direct methods. The solved structure indicated that the material crystallizes in the cubic $Pa\bar{3}$ unit cell, with a = 19.4821 Å, but the data had residual values of Rw = 20% probably due to solvent in the framework (CIF file available see the Appendix C). The diffraction peaks of the experimental pattern match well with the simulated pattern indicating the material is phase pure (Figure 5.7).

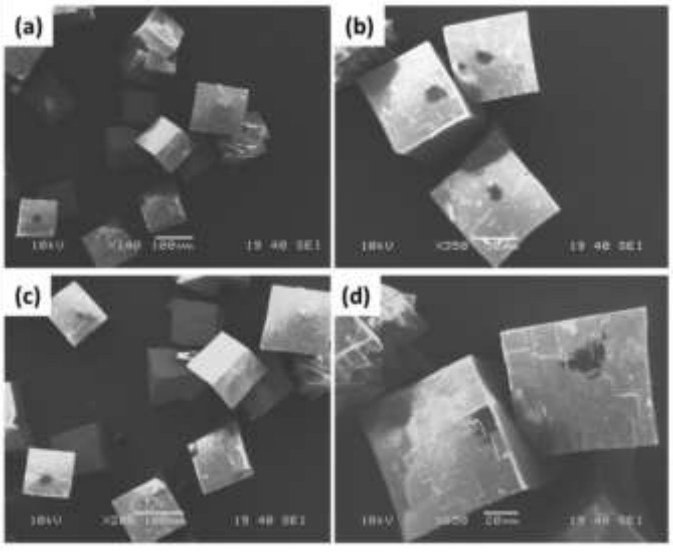

Figure 5.6: SEM images of Sc(IA)-1 cubic crystals.

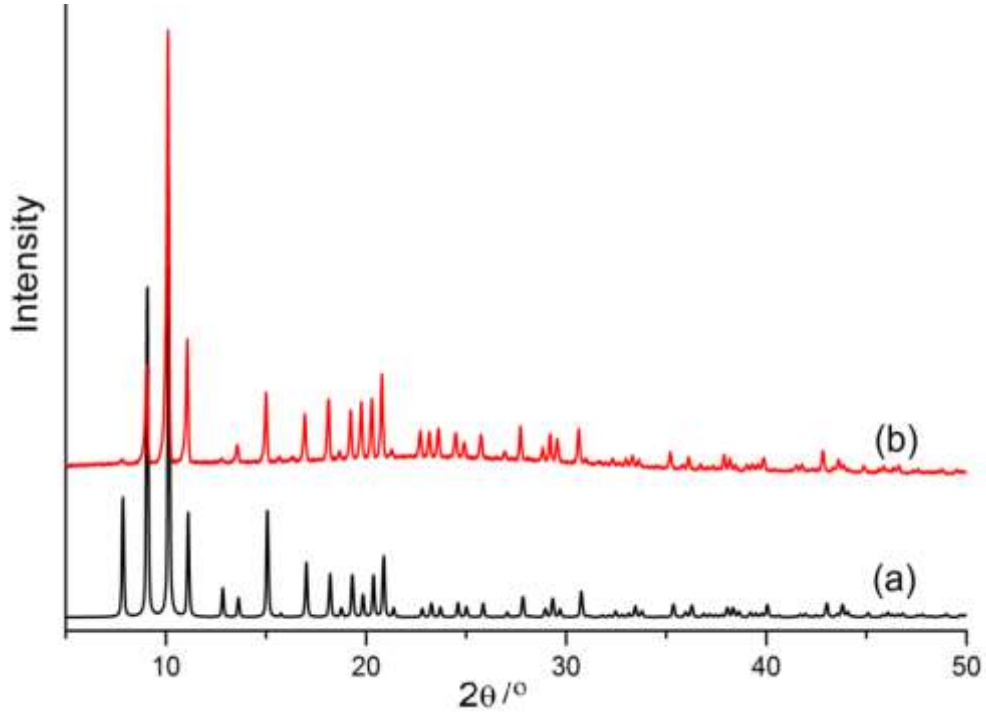

Figure 5.7: Experimental powder diffraction pattern of Sc(IA)-1 MOF (b) compared to the pattern simulated from the single crystal model (a).

Figure 5.8 shows the framework of the structure. The assembly of this structure is a three dimensional scandium isophthalate material built up from octahedral scandium trimers which shared an oxygen atom by linking as Sc-(μ_3-O)-Sc. Each trimer $[Sc_3O_4(O_2)_6]$ is coordinated via carboxylate groups of the isophthalate linker to six others, building up a 3D structure framework, similar to that reported for MIL-59(V) and another MOF prepared very recently with indium[9]. Elemental analysis on as-prepared Sc(IA)-1 $[Sc_3O(OH)(H_2O)_2(C_8H_4O_4)_3 \cdot DMF]$; found % (calc. %): C 40.84 (42.15), H 3.14 (1.74), N 2.51 (1.82). The traces of nitrogen present in the sample arise from the DMF used in the synthesis. This suggested that DMF is occluded into the structure. Table 5.5 gives the crystallographic data from the refinement.

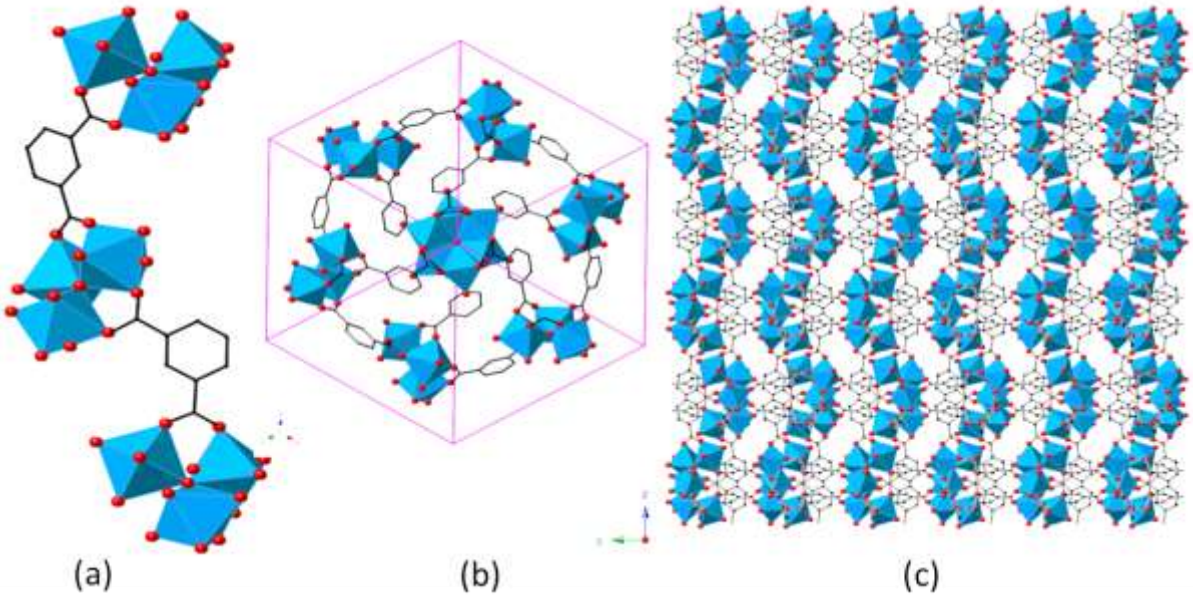

Figure 5.8: Images of the structure of Sc(IA)-1: (a) trimer linked by isophthalates, (b) cage of structure 1, (c) molecular packing. Scandium octahedra are shown in blue. Black and red spheres represent the carbon and oxygen atoms of the linker.

Table 5.5: Crystallographic data for the Rietveld refinement of Sc(IA)-1.

Structure	**Sc(IA)-1**
Formula unit	$Sc_3O(OH)(H_2O)_2(C_8H_4O_4)_3$
Crystal system	Cubic
Space group	$Pa\,\bar{3}$
X-ray source	Mo Kα
Diffractometer	STOE STADIP
Wavelength (Å)	0.71073
Unit cell (Å)	
a/Å	19.4824 (14)
b/Å	19.482114)
c/Å	19.4821(14)
Volume/Å3	7394.5(8)
R	0.10
Rw	0.20

The unit cell parameters were refined via Le Bail refinement against lab so the PXRD data to be 19.5821(14) Å.

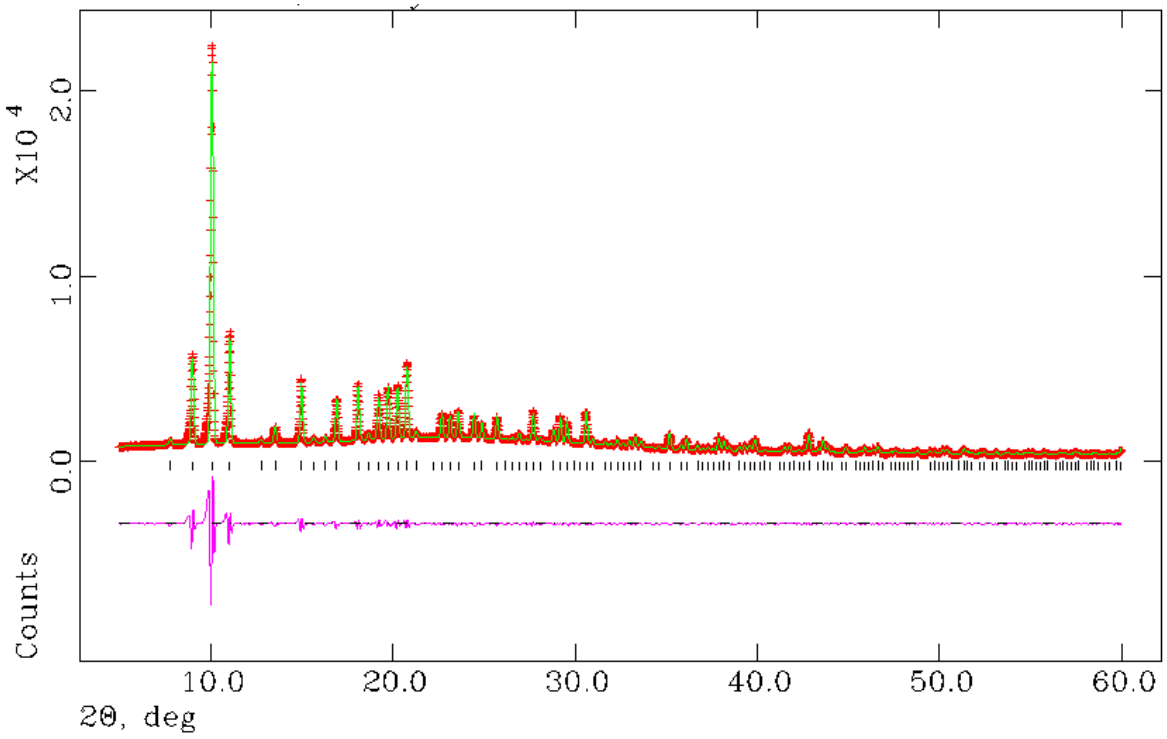

Figure 5.9: Le Bail plot for the unit cell refinement on Sc(IA)-1 [$Sc_3O(OH)(H_2O)_2(C_8H_4O_4)_3$].

TGA (Figure 5.10) indicates the structure loses around 10 wt% by 250 °C, which is attributed to the loss of solvent used in the synthesis. The decomposition of the framework starts at 500 ℃. In order to remove solvent (DMF) occluded in the framework, the sample was heated at 250 ℃ for 12 h under flowing nitrogen. The PXRD pattern was still crystalline. After heating, TGA was performed (Figure 5.10) and CHN analysis measured on the heated-sample resulted, found % (calc. %): C 41.60 (41.7), H 1.38 (1.74), N 0.1 (0.0) confirming that almost all solvent (DMF) has been removed. The small amount of weight loss from the sample heated at 250 ^{o}C (4 % in two steps) is attributed to loss of coordinated water.

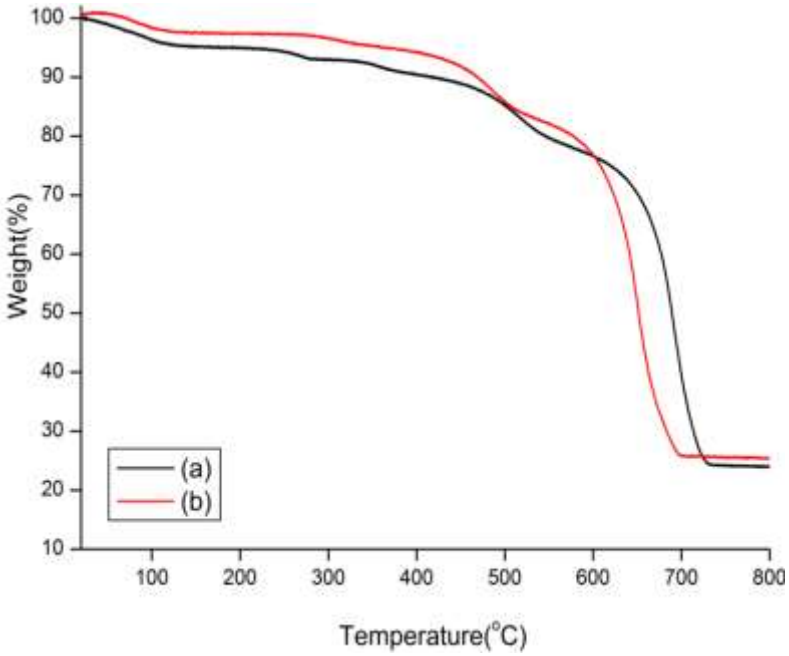

Figure 5.10: Thermogravimetric analysis of Sc(IA)-1 MOF, as-prepared (black) and pre-heated at 250℃ (red) under flowing air.

b) Structural analysis of Sc(IA)-2, $Sc_2(C_8H_4O_4)_3$

Figure 5.11 shows octahedral crystals of the as-prepared Sc(IA)-2, which crystallizes in the cubic system, unit cell of $a = 13.345$ *Å*. The PXRD diffraction pattern of the as-prepared material was compared with a simulated pattern from the crystal structure (Figure 5.12).

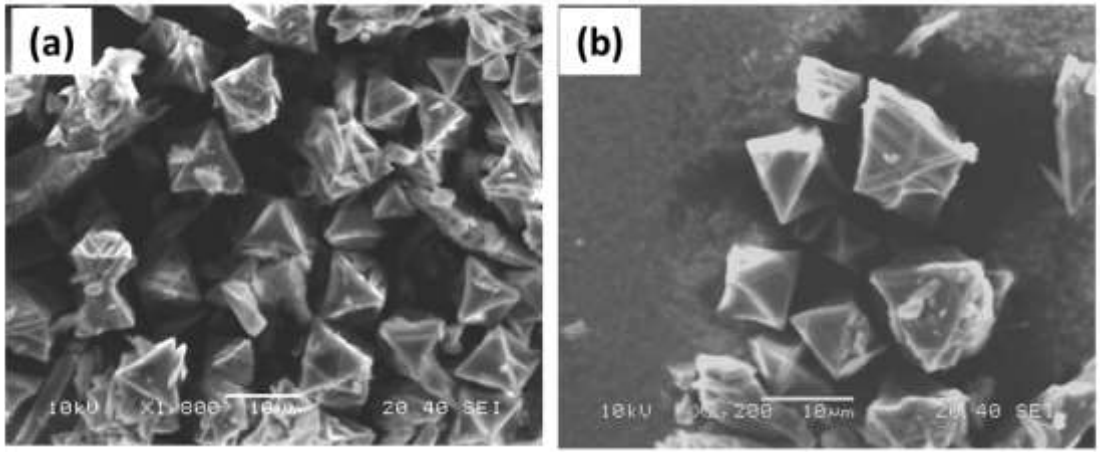

Figure 5.11: SEM images of Sc(IA)-2 octahedral crystals.

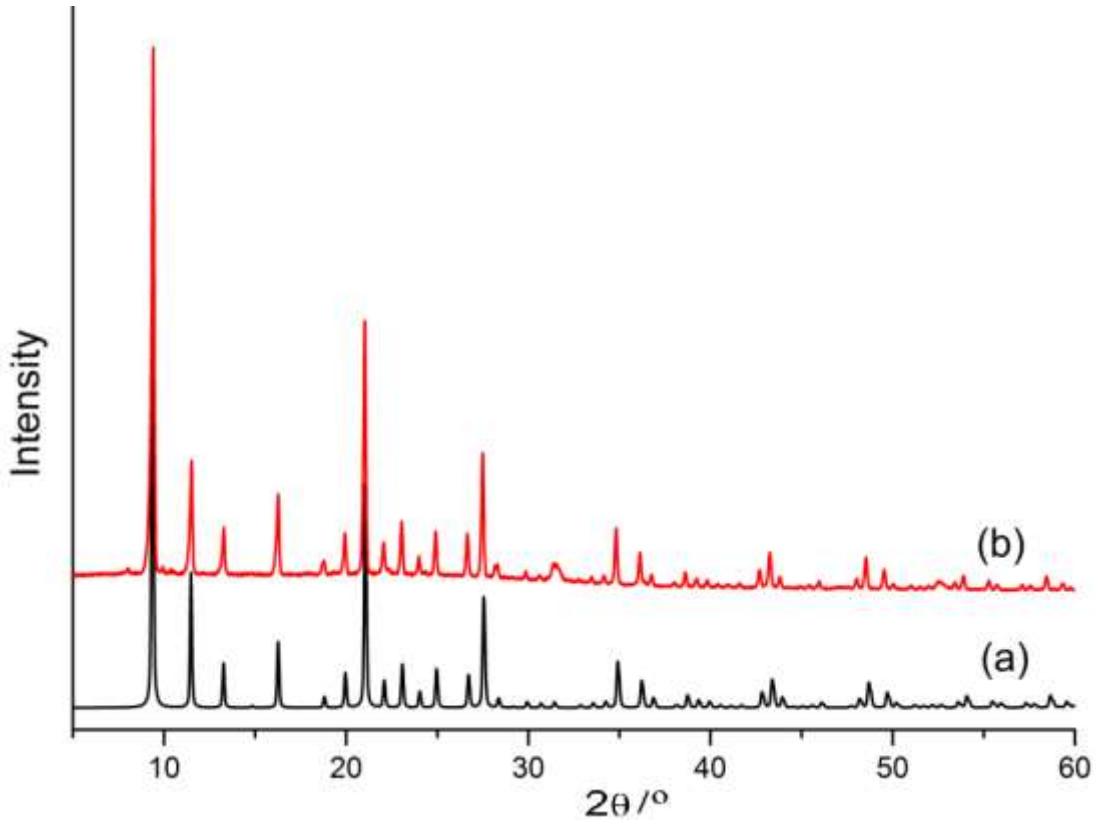

Figure 5.12: Experimental powder diffraction pattern of Sc(IA)-2 MOF (b) compared to the pattern simulated from the single crystal model(a).

Figure 5.13 shows the three-dimensional MOF, Sc(IA)-2. This structure has two crystallographically unique scandium sites in the structure (Figure 5.13a), each of which is coordinated to six oxygen atoms, where each ScO_6 octahedron is linked to 6 isophthalate groups, 2 of which bridge the scandium atoms in the asymmetric unit, 4 of the isophthalate groups act as linkers going to ScO_6 octahedra in different asymmetric units, and four bridging isophthalate groups are being received from independent asymmetric units. Table 5.6 gives details of crystallographic data for Sc(IA)-2 from single crystal diffraction data

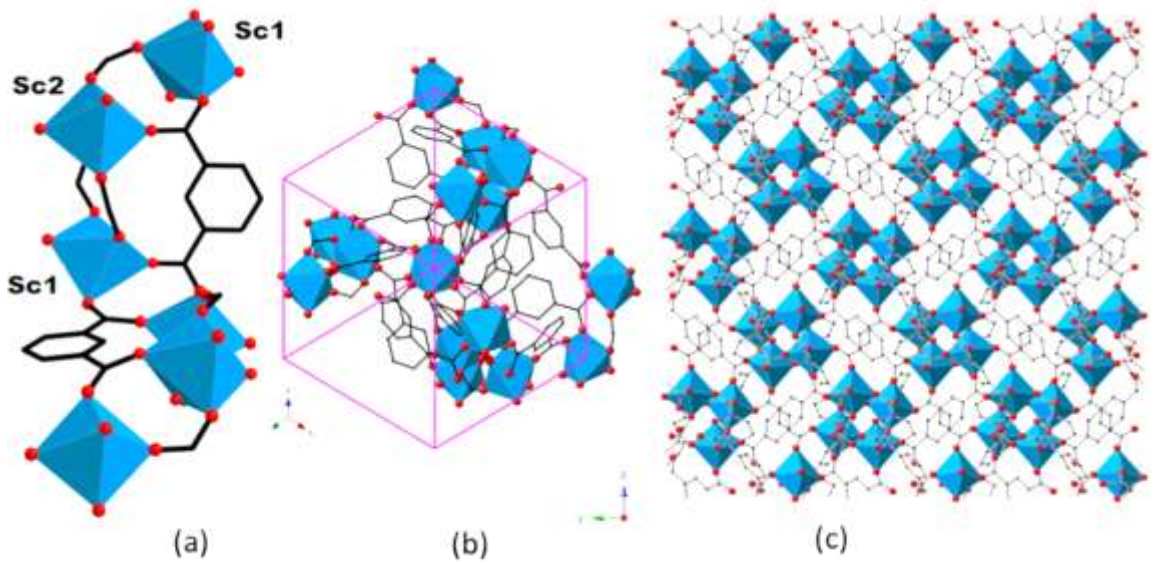

Figure 5.13: Crystal structure of Sc(IA)-2: (a) trimer linked by isophthalate group structure, (b) cage of structure, (c) molecular packing.

Table 5. 6: Crystallographic data for Sc(IA)-2 obtained by single crystal analysis.

Structure	**Sc(IA)-2**
Formula unit	$Sc_2(C_8H_4O_4)_3$
Crystal sytem	Cubic
Space group	P 2_1 3
X-ray source	Mo Kα
Diffractometer	
Wavelength (Å)	0.71073
Unit cell (Å)	
a/Å	13.345(3)
b/Å	13.345(3)
c/Å	13.345(3)
Volume/Å^3	2376.6(9)
R	0.033
Rw	0.0728

Thermogravimetric analysis in Figure 5.14 shows that the material is highly stable and no significant weight loss up to the final decomposition above 500 °C. Elemental analysis on as-prepared Sc(IA)-2 [$Sc_2(C_8H_4O_4)_3$] found % (calc. %): C 49.36 (49.50), H 2.18 (2.07), N 0.0 (0.0).

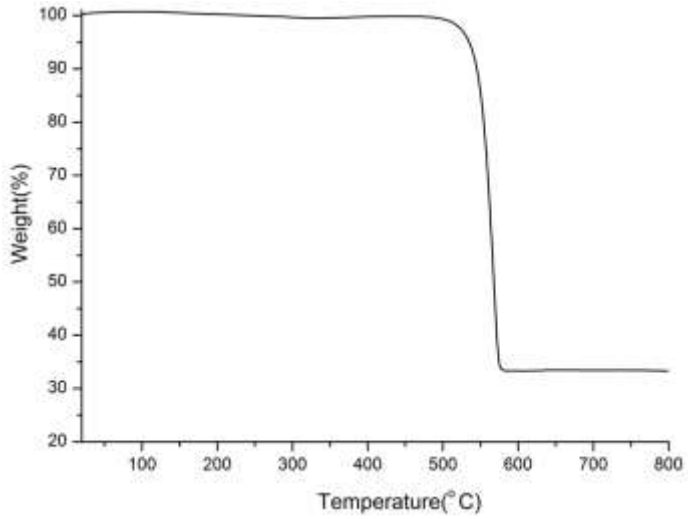

Figure 5. 14: Thermogravimetric analysis of Sc(IA)-2 under flowing air.

c) Adsorption properties of scandium isophthalates Sc(IA)-1 and 2

Analysis of the adsorption properties of both materials were studied using nitrogen and carbon dioxide adsorption. Adsorption studies of the Sc(IA)-2 indicated no porosity to gases N_2 and CO_2 owing to the small window diameters, whereas Sc(IA)-1 was porous to both N_2 and CO_2. Prior to adsorption analysis the sample was activated at 250 ℃ under vacuum for 4 h. Adsorption of CO_2 at 0 ℃ indicated porosity of the framework with uptake of ~ 1.8 mmol g^{-1} up to P/P_0 = 0.014 (P =1 bar), at -77 ℃ an uptake of 2.5 mmol g^{-1} was observed (pore volume 0.1 cm^3g^{-1}). The sample was analysed for N_2 adsorption at -196 ℃ giving an uptake of 2 mmol g^{-1} with a BET surface area of 334 m^2g^{-1}. These adsorption properties are better than these reported for the indium analogue, which was not accessible for N_2, and for which adsorption of CO_2 measured at 20 ℃ gave an uptake of only 0.18 mmol g^{-1}.

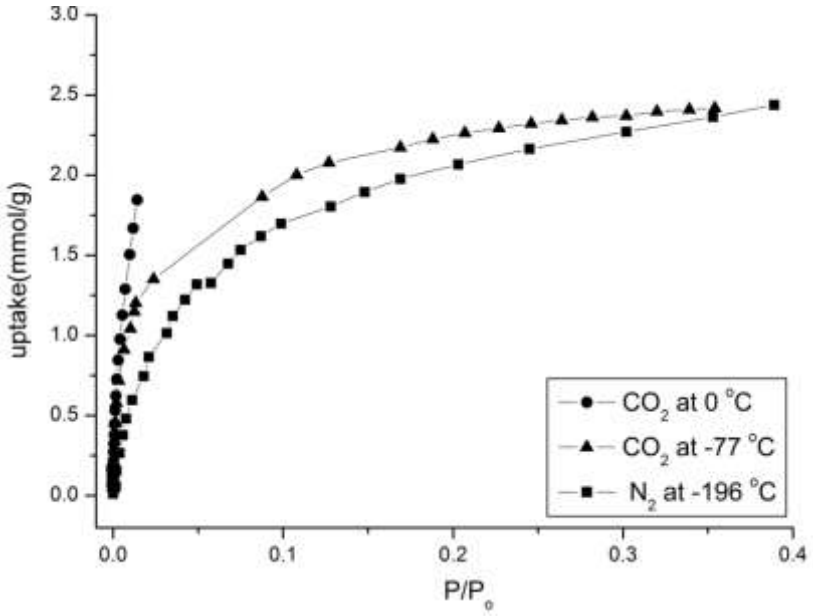

Figure 5.15: N_2 and CO_2 adsorption isotherms collected on Sc(IA)-1 measured at -196℃ and -77℃ respectively.

d) Solid-state MAS NMR of scandium isophthalates

Solid state ^{13}C and ^{1}H MAS NMR spectra of Sc(IA)-1 and Sc(IA)-2 are shown in Figure 5.16. Solid state ^{13}C NMR for the as-prepared and heated forms show the characteristic resonances for the linker. The ^{13}C spectrum for the as-prepared Sc(IA)-1 indicated the presence of DMF, which is only partially removed upon heating (Figure 5.16, ^{13}C). The ^{1}H spectra for as-prepared Sc(IA)-1 also indicate the initial presence of DMF and its subsequent partial removal by heating (Figure 5.16, ^{1}H). Strong changes in intensity of the ^{1}H signals between 0 and 5 ppm occur for Sc(IA)-1. This is attributed to removal of solvent and water bound to the trimer sites and trapped in the pores. ^{1}H NMR of Sc(IA)-2 shows characteristic signals from the linker, and does not change upon heating. The ^{45}Sc spectrum of Sc(IA)-1 (Figure 5.16) shows the broad signal characteristic of scandium trimer unit. The broad signal arises due to the linker disorder of OH and H_2O on the Sc^{3+} sites. For the sample calcined up to $250^{0}C$ the presence of a pair of much lower intensity peaks can be observed (b), possibly because of the small amounts of conversion to Sc(IA-2). However, no changes were observed by PXRD (Figure 5.17). The spectra (c, d) for structure Sc(IA)-1 shows the two scandium

signals which are attributed to the two crystallographically-distinct scandium environments is consistent with the crystal structure. The first peak at 3.0 ppm has a very symmetric lineshape, indicating a highly symmetric environment, whereas for the signal at -30 ppm a typical quadrupolar lineshape results due to deviation of the octahedral coordination from a regular octahedron. A comparison of the bond lengths and angles for Sc(1) and Sc(2) shows that Sc(1) is more asymmetric and is expected to be responsible for the signal at -30 ppm.

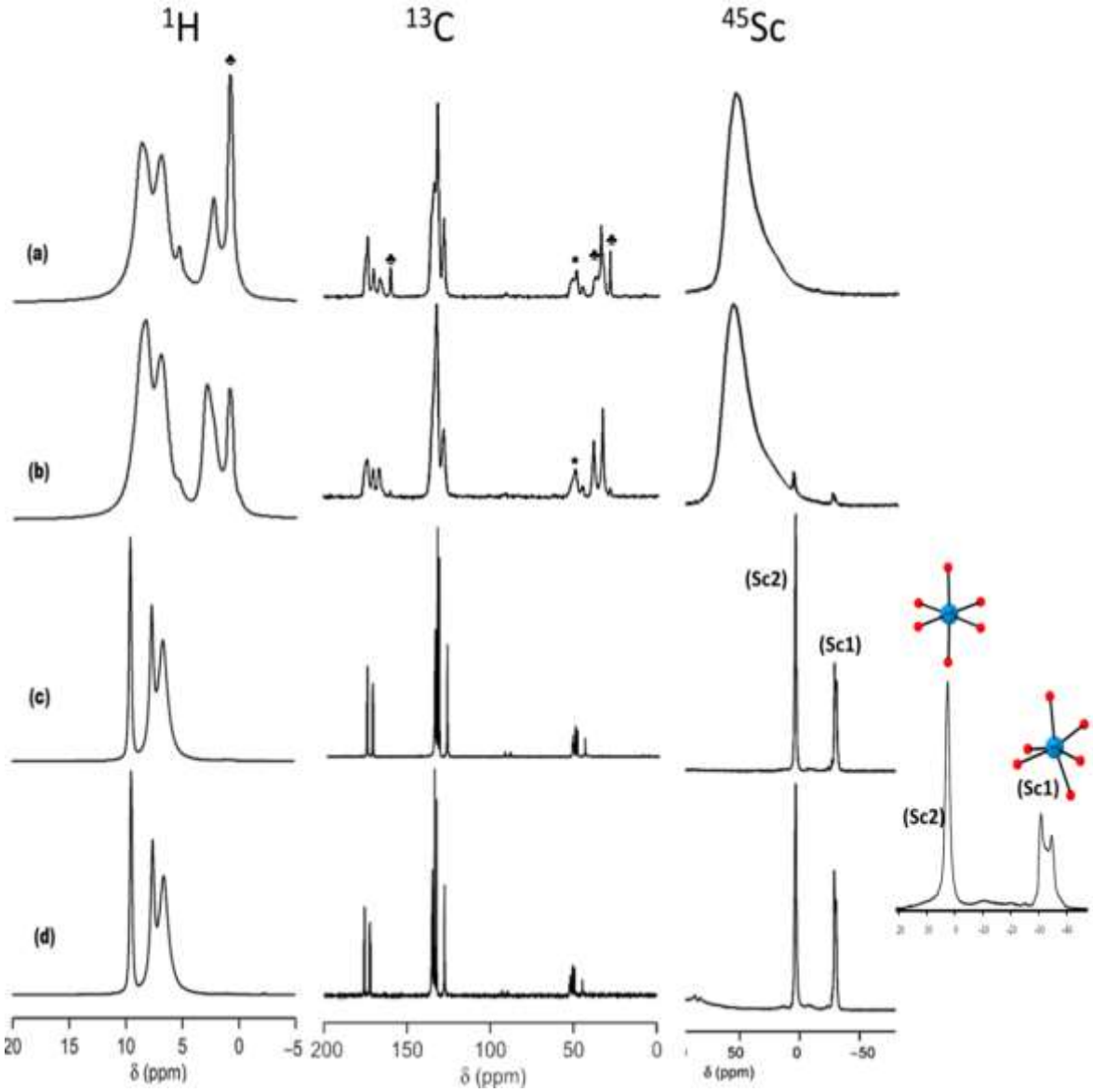

Figure 5.16: Solid state ^{1}H, ^{13}C and ^{45}Sc MAS spectra of (a,b) Sc(IA)-1 and (c,d) Sc(IA)-2, in as-prepared and heated (250 °C) forms, respectively. ^{1}H and ^{13}Sc spectra were recorded at MAS rates of (a) 24 kHz, (b) 30 kHz, (c,d) 40 kHz. For all ^{13}C spectra the MAS rate was 12.5 kHz. ♣ = DMF

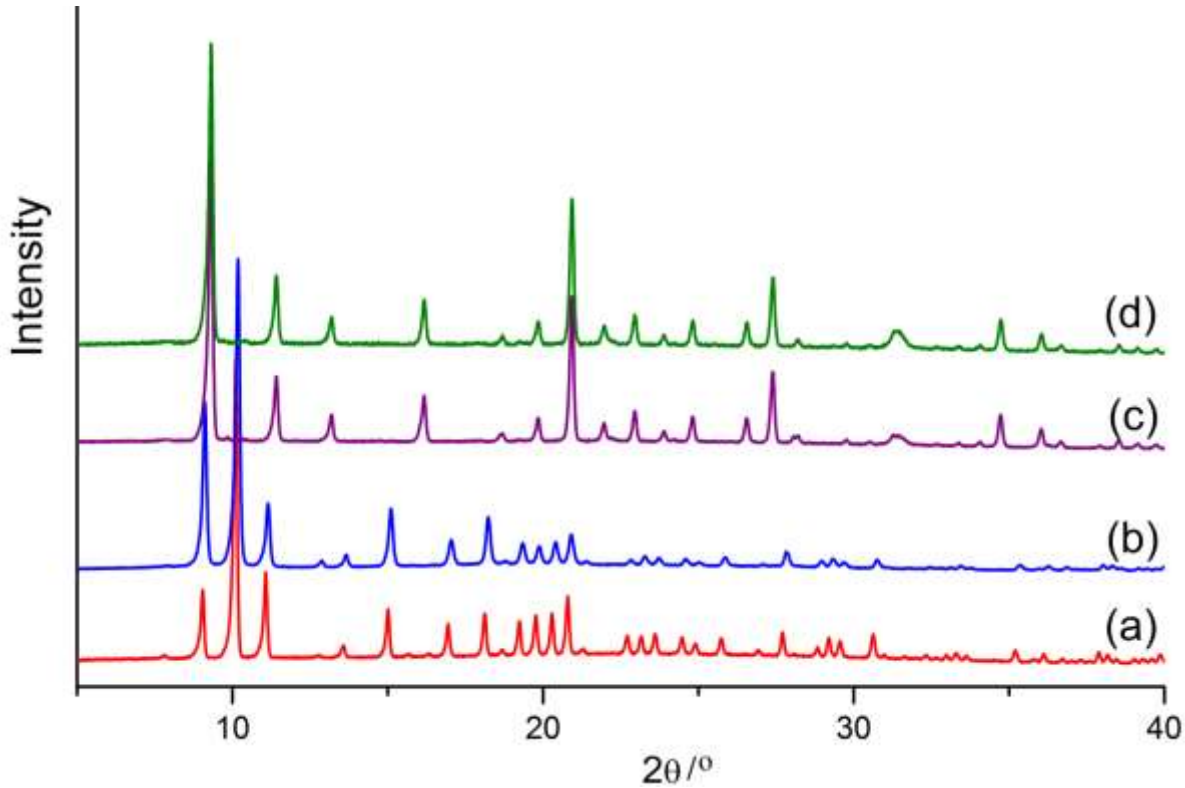

Figure 5. 17: PXRD of Sc(IA)-1(a,b) as-prepared and heated at 250 ℃, respectively, and Sc(IA)-2, (c and d) as-prepared and heated at 250 ℃ respectively.

5.4.1.2 Sc(NH_2-IA), [$Sc_2(NH_2$- $C_8H_4O_4)_3$]

Figure 5.18 shows the red cubic crystals obtained in this synthesis, which were suitable for single crystal analysis. The powder X-ray diffraction pattern of the as-prepared sample was compared with a simulated pattern derived from the single crystal structure (Figure 5.19). Single crystal analysis on the crystalline materials by using the CRYSTALS suite software[23] based on direct methods indicated that the cube-shape crystals crystallized in the crystal system cubic $I2_13$, unit cell of a = 13.909 Å. (CIF file available, see the Appendix C)Table 5.7 lists details of the structure solved from single crystal diffraction.

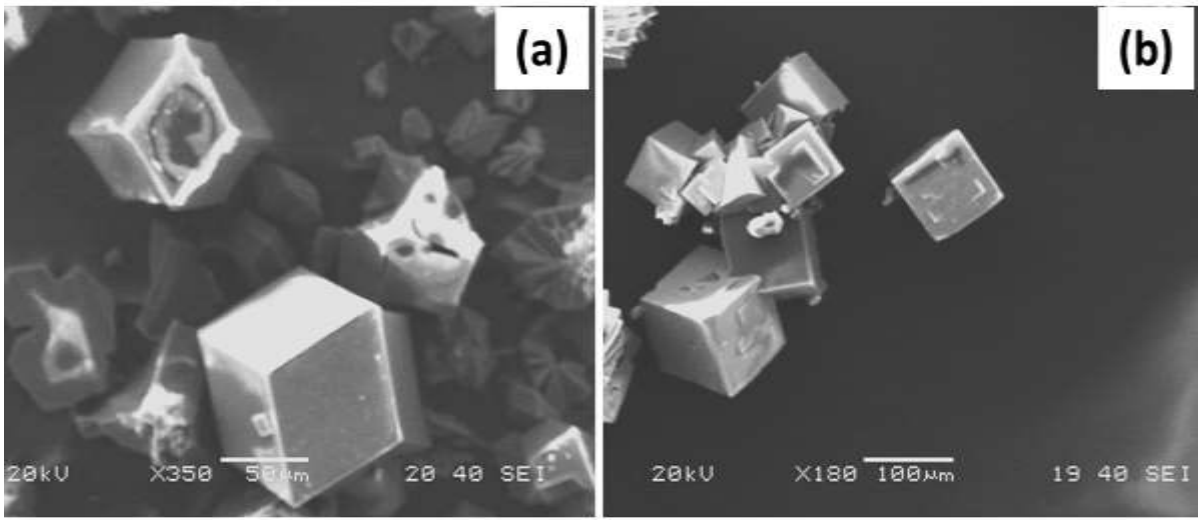

Figure 5.18: SEM images of Sc(NH_2-IA) cube shaped crystals.

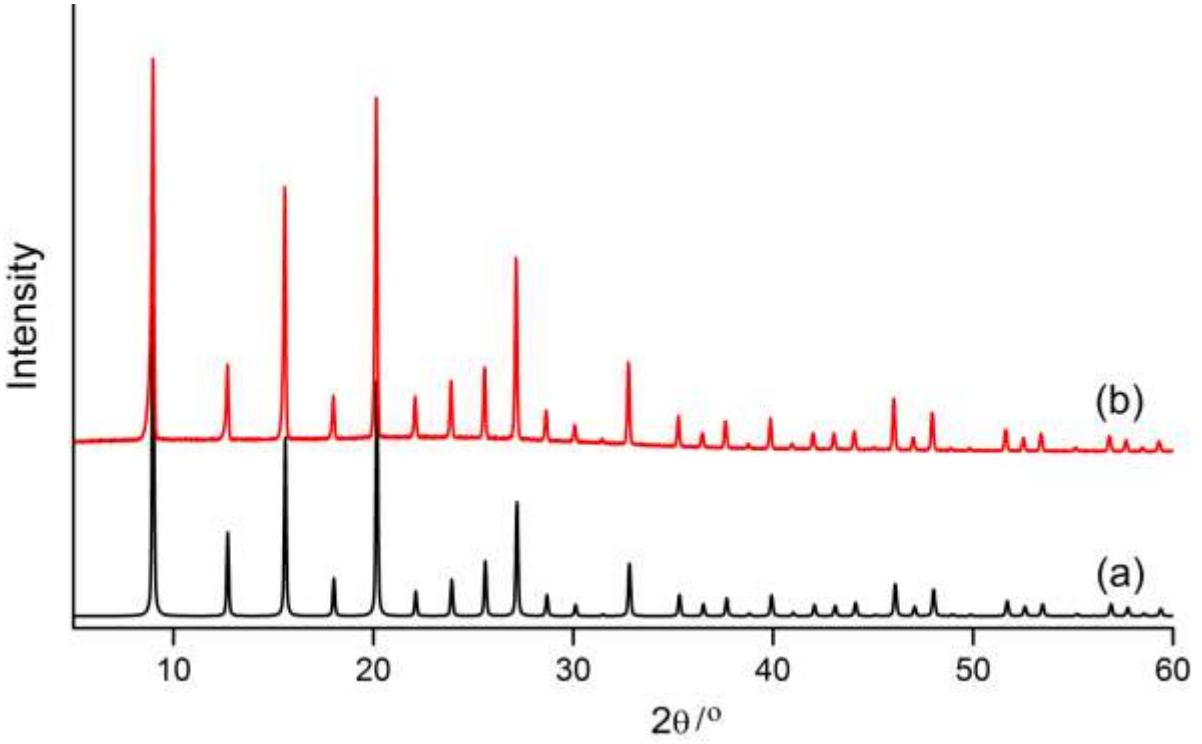

Figure 5.19: Experimental powder diffraction pattern of Sc(NH_2-IA) MOF (b) compared to the pattern simulated from the single crystal model(a).

Table 5.7: Crystallographic information for structure Sc(NH_2-IA).

Structure	$Sc_2(NH_2\text{-}IA)_3$
Formula unit	$Sc_2C_{24}H_{15}N_3O_{12}$
Crystal system	Cubic
Space group	$I\,2_13$
X-ray source	Mo Kα
Diffractometer	
Wavelength (Å)	0.71075
Unit cell (Å)	
a/Å	13.919(7)
Volume/Å^3	2696.4(2)
R	0.0606
Rw	0.0960

Figure 5.20(a) shows the assembly of this framework, where each amino-isophthalate molecule is bonded to 4 scandium cations and the scandium cation is linked octahedrally to six carboxylate O atoms. Figure 5.20(c) shows each ScO_6 octahedron is joined to three other octahedra, by sharing two carboxylate carbons, from the same edge of the octahedral unit. This assembly gives rise to undulating chains similar to those observed in the Sc(IA)-2 (Figure 5.21), but in this case the presence of amino groups appears to make the framework more symmetric, so that there is only one type of Sc^{3+} in this structure.

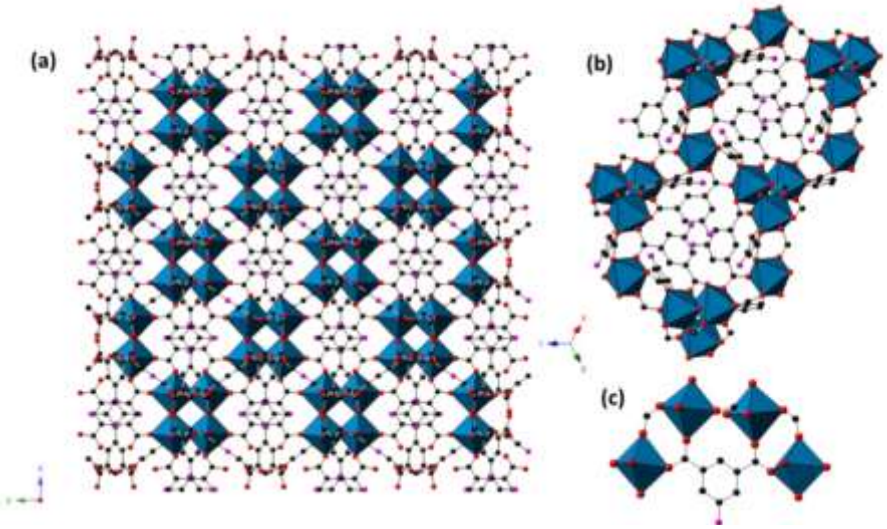

Figure 5.20: Crystal structure of $Sc_2(NH_2\text{-}IA)_3$: (a) molecular packing, (b) ScO_6 octahedron, (c) isophthalate linker bonding to four Sc^{3+} cations. ScO_6 are shown in blue. Black, magenta and red spheres represent the C, N, and O atoms respectively.

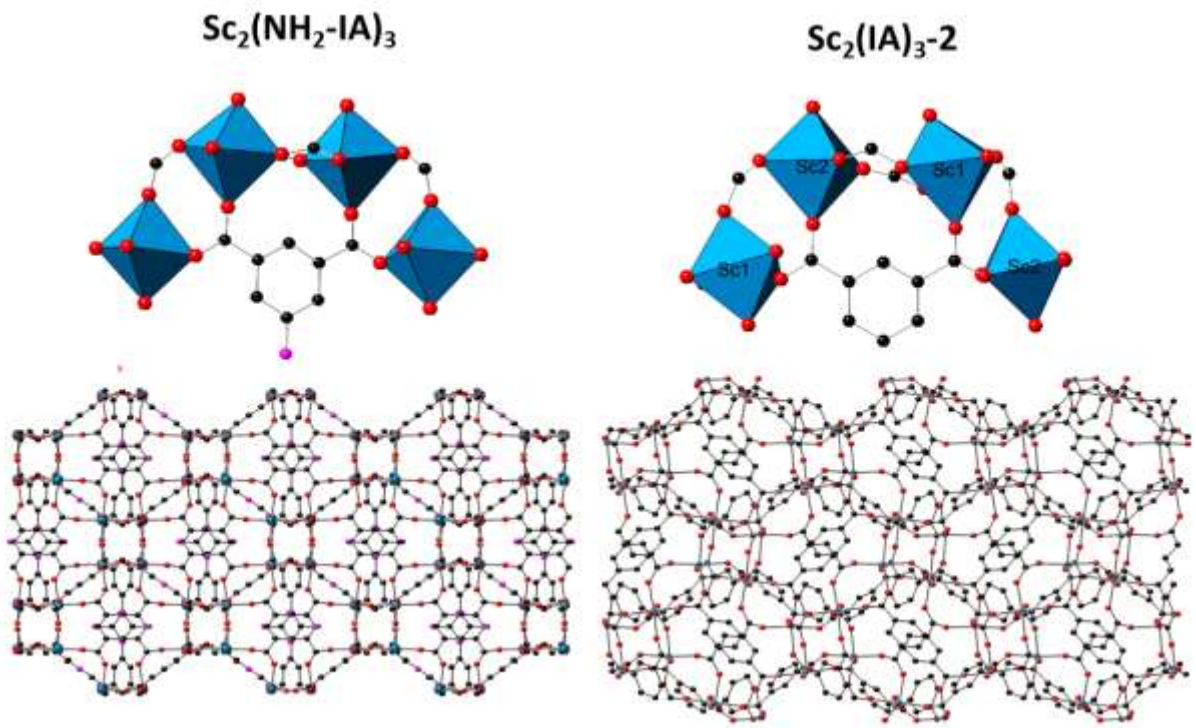

Figure 5.21: Comparison of $Sc_2(NH_2\text{-}IA)_3$ and $Sc_2(IA)_3$-2.

Thermogravimetric analysis shows that the framework is thermally stable up to 500 °C.

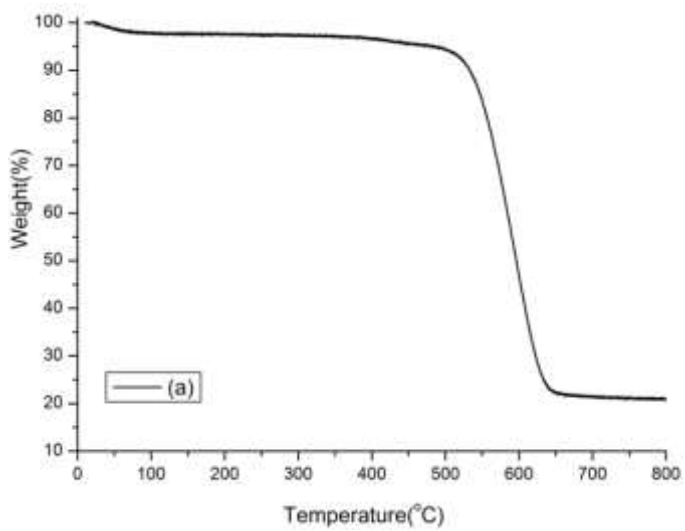

Figure 5.22: Thermogravimetric analysis of as-synthesised $Sc_2(NH_2\text{-}IA)_3$.

Figure 5.23 shows the solid-state ^{13}C, ^{1}H and ^{45}Sc MAS NMR for the as-prepared material and that heated at 250^{o}C (a and b respectively). The ^{13}C spectrum showed the characteristic peaks for the linker. ^{1}H spectrum has the broad peak at 1 ppm attributed to the amino-group

along with the other ^{1}H characteristic peaks in the linker. The ^{13}Sc MAS NMR exhibits a narrow single signal consistent with the highly symmetric scandium on the octahedral site.

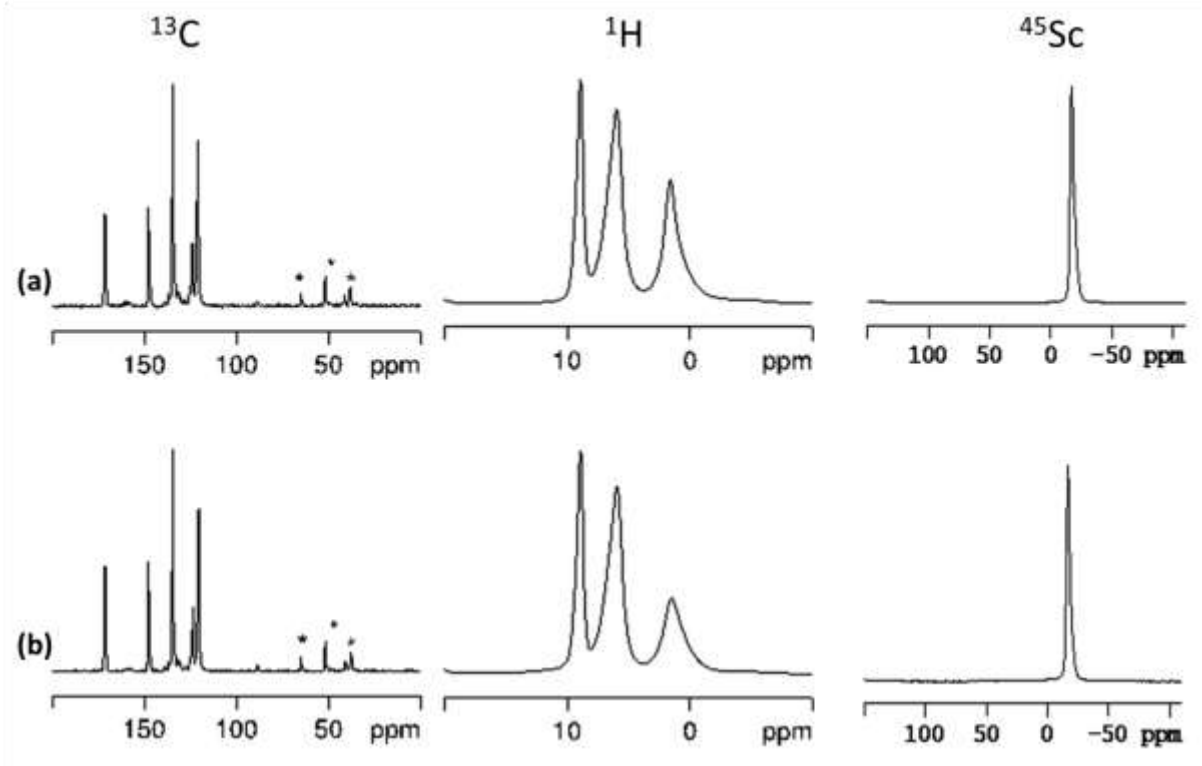

Figure 5.23: Solid state NMR spectra ^{1}H (14.1 T), ^{13}C MAS and ^{45}Sc (14.1 T) on as- prepared Sc-(NH_2-IA)-1(a) and (b) sample heated at 250℃ . The MAS rate was 12.5 kHz for ^{13}C and ^{1}H, and 25 for ^{45}Sc. * indicates spinning sidebands.

5.4.1.3 Sc(NO_2-IA), [$Sc_2(NO_2$- $C_8H_4O_4)_3$]

Syntheses with (NO_2-IA) were explored by following the conditions described in Table 5.2. Two microcrystalline samples were obtained (Figure 5.24). Sample 1 was obtained by using a molar ratio of 0.5 for Sc/L and heated at 120 ℃ for 12 h. Sample 2 was synthesized using a molar ratio of 1 and higher temperature 190 ℃ and using a mixture of DMF and water (using just water yielded the same material) . Figure 5.23 shows the patterns for both samples.

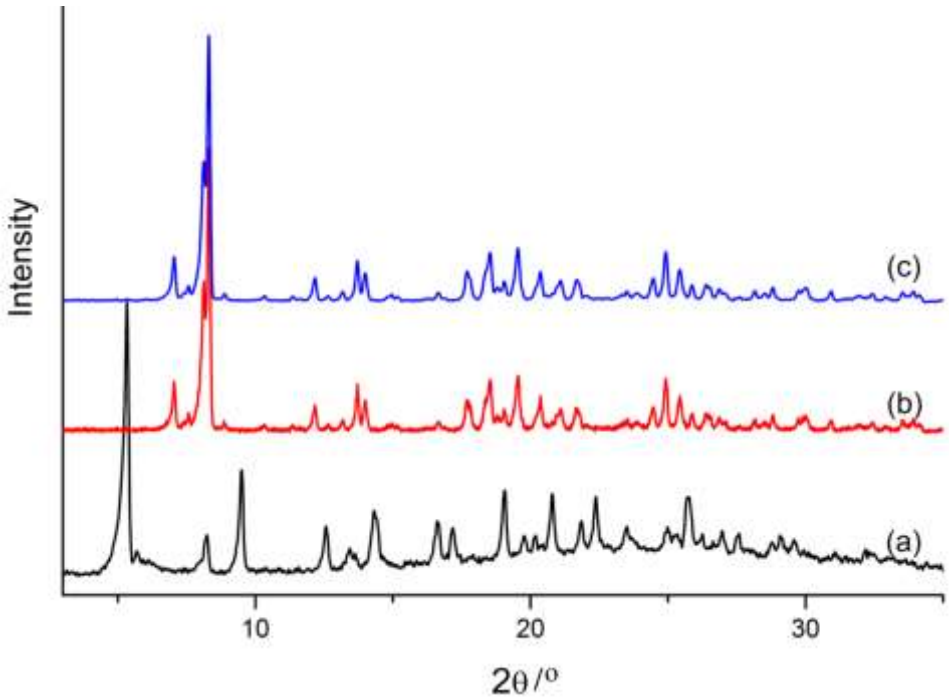

Figure 5.24: Experimental powder diffraction patterns of Sc(NO_2-IA)-1 materials, (a) sample 1 prepared with Sc/L(0.5) and (b and c) samples using a molar ratio Sc/L=1. (PXRD (c) correspond to the synthesis made using just water as solvent).

The characterisation by SEM microscopy showed that the product was a crystal aggregate. TGA shows that the samples are thermal stable up to 380 ℃ for 1 and 425 ^{o}C for 2. Sample 1 loses 5 wt % at 250 ℃ due to solvent, whereas sample 2 loses no solvent. Neither material is porous to N_2 or CO_2.

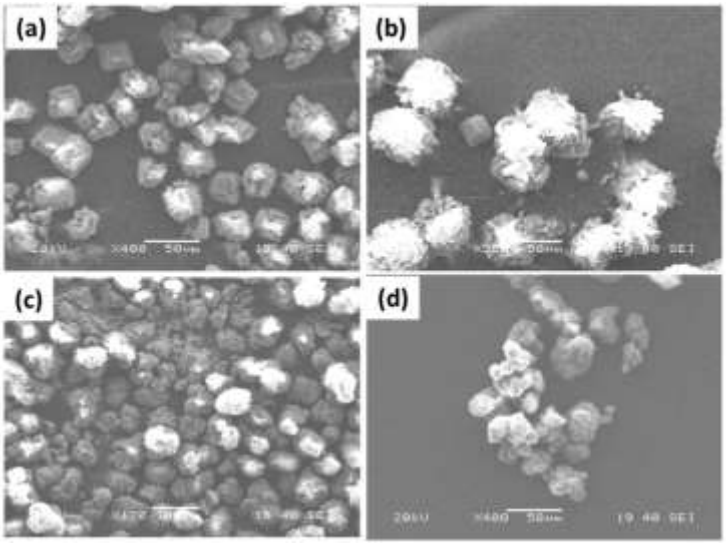

Figure 5.25: SEM images of samples 1(a, b) and 2(c, d) obtained for $Sc_x(NO_2\text{-}IA)_y$.

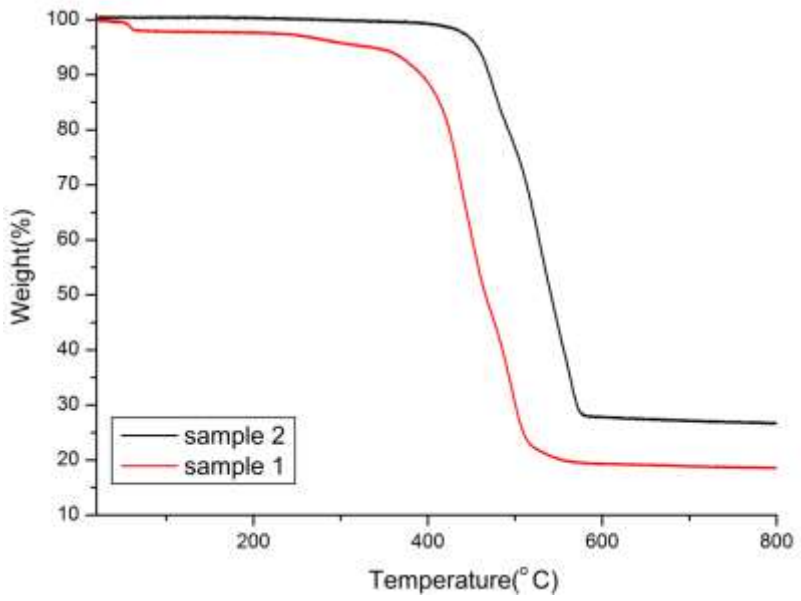

Figure 5.26: Thermogravimetric analysis measured on both samples obtained using Sc^{3+} and NO_2-IA.

All attempts to get single crystals were unsuccessful with nitro-isophthalic acid.

5.4.1.4 Discussion of scandium isophthalates

The solvothermal synthesis using mixed solvents, H_2O and DMF gave the Sc(IA)-1 material as cube shape morphology (Figure 5.6), with space group cubic *Pa-3*. The structure (Figure 5.8) is built up from octahedral scandium trimer similar to assembly of MIL-101 and MIL-100, sharing an oxygen atom as Sc-(μ_3-O)-Sc. Sc(IA)-1 is isostructural with a previously reported indium isophthalate.[9] The simulated X-ray diffraction pattern of this structure was then compared to experimental pattern, resulting in good agreement, and no second phases were observed (Figure 5.7).

The hydrothermal synthesis using the same linker and longer time of reaction at higher temperature (220 ℃) reported elsewhere[10] was performed for comparison. This synthesis yielded as octahedral crystals (Figure 5.11) and PXRD pattern of the as-prepared material Sc(IA)-2, showed the purity of the solid compared to the simulated pattern (Figure 5.12), with a cubic system, P 2_1 3 symmetry. The Sc(IA)-1 material is porous for both, N_2 and CO_2 (Figure 5.15). Sc(IA)-2 is not porous at all. This is consistent with the structural assembly

because the windows of Sc(IA)-2 are not large enough for the access of these gases. Solid-state MAS NMR (Figure 5.16) of these two scandium isophthalates, showed that Sc(IA)-1 has just one scandium site, in contrast to Sc(IA)-2, which has two. As-prepared Sc(IA)-1 has some residual solvent after synthesis, which is only partially removed by heating at 250 °C.

Remarkably, the amino-isophthalate isostructural with Sc(IA)-2 was prepared using mixed linker synthesis conditions that give rise to Sc(IA)-1. The structure crystallises with a higher symmetry, due to the presence of the bulk amino-group, and ^{45}Sc NMR confirms that there is only one type of Sc^{3+}. New phases were also prepared using the nitro-isophthalic acid, but only as microcrystalline powders and their structures were not solved. Of all the scandium isophthalates, only Sc(IA)-1 was porous. For the other materials the window size was too small to admit molecules.

5.4.2 Scandium 2, 5-furandicarboxylates

A series of experiments was carried out investigating different reaction conditions, listed in Table 5.2. Two novel crystalline scandium 2, 5-furancarboxylates were prepared, but just one of them was suitable for analysis by single crystal diffraction.

5.4.2.1 Analysis of Structure Sc(FDA)-1, $Sc_2(C_6H_2O_5)_3$

The sample obtained as colourless crystals was analysed by single crystal diffraction to determine the structure. Single crystal analysis using the CRYSTALS suite of programs indicated that the material crystallized in the triclinic space group *P-1* with unit cell *a* = 8.775(4) Å, *b* = 10.56(30) Å and *c*=11.854(4)9) Å, and α = 93.144 ^{o} (12), β = 91.464 ^{o}(8) and γ = 105.847 ^{o}(13) but the data had high residual values of Rw = 25.8%.

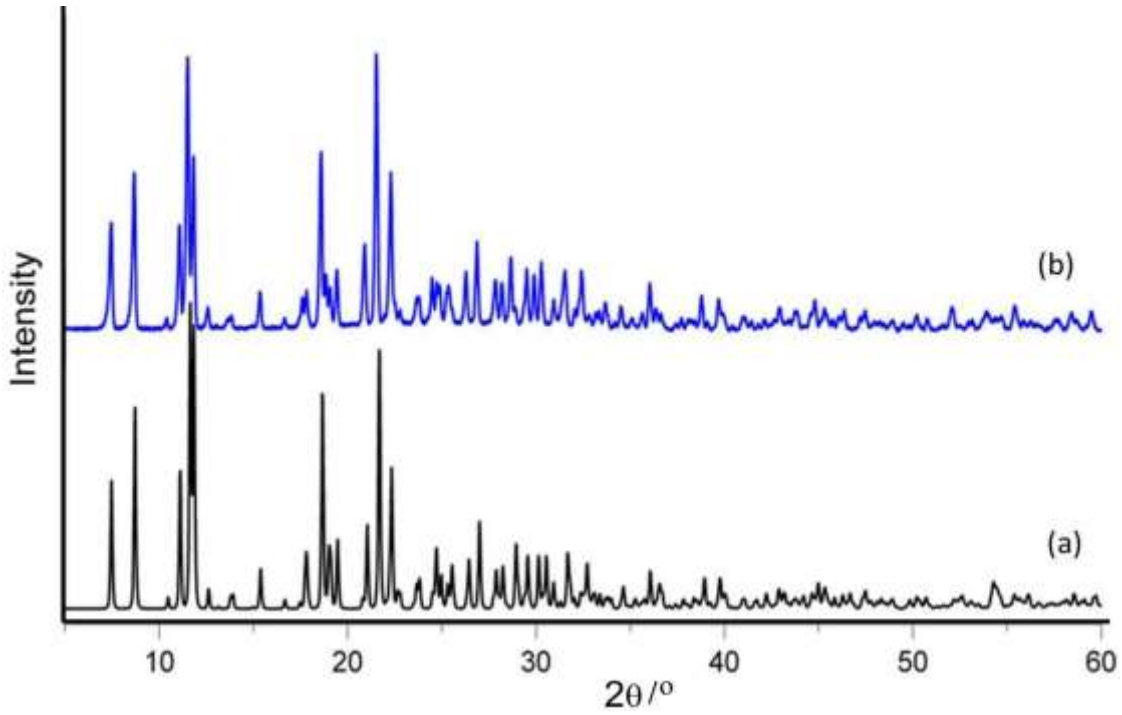

Figure 5.27: PXRD collected on sample Sc(FDA)-1 (a) simulated pattern and (b) as-prepared.

Rietveld refinement was performed using the single crystal structure, as a starting model, against laboratory powder XRD. The single crystal structure was used as a starting model that was Rietveld-refined against laboratory powder diffraction using the GSAS suite of programs, resulting in a good fit to the data (Rwp = 9.73, Rp = 7.18). Rietveld profile fit for the refinement of the triclinic structure is shown in Figure 5.28 and Table 5.8 gives the crystallographic data of refinement (CIF file available see the Appendix C).

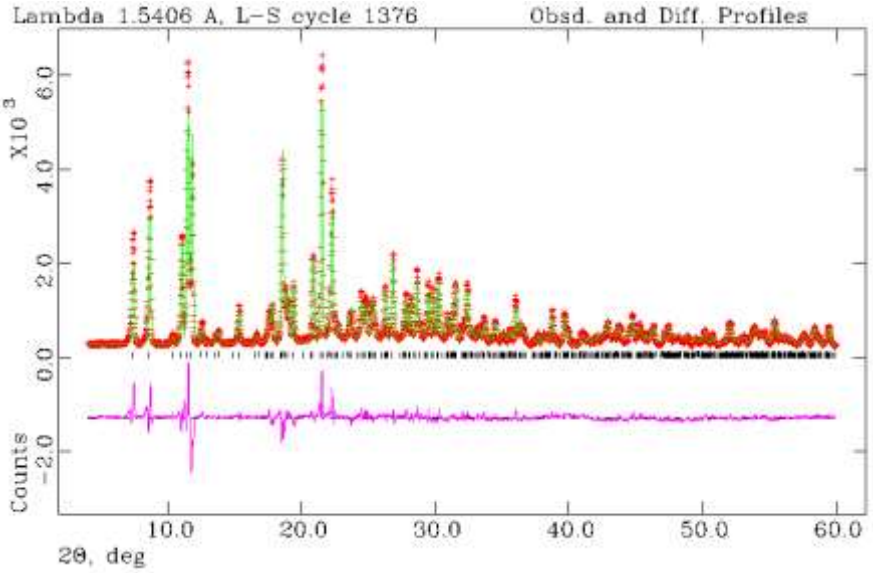

Figure 5.28: Rietveld profile fit for Sc(FDA)-1.

Table 5.8: Structural data from Rietveld refinement on the Sc(FDA)-1

Structure	**Sc(FDA)-1**
Formula unit	$Sc_2C_{18}H_6O_{15}$
Crystal system	Triclinic
Space group	P -1
X-ray source	Cu Kα
Diffractometer	STOE STADIP
Wavelength (Å)	1.54056
Unit cell (Å)	
a/Å	8.83219(19)
b/Å	10.58983(27)
c/Å	11.8206(4)
α/°	93.253(23)
β/°	91.13(30)
γ/°	106.343(27)
Volume/Å^3	1058.48
R	0.0718
Rwp	0.0973

The structure of this framework is built up from two crystallographically distinct ScO_6 octahedra, which are linked to the carboxy-groups of the linker. Each linker molecule is bonded with 4 ScO_6, where each carboxy terminal of the ligand is linked to a pair of identical scandium atoms, assembling chains. Each pair of identical scandium (Sc) is connected to the other pair of scandium (Sc) across the linker. Images of the framework are shown in Figure

5.29. TGA shows decomposition of the framework after 350℃. Analysis of gas adsorption demonstrated that the structure was not porous for gases.

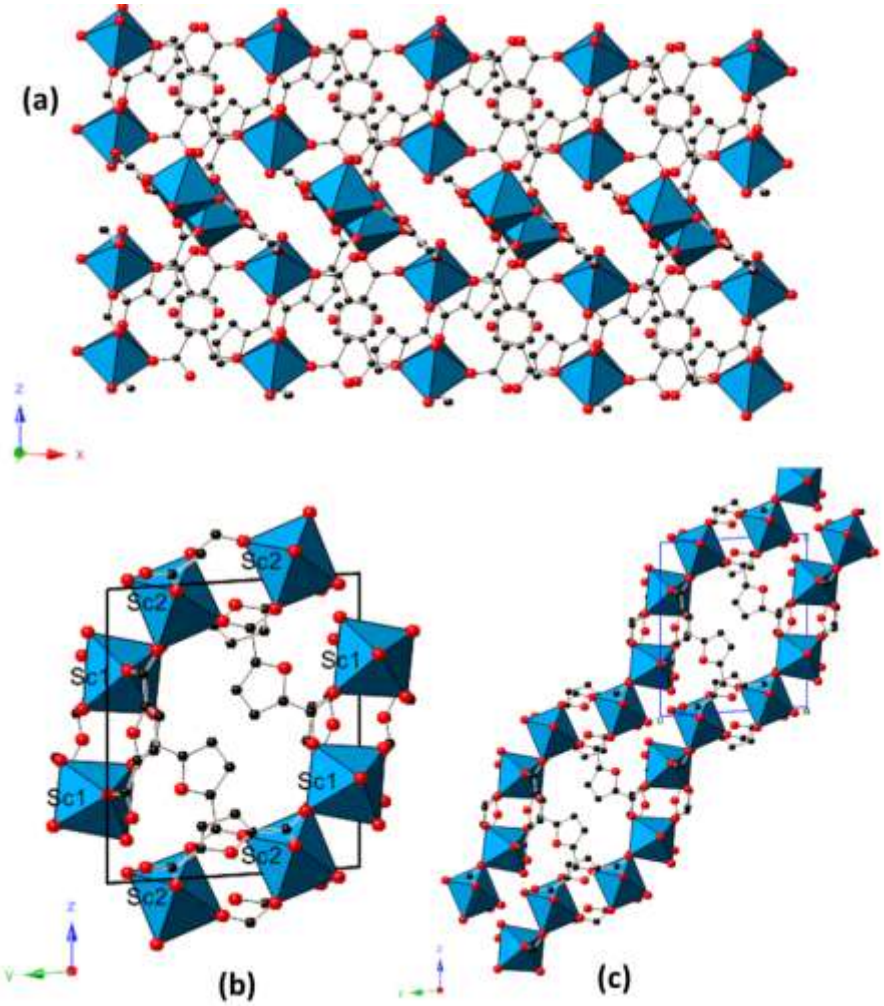

Figure 5.29: Representation of Sc(FDA)-1; Framework of the structure viewed the channels parallel to the y-axis (a), unit cell (b) and structure viewed the chains parallel to the x-axis (c). Scandium octahedra are shown in blue. Black and red spheres represent the carbon and oxygen atoms of the FDA linker.

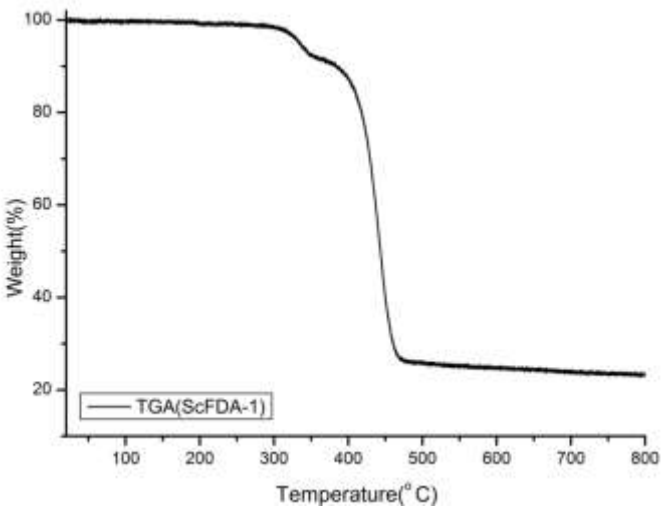

Figure 5.30: Thermogravimetric analysis of as-prepared Sc(FDA)-1 under flowing air.

5.4.2.2 Analysis of Structure Sc(FDA)-2

Many attempts to synthesize large crystals for Sc(FDA)-2 gave only microcrystalline powder. Figure 5.31 shows the PXRD collected on two as-prepared samples prepared at different temperature (160 ℃ and 190 ℃) under the reaction conditions found in Table 5.1. PXRD patterns are similar.

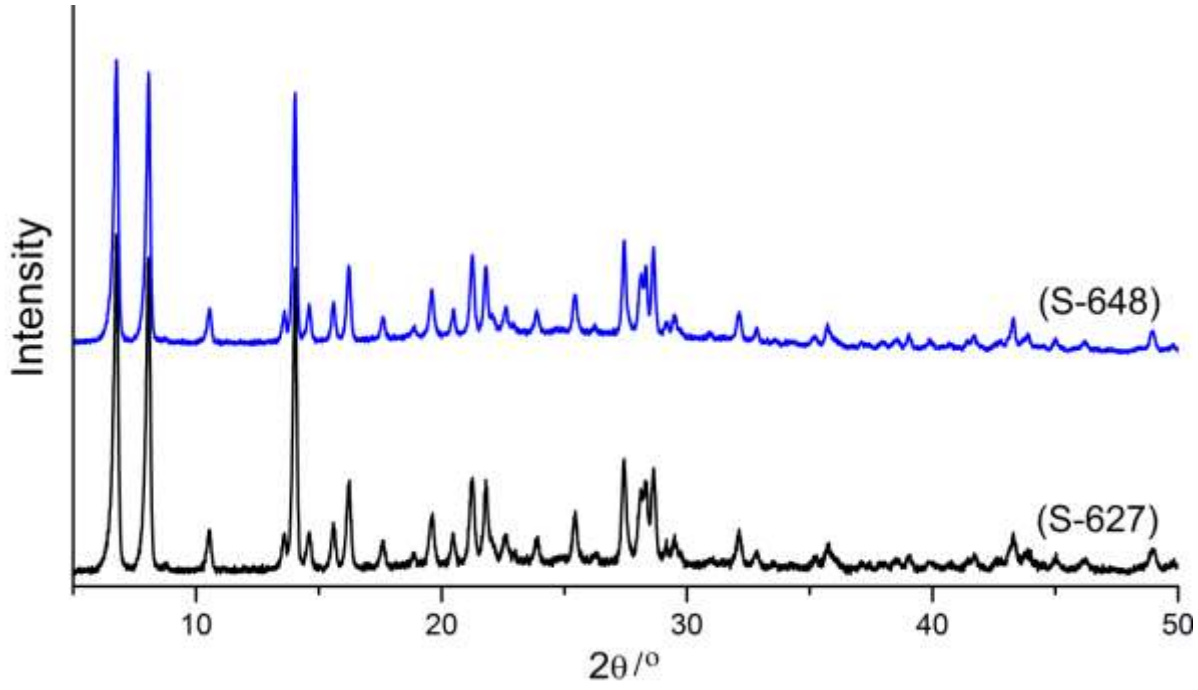

Figure 5.31: PXRD collected on sample Sc(FDA)-2; (a) as-prepared samples S-627 (prepared at 160 ℃) and S-648 (prepared at 190 ℃).

The unknown phase was indexed using different programs to get structural information of the crystalline material. Firstly, the EXPO2010[26] suite software was use. The peaks of the PXRD were automatically chosen in a range between 5-40° 2θ by using the algorithm N-TREOR, the pattern was indexed in the orthorhombic system *P* $b2_1$ *n* with unit cell parameters of *a* = 21.696 Å, *b* = 25.899 Å, *c* = 6.273 Å. These values for the indexed cell are similar to those obtained by using the algorithm DICVOL06 method in the FullProf suite program. It is interesting to note a certain similarity with the tetragonal structure reported by Ibarra et al.[11], *I* 4_1*/amd* unit cell *a* = *b* = 22.605 Å, *c* = 12.474 Å). That MOF (NOTT-401) was synthesized using the similar thiophene-2,5-dicarboxylic acid and scandium triflate, in a mixture of solvents (THF, DMF and H_2O) .

In order to get structural information of this unknown material, an attempt to obtain the assembly in the framework was carried out by starting from the structural model of NOTT-401. Thus, the space group was changed to orthorhombic along with the indexed unit cell. So far it was possible to match the more important peaks of our pattern (Figure 5.32); however as using the model which involves mixed solvents to synthesize the NOTT-401, it has not yet been possible to get a very close match for the other reflections. Figure 5.33 shows a possible motif for the unknown structure.

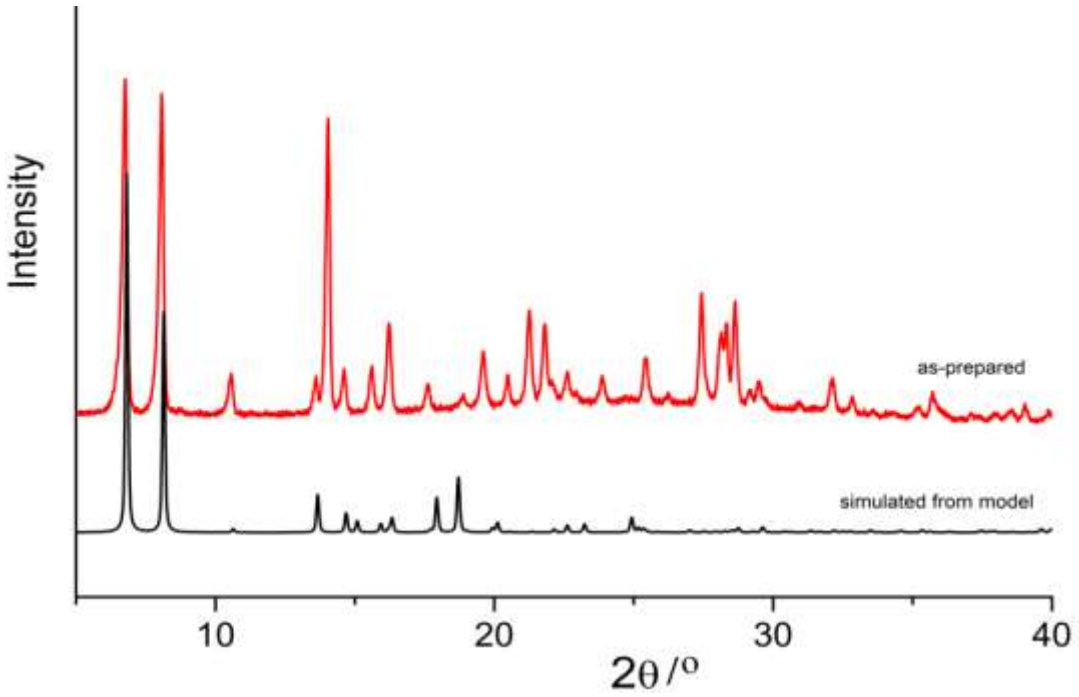

Figure 5.32: PXRD collected on sample Sc(FDA)-2 (a) compared with that simulated from the model (see text).

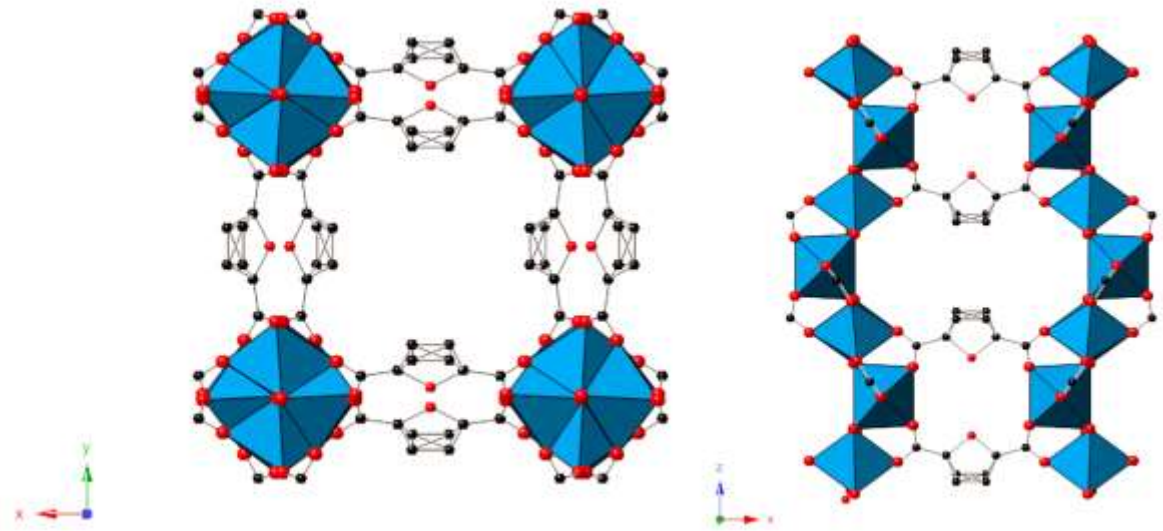

Figure 5.33: Possible assembly for unknown structure Sc(FDA)-2. Scandium is represented with blue polyhedral. Black and red spheres represent the carbon and oxygen atoms of the linker respectively.

The synthesis described here involves just DMF as solvent, and CHN analysis of the as-prepared sample gave the presence of the N (3.31%), which is attributed to DMF, which is also confirmed by TGA. TGA (Figure 5.34) shows that a 20% loss weight is observed up to

280 ℃. Thus the sample was heated at 250 ℃ for 8 h under flowing nitrogen to remove solvent. TGA of the heated samples was obtained and still showed some solvent in the framework, and the sample exhibited drastic changes in the PXRD pattern. The structural response of the Sc(FDA)-2 to temperature variation was studied in temperature arrange of 120, 200, 250 and 300 ℃. Comparison of the powder diffraction patterns of the material (Figure 5.35) after heating showed that the sample starts to change structure at 200 ℃.

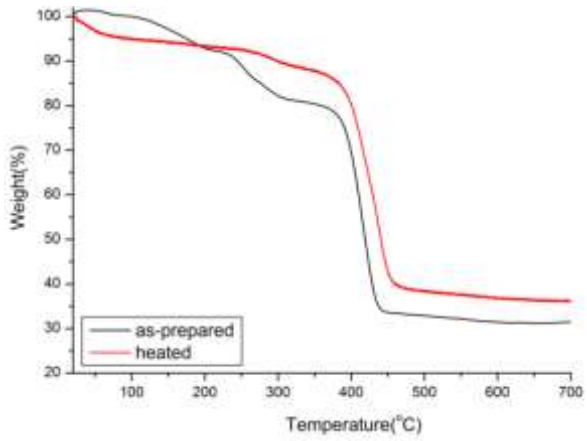

Figure 5.34: Thermogravimetric analysis of Sc(FDA)-2, as-prepared and heated at 250 ℃.

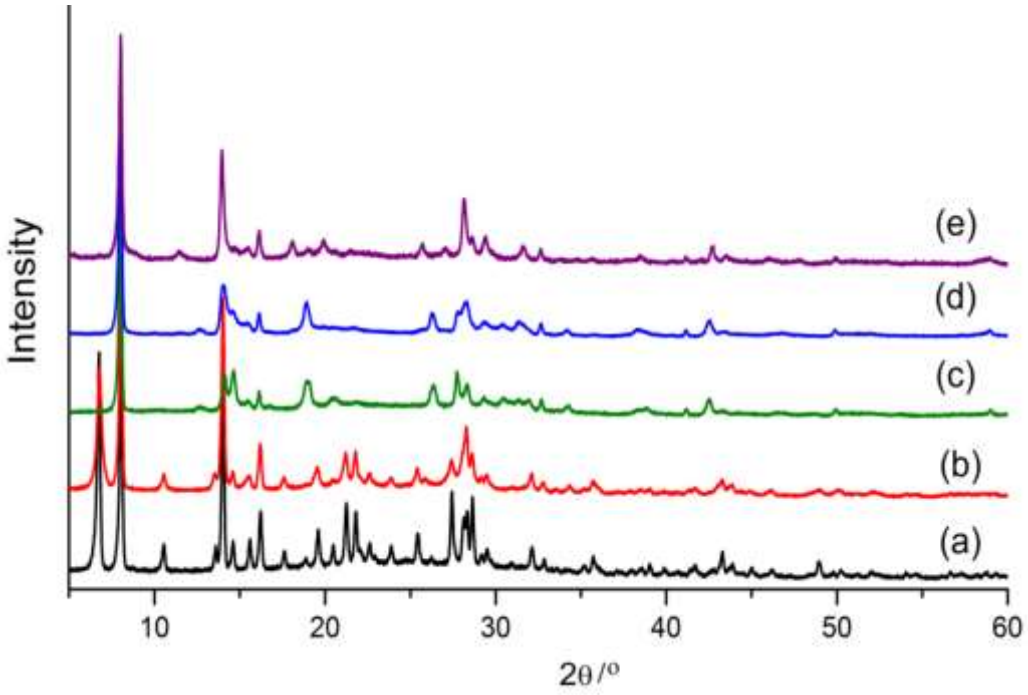

Figure 5.35: PXRD collected on sample Sc-FDA(2); (a) as-prepared, (b) heated at 120℃, (c) heated at 200 ℃, (d) heated at 250 ℃, (d) heated at 300 ℃

It has been observed for other MOFs, such as MIL-100(Sc) or MIL-88B(Sc) that solvent exchange from solution into framework is possible. So solvent exchange experiments were carried out on the sample by stirring for 24 h in solvents such as MeOH and acetone, followed by filtration and heating at 60 ℃ for 12 h, but the PRXD pattern did not show changes (Figure 5.36).

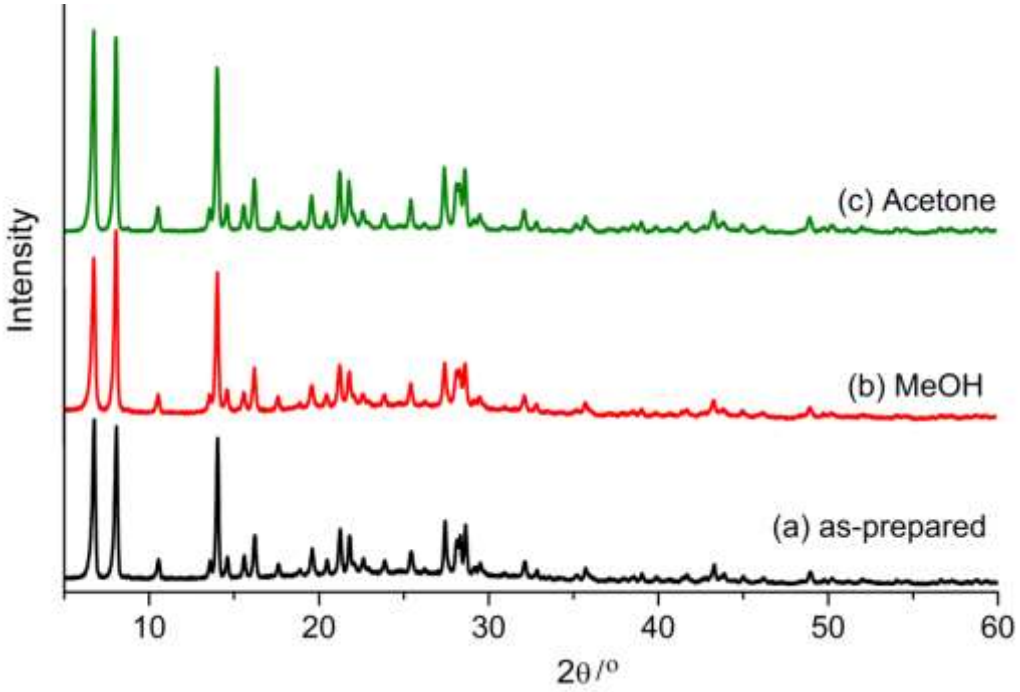

Figure 5.36: PXRD collected od Sc(FDA)-2; (a) as-prepared, (b) contacted with MeOH) and (c) contacted with acetone.

Elemental analysis confirmed DMF remained after contacting with acetone and methanol, with the wt% N reduced from 3.31 to 2.3 or 2.5 w%, similar to the residual values after heating at 120 °C.

Adsorption analysis showed that the material was porous to N_2 and CO_2. An as-prepared sample activated at 120 °C (S-120) under vacuum at 4 h gave the adsorption isotherms shown in Figure 5.37. N_2 adsorption at -196 activated sample gave a BET surface area of 100 m^2g^{-1} with an uptake of 1 mmol g^{-1}, while the measured adsorption for CO_2 at –77 °C gives an

uptake of 4.5 mmol g^{-1}. Also, studies of adsorption were carried out on the sample heated at 250 ^{o}C (Figure 5.37, labelled as S-250), which result did not absorb N_2, and gave a CO_2 adsorption gave an uptake of 1.5 mmol g^{-1}.

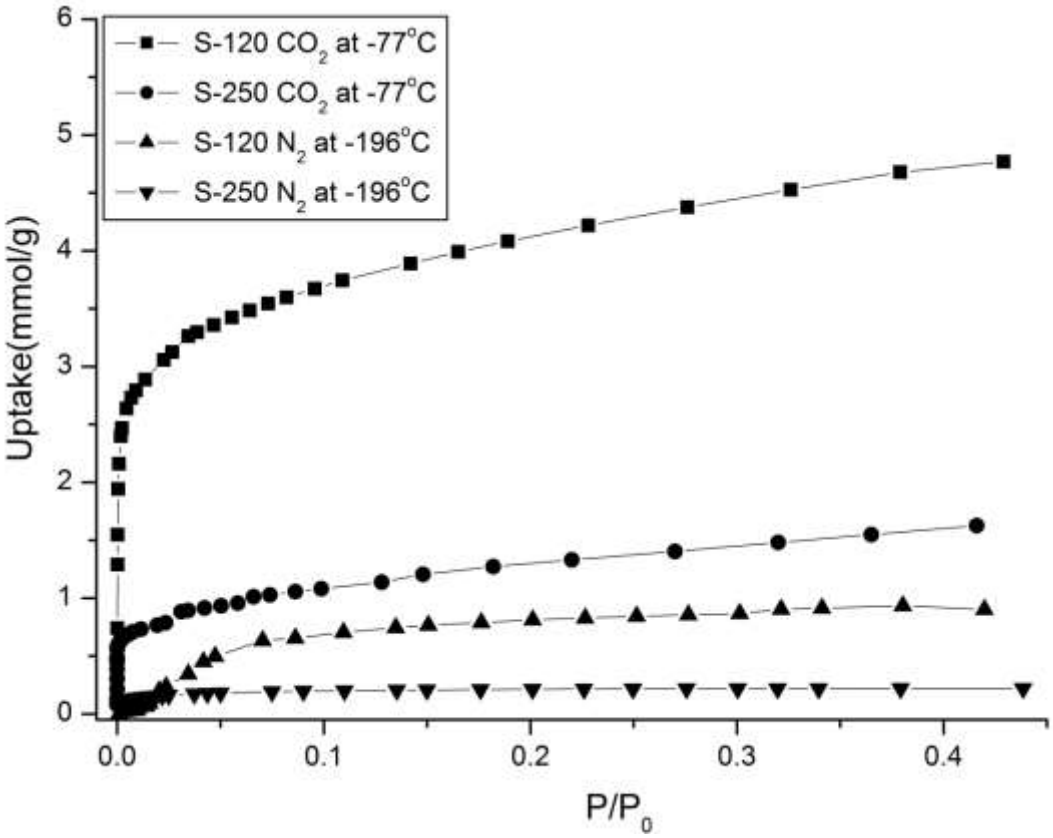

Figure 5. 37: CO_2 and N_2 adsorption isotherms measured at -77 ℃ and -196 ℃

As seen in the PXRD diffraction pattern (Figure 5.35) the structure changes at 200 ℃ , when the amount of DMF calculated by CHN analysis was reduced, (N only 1.0%). From these results it possible to say that structural change due to the solvent loss. DMF is not just occluded into the framework, because when part of the DMF is removed the uptake of CO_2 gas is reduced by 60%. Further analysis by solid state NMR was performed on the Sc(FDA)-2 (Figure 5.38). Three samples were analysed, as-prepared (a), heated at 120℃ (b) (S-120) and heated at 250℃ (c) (S-250). Figure 5.38 shows the solid-state NMR on samples for ^{1}H, ^{13}C and ^{45}Sc.

^{1}H MAS NMR spectra of as-prepared Sc(FDA)-2 indicates the presence of DMF in the solid. S-120 (Figure 5.38, sample heated at 120 ℃) still indicates the presence of DMF in the solid and other impurities (4.7 and 5.5 ppm). The peaks at 7.3 and 8.5 ppm in the ^{1}H MAS NMR spectrum of as-prepared sample remain in the spectrum of S-120, although shifted slightly upfield (to lower chemical shift). For sample S-250 (sample heated at 250 ℃), the peak at 2.7 ppm is much less intense when compared with the spectrum of S-120, corresponding to the removal of solvent. There is a presence of a new peak at 5.1 ppm, and at present it is not known what this new peak could correspond to.

The ^{13}C CPMAS NMR indicated that upon heating S-120, the spectrum changes slightly so that the peak split at 117 and 118 ppm in the as-prepared sample becomes one sharp peak at 117 ppm. This single peak is also seen in the ^{13}C spectrum of S-250, although much broader, possibly indicating disorder.

The ^{45}Sc MAS NMR spectra shows that for as-prepared ScFDA-2 the framework has two scandium sites and upon heating the sample (S-120) the position of the ^{45}Sc peak moves to lower chemical shift, the Sc site is becoming more shielded. The two sites remain one with a small quadrupolar coupling and one with a large quadrupolar coupling. The ^{45}Sc MAS NMR spectrum of S-250 shows a broader peak, which may contain two or more Sc signals. Further experiments are required to identify this, for example, ^{45}Sc triple quantum MQ-MAS.

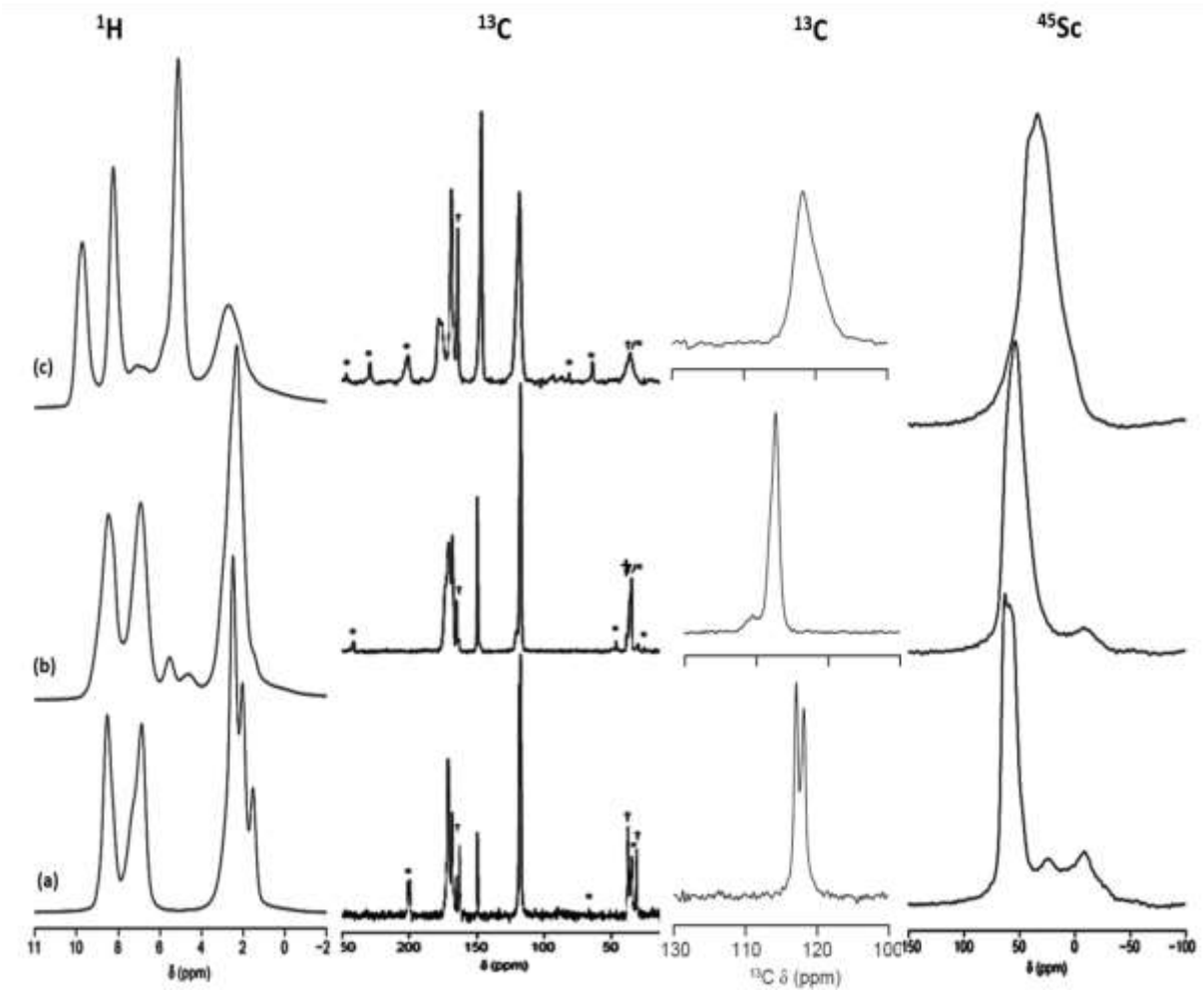

Figure 5.38: ^{1}H, ^{13}C and ^{45}Sc (14.1 T) MAS NMR spectra of Sc(FDA)-2, as-prepared (a), heated at 120℃ (b) and 250℃ (c). The MAS rate was 60, 12.5 and 25 kHz for ^{1}H, ^{13}C and 25 for ^{45}Sc respectively. ● indicates spinning sidebands, †=*DMF*.

From these results based on the analysis of NMR, gas adsorption and PXRD could suggest that DMF is coordinated to the framework, but to support our hypothesis the structure must be solved.

5.4.3 Scandium meso tetrakis(4-carboxyphenyl)porphyrin [TCPP]

The resultant reactions in the Sc-TCPP series yielded brown solids. The powder X-ray diffraction patterns of the different samples obtained are shown in Figure 5.39. Among the different conditions used, the best route to obtain the most crystalline solid is using low temperature in a range between 70 and 110 ℃.

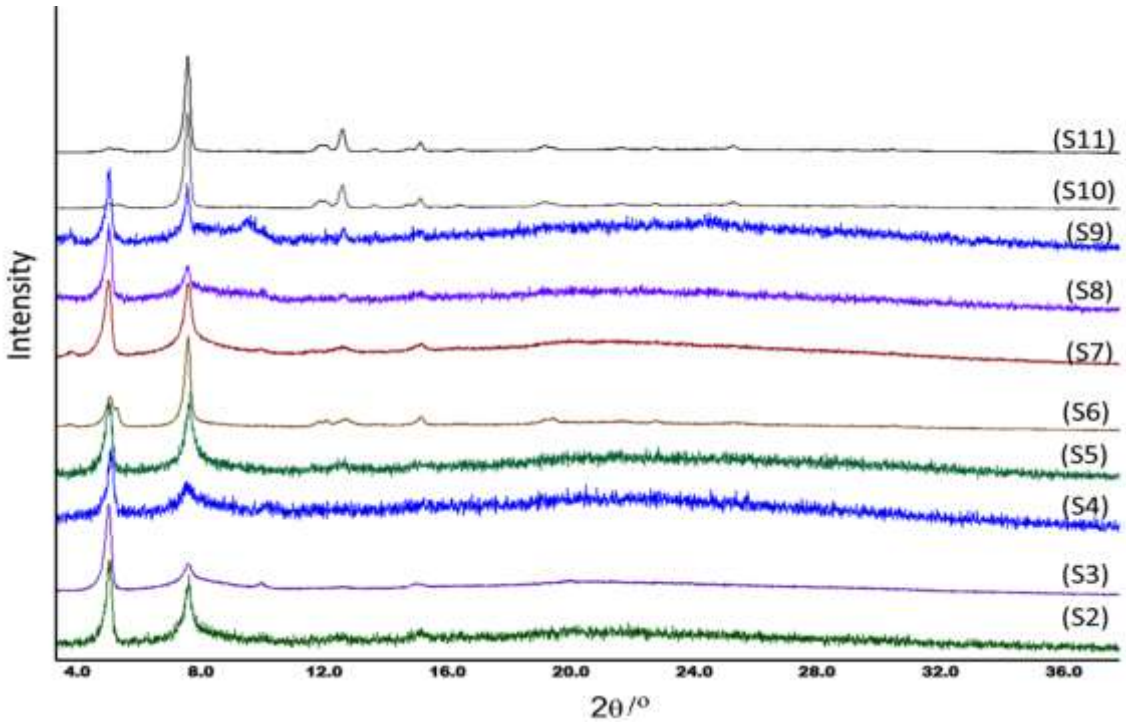

Figure 5.39: Experimental powder diffraction pattern of different samples of Sc-TCPP

The principal reflections (Figure 5.40) were chosen to obtain a possible unit cell. This was performed using the FullProf suite program[27] by using the algorithm N-TREOR. The pattern gave a potential monoclinic system *C2*, unit cell parameters of *a*= 24.086 Å, *b* = 10.423 Å, *c* = 21.947 Å, $\alpha = 90$ ℃, $\beta = 129.84$ ℃ and $\gamma = 90$ ℃.

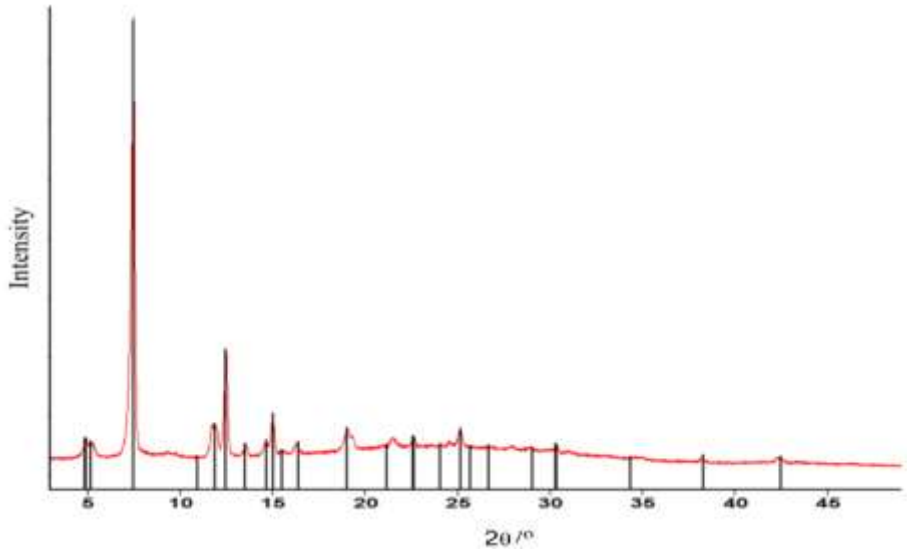

Figure 5.40: PXRD indicated the principal reflections of the cell indexed.

EDX confirms the presence of scandium in the samples, however it was not possible to get an accurate Sc:TCPP ratio. Figure 5.41 shows the TGA analysing two samples, sample S11 has a significant loss weight compared to sample S7. Sample S7 has 10% solvent loss by 300 ℃, whereas sample S11 has an 18% loss solvent at 250 ℃.

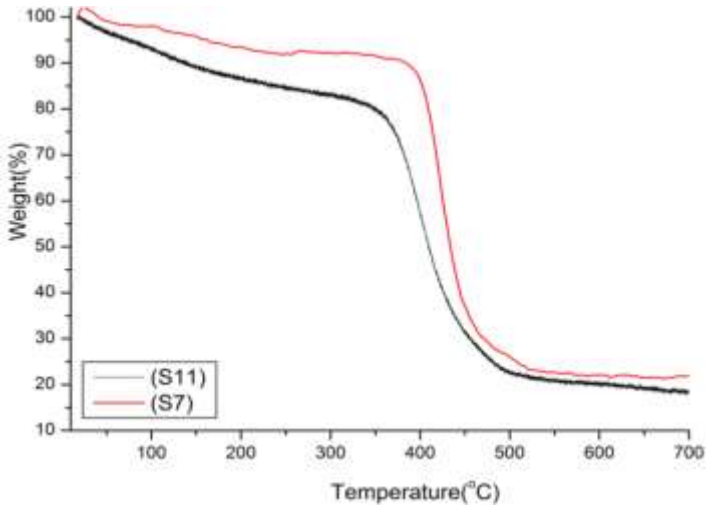

Figure 5.41: Thermogravimetric analysis of Sc-TCPP, samples S7 and S11.

Samples (S7 and S11) were heated at 65 and 150 ℃ for 6 h to remove the solvent, these remain crystalline after heating at 65 ℃, but after treatment at 150 ℃, demonstrated loss of crystallinity (Figure 5.42).

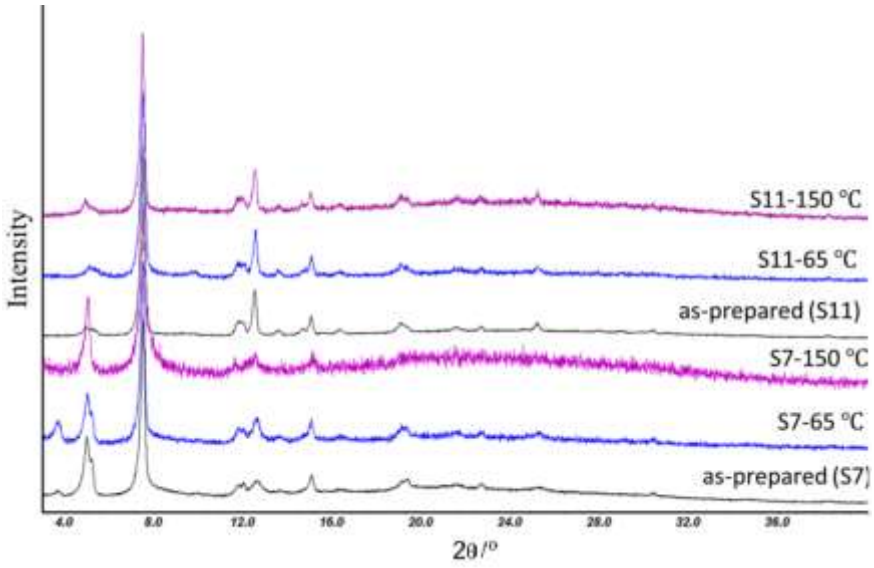

Figure 5.42: PXRD of Sc-(TCPP) of samples S7 and S11, as-prepared, heated at 60 ℃ and 150 ℃.

Characterisation by SEM microscopy was performed on the as-prepared samples (Figure 5.43). Sample S7 involves DMF in the synthesis and sample S11 was prepared using a mixture of DMF and H_2O. These materials exhibited morphology like long fibres (or wires). The fibres in sample S7 are so long that it was not possible to determine their length. However, for the solid which involved water in the synthesis crystals were 20 - 30 µm in length and 0.5 -1.5 width.

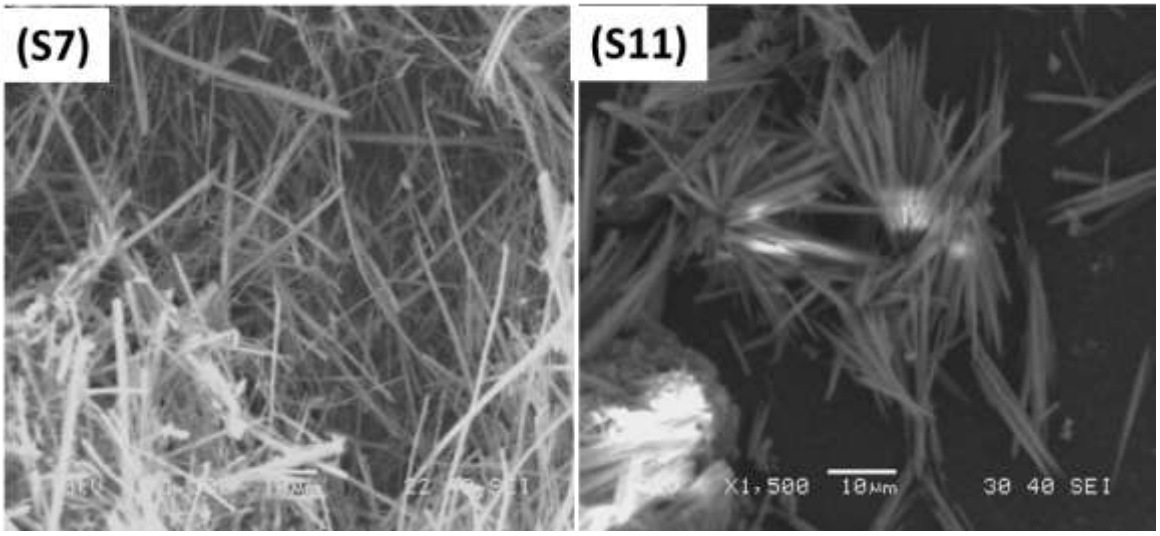

Figure 5.43: SEM images of Sc-TCPP different samples. S7 prepared in DMF and S11 prepared using a mixture of solvents DMF and H_2O.

Adsorption of N_2 at -196 to measure the porosity of the samples was performed by outgassing at 65 °C for 4 h under vacuum prior to analysis. The highest observed uptake of 12 mmol g^{-1} with a BET surface area of 784 m^2 g^{-1} , was higher than the PIZA-1[16] network and closer to those values obtained for the iron TCPP, MIL-141(Fe). [18] Figure 5.44 shows the isotherms and table 5.9 list the BET surface area of the several samples prepared under different conditions.

Table 5.9: BET Surface area of Sc-TCPP

Molar ratio (Sc/TCPP)	Sample	BET surface area ($m^2 g^{-1}$)	Time (day)	Temperature (℃)
6.9	S2	370	1	70
6.9	S5	310	2	70
4.6	S6	783	3	70
4.6	S7	784	5	70
4.6	S8	316	3	110
4.6	S9	278	5	110
4.6	S10	542	5	110
2.3	S11	452	3	70

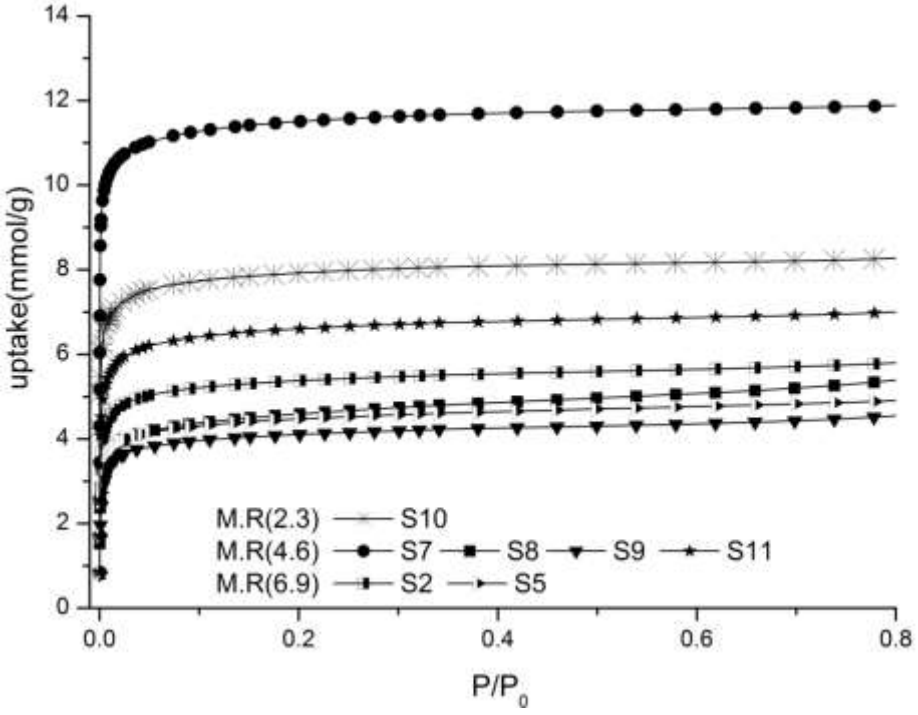

Figure 5.44: N_2 adsorption isotherms collected on Sc-TCPP (-196℃) .

Extensive research on porphyrin systems has reported assembly of nanowires or nanorods. This could suggest that further work to optimize the synthesis can address to this point. A possible arrangement of the Sc^{3+} into the square planar molecule might be by linking to the carboxy groups of the square planar molecule and growing in layers (Figure 5.45).

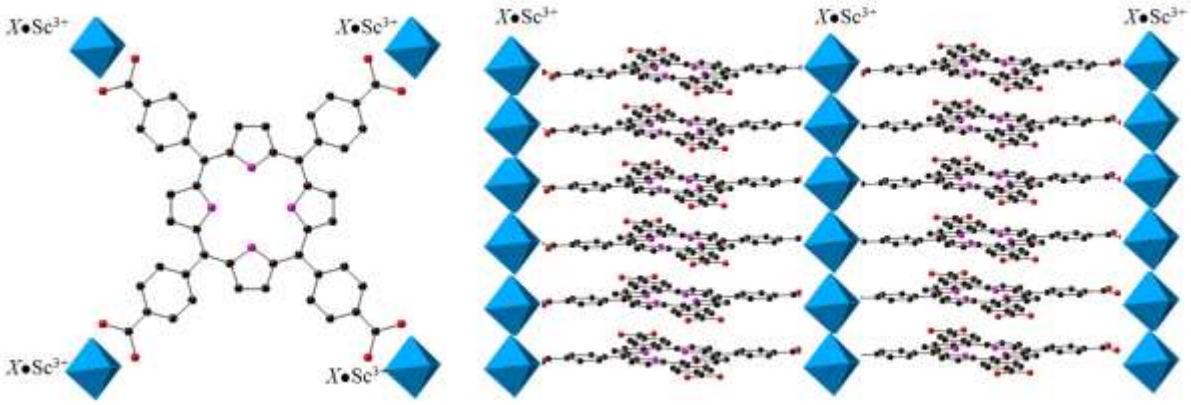

Figure 5.45: Possibly assembly for Sc-TCPP.

5.6 Conclusion

In this chapter a series of novel materials has been prepared and characterized by PXRD, TGA, gas adsorption and solid-state NMR. Among the three ligands used in the syntheses of novel scandium MOFs by using isophthalic acid and its amino derivative two new structures were found and solved by single crystal X-ray analysis. In the case of 2,5-furandicarboxylic acid as ligand, also two structures were prepared but just one was solved by single crystal and for the unknown material, a structural model was proposed. The macromolecule TCPP as linker gives rise a porous scandium carboxylate but no structural solution to this material has been found due to limitations to grow crystals. At least six novel phases were produced, three of which show porosity for N_2 and/or CO_2.

The scandium isophthalate (named here as (Sc(IA)-1) was prepared by solvothermal synthesis using mixed solvent (DMF and H_2O) at lower temperature (120 ℃) and shorter time of reaction (12 h) by comparison with the other scandium isophthalate (labelled here as Sc(IA)-2) which was prepared hydrothermally at higher temperature 220 ℃ and 48 h. Both materials crystallise in the cubic system but with different symmetry and morphology, Sc(IA)-1 cube shaped, $Pa\bar{3}$, crystallised as cubes whereas Sc(IA)-2, $P2_13$, crystallised

octahedra. Scandium 2-aminoisophthalate crystallises as a form isostructural to Sc(IA)-2, but in the higher symmetry space group $I2_13$. This is clearly manifested in the ^{45}Sc MASNMR, where there is a single resonance, rather than two.

Of these novel scandium carboxylates, only the Sc(IA)-1 is porous, exhibiting an uptake of 2.5 mmol g^{-1} at -77 ℃ and 1 bar for CO_2. This is much higher than the observed porosity for the indium analogue. The structure of Sc(IA)-1 contains $Sc_3O(L)_3(O_2C)_6$ trimer similar to those found in MIL-88, MIL100 and MIL-101 reported earlier in this thesis, but the pore size is too small for the materials to act as a catalyst. It would be expected to be a selective adsorbent for CO_2 over larger molecules such as hydrocarbons.

Of the two crystalline scandium MOFs obtained by using 2, 5-furancarboxylic acid, just one of them crystallizing as large colourless chips (Sc(FDA)-1), which was analysed by single crystal diffraction. This showed that the Sc(FDA)-1 solid crystallized in the triclinic space group (*P-1)* but the data had high residual values. Then single crystal structure was Rietveld-refined against powder X-ray diffraction using the GSAS suite of programs, resulting in a good fit to the data. This novel solid was not porous in contrast with the other material prepared Sc(FDA)-2, which was porous for both, N_2 and CO_2, but drastic changes were observed upon heating at 250 ℃. The unknown porous structure, Sc(FDA)-2 is found to lose DMF from the pores upon thermal treatment, resulting change and loss (rather than gain) of porosity. Also, these changes were confirmed by solid state NMR but further work are required to understand this solid, starting for the structural solution as all the attempts yielded as microcrystalline powder it is necessary to solve the structure, it might be by using synchrotron analysis or change the synthetic conditions or even the reactor to obtain large crystals.

The novel porphyrin-based scandium MOFs crystallised as poorly crystalline fibres or wires, with relatively low thermal stability. Nevertheless they possess large surface areas when activated at low temperatures under vacuum (70 °C), which achieve nearly 800 m^2 g^{-1}. Further studies are required to enhance the crystallinity of this material to give crystals amenable to structure solution.

5.6 References

1. S. R. Miller, P. A. Wright, T. Devic, C. Serre, G. Ferey, P. L. Llewellyn, R. Denoyel, L. Gaberova and Y. Filinchuk, *Langmuir*, 2009, 25, 3618-3626.

2. J. P. S. Mowat, S. R. Miller, A. M. Z. Slawin, V. R. Seymour, S. E. Ashbrook and P. A. Wright, *Micropor. Mesopor. Mat.*, 2011, 142, 322-333.

3. J. P. S. Mowat, S. R. Miller, J. M. Griffin, V. R. Seymour, S. E. Ashbrook, S. P. Thompson, D. Fairen-Jimenez, A.-M. Banu, T. Düren and P. A. Wright, *Inorg. Chem.*, 2011, 50, 10844-10858.

4. J. P. S. Mowat, V. R. Seymour, J. M. Griffin, S. P. Thompson, A. M. Z. Slawin, D. Fairen-Jimenez, T. Duren, S. E. Ashbrook and P. A. Wright, *Dalton Trans.*, 2012, 41, 3937-3941.

5. L. Mitchell, B. Gonzalez-Santiago, J. P. S. Mowat, M. E. Gunn, P. Williamson, N. Acerbi, M. L. Clarke and P. A. Wright, *Cat. Sci. Tech.*, 2013, 3, 606-617.

6. K. Barthelet, D. Riou and G. Ferey, *Chem. Commun.*, 2002, 1492-1493.

7. H. Reinsch, M. A. van der Veen, B. Gil, B. Marszalek, T. Verbiest, D. de Vos and N. Stock, *Chem. Mat.*, 2013, 25, 17-26.

8. T. Panda, T. Kundu and R. Banerjee, *Chem. Commun.* , 2013, 49, 6197-6199.

9. W. Ji, H. Hu, W. Zhang, H. Huang, X. He, X. Han, F. Zhao, Y. Liu and Z. Kang, *Dalton Trans.*, 2013, 42, 10690-10693.

10. S. R. Miller, PhD, University of St. Andrews, 2007.

11. I. A. Ibarra, S. Yang, X. Lin, A. J. Blake, P. J. Rizkallah, H. Nowell, D. R. Allan, N. R. Champness, P. Hubberstey and M. Schroder, *Chem. Commun.*, 2011, 47, 8304-8306.

12. H.-H. Li, W. Shi, N. Xu, Z.-J. Zhang, Z. Niu, T. Han and P. Cheng, *Cryst. Growth Des.*, 2012, 12, 2602-2612.

13. F.-N. Shi, D. Ananias, T.-H. Yang and J. Rocha, *J. Solid State Chem.*, 2013, 204, 321-328.

14. W.-Y. Gao, M. Chrzanowski and S. Ma, *Chem. Soc. Rev.*, 2014, 43, 5841-5866.

15. G. l. K. B. F. S. Nakagaki , G. M. Ucoski and and K. A. D. d. F. Castro, *Molecules*, 2013, 18, 7279-7308.

16. M. E. Kosal, J.-H. Chou, S. R. Wilson and K. S. Suslick, *Nat Mater*, 2002, 1, 118-121.

17. S. Lipstman, S. Muniappan, S. George and I. Goldberg, *Dalton Trans.*, 2007, 3273-3281.

18. A. Fateeva, S. Devautour-Vinot, N. Heymans, T. Devic, J.-M. Grenèche, S. Wuttke, S. Miller, A. Lago, C. Serre, G. De Weireld, G. Maurin, A. Vimont and G. Férey, *Chem. Mat.*, 2011, 23, 4641-4651.

19. C. Zou, M. H. Xie, G. Q. Kong and C. D. Wu, *CrystEngComm*, 2012, 14, 4850-4856.

20. H.-J. Son, S. Jin, S. Patwardhan, S. J. Wezenberg, N. C. Jeong, M. So, C. E. Wilmer, A. A. Sarjeant, G. C. Schatz, R. Q. Snurr, O. K. Farha, G. P. Wiederrecht and J. T. Hupp, *J. Am. Chem. Soc.*, 2014, 135, 862-869.

21. B. J. Deibert and J. Li, *Chem. Commun.* , 2014, 50, 9636-9639.

22. W. Morris, B. Volosskiy, S. Demir, F. Gándara, P. L. McGrier, H. Furukawa, D. Cascio, J. F. Stoddart and O. M. Yaghi, *Inorg. Chem.*, 2012, 51, 6443-6445.

23. P. W. Betteridge, J. R. Carruthers, R. I. Cooper, K. Prout and D. J. Watkin, *J. Appl. Crystallogr.*, 2003, 36, 1487.

24. C. Larson and R. B. von Dreele, *Los Alamos National Labaratory: Los Alamos, NM*, 2001.

25. B. H. Toby, *J. Appl. Crystallogr.*, 2001, 210-213.

26. A. Altomare, M. Camalli, C. Cuocci, C. Giacovazzo, A. Moliterni and R. Rizzi, *J. Appl. Crystallogr.*, 2009, 42, 1197-1202.

27. J. Rodriguez-Carvajal, *J. Physica B.*, 1990, 192, 55.

Chapter 6: General conclusions and further work

6.1 General conclusions

This chapter summarises the results obtained in this investigation. The main aim of this thesis was to explore the synthesis and properties of scandium carboxylate metal-organic frameworks. The properties of known and novel scandium metal-organic frameworks for adsorption and catalysis were then examined.

The first part detailed the application of scandium MOFs as catalysts. The synthesis of MOFs such as MIL-100(Sc) and the isoreticular MIL-88(B)(Sc) and MIL-88D(Sc) were prepared following reaction conditions from the literature. MIL-101(Sc) was prepared as a single phase by using a mixture of solvents (DMF and EtOH). Upon heating, MIL-101(Sc-) recrystallized into MIL-88B(Sc). Slightly modification on this route, by changing the molar ratio and the addition of a third solvent (H_2O) to the mixture gave the preparation of MIL-68(Sc) for the first time. Characterisation by single crystal diffraction was performed and its structure was solved in the orthorhombic system (*Cmcm*). Chromium MOFs (MIL-101 and MIL-100) and scandium-exchanged zeolites were prepared to compare their catalytic activity with scandium MOFs.

The direct encapsulation of polyoxometallates (POMs) in MOFs during synthesis was also explored. Polytungstic acid (PTA) could be encapsulated within the pores of MIL-101(Sc) to make it more thermally stable and so to greatly enhance its surface area for N_2 adsorption. Attempts at POM encapsulation in MIL-100(Sc) and MIL-88D(Sc) were unsuccessful. A series of scandium and chromium MOFs, POM/MIL-100(Sc) and scandium-exchanged zeolites were tested as heterogeneous catalysts in the carbonyl ene reaction between α-methyl styrene and ethyl trifluoropyruvate. Results of this test showed that MIL-100(Sc) was the best catalyst for this reaction, achieving a conversion of 99% to the desired product and showing recyclability. The other reaction studied was acetalization of benzaldehyde and acetophenone,

and in this case the isoreticular MOFs MIL-88(B) and MIL-88D(Sc) were the most selective catalysts. This was due to the solvent used in the reaction, which allowed the pores of the framework to open, whereas the reaction was slow in MIL-100(Sc), suggesting that the reactants and products are adsorbed strongly in the pores or the Lewis acid sites are blocked by coordination to the methanol.

Functionalisation of scandium terephthalates such as MIL-101(Sc), MIL-88B(Sc) and MIL-68(Sc), Sc_2BDC_3, and MIL-53(Sc) were explored in the second part in this thesis. Functionalisation by using amino functional groups was performed on those materials for the first time and their properties compared to those of their unfunctionalised forms.

The amino-functionalised NH_2-MIL-101(Sc) was prepared but recrystallization occurs readily upon heating. Meanwhile, several routes were found to synthesize NH_2-MIL-88B(Sc) and analysis of their adsorption properties were studied with CO_2. Gas adsorption studies suggested that the functionalised NH_2-MIL-88B(Sc) is selective for CO_2 with an uptake of 2.5 mmol g^{-1}. This is due to the amino groups in the framework, which increases the affinity to that gas. In fact the non-functionalised MIL-88B(Sc) was not porous either for N_2 or CO_2. NH_2-MIL-68(Sc) adsorbs less CO_2 compared to MIL-68(Sc), 9 of 20 mmol g^{-1}.

Although the synthesis of amino-Sc_2BDC_3 was reported previously, here an optimized solvothermal route was discovered, which involves lower temperatures and mixed solvents, and this gave $Sc_2(NH_2\text{-}BDC)_3$ as a single phase and large crystals. In addition its post-synthetic modification by using nitro-groups was studied. Also, the synthesis of $Sc_2(Br\text{-}BDC)_3$ was prepared for first time and analysed by single crystal diffraction. In order to compare the adsorption properties of these MOFs and post-modified material, Sc_2BDC_3 and $Sc_2(NO_2\text{-}BDC)_3$ were synthesized. These five materials were used as adsorbents for methanol and hydrocarbons. Results of this study demonstrated that Sc_2BDC_3 and $Sc_2(NH_2\text{-}BDC)_3$

gave the highest uptakes for methanol, while the other MOFs with nitro-and bromo-groups showed lower uptakes because of the presence of bulky groups. In addition, these block access of more sterically-demanding adsorbates, such as branched alkanes.

Amino-functionalised MIL-53(Sc) was prepared for the first time. The synthesis was achieved using a mixed ligand approach. The material was characterised using PXRD, TGA and gas adsorption, which confirms the sample adsorbs CO_2.

The synthesis of novel scandium MOFs using the linkers isophthalate and its amino- and nitro- derivatives, 2,5-furandicarboxylate and the porphyrin tetra(carboxyphenyl)porphyrin (TCPP) and six novel materials were prepared. For three of these MOFs, Sc(IA)-1 with formula $Sc_3O(OH)(H_2O)_2(C_8H_4O_4)_3]$, Sc($NH_2$-IA) [$Sc_2(NH_2$- $C_8H_4O_4)_3$] and Sc(FDA)-1, $Sc_2(C_6H_2O_5)_3$ their structure was solved by single crystal diffraction. Three of the new materials, Sc(IA)-1, Sc(FDA)-2 and the scandium TCPP were found to be porous to N_2 and CO_2.

6.2 Further work

Functionalisation of scandium terephthalate MOFs using amino groups have demonstrated to enhance CO_2 adsorption in NH_2-MIL-88B(Sc), so the synthesis of amino-MIL-88D(Sc) can be explored further. Attempts in the amino-functionalisation of MIL-101(Sc) were unsuccessful recrystallization into NH_2-MIL-88B(Sc) but since the encapsulation of polyoxometalate phosphotungstate PTA was successful and have increased the stability of MIL-101(Sc), further investigation for the synthesis of amino-MIL-101(Sc) encapsulating PTA could be explored, with the aim of making the amino-MIL-101(Sc) framework stable to heating.

Further studies are required to determine the unsolved structures. This may be possible for highly crystalline powders via ab initio methods using synchrotron high resolution powder data, or by using different crystallisation conditions (time, dilution, solvents) For the poorly crystalline porphyrins, this is likely to be a challenge, but an idea of the scandium coordination geometry could be achieved by solid state NMR.

Appendices: Attached CD

Appendix A: Crystallographic information files for MIL-68(Sc)

A1: MIL-68(Sc)

Appendix B: Crystallographic information files for the functionalised-scandium carboxylates

B1: $Sc_2(NH_2\text{-}BDC)_3$

B2: $Sc_2(Br\text{-}BDC)_3$

B3: NH_2-MIL-53(Sc)

Appendix C: Crystallographic information files for novel scandium carboxylates

C1: Sc(IA)-1

C2: Sc(NH_2-IA)

C3: Sc(FDA)-1